AVIAN VIRAL IMMUNOSUPPRESSIVE DISEASE

EDITED BY: Yulong Gao, Aijian Qin, Yongxiu Yao and Ziqiang Cheng
PUBLISHED IN: Frontiers in Veterinary Science and Frontiers in Microbiology

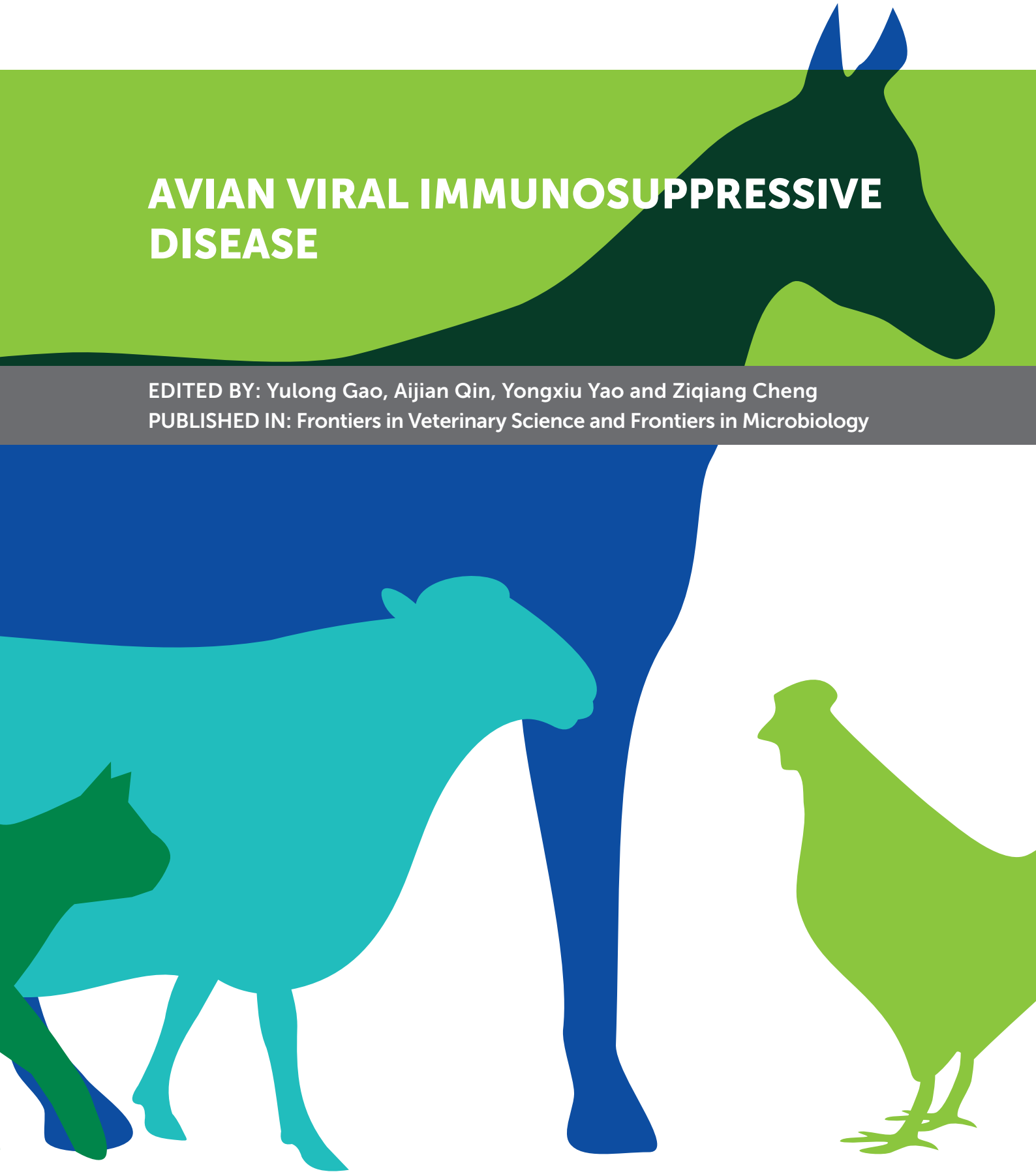

frontiers Research Topics

frontiers

ISSN 1664-8714
ISBN 978-2-83250-499-4
DOI 10.3389/978-2-83250-499-4

About Frontiers

Frontiers is more than just an open-access publisher of scholarly articles: it is a pioneering approach to the world of academia, radically improving the way scholarly research is managed. The grand vision of Frontiers is a world where all people have an equal opportunity to seek, share and generate knowledge. Frontiers provides immediate and permanent online open access to all its publications, but this alone is not enough to realize our grand goals.

Frontiers Journal Series

The Frontiers Journal Series is a multi-tier and interdisciplinary set of open-access, online journals, promising a paradigm shift from the current review, selection and dissemination processes in academic publishing. All Frontiers journals are driven by researchers for researchers; therefore, they constitute a service to the scholarly community. At the same time, the Frontiers Journal Series operates on a revolutionary invention, the tiered publishing system, initially addressing specific communities of scholars, and gradually climbing up to broader public understanding, thus serving the interests of the lay society, too.

Dedication to Quality

Each Frontiers article is a landmark of the highest quality, thanks to genuinely collaborative interactions between authors and review editors, who include some of the world's best academicians. Research must be certified by peers before entering a stream of knowledge that may eventually reach the public - and shape society; therefore, Frontiers only applies the most rigorous and unbiased reviews.
Frontiers revolutionizes research publishing by freely delivering the most outstanding research, evaluated with no bias from both the academic and social point of view. By applying the most advanced information technologies, Frontiers is catapulting scholarly publishing into a new generation.

What are Frontiers Research Topics?

Frontiers Research Topics are very popular trademarks of the Frontiers Journals Series: they are collections of at least ten articles, all centered on a particular subject. With their unique mix of varied contributions from Original Research to Review Articles, Frontiers Research Topics unify the most influential researchers, the latest key findings and historical advances in a hot research area! Find out more on how to host your own Frontiers Research Topic or contribute to one as an author by contacting the Frontiers Editorial Office: frontiersin.org/about/contact

AVIAN VIRAL IMMUNOSUPPRESSIVE DISEASE

Topic Editors:
Yulong Gao, Harbin Veterinary Research Institute, Chinese Academy of Agricultural Sciences, China
Aijian Qin, Yangzhou University, China
Yongxiu Yao, The Pirbright Institute, United Kingdom
Ziqiang Cheng, Shandong Agricultural University, China

Citation: Gao, Y., Qin, A., Yao, Y., Cheng, Z., eds. (2022). Avian Viral Immunosuppressive Disease. Lausanne: Frontiers Media SA.
doi: 10.3389/978-2-83250-499-4

Table of Contents

frontiers in Veterinary Science

BRIEF RESEARCH REPORT
published: 11 January 2022
doi: 10.3389/fvets.2021.813397

Molecular Characterization of a Novel Budgerigar Fledgling Disease Virus Strain From Budgerigars in China

Xiaoliang Hu[1], Dongdong Cai[2], Siru Liu[1], Yan Li[3], Lulu Chen[1], Guangmei Luo[1], Hongli Pu[1], Yucan He[1], Xiangxiao Liu[1], Lili Zhao[4], Hongzhi Cao[5], Tiankuo Yang[6] and Zhige Tian[1]**

[1] Yibin Key Laboratory of Zoological Diversity and Ecological Conservation, Solid-State Fermentation Resource Utilization Key Laboratory of Sichuan Province, Faculty of Agriculture, Forestry and Food Engineering, Yibin University, Yibin, China, [2] Sichuan Animal Disease Control Central, Chengdu, China, [3] Animal Breeding and Genetics Key Laboratory of Sichuan Province, Sichuan Animal Sciences Academy, Chengdu, China, [4] College of Veterinary Medicine, Jilin University, Changchun, China, [5] Department of Animal Husbandry and Veterinary Medicine, Modern Agricultural College, Yibin Vocational and Technical College, Yibin, China, [6] Aviation Medical Appraisal Center, Civil Aviation Flight University of China, Guanghan, China

OPEN ACCESS

Edited by:
Yulong Gao,
Harbin Veterinary Research Institute, Chinese Academy of Agricultural Sciences (CAAS), China

Reviewed by:
Yanbing Li,
Harbin Veterinary Research Institute, Chinese Academy of Agricultural Sciences (CAAS), China
Stefan Vilcek,
University of Veterinary Medicine in Kosice, Slovakia
Ugo Moens,
Arctic University of Norway, Norway

***Correspondence:**
Zhige Tian
beishugege@126.com
Tiankuo Yang
yangtiankuo@hotmail.com

Specialty section:
This article was submitted to Veterinary Infectious Diseases, a section of the journal Frontiers in Veterinary Science

Received: 11 November 2021
Accepted: 17 December 2021
Published: 11 January 2022

Citation:
Hu X, Cai D, Liu S, Li Y, Chen L, Luo G, Pu H, He Y, Liu X, Zhao L, Cao H, Yang T and Tian Z (2022) Molecular Characterization of a Novel Budgerigar Fledgling Disease Virus Strain From Budgerigars in China. Front. Vet. Sci. 8:813397. doi: 10.3389/fvets.2021.813397

Budgerigar fledgling disease virus (BFDV) is the causative polyomavirus of budgerigar fledgling disease, an important avian immunosuppressive disease in budgerigars (*Melopsittacus undulatus*). In the current study, we explored the etiological role and molecular characteristics of BFDV. We identified a novel BFDV strain, designated as SC-YB19, belonging to a unique cluster with three other domestic strains (WF-GM01, SD18, and APV-P) and closely related to Polish isolates based on complete sequences. Sequence analysis showed that SC-YB19 had an 18-nucleotide (nt) deletion in the enhancer region, corresponding to the sequence position 164–181 nt, which differed significantly from all other BFDV strains. Based on sequence alignment, three unique nucleotide substitutions were found in VP4 (position 821), VP1 (position 2,383), and T-antigen (position 3,517) of SC-YB19, compared with SD18, WF-GM01, QDJM01, HBYM02, APV7, and BFDV1. Phylogenetic analyses based on complete sequences suggested that SC-YB19, along with the domestic WF-GM01, SD18, and APV-P strains, formed a single branch and were closely related to Polish, Japanese, and American isolates. These results demonstrate that BFDV genotype variations are co-circulating in China, thus providing important insight into BFDV evolution.

Keywords: budgerigar fledgling disease virus, deletion, phylogenetic analysis, genotype variation, enhancer element

BACKGROUND

Budgerigar fledgling disease virus (BFDV), also called avian polyomavirus (APV), is the causative agent of budgerigar fledgling disease, an important immunosuppressive disease in budgerigars (*Melopsittacus undulatus*). The disease was first reported in 1981, with typical symptoms including abdominal distention, lack of down feathers on the back and abdomen, subcutaneous hemorrhage of nestlings, and acute death (1–3). Polyomaviruses have a wide host range, and have been identified in vertebrates such as humans (4, 5), bats (6, 7), non-human primates (8), and horses (9). In China, a BFDV strain, HBYM02, was first reported and isolated in Hubei Province in 1994. Since

then, sporadic infections have occurred across the country, resulting in considerable losses to the budgerigar breeding industry (10).

BFDV was identified as the first non-mammalian member of the genus *polyomavirus* (11, 12). BFDV is a circular, double-stranded molecule with a 4 981-nt genome, which can be divided into early and late regions. The early region codes for two non-structural proteins, i.e., large T and small t antigens. The late region contains four structural proteins, i.e., VP1, VP2, VP3, and VP4 (13). The genome also contains four regulatory elements, i.e., promoter, polyadenylation signal, DNA replication origin, and enhancer regions (14).

In the present study, we report on BFDV infection in budgerigars from Sichuan Province, China, for the first time. To better understand the molecular characteristics of the identified strain, sequencing analysis was performed and a phylogenetic tree was constructed based on its complete genome. Our results should assist in elucidating the genetic evolution of BFDV in China.

METHODS

Ethics Statement

No animals were sacrificed for this study.

Abbreviations: BFDV, Budgerigar fledgling disease virus; APV, avian polyomavirus; NJ, neighbor-joining; nt, nucleotides; PCR, polymerase chain reaction; RT, reverse transcription.

Clinical Cases and Virus Identification

During the spring of 2019, dozens of budgerigars died at a budgerigar breeding farm in Sichuan, China. The birds showed rapid weight loss and exhibited liver and lung congestion, splenomegaly, swollen kidneys, and liver hemorrhage. Heart, liver, lung, and fecal samples were collected from the dead budgerigars. The samples were ground and centrifuged at 8,000 rpm for 10 min. DNA/RNA was extracted from the resulting supernatants, then identified using primers (15). Polymerase chain reaction (PCR) primers were employed to amplify the complete sequence, as described previously (16). Samples were examined by blood agglutination assay, PCR, or reverse transcription (RT) -PCR for the presence of DNA or RNA viruses, including avian reovirus (17), infectious bursal disease virus (18), reticuloendotheliosis virus (19), avian influenza virus (20), Newcastle disease virus (21), avian leukosis virus (22), and avian adenovirus 4 (23), according to previously described methods.

Sequence Alignment and Phylogenetic Analysis

Complete sequences were manually assembled using ClustalX (v1.83), Vector 10, and DNASTAR. Multiple sequence alignments were conducted using ClustalW in MEGA v6.0. Phylogenetic trees were constructed using the neighbor-joining (NJ) method in MEGA (v4.0). Bootstrap values were estimated for 1,000 replicates. The sequences obtained in this study were assembled and submitted to GenBank under accession number MT119153.

TABLE 1 | Point mutations in seven strains of BFDVs compared with SC-YB19.

Nucleotide number	Region	SC-YB19	Nucleotide exchange compared with SC-YB19 (amino acid substitution compared with predicted amino acid sequence of SC-YB19)					
			SD18	WF-GM01	QDJM01	HBYM02	APV7	BFDV1
386	VP4(inton)	G	G	G	G	G	G	C
387	VP4(inton)	C	C	C	C	C	C	G
623	VP4(inton)	C	C	C	T	T	T	T
821	VP4	C(123T)	T(123T)	T(123T)	T(123T)	T(123T)	T(123T)	T(123T)
1652	VP2/VP3	G(115G)	G(115G)	G(115G)	G(115G)	G(115G)	G(115G)	T(115A)
2383	VP1	T(157S)	A(157S)	A(157S)	A(157S)	A(157S)	A(157S)	A(157S)
2488	VP1	C(192G)	C(192G)	C(192G)	T(192G)	T(192G)	C(192G)	T(192G)
2572	VP1	A(220E)	A(220E)	A(220E)	G(220E)	G(220E)	A(220E)	G(220E)
2677	VP1	C(255A)	C(255A)	C(255A)	A(255A)	A(255A)	C(255A)	A(255A)
2758	VP1	A(282R)	A(282R)	A(282R)	G(282R)	G(282R)	A(282R)	G(282R)
2920	VP1	T(336D)	T(336D)	T(336D)	C(336D)	C(336D)	T(336D)	C(336D)
2959	Non-coding region	A	A	A	C	C	A	C
3256	T-antigen	G(515T)	G(515T)	G(515T)	A(515T)	A(515T)	A(515T)	A(515T)
3457	T-antigen	C(448K)	C(448K)	T(448K)	T(448K)	T(448K)	T(448K)	T(448K)
3517	T-antigen	G(428R)	T(428R)	T(428R)	T(428R)	T(428R)	T(428R)	T(428R)
3657	T-antigen	T(382K)	T(382K)	G(382Q)	G(382Q)	G(382Q)	G(382Q)	G(382Q)
3739	T-antigen	G(354T)	G(354G)	G(354G)	A(354T)	A(354T)	A(354T)	A(354T)
4139	T-antigen	G(221P)	G(221P)	G(221P)	G(221P)	A(221L)	A(221L)	A(221L)
4986	T/t-antigen	G(4L)	G(4L)	G(4L)	A(4L)	G(4L)	G(4L)	A(4L)

Highlights indicate the mutant position.

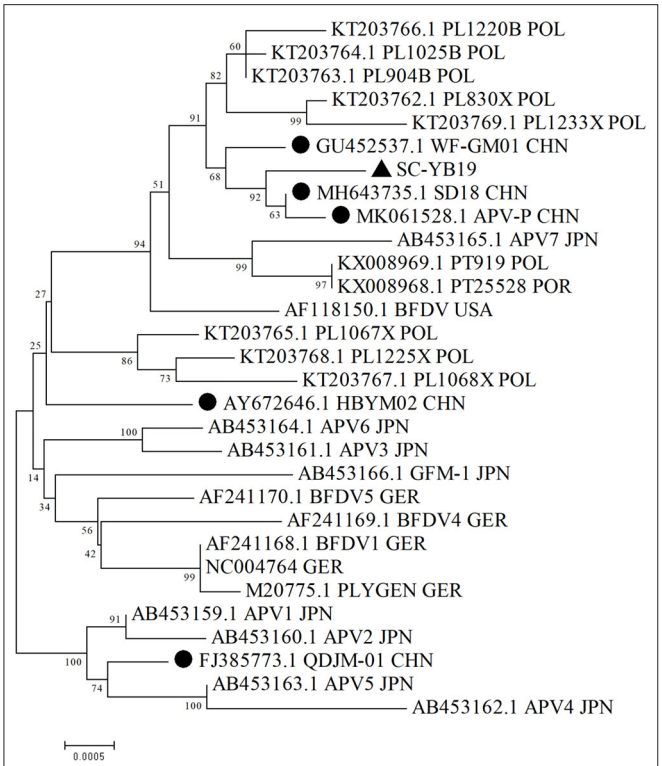

FIGURE 1 | Phylogenetic analysis of complete SC-YB19 sequence and related whole-genome strains from GenBank. Neighbor-joining was used to construct a phylogenetic tree, with bootstrap values of 1,000 replicates shown on branches. Scale bar represents *p*-distance. ● presents the domestic strains. ▲ presents the strains isolated in this study. CHN, China; GER, Germany; POL, Poland; POR, Portugal; USA, United States Of Amrica; JPN, Japan.

TABLE 2 | Source of Budgerigar fledgling disease polyomavirus (BFDV) sequences used in the experiment.

Name	Genbank	Collection date	Country
SC-YB19	MT119153	2019	CHN
BFDV1	AF241168	1984	GER
BFDV4	AF241169	1981	GER
BFDV5	AF241170	1995	GER
GFM-1	AB477106	1982	JPN
BFDV	AF118150	1999	USA
APV1	AB453159	2003	JPN
APV2	AB453160	2003	JPN
APV3	AB453161	2004	JPN
APV4	AB453162	2005	JPN
APV5	AB453163	2005	JPN
APV6	AB453164	2005	JPN
APV7	AB453165	2006	JPN
PLYGEN	M20775	1988	GER
WF-GM01	GU452537	2009	CHN
SD18	MH643735	2018	CHN
APV-P	MK061528	2018	CHN
QDJM-01	FJ385773	2008	CHN
HBYM02	AY672646	1994	CHN
PL830X	KT203762	2009	POL
PL1220B	KT203766	2010	POL
PT25528	KX008968	2015	POR
PT919	KX008969	2016	POL
PL1025B	KT203764.1	2010	POL
PL904B	KT203763.1	2009	POL
PL1233X	KT203769.1	2011	POL
PL1067X	KT203765	2010	POL
PL1225X	KT203768	2010	POL
PL1068X	KT203767	2010	POL
/	NC004764	1984	GER

RESULTS AND DISCUSSION

In 2019, more than 20 two-week-old budgerigars died at a breeding farm and were thus collected for laboratory investigation. Tissue samples from the liver and lungs were only positive for BFDV. No other viruses were identified in the samples (data not shown). To analyze genomic characteristics, PCR was employed to amplify and sequence the complete viral genome (termed SC-YB19). The genome was 4,963-nt long and composed of six regions, including early, late, promoter, polyadenylation signal, DNA replication origin, and enhancer regions. The positions 80–126, 131–178, 180–193, 682–693, and 706–715 are speculated to be enhancer elements (14) (**Supplementary Figure 1**), which affect interactions with cellular transcription and replication factors and regulate viral and cellular gene products (24–27). We identified an 18-nt deletion (position 164–182) in the enhancer section (positions 131–178 and 180–193) in SC-YB19, but not in the other BFDV isolates (**Supplementary Figures 2A,B**). However, whether this deletion affects the transcription, replication, and virulence of SC-YB19 is unknown, and further experiments are required to investigate its potential influence on biological effects. In addition, compared with SD18, WF-GM01, QDJM01, HBYM02, APV7, and BFDV1, nucleotide substitutions were observed at 19 loci in VP4, VP2/VP3, VP1, non-coding region, T-antigen, and T/t-antigen of SC-YB19. Three nucleotide substitutions in VP4 (position 821), VP1 (position 2,383), and T-antigen (position 3,517) were only found in SC-YB19, not in the other domestic strains (**Table 1**). All nucleotide substitutions in SC-YB19 were nonsense mutations (**Table 1**). Based on sequence alignment, position 2488, 2572, 2677, 2758, 2920, 2959, 3256, and 4139 of SC-YB19, SD18, and WF-JM01 were identified to that of BFDV and APV-7, which were isolated from the USA and Japan, respectively, while position 623, 2488, 2572, 2677, 2758, 2920, 2959, 3256, 3739, 4139, and 4986 of QDJM01 and HBYM02 were identified to the German strains (BFDV1, BFDV4, BFDV5, PLYGEN, and NC004764) (**Supplementary Figures 3**, **4**). These results indicate that domestic strains show genetic diversity and may have different ancestors. We suppose that BFDVs have undergone evolution in China.

Phylogenetic analyses based on complete sequences suggested that SC-YB19, along with the domestic WF-GM01, SD18, and

APV-P strains, formed a single branch and were closely related to Polish, Japanese, and American isolates (**Figure 1**; **Table 2**). QD-JM01 was clustered with the APV1, APV2, APV4, and APV5 strains isolated from the Japanese black-headed caique (*Pionites melanocephalus*). HBYM02 was distinct from the five other domestic strains and did not belong to any cluster (**Figure 1**). Thus, our data show that different BFDV genotypes are co-circulating in China.

CONCLUSIONS

We report on a novel BFDV enhancer deletion mutant (SC-YB19 strain) in China. The strain forms a unique cluster with three other domestic strains. This study improves our understanding of the genetic structure, diversity, and evolution of SC-YB19.

DATA AVAILABILITY STATEMENT

The datasets presented in this study can be found in online repositories. The names of the repository/repositories and accession number(s) can be found in the article/**Supplementary Material**.

ETHICS STATEMENT

The animal study was reviewed and approved by Animal Ethics Committee of Yibin University.

AUTHOR CONTRIBUTIONS

ZT and TY designed the study and revised the draft. XH, DC, SL, and ZT performed the experiments. YL, LC, GL, HP, YH, XL, LZ, and HC collected the samples. ZT, XH, and TY drafted the manuscript. All authors revised and approved the paper for publication.

FUNDING

This work was supported by the Doctor Launch Project of Yibin University (2019QD09 and 2019QD10) and Foundation of General Program in Civil Aviation Flight University of China (J2021-134).

SUPPLEMENTARY MATERIAL

The Supplementary Material for this article can be found online at: https://www.frontiersin.org/articles/10.3389/fvets.2021.813397/full#supplementary-material

Supplementary Figure 1 | Draft enhancer element of SC-YB19 (in red box).

Supplementary Figure 2 | (A) 18-nt deletion in the enhance element at nucleotide position 164–182 of the SC-YB19; **(B)** Result of the ABI sequencing for SC-YB19.

Supplementary Figure 3 | Nucleotide sequences alignments between SC-YB19 and SD18, WF-GM01, QDJM01, AY672646, AF118150, APV-7, AF241168, AF241169, AF241170, M20775, and NC004764.

Supplementary Figure 4 | Multiple sequence alignment of complete sequences in BFDV strains.

REFERENCES

1. Davis R, Bozeman L, Gaudry D, Fletcher O, Lukert P, Dykstra M. A viral disease of fledgling budgerigars. *Avian Dis.* (1981) 25:179–83. doi: 10.2307/1589839
2. Bernier G, Morin M, Marsolais G. A generalized inclusion body disease in the budgerigar (Melopsittacus undulatus) caused by a papovavirus-like agent. *Avian Dis.* (1981) 25:1083–92. doi: 10.2307/1590087
3. Feng H, Shuda M, Chang Y, Moore PS. Clonal integration of a polyomavirus in human Merkel cell carcinoma. *Science.* (2008) 319:1096–100. doi: 10.1126/science.1152586
4. Allander T, Andreasson K, Gupta S, Bjerkner A, Bogdanovic G, Persson MA, et al. Identification of a third human polyomavirus. *J Virol.* (2007) 81:4130–6. doi: 10.1128/JVI.00028-07
5. Gaynor AM, Nissen MD, Whiley DM, Mackay IM, Lambert SB, Wu G, et al. Identification of a novel polyomavirus from patients with acute respiratory tract infections. *PLoS Pathogens.* (2007) 3:e64. doi: 10.1371/journal.ppat.0030064
6. Tao Y, Shi M, Conrardy C, Kuzmin IV, Recuenco S, Agwanda B, et al. Discovery of diverse polyomaviruses in bats and the evolutionary history of the Polyomaviridae. *J Gen Virol.* (2013) 94:738–748. doi: 10.1099/vir.0.047928-0
7. Fagrouch Z, Sarwari R, Lavergne A, Delaval M, De Thoisy B, Lacoste V, et al. Novel polyomaviruses in South American bats and their relationship to other members of the family Polyomaviridae. *J Gen Virol.* (2012) 93:2652–7. doi: 10.1099/vir.0.044149-0
8. Deuzing I, Fagrouch Z, Groenewoud MJ, Niphuis H, Kondova I, Bogers W, et al. Detection and characterization of two chimpanzee polyomavirus genotypes from different subspecies. *Virol J.* (2010) 7:347. doi: 10.1186/1743-422X-7-347
9. Renshaw RW, Wise AG, Maes RK, Dubovi EJ. Complete genome sequence of a polyomavirus isolated from horses. *Am Soc Microbiol.* (2012) 86:8903. doi: 10.1128/JVI.01261-12
10. Xia W, Feng F, Li T, Chen S, Zhao L. Identification and biochemical characteristics of a new psittacine virus in China. *Virol Sinica.* (1999) 14:265–272.
11. Bozeman L, Davis R, Gaudry D, Lukert P, Fletcher O, Dykstra M. Characterization of a papovavirus isolated from fledgling budgerigars. *Avian Dis.* (1981) 25:972–80. doi: 10.2307/1590072
12. Lehn H, Müller H. Cloning and characterization of budgerigar fledgling disease virus, an avian polyomavirus. *Virology.* (1986) 151:362–70. doi: 10.1016/0042-6822(86)90056-5
13. Johne R, Paul G, Enderlein D, Stahl T, Grund C, Müller H. Avian polyomavirus mutants with deletions in the VP4-encoding region show deficiencies in capsid assembly and virus release, and have reduced infectivity in chicken. *J Gen Virol.* (2007) 88:823–30. doi: 10.1099/vir.0.82506-0
14. Rott O, Kröger M, Müller H, Hobom G. The genome of budgerigar fledgling disease virus, an avian polyomavirus. *Virology.* (1988) 165:74–86. doi: 10.1016/0042-6822(88)90660-5
15. Zhuang Q, Chen J, Mushtaq MH, Chen J, Liu S, Hou G, et al. Prevalence and genetic characterization of avian polyomavirus and psittacine beak and feather disease virus isolated from budgerigars in Mainland China. *Arch Virol.* (2012) 157:53–61. doi: 10.1007/s00705-011-1138-1
16. Ma J, Wu R, Tian Y, Zhang M, Wang W, Li Y, et al. Isolation and characterization of an Aves polyomavirus 1 from diseased budgerigars in China. *Vet Microbiol.* (2019) 237:108397. doi: 10.1016/j.vetmic.2019.108397
17. Zhong L, Gao L, Liu Y, Li K, Wang M, Qi X, et al. Genetic and pathogenic characterisation of 11 avian reovirus isolates from northern China suggests continued evolution of virulence. *Sci Rep.* (2016) 6:35271. doi: 10.1038/srep35271

18. Lu Z, Zhang L, Wang N, Chen Y, Gao L, Wang Y, et al. Naturally occurring reassortant infectious bursal disease virus in northern China. *Virus Res.* (2015) 203:92–5. doi: 10.1016/j.virusres.2015.04.003
19. Jiang L, Qi X, Gao Y, Hua Y, Li K, Deng X, et al. Molecular characterization and phylogenetic analysis of the reticuloendotheliosis virus isolated from wild birds in Northeast China. *Vet Microbiol.* (2013) 166:68–75. doi: 10.1016/j.vetmic.2013.05.008
20. Li Y, Li C, Liu L, Wang H, Wang C, Tian G, et al. Characterization of an avian influenza virus of subtype H7N2 isolated from chickens in northern China. *Virus Genes.* (2006) 33:117–22. doi: 10.1007/s11262-005-0042-8
21. Zhu J, Hu S, Xu H, Liu J, Zhao Z, Wang X, et al. Characterization of virulent Newcastle disease viruses from vaccinated chicken flocks in Eastern China. *BMC Vet Res.* (2016) 12:113. doi: 10.1186/s12917-016-0732-6
22. Wang Q, Li X, Ji X, Wang J, Shen N, Gao Y, et al. A recombinant avian leukosis virus subgroup j for directly monitoring viral infection and the selection of neutralizing antibodies. *PLoS ONE.* (2014) 9:e115422. doi: 10.1371/journal.pone.0115422
23. Pan Q, Liu L, Wang Y, Zhang Y, Qi X, Liu C, et al. The first whole genome sequence and pathogenicity characterization of a fowl adenovirus 4 isolated from ducks associated with inclusion body hepatitis and hydropericardium syndrome. *Avian Pathol J WVPA.* (2017) 46:571–578. doi: 10.1080/03079457.2017.1311006
24. Maniatis T, Goodbourn S, Fischer JA. Regulation of inducible and tissue-specific gene expression. *Science.* (1987) 236:1237–45. doi: 10.1126/science.3296191
25. Ondek B, Shepard A, Herr W. Discrete elements within the SV40 enhancer region display different cell-specific enhancer activities. *EMBO J.* (1987) 6:1017–25. doi: 10.1002/j.1460-2075.1987.tb04854.x
26. Chakraborty T, Das GC. Proteins of the nuclear factor-1 family act as an activator of the late promoter in human polyomavirus BK *in vitro*. *J Gen Virol.* (1991) 72:1935–42. doi: 10.1099/0022-1317-72-8-1935
27. Prives C, Murakami Y, Kern FG, Folk W, Basilico C, Hurwitz J. DNA sequence requirements for replication of polyomavirus DNA *in vivo* and *in vitro*. *Mol Cell Biol.* (1987) 7:3694–704. doi: 10.1128/mcb.7.10.3694-3704.1987

Conflict of Interest: The authors declare that the research was conducted in the absence of any commercial or financial relationships that could be construed as a potential conflict of interest.

Publisher's Note: All claims expressed in this article are solely those of the authors and do not necessarily represent those of their affiliated organizations, or those of the publisher, the editors and the reviewers. Any product that may be evaluated in this article, or claim that may be made by its manufacturer, is not guaranteed or endorsed by the publisher.

frontiers in Microbiology

ORIGINAL RESEARCH
published: 14 March 2022
doi: 10.3389/fmicb.2022.800618

Chicken Peripheral Blood Mononuclear Cells Response to Avian Leukosis Virus Subgroup J Infection Assessed by Single-Cell RNA Sequencing

Xiaoyun Qu[1†], Xiaobo Li[2†], Ziwei Li[1], Ming Liao[1] and Manman Dai[1*]*

[1] National and Regional Joint Engineering Laboratory for Medicament of Zoonosis Prevention and Control, Guangdong Provincial Key Laboratory of Zoonosis Prevention and Control, College of Veterinary Medicine, South China Agricultural University, Guangzhou, China, [2] Core Facilities for Medical Science, Sun Yat-sen University, Guangzhou, China

OPEN ACCESS

Edited by:
Aijian Qin,
Yangzhou University, China

Reviewed by:
Jianqiang Ye,
Yangzhou University, China
Qing Pan,
Harbin Veterinary Research Institute (CAAS), China
Shuang Chang,
Shandong Agricultural University, China

***Correspondence:**
Ming Liao
mliao@scau.edu.cn
Manman Dai
daimanman1229@scau.edu.cn

[†] These authors have contributed equally to this work

Specialty section:
This article was submitted to Virology, a section of the journal Frontiers in Microbiology

Received: *23 October 2021*
Accepted: *21 February 2022*
Published: *14 March 2022*

Citation:
Qu X, Li X, Li Z, Liao M and Dai M (2022) Chicken Peripheral Blood Mononuclear Cells Response to Avian Leukosis Virus Subgroup J Infection Assessed by Single-Cell RNA Sequencing. Front. Microbiol. 13:800618. doi: 10.3389/fmicb.2022.800618

Chicken peripheral blood mononuclear cells (PBMCs) exhibit wide-ranging cell types, but current understanding of their subclasses, immune cell classification, and function is limited and incomplete. Here we performed single-cell RNA sequencing (scRNA-seq) of PBMCs in Avian leukosis virus subgroup J (ALV-J) infected and control chickens at 21 days post infection (DPI) to determine chicken PBMCs subsets and their specific molecular and cellular characteristics. Eight cell populations and their potential marker genes were identified in PBMCs. T cell populations had the strongest response to (ALV-J) infection, based on the detection of the largest number of differentially expressed genes (DEGs), and could be further grouped into four subsets: activated $CD4^+$ T cells, Th1-like cells, Th2-like cells, and cytotoxic $CD8^+$ T cells. Furthermore, pseudotime analysis results suggested that chicken $CD4^+$ T cells could potentially differentiate into Th1-like and Th2-like cells. Moreover, ALV-J infection activated $CD4^+$ T cell was probably inclined to differentiate into Th1-like cells. Compared to the control PBMCs, ALV-J infection also had an obvious impact on PBMCs composition. B cells showed inconspicuous response and their numbers decreased in PBMCs from ALV-J infected chicken. Proportions of cytotoxic Th1-like cells and $CD8^+$ T cells increased in the T cell population of PBMCs from ALV-J infected chicken, which were potentially key mitigating effectors against ALV-J infection. More importantly, our results provide a rich resource of gene expression profiles of chicken PBMCs subsets for a systems-level understanding of their function in homeostatic condition as well as in response to viral infection.

Keywords: scRNA-seq, chicken, PBMCs, ALV-J, T cell

INTRODUCTION

Adaptive immunity is known to play a vital protective role against avian viral infections. However, many interesting scientific questions about avian T cell or B cell immunity remain unresolved (Dai et al., 2019). For example, many important marker genes of the chicken immune cells are unknown, including effector or memory T cells and B cells. This greatly limit the immune cell

phenotyping and subsequent immune function and mechanistic studies. Specifically, effector $CD4^+$ T cells can differentiate into many T helper (Th) subsets, resulting in the production of different cytokines and effector functions. The Th1-Th2 paradigm is reported to exist in chickens (Degen et al., 2005). However, whether this paradigm holds true at the cellular and molecular levels and whether chicken Th cells can become terminally polarized to a Th1 or Th2 phenotype remain to be verified. Furthermore, it is also important and interesting to thoroughly characterize the molecular signatures of the $CD4^+$ T, $CD8^+$ T cells, and B cells during homeostasis and after pathogen exposure.

Chicken peripheral blood mononuclear cells (PBMCs), which contain various cells including T cells, B cells, natural killer (NK) cells, monocytes, and dendritic cells (DCs), are reported to execute important functions in eliminating avian viral infections (Bi et al., 2018; Dai et al., 2020a; Dai et al., 2021). However, such studies are usually based on bulk PBMCs measurements overlooking the complexity of diverse cell types. Recent advances in single-cell RNA-seq (scRNA-seq) allow the breakdown of complex tissues or host compartments into individual cell types for exploring their relevance in health and disease (Hen-Avivi and Avraham, 2018). scRNA-seq has already been used to investigate the immune response of human peripheral blood cells under infection of pathogenic microorganisms including salmonella, severe acute respiratory syndrome corona virus 2 (SARS-CoV-2), and influenza virus (Ben-Moshe et al., 2019; Wilk et al., 2020; Zhu et al., 2020). In chickens, the cell lineage characteristics in some tissues have been identified using scRNA-seq, such as the developing chicken limb (Feregrino et al., 2019), chicken skeletal muscle (Li et al., 2020), and embryonic chicken gonad (Estermann et al., 2020). However, no reported study used scRNA-seq to determine chicken immune cell subsets or lineages. Moreover, to our knowledge, scRNA-seq technology has not even been applied to study chicken PBMCs responses to any viral infection.

Avian leukosis virus subgroup J (ALV-J), an avian oncogenic retrovirus, causes enormous economic losses in the global poultry industry as there are currently no vaccines or drug treatments (Feng and Zhang, 2016). A potential vaccine for ALV-J has been reported to induce significantly increased $CD4^+$ and $CD8^+$ T cell proportion as well as IL-4 and IFN-γ levels in immunized chickens (Xu et al., 2015). Unfortunately, few studies explored the specific T cell phenotype or function against ALV. A full understanding of the ALV-specific cellular immune response in chickens is likely the premise for developing effective vaccines. In our previous study, we found that ALV-J viremia was eliminated by 21 days post infection (DPI) when a significantly up-regulated $CD8^+$T cell proportion and a very low serum antibody level in the peripheral blood were detected (Dai et al., 2020a). As described above, PBMCs contains many cell types besides $CD8^+$ T cells and B cells. Usually, these immune cells are able to form a complex network of communications that maintains an orchestrated and dynamic immune response to eliminate invading pathogens (Ben-Moshe et al., 2019). Hence, elucidating different chicken PBMCs subsets responding to viral infection is very important.

In the current study, we performed 10x scRNAseq on PBMCs from ALV-J infected and uninfected chickens at 21 DPI to comprehensively identify PBMCs subsets and characterize their specific cellular and molecular responses after viral infection. More importantly, we provide evidence to show that chicken Th cells can be terminally polarized to a Th1 or Th2 phenotype. Moreover, we have developed an extensive catalog of candidate marker genes and immune factors for identifying known and unknown chicken immune cells and their functions.

MATERIALS AND METHODS

Ethics Statement

All animal research projects were sanctioned by the South China Agriculture University Institutional Animal Care and Use Committee (identification code: 2019076, 10 June, 2019). All animal procedures were performed according to the regulations and guidelines established by this committee and international standards for animal welfare.

Sample Preparation

Peripheral blood mononuclear cells samples from ALV-J infected and control chickens at 21 DPI were prepared as previously described (Dai et al., 2020a). Briefly, 4-week-old specific-pathogen-free (SPF) chickens were inoculated intraperitoneally at a dose of 0.8 mL (10^4 $TCID_{50}$/0.1 mL) of ALV-J strain CHN06, and the virus was eliminated at 21 DPI when a significantly up-regulated $CD8^+$ T cell ratio in PBMCs was detected compared to the control group injected with 0.8 mL PBS alone (Dai et al., 2020a). To further explore the immune signature of various lymphocytes in PBMCs, we further investigated the single-cell survey of the chicken PBMCs response to ALV-J infection at 21 DPI.

Single Cell Suspension for 10x scRNAseq

Pooled PBMCs from blood of three ALV-J infected chickens or three control chickens at 21 DPI were, respectively, resuspended in PBS (calcium and magnesium-free; Gibco, Thermo Fisher Scientific, Waltham, MA, United States) with 0.4% bovine serum albumin (BSA; Solarbio, China), followed by passing through a 40 μm cell strainer (Biosharp, China). Cell concentration and viability were assessed using Trypan Blue and a Neubauer hemocytometer (Sigma-Aldrich, St. Louis, MO, United States). Cell viability in both samples was about 80%. Subsequently, the cell density was adjusted to 1×10^6 cells/mL. High quality single cell suspensions were subjected to encapsulation using a 10x Genomics v.3 kit (10x Genomics, United States).

Library Preparation for 10x scRNAseq

Single cell encapsulation, complementary DNA (cDNA) library synthesis, RNA-sequencing, and data analysis were completed by Gene *Denovo* (Guangzhou, China). The single-cell suspensions were bar-coded and reverse-transcribed into scRNA-seq libraries using the Chromium Single Cell 3′ Gel Bead-in Emulsion

(GEM) Library and Gel Bead Kit (10x Genomics) according to the manufacturer's protocol. Briefly, single cells of the ALV-J infected and control PBMCs at 21 DPI were separately barcode-labeled and mixed with reverse transcriptase into GEMs; the cDNA library was then using PCR with the sequencing primers R1 and R2, and subsequently ligated to Illumina sequencing adapters with P5 and P7. Finally, the cDNA libraries were sequenced on the Illumina 10x Genomics Chromium platform (Illumina Novaseq 6000). An average of 18,895 reads per cell in the ALV-J infected PBMCs and 30,540 mean reads per cell in the control PBMCs were obtained, respectively.

Single-Cell RNA Sequencing Data Processing and Analysis

Data Processing

Cell Ranger[1] (v3.1.0) uses an aligner called STAR,[2] which performs splicing-aware alignment of reads to the chicken genome of GRCg6a (Zerbino et al., 2018). Only reads that are confidently mapped to the transcriptome are used for Unique Molecular Identifier (UMI) counting. Cells with unusually high numbers of UMIs ($\geq$8,000) or mitochondrial gene percentage ($\geq$10%) were filtered out. Cells with $<$500 or $>$4,000 gene counts were also excluded. Using the R package Seurat v.2.3.2 (Butler et al., 2018), UMI counts were then Log-normalized and any variation due to the library size or mitochondrial UMI count proportion was then regressed via a variance correction using the function ScaleData.

Dimensionality Reduction and Visualization

Top 50 significant principal components (PCs) were determined for downstream clustering and dimensional reduction following the jackStraw procedure (Butler et al., 2018). Then, Seurat was used to implement the graph-based clustering approach (resolution setting as 0.6) (Levine et al., 2015; Xu and Su, 2015). T-distributed Stochastic Neighbor Embedding (t-SNE) (Linderman et al., 2019) or Uniform Manifold Approximation and Projection (UMAP) (Becht et al., 2019) in Seurat were used to visualize and explore these datasets.

Differentially Expressed Gene (Up-Regulation) Analysis per Cluster

We used the Wilcoxon rank sum test (Camp et al., 2017) to identify differential expression for a single cluster, compared to all other cells. We identified up-regulated DEGs according to the following criteria: (1) P value $\leq$ 0.01; (2) logFC $\geq$ 0.360674 (logFC means log fold-change of the average expression between the two compared groups); (3) The proportion of cells in which the gene is detected in a specific cluster $>$25%. Gene ontology (GO) enrichment analysis selects all GO terms that are significantly enriched in DEGs compared to the genome background; furthermore, the DEGs are filtered to correspond to biological functions. All DEGs were mapped to GO terms in the Gene Ontology database (The Gene Ontology Consortium [GOC], 2019), gene numbers were calculated for every term, and significantly enriched GO terms in DEGs compared to the genome background were identified by hypergeometric testing to identify the main features of each cluster. Finally, Pearson's correlation analysis was performed to investigate correlations between different clusters based on the levels of gene expression.

Marker Gene Analysis

We further selected the top five expressed genes in each cluster as marker genes according to the result of differentially expressed genes (parameters used: logFC $>$ 0.25; min_pct $>$ 0.25; p value $<$ 0.01). The expression distribution of each marker gene was then demonstrated using bubble diagrams. We also checked the expression of classical marker genes of chicken immune cells, e.g., CD4 T cell (*CD3D*, *IL7R*, and *CD4*), B cell (BCL11A, Bu-1, and BLB2), CD8 T cell (*CD3D*, *CD8A*, and *GNLY*), Dendritic Cell (DC, *CD80*, *CD86*, and *BLB2*), and Natural killer cell (NK, *CD8A*, *CD5*, and *CD44*) (see Additional file 2 in **Supplementary Material**, **Figures 2**, **4**) (Stewart et al., 2013).

Pseudo Temporal Ordering of Cells

Single cell trajectory was analyzed using a matrix of cells and gene expressions in Monocle 2 (v.2.6.4) (Trapnell et al., 2014). Monocle reduces the space in which cells are embedded to two dimensions and orders the cells (parameters used: sigma = 0.001, lambda = NULL, param.gamma = 10, tol = 0.001). Once the cells were ordered, the trajectory (with a tree-like structure, including tips and branches) could be visualized in the reduced dimensional space.

Differentially Expressed Gene Analysis in Cell Populations of the Peripheral Blood Mononuclear Cells From the Avian Leukosis Virus Subgroup J Infected and Control Chickens

To explore the response of each cluster in PBMCs, we further analyzed the DEGs in cell populations of PBMCs from the infected and control chickens using Seurat's R package. A hurdle model in MAST (Model-based Analysis of Single-cell Transcriptomics) (Finak et al., 2015) was used to identify DEG group in one cluster. DEGs between the ALV-J infected and control samples were identified by the following criteria: (1) $|\log2FC| \geq 1$; (2) P value $\leq$ 0.01; and (3) proportion of cells in which the gene was detected in a specific cluster $>$25%. Identified DEGs were subsequently subjected to GO enrichment analysis as described above.

Protein-Protein Interaction Network Analysis

The interaction network of the candidate DEGs was constructed using String v.10.0 and Cytoscape (v.3.3.0) software. Specifically, the protein-protein interaction network was identified using

[1]https://support.10xgenomics.com/single-cell-gene-expression/software/overview/welcome

[2]https://github.com/alexdobin/STAR

String (Szklarczyk et al., 2015), which determined genes as nodes and interactions as lines in a network. The final network file was visualized using Cytoscape software (Shannon et al., 2003) to present a core and hub gene biological interaction.

RESULTS

Single-Cell Transcriptomics Identified Eight Distinct Cell Populations in the Peripheral Blood Mononuclear Cells Collected From Avian Leukosis Virus Subgroup J-Infected and Control Chickens at 21 Days Post Infection

We used the 10x Genomics platforms to perform 3′ scRNA-seq on PBMCs collected from ALV-J infected and PBS-treated control chickens at 21 DPI, respectively. Details on the statistics of scRNA-seq are summarized in Additional file 1 in **Supplementary Material**. A total of 13, 766 cells in the PBMCs from ALV-J infected chicken and 9,786 cells in the control PBMCs were profiled, and eight distinct clusters were obtained and visualized using UMAP (**Figure 1**) or t-SNE (**Figure 2A**). Clusters 6, 7, and 8 occupied a very small proportion in chicken PBMCs (**Figure 1C**), and the proportion of clusters 0, 1, and 3 were increased in the PBMCs from ALV-J infected chicken when compared to the control. Conversely, the proportion of clusters 2, 6, 7, and 8 were distinctly reduced in the PBMCs from ALV-J infected chicken at 21 DPI (**Figures 1A–C**).

For further analyzing the immune signatures of each cluster in chicken PBMCs, we identified the up-regulated DEGs in a single cluster compared to all other cells, and analyzed the DEGs enriched in the GO terms "immune system process," "response to stimulus," and "defense response to virus." The results showed that most immune-related DEGs (DEGs enriched in the above three Go terms) were mainly detected in clusters 6, 7, and 8 (**Figure 2B**, Additional files 2, 3 in **Supplementary Material**), which implied that, in PBMCs, these clusters are the main effectors responded to pathogenic stimuli. Additionally, the expression levels and the proportion of cells expressing the top five genes in each cluster are shown in a dot plot (**Figure 2C**, Additional files 4, 5 in **Supplementary Material**); these need to be confirmed in future research and are proposed to be used as marker genes for each cluster of chicken PBMCs.

Based on the expression of classical CD3 marker, we could define clusters 6 and 7 as T cells (**Figure 2D**). Cluster 6 mainly included $CD4^+$ T cells ($CD3^+CD4^+IL7R^+CD28^+$) (**Figures 2C,D**). The marker gene, *KK34* in Cluster 7 is reported to encode an IL-5-like transcript that was specifically expressed by avian γδT cells in the peripheral blood, which may mediate T helper 2 (Th2)-cytokine-dependent allergy (Koskela et al., 2004). Meanwhile, other studies reported that dopamine receptor (*DRD4*) is involved in Th2 cell differentiation and inflammation (Wang W. et al., 2019). Therefore, we defined cluster 7 as Th2-like cell ($CD3^+KK34^+DRD4^+$; **Figures 2C,D**). In addition, we found that a few cytotoxic $CD8^+$ T cells ($CD3^+CD8^+GNLY^+$) mixed in clusters 6 and 7 (**Figure 2D**). Therefore, we planned to subdivide clusters 6 and 7 for a more detailed display of data in the following analysis. Additionally, cluster 8 should be B cells according to the expression of the known marker genes, BCL11A, Bu-1 (ENSGALG00000015461), and Class II (also named as BLB2) (**Figures 2C,D**). Interestingly, the top five genes in cluster 4 were mainly interferon stimulating genes (ISGs), including *RSAD2*, *TRIM25*, *OASL*, and *IFIT5*, which implied that cluster 4 also contained a type of important antiviral immune cell (**Figure 2C**). Therefore, we defined cluster 4 as ISG expressing cells in PBMCs, which needs to be further verified in future studies. Unfortunately, we were unable to define clusters 0, 1, 2, 3, and 5 based on the limited known chicken cell-type markers and the top five genes expressed by cells in these clusters.

Most Differentially Expressed Genes Were Detected in the T Cell Population (Clusters 6 and 7) in Response to Avian Leukosis Virus Subgroup J Infection at 21 Days Post Infection

We calculated the DEGs between cell populations of PBMCs from the ALV-J infected and control chickens at 21 DPI using Seurat. It was found that the total number of DEGs and the DEGs enriched in the GO terms "response to stimulus" and "cell proliferation" were largely detected in clusters 6 and 7 (**Figure 3A**, Additional file 6 in **Supplementary Material**), indicating that cells in clusters 6 and 7 might have played an important role during the antiviral response to ALV-J in the infected chicken. We further discovered that the decreased proportion of clusters 6 and 7 in PBMCs from ALV-J infected chicken might be a result of the up-regulated pro-apoptotic factors, *ITPR2* (van Es et al., 2007) and *JARID2* (Gennart et al., 2015) (**Figures 1C**, **3B**, Additional file 6 in **Supplementary Material**). Next, an immune related DEG analysis was performed after sub clustering of clusters 6 and 7 in the study outlined below.

Meanwhile, some DEGs in other clusters were analyzed. We found that an important immune gene, interferon regulator 7 (*IRF7*), revealed up-regulation in clusters 0, 1, 2, and 3 in response to ALV-J infection at 21 DPI (**Figure 3B**, Additional file 6 in **Supplementary Material**). We also found that the anti-apoptotic gene *BCL2L10* (Zang et al., 2015) was up-regulated in clusters 0, 1, 3, 4, and 5 of PBMCs from ALV-J infected chicken (**Figure 3B**, Additional file 6 in **Supplementary Material**). Besides, Pearson's correlation analysis indicated that clusters 0, 1, 2, 3, 4, and 5 were strongly correlated between each other, but displayed very low correlation with clusters 6, 7, and 8 (corresponding to T cells and B cells; **Figure 3C**). And at 21 DPI, the late infection stage, we detected most DEGs in the T cell population (clusters 6 and 7) (**Figure 3A**, Additional file 6 in **Supplementary Material**). So, the function of cells in clusters 0, 1, 2, 3, 4, and 5 may be worked at other infection stage such as the early infection stage.

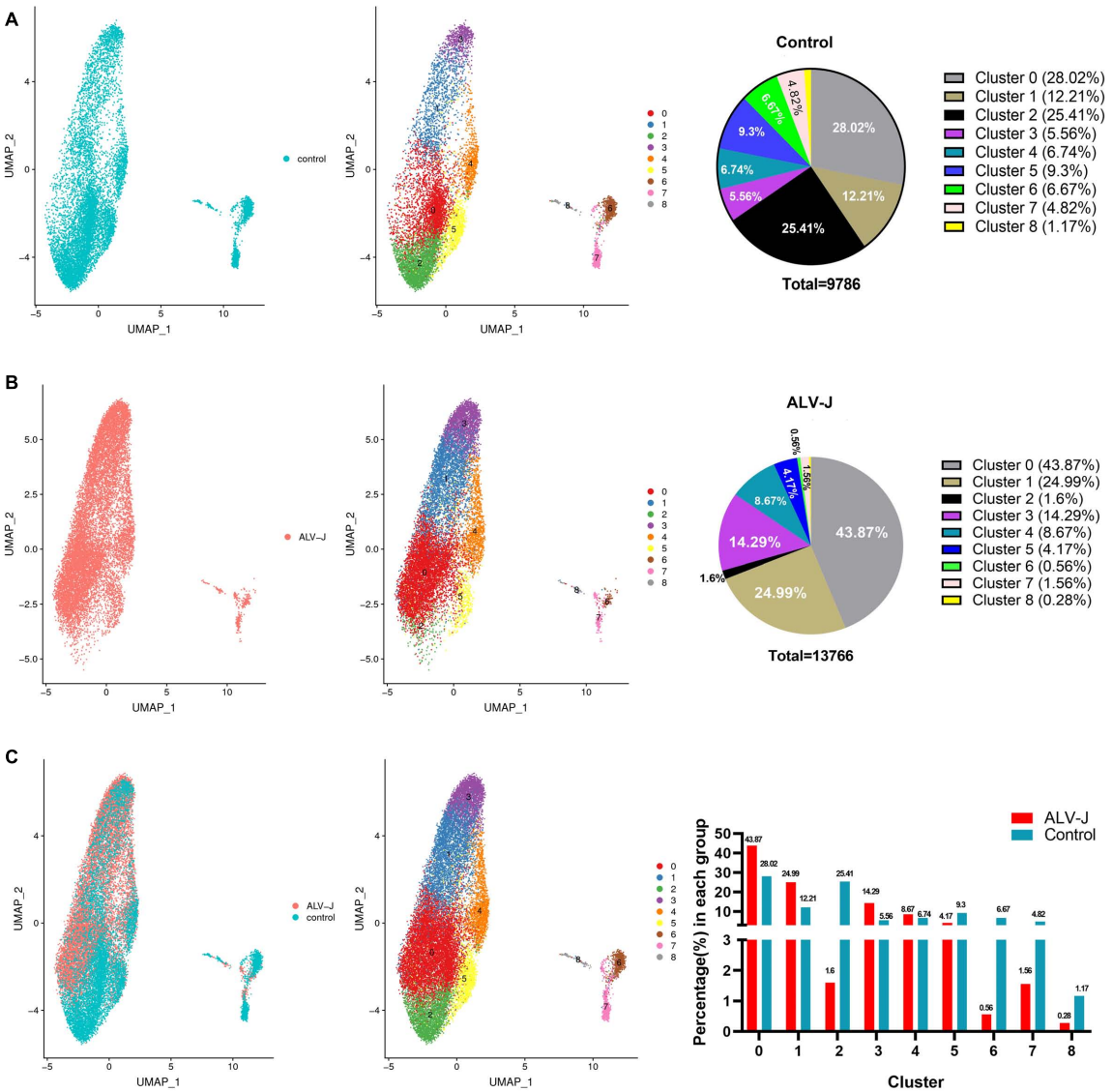

FIGURE 1 | Single-cell profiling of cell populations in chicken peripheral blood mononuclear cells (PBMCs) collected from avian leukosis virus subgroup-J (ALV-J)-infected and control chickens at 21 days post infection (DPI). **(A)** Uniform Manifold Approximation and Projection (UMAP) display of all cell populations and their proportions in the control PBMCs. **(B)** UMAP display of all cell populations and their proportions in PBMCs from ALV-J infected chicken. **(C)** Cell distribution and proportion of each cluster in PBMCs from ALV-J infected and control chickens.

T Cell Populations of Clusters 6 and 7 Could Be Further Divided Into Four Distinct Cell Populations in the Peripheral Blood Mononuclear Cells

The above-mentioned T cell populations of clusters 6 and 7, both in PBMCs from the ALV-J infected or control chicken, were further divided into four distinct clusters (named as clusters A0–A3) and visualized using UMAP (**Figures 4A–C**). Compared to those in the control PBMCs, the proportions of clusters A0 and A1 in the PBMCs from ALV-J infected chicken decreased. Conversely, the proportions of clusters A2 and A3 significantly increased in PBMCs from ALV-J infected chicken (**Figure 4C**). Next, the top five genes expressed in clusters A0–A3 were picked as potential marker genes and they are shown in a dot plot (**Figure 4D**, Additional files 7, 8 in **Supplementary Material**). Based on the classical marker genes and our above analysis, we considered cluster A0 as $CD4^+$ T cells ($CD3^+CD4^+IL7R^+CD28^+$), cluster A3 as cytotoxic $CD8^+$ T cells ($CD3^+CD8^+IL2RB^+GNLY^+$), and cluster A1 as Th2 like cells ($CD3^+KK34^+DRD4^+$) (**Figures 4D,E**). Besides, cluster A0 contained some $CD4^+$ $CD8^+$T cells based on the low expression level of CD8A (**Figure 4E**), which could not be separated with $CD4^+$ T cells.

Although we were unable to define cluster A2 based on their top five genes and a few known markers of

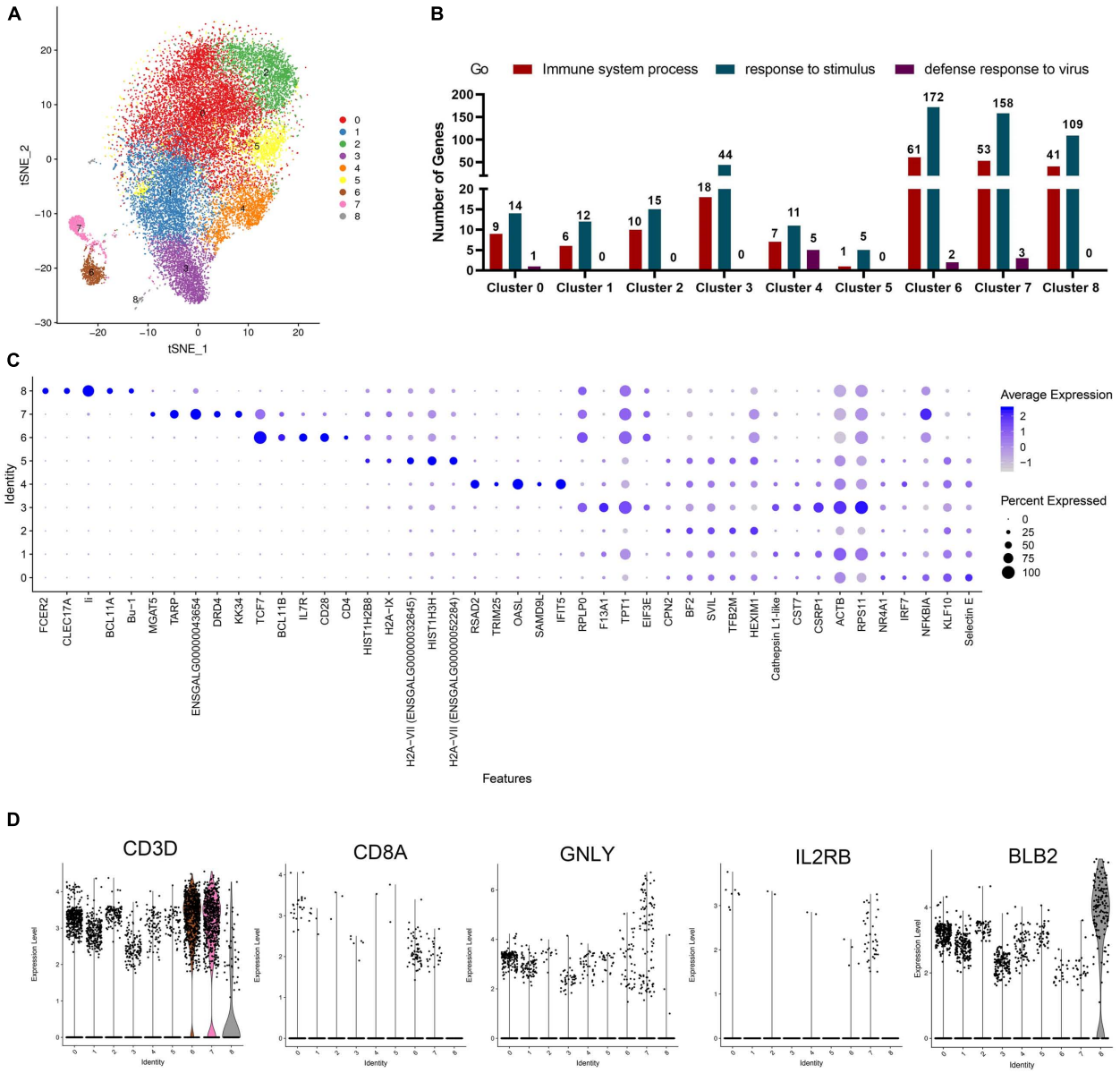

FIGURE 2 | Analysis of cell types of each cluster in chicken PBMCs. **(A)** t-Distributed Stochastic Neighbor Embedding (t-SNE) projection representing the eight clusters of cells identified in the chicken PBMCs (unified set of control and ALV-J infection samples). **(B)** The statistics of genes involved in the GO terms "immune system process," "response to stimulus," and "defense response to virus," as analyzed in each cluster. **(C)** Top five DEGs (x-axis) identified in each cluster (y-axis). Dot size represents the proportion of cells in the cluster that express the gene; intensity indicates the mean expression level (*Z*-score) in the cells, relative to those from other clusters. **(D)** Expression levels of the characteristic marker genes (*CD3D*, *CD8A*, *GNLY*, *IL2RB*, and *BLB2*) in PBMCs clusters.

various chicken cell-types, using pseudotime analysis, we believe that clusters A0 (activated $CD4^+$ T cells, namely Th0 cells), A1 (Th2-like cells), and A2, in both ALV-J infected and control samples, demonstrated a potential differentiation correlation (**Figure 5A**). Cluster A0 (Th0 cells) is mainly located at the early stage of the pseudo-time trajectories, whereas clusters A2 and A1 (Th2-like cells) are mainly located at the late stage (**Figures 5A,B**). These results suggest that clusters A2 and A1 are likely differentiated from A0 and imply that cluster A2 might represent Th1-like cells. Interestingly, cells in the control PBMCs are mainly distributed in the A0 (Th0) and A1 (Th2-like) cell populations (**Figures 5C–E**). Conversely, ALV-J-infected PBMCs are highly enriched in the terminally differentiated A2 cell populations (Th1-like; **Figures 5C–E**), which indicates that ALV-J infection induced $CD4^+$ T cell activation and differentiation into the Th1 phenotype. Finally, the branch-dependent differential gene hierarchy clustering heat map is

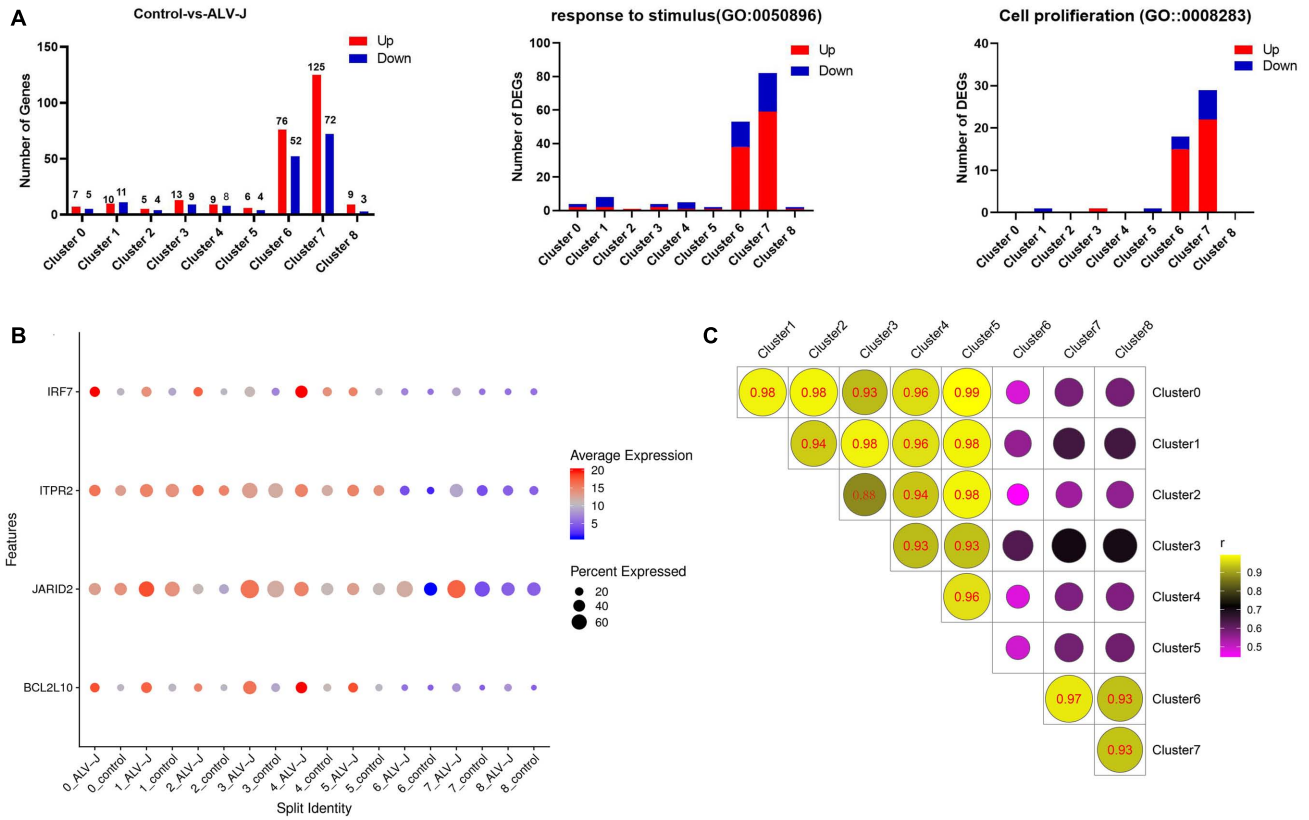

FIGURE 3 | Differentially expressed gene (DEG) analysis in PBMCs from ALV-J infected and control chickens within cell populations**. (A)** Bar graphs showing all up-regulated (red) and down-regulated (blue) DEGs, and the number of DEGs involved in the GO terms "response to stimulus" and "cell proliferation" in PBMCs from ALV-J infected chicken compared to control PBMCs within each cluster. **(B)** Dot plot representing selected DEGs (*IRF7*, *ITPR2*, *JARID2*, and *BCL2L10*) expressed in eight clusters within which cells from the ALV-J infected sample were compared with the control sample. The intensity represents the expression level, while dot size represents the proportion of cells expressing each gene. **(C)** Pearson's Correlation analysis of different cell populations based on gene expression levels.

shown in Additional file 9 in **Supplementary Material**; it contains the top 10 branching DEGs displayed in **Figure 5F**. Of note, *BRT-1*, *CSTA*, *ENSGALG00000046729*, *HPSE*, *IFI6*, *ITGB3*, and *TUBB1* may be associated with Th1 cell differentiation (**Figures 5D–F**).

Cluster A2 (Th1-Like) Is the Vital Cell Type in Response to Avian Leukosis Virus Subgroup J Infection

Our above results showed that cells in clusters 6 and 7 might have played a potentially important role in the antiviral response during ALV-J infection based on their largely immune-related DEG expression (**Figure 3A**, Additional file 6 in **Supplementary Material**). Meanwhile, the T cell populations in clusters 6 and 7 could be further grouped into four distinct sub clusters (**Figure 4**). To further investigate each T cell population, we first calculated the DEGs between corresponding T cell population in the PBMCs from ALV-J infected and control chickens at 21 DPI using Seurat. Strikingly, the highest numbers of total DEGs and the DEGs enriched in the GO terms "response to stimulus" and "cell proliferation" were predominant in cluster A2 (Th1-like T cells; **Figure 6A**, Additional file 10 in **Supplementary Material**), suggesting that cluster A2 represents likely the most vital effectors among PBMCs of the ALV-J infected host.

Next, the specific DEGs of the four sub clusters enrichment in "response to stimulus" (GO:0050896) were exhibited using a volcano plot (Additional file 11 in **Supplementary Material**). Moreover, a total of 33 important immune-related genes were screened from clusters A0 to A3 and their expression levels were quantified in a heat map and a dot plot (**Figures 6B,C**, Additional file 10 in **Supplementary Material**). We also observed that most of these immune-related genes were highly expressed in cluster A2. It is worth noting that *BCL2L10*, *H-RAS*, *IRF7*, *NOX1*, *SEC14L1*, *IL1RAP*, *FLNB*, *CDK17*, *ZEB2*, *PIK3R6*, *CREG1*, *CTSB*, and *ITGA2* were up-regulated in cluster A2, rather than in the other three clusters (**Figure 6C**, Additional file 10 in **Supplementary Material**). Moreover, it is reported that H-RAS act as critical controllers of Th1 responses via transmitting TCR signals for the Th1 priming of $CD4^+$ T cells (Iborra et al., 2011), which further supports the results we described above that cluster A2 may represent Th1 cells. Besides, we found that *PDE3B*, *RARA*, and *CD164* were only up-regulated in cluster A1, while *IRAK2*, *CD82*, *IRF2*, *MAPK6*, *TGFBR2*,

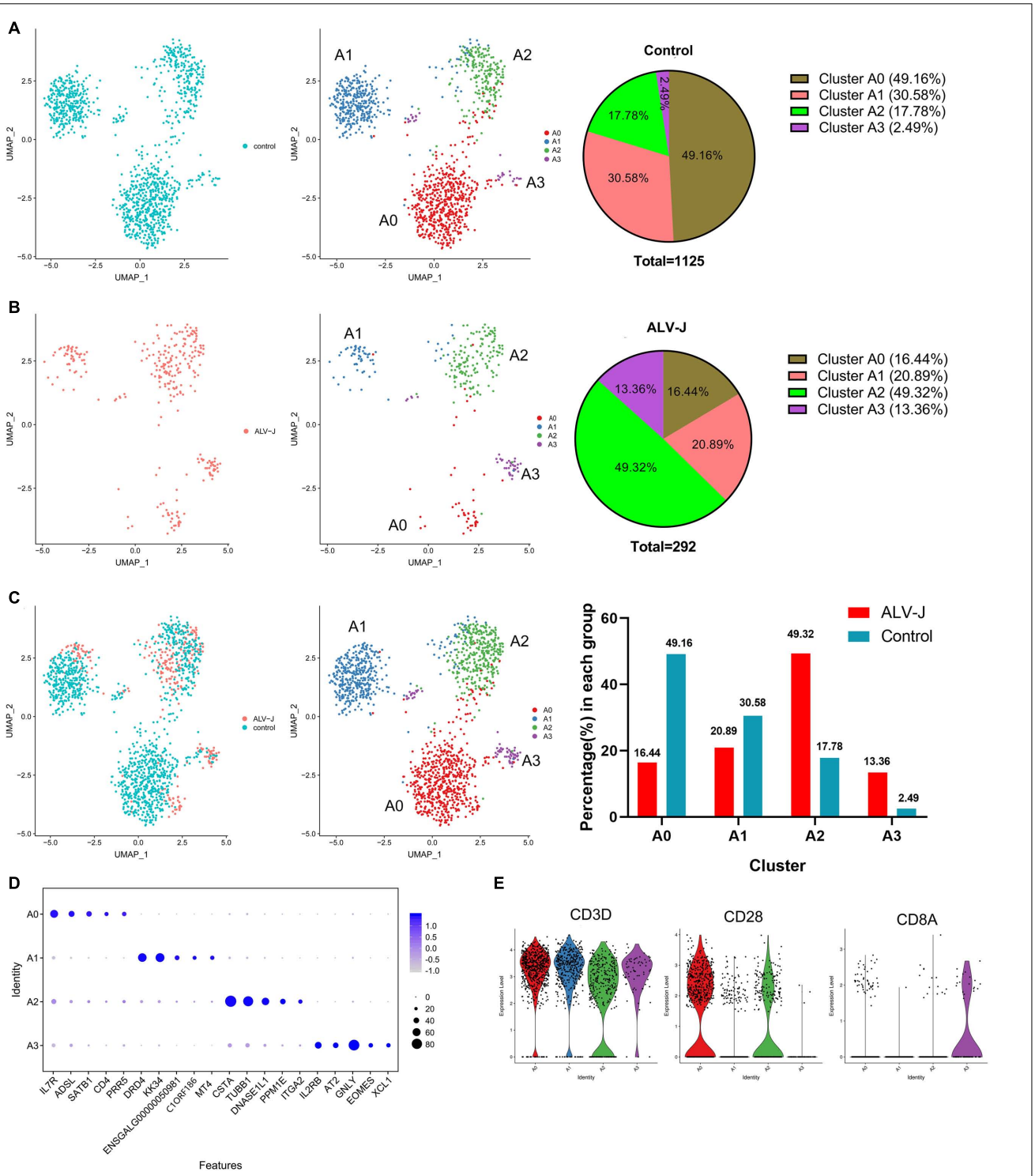

FIGURE 4 | T cell population of clusters 6 and 7 were further divided into four distinct cell populations**. (A)** UMAP display of the cell populations and their proportions of the T cell sub clustering (clusters 6 and 7) in the control PBMCs. **(B)** UMAP display of the cell populations and their proportions of the T cell sub clustering (clusters 6 and 7) in PBMCs from ALV-J infected chicken. **(C)** The regrouped T cell distribution and proportion of each cluster in PBMCs from ALV-J infected and control chickens. **(D)** Top five DEGs (x-axis) identified in clusters A0–A3 (y-axis). **(E)** Expression levels of characteristic marker genes (*CD3D*, *CD28*, and *CD8A*) in clusters A0–A3.

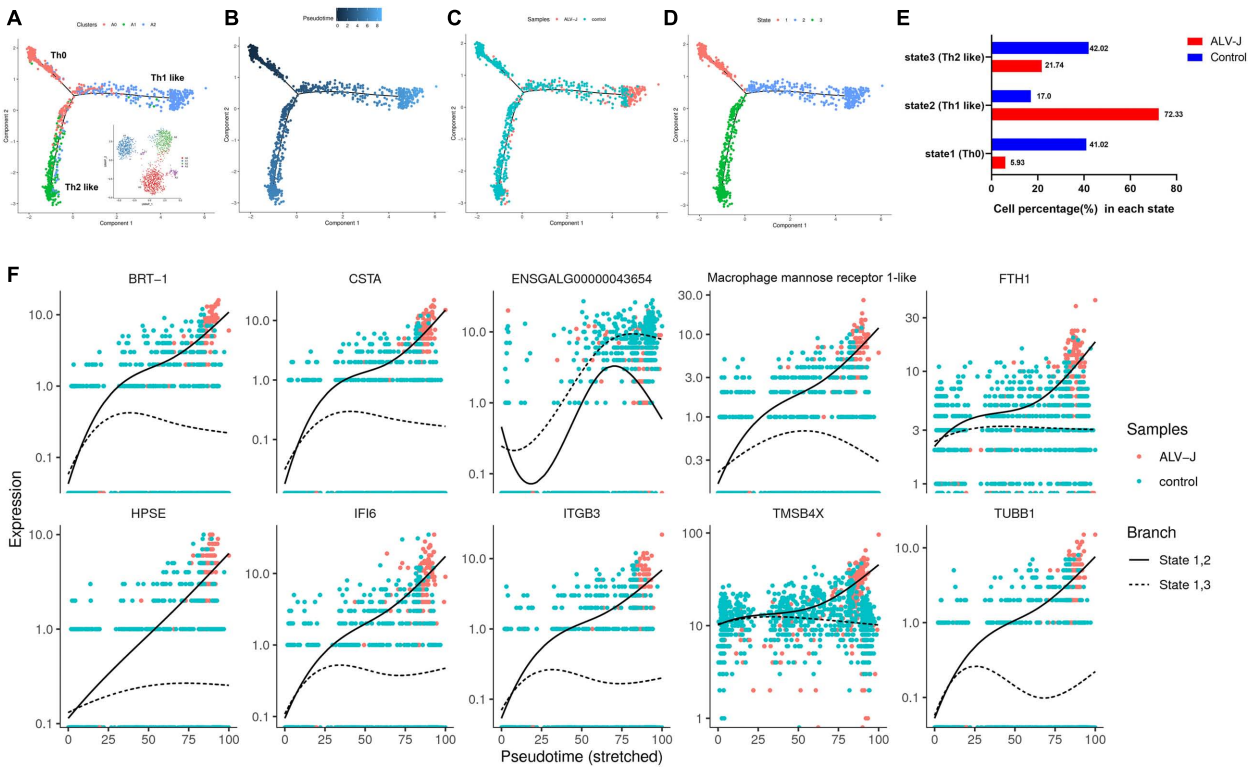

FIGURE 5 | Pseudotime analysis of clusters A0, A1, and A2**. (A)** Mapping of clusters A0 (Th0), A1 (Th2-like), and A2 (Thl-like) to the pseudotime trajectory. **(B)** Pseudotime trajectory calculated from all cells of clusters A0–A2 in the control and ALV-J infected samples. Darker colored dots represent a shorter pseudotime and earlier differentiation period. **(C)** Mapping of cells in control and ALV-J infected samples to the pseudotime trajectory. **(D)** The cell states of pseudotime trajectory partitioned from all cells of clusters A0–A2 in the control and ALV-J infected samples. **(E)** Cell proportion of each state between the ALV-J infected and control samples. **(F)** Dynamics of the top 10 branching DEGs. Full line: state 1, 2; imaginary line: state 1, 3.

and *CTLA4* were only up-regulated in cluster A0. Furthermore, the apoptosis-associated gene, *CASP8AP2* (Wang et al., 2018), exhibited increased expression in clusters A0 and A1, which could potentially explain their proportional decrease in PBMCs after infection. Taken together, these up-regulated genes could potentially serve as marker genes for chicken Th1-like cells (cluster A2), Th2-like cells (cluster A1), and Th0 cells (cluster A0), respectively.

Finally, we conducted an interaction network analysis of the 33 candidate DEGs based on the STRING database (**Figure 7**). The results implied that the 13 DEGs marked in red are likely the more important hub genes. Specifically, four hub genes including *ITGA2*, *IL1RAP*, *NOX1*, and *CDK17* were up-regulated in cluster A2 (Th1-like cells, **Figure 6C**, Additional file 10 in **Supplementary Material**). Three hub genes including *IRAK2*, *CTLA4*, and *TGFBR2* were up-regulated in cluster A0 (Th0 cells, **Figure 6C**, Additional file 10 in **Supplementary Material**). Two hub genes including *MYO9B* and *ZNFX1* were up-regulated in Th1-like cells and cluster A1 (Th2-like cells, **Figure 6C**, Additional file 10 in **Supplementary Material**). Besides, identified hub gene *PDE3B* was up-regulated in Th2 like cell; *ITGAV* was up-regulated in Th1-like, Th2-like, and cytotoxic $CD8^+$ T cell populations; *CASP8AP2* was up-regulated in Th0 and Th2-like cells; *JARID2* was up-regulated in Th0, Th1-like, and cytotoxic $CD8^+$ T cell populations (**Figure 6C**, Additional file 10 in **Supplementary Material**).

DISCUSSION

Adaptive immunity, including T cell and B cell response, is the foundation upon which vaccines are developed. Despite decades of research, we still have limited insights into the ability of the avian immune response to pathogens at both cellular and molecular levels. For example, antibody level and T cell proportional change in the peripheral blood are usually used to evaluate a virus-induce immune response (Feng and Zhang, 2016; Ruan et al., 2020; Dai et al., 2020a, 2021). Flowcytometry-based phenotyping and functional evaluation of chicken T cells are limited by reagents and methods availability (Dai et al., 2019). Fortunately, advances in scRNA-seq allow us to at least partially overcome these defects to gain insight into the molecular signature of avian immune responses to viral infections. Previously, we found that ALV-J viremia was eliminated by 21 DPI when an up-regulated $CD8^+$ T cell proportion and low antibody levels were detected (Dai et al., 2020a). In the current study, we used 10x scRNAseq on PBMCs in ALV-J infected chicken and uninfected chicken (control) at

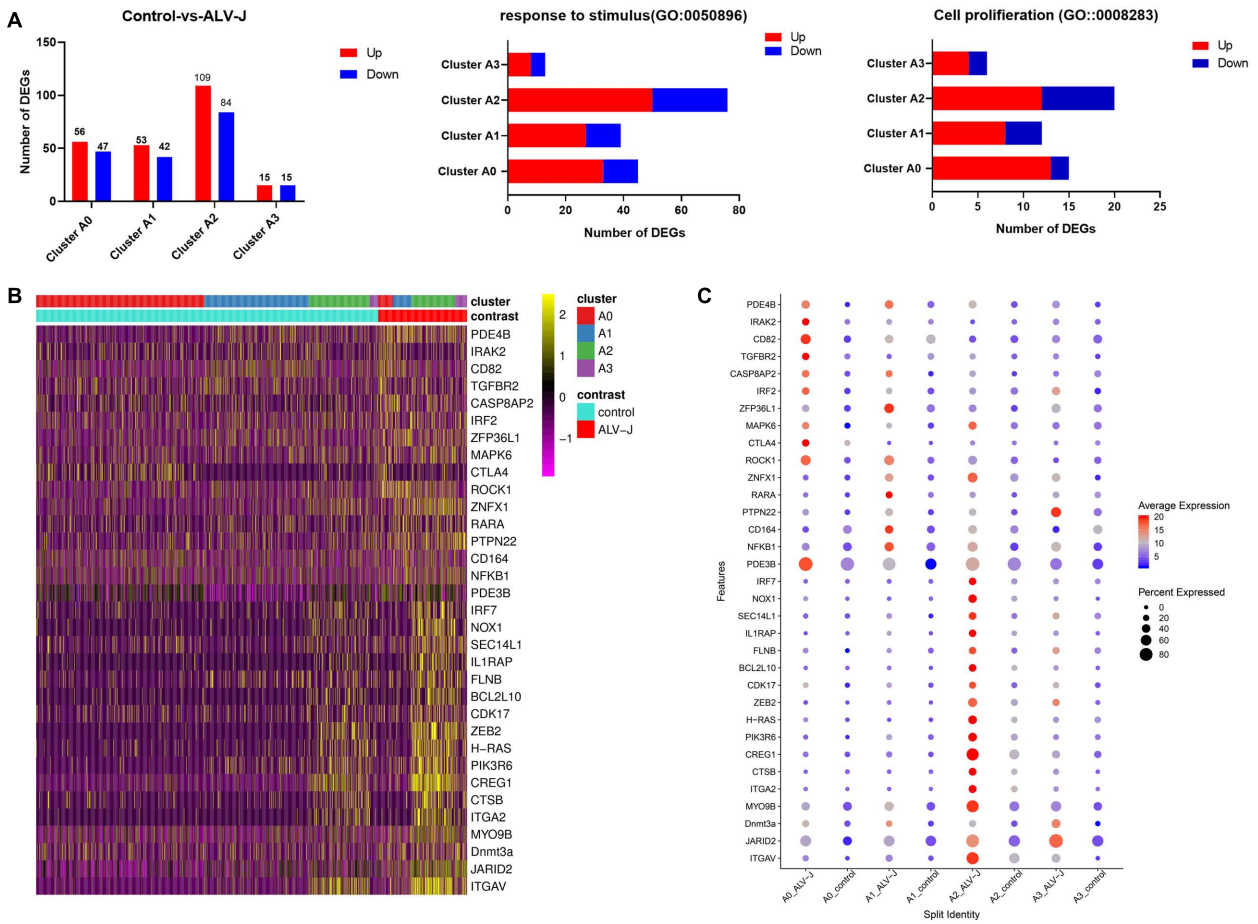

FIGURE 6 | Landscape of immune-related gene expression in clusters A0–A3 of the ALV-J infected and control samples. **(A)** Histogram shows all the up-regulated (red) and down-regulated (green) DEGs, and the number of DEGs involved in GO terms "response to stimulus" and "cell proliferation" in cells of clusters A0–A3 from ALV-J infected chicken compared to those from the control. **(B)** Heatmap shows the normalized expression (*Z*-score) of all immune-related DEGs in cells of clusters A0–A3 from the ALV-J infected sample compared with the control one. **(C)** Dot plot representing DEGs expressed in clusters A0–A3 from the ALV-J infected sample is compared with those from the control sample. The intensity represents the expression level, while the size of the dots represents the proportion of cells expressing each gene.

21 DPI to characterize two major aspects of immune response against the invading pathogen: the immune cell composition and their responses to infection.

In this study, eight distinct cell populations in chicken PBMCs were identified following analysis of scRNA-seq data. Strikingly, we found that known T cell populations (clusters 6 and 7) and B cell populations (cluster 8) occupied a very small proportion in chicken PBMCs. Of note, ALV-J infection had an obvious impact on the cell composition of PBMCs. Specifically, the total number and proportion of T cells, B cells, and the cells in cluster 2 were distinctly reduced in PBMCs from ALV-J infected chicken compared to those in the control PBMCs. Furthermore, up-regulated *ITPR2* (van Es et al., 2007) and *JARID2* (Gennart et al., 2015) expression might be involved in T cell apoptosis in PBMCs from ALV-J infected chicken (**Figures 1C**, **3B**, Additional file 6 in **Supplementary Material**). On the other hand, the proportion of clusters 0, 1, and 3 were obviously increased in PBMCs from ALV-J infected chicken compared to that of the control PBMCs, which could be associated with the up-regulation of the anti-apoptotic gene, *BCL2L10* (Zang et al., 2015). In future, experiment *in vitro* about ALV-J infection of cells of each cluster are needed in order to further confirm our above observation for exclusion scRNA-seq technical or sampling effects.

Additionally, Pearson's correlation analysis showed that clusters 0, 1, 2, 3, 4, and 5 exhibited strong correlation, but much less so with the T cell and B cell populations (clusters 6, 7, and 8; **Figure 3C**). Unfortunately, clusters 0, 1, 2, 3, 4, and 5 were unable to be defined based on the limited known chicken cell-type markers and the five most highly expressed genes in these clusters. Interestingly, the top expressed genes in cluster 4 were mainly chicken ISGs including *RSAD2*, *TRIM25*, *OASL*, and *IFIT5* (Dai et al., 2020b), which implied that cluster 4 contained important antiviral immune cells (**Figure 2C**). Moreover, *IRF7* which is involved in IFN-β signaling and ISGs inducer (Cheng et al., 2019; Dai et al., 2020b), revealed up-regulation in clusters 0, 1, 2, and 3 response to ALV-J infection at 21 DPI (**Figure 3B**,

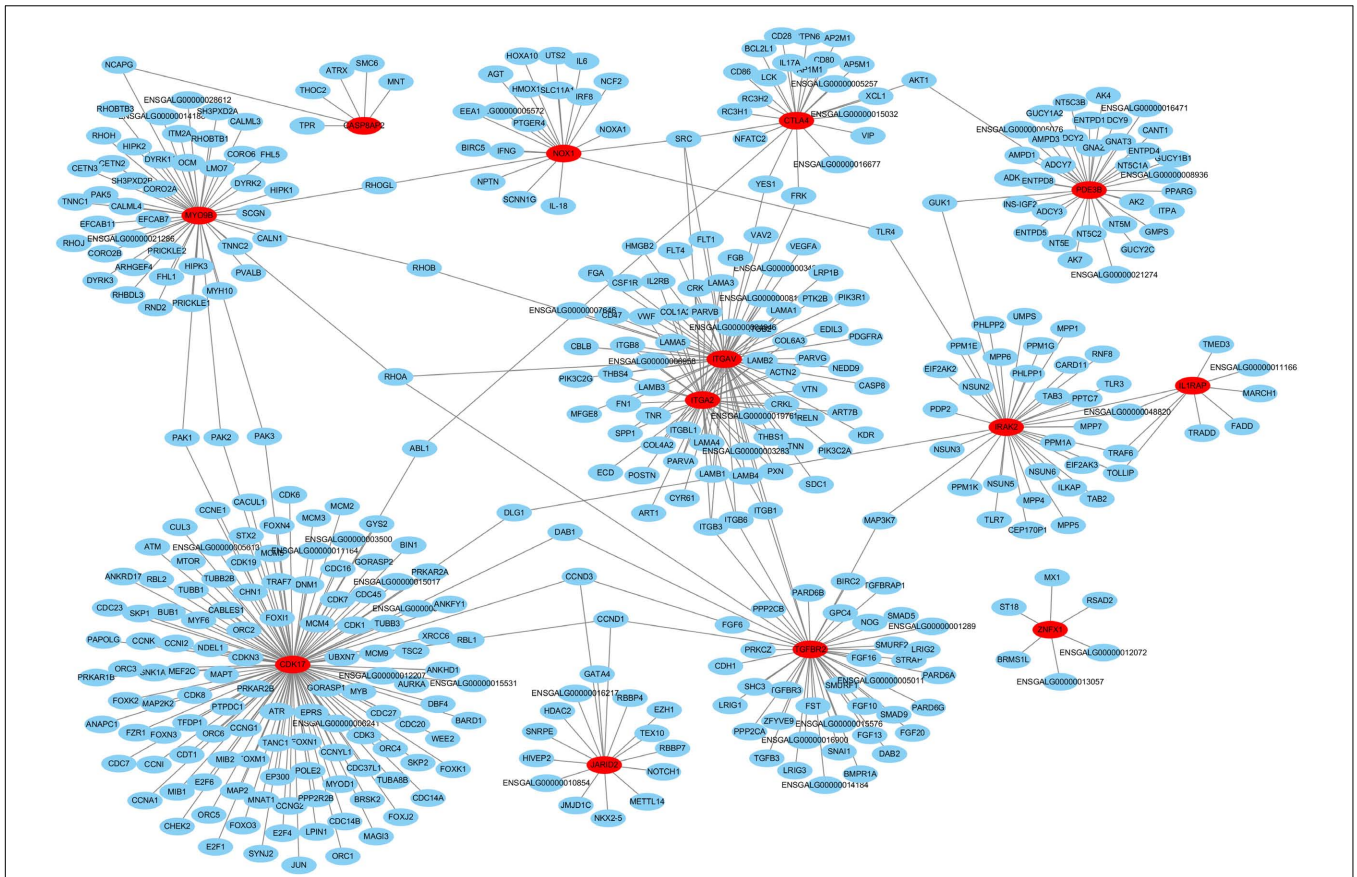

FIGURE 7 | The interaction network analysis of the 33 candidate DEGs based on the STRING database. In this network, red nodes represent hub genes, and lines represent potential associations.

Additional file 6 in **Supplementary Material**). According to these results, the function of clusters 0, 1, 2, 3, 4, and 5 may be related to innate immune response at the early infection stage. The specific cell types and function of these clusters need to be further confirmed in future studies. Besides, the inability to detect the DC or NK cell population and so on may be largely due to limited cell numbers for scRNA-seq in this study. In future, more samples and cell numbers were necessary for identifying more cell types that occupied very small proportions in PBMCs.

Most DEGs were detected in the T cell population (clusters 6 and 7) response to ALV-J infection at 21 DPI (**Figure 3A**, Additional file 6 in **Supplementary Material**). Furthermore, the T cell population could be further divided into four distinct cell populations including $CD4^+$ T cells (Cluster A0), Th2-like cells (Cluster A1), Th1-like cells (Cluster A2), and cytotoxic $CD8^+$ T cells (Cluster A3), based on their marker genes expression and pseudotime analysis results. Here, pseudotime analysis implied that $CD4^+$ T cells in chicken PBMCs could become terminally polarized to a Th1 or Th2 phenotype. Moreover, ALV-J infection induced $CD4^+$ T cell activation and differentiation into a Th1 phenotype was likely associated with the expression of the top 10 branching DEGs (**Figures 5D–F**). In addition, the Th1-like cell population (Cluster A2) was vital in response to ALV-J infection at 21 DPI based on the expression of largely immune-related DEGs. Compared to the control PBMCs, the proportion of Th1-like cells (cluster A2) and cytotoxic $CD8^+$ T cells (cluster A3) were increased in the T cell population of PBMCs from ALV-J infected chicken. It is also known that Th1 cells can help cytotoxic $CD8^+$ T cell activation, survival, and memory generation (Huang et al., 2007). Conversely, B cell proportion was decreased, and fewer DEGs were detected after ALV-J infection (**Figures 1C**, **3A**). It is also reported that ALV-J infection inhibits the proliferation, maturity, and responing of B cells (He et al., 2019). Therefore, we speculated that it was the T cell response, including Th1-like cells and cytotoxic $CD8^+$ T cells, instead of the B cell response that eliminated ALV-J viremia before 21 DPI. Our previous animal experiments also verified that T cell response as opposed to humoral immunity was the key factor defending against ALV-J infection (Dai et al., 2020a).

More importantly, we identified 13 hub genes for the first time that were up-regulated in each chicken T cell population after ALV-J infection. Of note, *CDK17*, reported to inhibit porcine reproductive and respiratory syndrome virus (PRRSV) infection (Bai et al., 2019); *Nox1*, reported to suppress influenza A virus induced lung inflammation and oxidative stress (Selemidis et al., 2013); and *IL1RAP*, reported to negatively

regulate Transmissible gastroenteritis virus (TGEV) induced mitochondrial damage (Zhao et al., 2018), were all up-regulated in the Th1-like cells of PBMCs from ALV-J infected chicken. The information reminded us that *IL1RAP*, *NOX1*, and *CDK17* could potentially serve as marker genes of Th1-like cells exerting antiviral function. Furthermore, we found that *ZNFX1* was up-regulated in Th1-like and Th2-like cells, and was involved in inducing IFN gene and ISG expression (Wang Y. et al., 2019), which indicated the complexity of antiviral immunity in T cells. On the other hand, *IRAK2*, reported to potentially suppress avian infectious bronchitis virus (IBV) infection (Liu et al., 2018), exhibited up-regulated expression in activated $CD4^+$ T cells (cluster A0, Th0 cell) of PBMCs from ALV-J infected chicken. Interestingly, *CTLA4*, a critical co-receptor for Treg cell function (Friedline et al., 2009; Kerdiles et al., 2010), and *TGFBR2*, the important TGF-β receptor suppressing proliferation and terminal differentiation of antiviral $CD4^+$ T cells (Lewis et al., 2016), also exhibited up-regulated expression in activated $CD4^+$ T cells. In the current study, we did not identify the two subpopulations of chicken regulatory T cells (Treg cells) including TGF-beta$^+$CD4$^+$ T cells and CD4$^+$CD25$^+$ T cells (Shanmugasundaram and Selvaraj, 2011; Gurung et al., 2017). We hypothesize that Th0 cells may negatively regulate T cell response to homeostatic control through *CTLA4* and *TGFBR2*. Therefore, further scRNA-seq experiments with additional pathogens and preferentially at various time-points during the infections are needed in order to further confirm our above observation. Ultimately, such function should be demonstrated in a functional assessment using isolated cell types. Besides, given that the annotation of chicken genome, GRCg6a is incomplete, the information and function of many novel genes are not clear, which limits the effective analysis of scRNAseq results.

In summary, our scRNA-seq study based on PBMCs from chickens generated a rich data resource that could be mined in future experiments to address the function of these cells throughout development and in response to pathogen infection. The "marker genes" that were assigned to different clusters need to be verified using specific antibodies to their gene products. To the best of our knowledge, the mark genes for each T cell population involved in ALV-J infection are identified here for the first time. Moreover, using pseudotime analysis, we found that chicken $CD4^+$ T cells could differentiate into Th1-like and Th2-like cells. With respect to the control PBMCs, ALV-J infection had an obvious impact on PBMCs composition. B cells were decreased and inconspicuous in response in PBMCs from ALV-J infected chicken at 21 DPI. Cytotoxic Th1-like cells and $CD8^+$ T cells are potential key effectors in the defense against ALV-J infection.

DATA AVAILABILITY STATEMENT

The datasets presented in this study can be found in online repositories. The name of the repository and accession number can be found below: SRA, NCBI; PRJNA687808.

ETHICS STATEMENT

The animal research projects were sanctioned by the South China Agriculture University Institutional Animal Care and Use Committee (identification code: 2019076, 10 June, 2019).

AUTHOR CONTRIBUTIONS

XQ, XL, and ZL assisted with data analysis. MD designed the study, performed experiments, collected and analyzed data, and drafted the manuscript. ML coordinated the study and revised the manuscript. All authors have read and approved the final manuscript.

FUNDING

This work was supported by the National Natural Science Foundation of China (32172868, 31802174, and 31830097), Young Elite Scientists Sponsorship Program by CAST (2020QNRC001), and 111 Project (D20008).

ACKNOWLEDGMENTS

We are grateful to the South China Agricultural University's high-level talent launch program and the "Fuji Peiyou" program of College of Veterinary Medicine, South China Agricultural University. We are extremely appreciative of the help given by Gene *Denovo* Corp. during bioinformatics analysis. Special thanks are given to Jingjing Ning for providing project coordination.

SUPPLEMENTARY MATERIAL

The Supplementary Material for this article can be found online at: https://www.frontiersin.org/articles/10.3389/fmicb.2022.800618/full#supplementary-material

REFERENCES

Bai, J. H., Li, K. P., Tang, W. D., Liang, Z. X., Wang, X. F., Feng, W. H., et al. (2019). A high-throughput screen for genes essential for PRRSV infection using a piggyBac-based system. *Virology* 531, 19–30. doi: 10.1016/j.virol.2019.03.001

Becht, E., McInnes, L., Healy, J., Dutertre, C. A., Kwok, I. W. H., Ng, L. G., et al. (2019). Dimensionality reduction for visualizing single-cell data using UMAP. *Nat. Biotechnol.* 37, 38–44. doi: 10.1038/nbt.4314

Ben-Moshe, N. B., Hen-Avivi, S., Levitin, N., Yehezkel, D., Oosting, M., Joosten, L. A. B., et al. (2019). Predicting bacterial infection outcomes using single cell RNA-sequencing analysis of human immune cells. *Nat. Commun.* 10:3266. doi: 10.1038/s41467-019-11257-y

Bi, Y. L., Xu, L., Qiu, L. L., Wang, S. S., Liu, X. P., Zhang, Y. N., et al. (2018). Reticuloendotheliosis virus inhibits the immune response acting on lymphocytes from peripheral blood of chicken. *Front. Physiol.* 9:4. doi: 10.3389/fphys.2018.00004

Butler, A., Hoffman, P., Smibert, P., Papalexi, E., and Satija, R. (2018). Integrating single-cell transcriptomic data across different conditions, technologies, and species. *Nat. Biotechnol.* 36, 411–420. doi: 10.1038/nbt.4096

Camp, J. G., Sekine, K., Gerber, T., Loeffler-Wirth, H., Binder, H., Gac, M., et al. (2017). Multilineage communication regulates human liver bud development from pluripotency. *Nature* 546, 533–538. doi: 10.1038/nature22796

Cheng, Y. Q., Zhu, W. X., Ding, C., Niu, Q. N., Wang, H. G., Yan, Y. X., et al. (2019). IRF7 Is Involved in Both STING and MAVS Mediating IFN- beta Signaling in IRF3-Lacking Chickens. *J. Immunol.* 203, 1930–1942. doi: 10.4049/jimmunol.1900293

Dai, M., Li, S., Keyi, S., Sun, H., Zhao, L., Deshui, Y., et al. (2021). Comparative analysis of key immune protection factors in H9N2 avian influenza viruses infected and immunized specific pathogen-free chicken. *Poult. Sci.* 100, 39–46. doi: 10.1016/j.psj.2020.09.080

Dai, M., Li, S., Shi, K., Liao, J., Sun, H., and Liao, M. (2020a). Systematic identification of host immune key factors influencing viral infection in PBL of ALV-J infected SPF chicken. *Viruses* 12:114. doi: 10.3390/v12010114

Dai, M., Xie, T., Liao, M., Zhang, X., and Feng, M. (2020b). Systematic identification of chicken type I, II and III interferon-stimulated genes. *Vet. Res.* 51:70. doi: 10.1186/s13567-020-00793-x

Dai, M., Xu, C., Chen, W., and Liao, M. (2019). Progress on chicken T cell immunity to viruses. *Cell. Mol. Life Sci.* 76, 2779–2788. doi: 10.1007/s00018-019-03117-1

Degen, W. G., van Daal, N., Rothwell, L., Kaiser, P., and Schijns, V. E. (2005). Th1/Th2 polarization by viral and helminth infection in birds. *Vet. Microbiol.* 105, 163–167. doi: 10.1016/j.vetmic.2004.12.001

Estermann, M. A., Williams, S., Hirst, C. E., Roly, Z. Y., Serralbo, O., Adhikari, D., et al. (2020). Insights into gonadal sex differentiation provided by single-cell transcriptomics in the chicken embryo. *Cell Rep.* 31:107491. doi: 10.1016/j.celrep.2020.03.055

Feng, M., and Zhang, X. (2016). Immunity to avian Leukosis virus: where are we now and what should we do? *Front. Immunol.* 7:624. doi: 10.3389/fimmu.2016.00624

Feregrino, C., Sacher, F., Parnas, O., and Tschopp, P. (2019). A single-cell transcriptomic atlas of the developing chicken limb. *BMC Genomics* 20:401. doi: 10.1186/s12864-019-5802-2

Finak, G., McDavid, A., Yajima, M., Deng, J. Y., Gersuk, V., Shalek, A. K., et al. (2015). MAST: a flexible statistical framework for assessing transcriptional changes and characterizing heterogeneity in single-cell RNA sequencing data. *Genome Biol.* 16:278. doi: 10.1186/s13059-015-0844-5

Friedline, R. H., Brown, D. S., Nguyen, H., Kornfeld, H., Lee, J., Zhang, Y., et al. (2009). CD4+ regulatory T cells require CTLA-4 for the maintenance of systemic tolerance. *J. Exp. Med.* 206, 421–434. doi: 10.1084/jem.20081811

Gennart, I., Coupeau, D., Pejakovic, S., Laurent, S., Rasschaert, D., and Muylkens, B. (2015). Marek's disease: genetic regulation of gallid herpesvirus 2 infection and latency. *Vet. J.* 205, 339–348. doi: 10.1016/j.tvjl.2015.04.038

Gurung, A., Kamble, N., Kaufer, B. B., Pathan, A., and Behboudi, S. (2017). Association of Marek's Disease induced immunosuppression with activation of a novel regulatory T cells in chickens. *PLoS Pathog.* 13:e1006745. doi: 10.1371/journal.ppat.1006745

He, S. H., Zheng, G. Y., Zhou, D. F., Li, G., Zhu, M. J., Du, X. S., et al. (2019). Clonal anergy of CD117(+)chB6(+) B cell progenitors induced by avian leukosis virus subgroup J is associated with immunological tolerance. *Retrovirology* 16:1. doi: 10.1186/s12977-018-0463-9

Hen-Avivi, S., and Avraham, R. (2018). Immune cell type 'fingerprints' at the basis of outcome diversity of human infection. *Curr. Opin. Microbiol.* 42, 31–39. doi: 10.1016/j.mib.2017.09.012

Huang, H., Hao, S. G., Li, F., Ye, Z. M., Yang, J. B., and Xiang, J. (2007). CD4(+) Th1 cells promote CD8(+) Tc1 cell survival, memory response, tumor localization and therapy by targeted delivery of interleukin 2 via acquired pMHC I complexes. *Immunology* 120, 148–159. doi: 10.1111/j.1365-2567.2006.02452.x

Iborra, S., Soto, M., Stark-Aroeira, L., Castellano, E., Alarcon, B., Alonso, C., et al. (2011). H-ras and N-ras are dispensable for T-cell development and activation but critical for protective Th1 immunity. *Blood* 117, 5102–5111. doi: 10.1182/blood-2010-10-315770

Kerdiles, Y. M., Stone, E. L., Beisner, D. R., McGargill, M. A., Ch'en, I. L., Stockmann, C., et al. (2010). Foxo transcription factors control regulatory T cell development and function. *Immunity* 33, 890–904. doi: 10.1016/j.immuni.2010.12.002

Koskela, K., Kohonen, P., Salminen, H., Uchida, T., Buerstedde, J. M., and Lassila, O. (2004). Identification of a novel cytokine-like transcript differentially expressed in avian gamma delta T cells. *Immunogenetics* 55, 845–854. doi: 10.1007/s00251-004-0643-8

Levine, J. H., Simonds, E. F., Bendall, S. C., Davis, K. L., Amir el, A. D., Tadmor, M. D., et al. (2015). Data-driven phenotypic dissection of AML reveals progenitor-like cells that correlate with prognosis. *Cell* 162, 184–197. doi: 10.1016/j.cell.2015.05.047

Lewis, G. M., Wehrens, E. J., Labarta-Bajo, L., Streeck, H., and Zuniga, E. I. (2016). TGF-beta receptor maintains CD4 T helper cell identity during chronic viral infections. *J. Clin. Investig.* 126, 3799–3813. doi: 10.1172/JCI87041

Li, J., Xing, S., Zhao, G., Zheng, M., Yang, X., Sun, J., et al. (2020). Identification of diverse cell populations in skeletal muscles and biomarkers for intramuscular fat of chicken by single-cell RNA sequencing. *BMC Genomics* 21:752. doi: 10.1186/s12864-020-07136-2

Linderman, G. C., Rachh, M., Hoskins, J. G., Steinerberger, S., and Kluger, Y. (2019). Fast interpolation-based t-SNE for improved visualization of single-cell RNA-seq data. *Nat. Methods* 16, 243–245. doi: 10.1038/s41592-018-0308-4

Liu, H., Yang, X., Zhang, Z. K., Zou, W. C., and Wang, H. N. (2018). miR-146a-5p promotes replication of infectious bronchitis virus by targeting IRAK2 and TNFRSF18. *Microb. Pathog.* 120, 32–36. doi: 10.1016/j.micpath.2018.04.046

Ruan, Y., Wang, Y., Guo, Y., Xiong, Y., Chen, M., Zhao, A., et al. (2020). T cell subset profile and inflammatory cytokine properties in the gut-associated lymphoid tissues of chickens during infectious bursal disease virus (IBDV) infection. *Arch. Virol.* 165, 2249–2258. doi: 10.1007/s00705-020-04735-y

Selemidis, S., Seow, H. J., Broughton, B. R. S., Vinh, A., Bozinovski, S., Sobey, C. G., et al. (2013). Nox1 Oxidase Suppresses Influenza A virus-induced lung inflammation and oxidative stress. *PLoS One* 8:e60792. doi: 10.1371/journal.pone.0060792

Shanmugasundaram, R., and Selvaraj, R. K. (2011). Regulatory T cell properties of chicken CD4+CD25+ cells. *J. Immunol.* 186, 1997–2002. doi: 10.4049/jimmunol.1002040

Shannon, P., Markiel, A., Ozier, O., Baliga, N. S., Wang, J. T., Ramage, D., et al. (2003). Cytoscape: a software environment for integrated models of biomolecular interaction networks. *Genome Res.* 13, 2498–2504. doi: 10.1101/gr.1239303

Stewart, C. R., Keyburn, A. L., Deffrasnes, C., and Tompkins, S. M. (2013). Potential directions for chicken immunology research. *Dev. Comp. Immunol.* 41, 463–468. doi: 10.1016/j.dci.2013.05.011

Szklarczyk, D., Franceschini, A., Wyder, S., Forslund, K., Heller, D., Huerta-Cepas, J., et al. (2015). STRING v10: protein-protein interaction networks, integrated over the tree of life. *Nucleic Acids Res.* 43, D447–D452. doi: 10.1093/nar/gku1003

The Gene Ontology Consortium [GOC] (2019). The Gene Ontology Resource: 20 years and still GOing strong. *Nucleic Acids Res.* 47, D330–D338. doi: 10.1093/nar/gky1055

Trapnell, C., Cacchiarelli, D., Grimsby, J., Pokharel, P., Li, S. Q., Morse, M., et al. (2014). The dynamics and regulators of cell fate decisions are revealed by pseudotemporal ordering of single cells. *Nat. Biotechnol.* 32, 381–386. doi: 10.1038/nbt.2859

van Es, M. A., Van Vught, P. W., Blauw, H. M., Franke, L., Saris, C. G., Andersen, P. M., et al. (2007). ITPR2 as a susceptibility gene in sporadic arnyotrophic lateral sclerosis: a genorne-wide association study. *Lancet Neurol.* 6, 869–877.

Wang, B., Gu, T. X., Yu, F. M., Zhang, G. W., and Zhao, Y. (2018). Overexpression of miR-210 promotes the potential of cardiac stem cells against hypoxia. *Scand. Cardiovasc. J.* 52, 367–371. doi: 10.1080/14017431.2019.1567932

Wang, W., Cohen, J. A., Wallrapp, A., Trieu, K. G., Barrios, J., Shao, F. Z., et al. (2019). Age-Related dopaminergic innervation augments T Helper 2-Type allergic inflammation in the postnatal lung. *Immunity* 51, 1102–1118.e7. doi: 10.1016/j.immuni.2019.10.002

Wang, Y., Yuan, S., Jia, X., Ge, Y., Ling, T., Nie, M., et al. (2019). Mitochondria-localised ZNFX1 functions as a dsRNA sensor to initiate antiviral responses through MAVS. *Nat. Cell Biol.* 21, 1346–1356. doi: 10.1038/s41556-019-0416-0

Wilk, A. J., Rustagi, A., Zhao, N. Q., Roque, J., Martinez-Colon, G. J., McKechnie, J. L., et al. (2020). A single-cell atlas of the peripheral immune response in

patients with severe COVID-19. *Nat. Med.* 26, 1070–1076. doi: 10.1038/s41591-020-0944-y

Xu, C., and Su, Z. (2015). Identification of cell types from single-cell transcriptomes using a novel clustering method. *Bioinformatics* 31, 1974–1980. doi: 10.1093/bioinformatics/btv088

Xu, Q., Ma, X., Wang, F., Li, H., and Zhao, X. (2015). Evaluation of a multi-epitope subunit vaccine against avian leukosis virus subgroup J in chickens. *Virus Res.* 210, 62–68. doi: 10.1016/j.virusres.2015.06.024

Zang, W., Wang, T., Huang, J., Li, M., Wang, Y., Du, Y., et al. (2015). Long noncoding RNA PEG10 regulates proliferation and invasion of esophageal cancer cells. *Cancer Gene Ther.* 22, 138–144. doi: 10.1038/cgt.2014.77

Zerbino, D. R., Achuthan, P., Akanni, W., Amode, M. R., Barrell, D., Bhai, J., et al. (2018). Ensembl 2018. *Nucleic Acids Res.* 46, D754–D761.

Zhao, X., Bai, X., Guan, L., Li, J., Song, X., Ma, X., et al. (2018). microRNA-4331 Promotes Transmissible Gastroenteritis Virus (TGEV)-induced Mitochondrial Damage Via Targeting RB1, Upregulating Interleukin-1 Receptor Accessory Protein (IL1RAP), and Activating p38 MAPK pathway in vitro. *Mol. Cell. Proteomics* 17, 190–204. doi: 10.1074/mcp.RA117.000432

Zhu, L. N., Yang, P. H., Zhao, Y. Z., Zhuang, Z. K., Wang, Z. F., Son, R., et al. (2020). Single-cell sequencing of peripheral mononuclear cells reveals distinct immune response landscapes of COVID-19 and influenza patients. *Immunity* 53, 685–696.e3. doi: 10.1016/j.immuni.2020.07.009

Conflict of Interest: The authors declare that the research was conducted in the absence of any commercial or financial relationships that could be construed as a potential conflict of interest.

Publisher's Note: All claims expressed in this article are solely those of the authors and do not necessarily represent those of their affiliated organizations, or those of the publisher, the editors and the reviewers. Any product that may be evaluated in this article, or claim that may be made by its manufacturer, is not guaranteed or endorsed by the publisher.

frontiers in Veterinary Science

ORIGINAL RESEARCH
published: 22 March 2022
doi: 10.3389/fvets.2022.854007

Marek's Disease Virus and Reticuloendotheliosis Virus Coinfection Enhances Viral Replication and Alters Cellular Protein Profiles

*Xusheng Du, Defang Zhou, Jing Zhou, Jingwen Xue and Ziqiang Cheng**

College of Veterinary Medicine, Shandong Agricultural University, Tai'an, China

Coinfection with Marek's disease virus (MDV) and reticuloendotheliosis virus (REV) causes synergistic pathogenic effects and serious losses to the poultry industry. However, whether there is a synergism between the two viruses in viral replication and the roles of host factors in regulating MDV and REV coinfection remains elusive. In this study, we found that MDV and REV coinfection increased viral replication in coinfected cells as compared to a single infection in a limited period. Further, we explore the host cell responses to MDV and REV coinfection using tandem mass tag (TMT) peptide labeling coupled with liquid chromatography–tandem mass spectrometry (LC-MS/MS). Compared with MDV/REV-infected cells, 38 proteins increased (fold change $>$ 1.2) and 60 decreased (fold change $<$ 0.83) their abundance in MDV and REV coinfected cells. Differentially accumulated proteins (DAPs) were involved in important biological processes involved in the immune system process, cell adhesion and migration, cellular processes, and multicellular organismal systems. STRING analysis found that IRF7, MX1, TIMP3, and AKT1 may be associated with MDV and REV synergistic replication in chicken embryo fibroblasts (CEFs). Western blotting analysis showed that the selected DAPs were identical to the quantitative proteomics data. Taken together, we verified that MDV and REV can synergistically replicate in coinfected cells and revealed the host molecules involved in it. However, the synergistic pathogenesis of MDV and REV needs to be further studied.

Keywords: proteomic analysis, coinfection, Marek's disease virus, reticuloendotheliosis virus, TMT

OPEN ACCESS

Edited by:
Guillermo Tellez-Isaias, University of Arkansas, United States

Reviewed by:
I. Castellanos-Huerta, National Autonomous University of Mexico, Mexico
Victor Manuel Petrone-García, National Autonomous University of Mexico, Mexico

****Correspondence:***
Ziqiang Cheng
czqsd@126.com

Specialty section:
This article was submitted to Veterinary Infectious Diseases, a section of the journal Frontiers in Veterinary Science

Received: *13 January 2022*
Accepted: *08 February 2022*
Published: *22 March 2022*

Citation:
Du X, Zhou D, Zhou J, Xue J and Cheng Z (2022) Marek's Disease Virus and Reticuloendotheliosis Virus Coinfection Enhances Viral Replication and Alters Cellular Protein Profiles. Front. Vet. Sci. 9:854007. doi: 10.3389/fvets.2022.854007

INTRODUCTION

Marek's disease virus (MDV), an oncogenic alpha-herpesvirus, causes Marek's disease (MD) (1). Reticuloendotheliosis virus (REV), an oncogenic and immunosuppressive retrovirus, causes reticuloendotheliosis (RE) (2). Two contagious, immunosuppressive, and oncogenic diseases in chickens affect poultry production, and mixed infection of MDV and REV has become an important epidemiologic situation worldwide (3–5). Synergistic pathogenicity usually occurred between MDV and REV, as MDV and REV coinfection significantly increased disease severity (6, 7). The common occurrence of REV among MDV-infected chickens may be linked to contaminated

vaccine stocks (8), and MDV due to REV long terminal repeat (LTR) recombinant increased horizontal transmission (9, 10). Generally, virus pathogenicity is related to the ability of viral replication. MDV and REV genome load contributes to our understanding of the pathogenesis of two virus infections. However, the effects of coinfection with MDV and REV on replication remain unknown.

To further understand the synergistic pathogenesis of MDV and REV coinfection, research on virus–host interaction is critical. Virus infection can affect host cell morphology, the cytoskeleton, the cell cycle, transcription and translation patterns, and innate immune responses of the host, the apoptosis pathway (11, 12). The morphological and functional changes are associated with significant changes in the patterns of expression of host cells (13, 14). Consequently, information on proteome changes in the host following MDV and REV coinfection may be crucial to understanding the host response to viral pathogenesis. In recent years, the development of comparative proteomics has facilitated the study of host cellular responses to pathogen infection (15). Proteomics technologies have been used to characterize the pathogenesis of MDV and REV infection, recently. Protein expression of chicken embryo fibroblast (CEF) cells infected with MDV has been studied using a modified MudPIT analysis involving strong cation exchange chromatography and microcapillary reversed-phase liquid chromatography–tandem mass spectrometry (LC-MS/MS) (16). Isobaric tags for relative and absolute quantification (iTRAQ) approach were used to analyze the protein profile of REV-infected CEFs (17). Among the current proteomics methods, tandem mass tag (TMT) quantitative proteomics techniques, the highly sensitive proteomic platform based on the isobaric labels TMTs as one of the most robust proteomics techniques, are useful for the analysis of infection-associated proteins (18).

However, to the best of our knowledge, no previous study has analyzed the proteomic changes in MDV/REV coinfected CEF cells. We examined the effects of coinfection on REV and MDV replication and used the TMT-labeling quantitative detection technique to quantify CEF cells proteins that are differentially expressed after infection by REV alone, MDV alone, or coinfection by both agents. A total of 98 common differentially expressed proteins were identified at 48 h post-infection (hpi). Analysis of these altered expression proteins might provide fundamental information for the study of virus–host interactions and the molecular basis underlying MDV and REV synergistic replication *in vitro*.

MATERIALS AND METHODS

Cells and Viruses

The Md5 strain of MDV (10^3 PFU/0.2 ml) and the single-nucleotide variant (SNV) strain of REV (10^4 $TCID_{50}$/0.2 ml) were maintained in our laboratory (19, 20). CEF cells were maintained in Dulbecco's Modified Eagle's Medium (DMEM; Sigma, CA, USA) supplemented with 10% fetal bovine serum (FBS; HyClone, UT, USA) in a 5% CO_2 incubator at 37°C. The replication of MDV and REV was measured using the pfu and $TCID_{50}$ methods in the CEF cells at various time points, respectively.

Overview of the Experimental Design

To study the effects of coinfection *in vitro*, CEF cell monolayers were subjected to one of four conditions (**Figure 1D**): (a) non-infected cells served as negative controls; (b) cells infected with REV only; (c) cells infected with MDV only; and d) cells infected with REV for 24 h and then infected with MDV (coinfected group). The multiplicity of infection (MOI) and incubation time of viruses were selected to allow replication while causing minimal damage to CEF cells. Confocal imaging, Western blotting, and qRT-PCR were used to detect viral infection and proliferation. Every sample was repeated in three technical replicates, and each experiment was conducted three times. The above samples were prepared for comparative proteomic analysis at the appropriate time intervals.

mRNA Quantitation by qRT-PCR

Total cellular RNA was extracted from the MDV-infected, REV-infected, MDV/REV coinfected, and mock-infected CEF cells using RNAiso Plus (TaKaRa, Dalian, China) following the manufacturer's instructions. cDNA was prepared from the RNA using ReverTra Ace qPCR RT Master Mix (TOYOBO, Shanghai, China) and used as a template for quantitative reverse transcription PCR (qRT-qPCR). Whereafter qRT-PCR was performed using the SYBR Premix Ex Taq™ II Kit (TaKaRa) on a Roche LightCycler 96 system (Roche, Basel, Switzerland). Real-time quantitative PCR (qPCR) detection was performed as previously described (20). Specific primers for amplifying various genes were as follows: for GAPDH mRNA analysis, 5′-GAACATCATCCCAGCGTCCA-3′ (forward) and 5′-GGTCATAAGTCCCTCCACGA-3′ (reverse) were used; for REV gp90 analysis, 5′-GGCATCAATCGTACCCGACA-3′ (forward) and 5′-GGGGGATAAACTGGACTGCC-3′ (reverse) were used; for MDV pp38 analysis, 5′-GCTGCAGCTGTCCATTTTCC-3′ (forward) and 5′-TACAGTGTAGCCGTACCCGA-3′ (reverse) were used. GAPDH was employed as an internal reference gene. The relative expression level of each mRNA was calculated by the $2^{-\Delta\Delta ct}$ method. Three independent biological replicates were performed for each gene.

Immunofluorescence Assay and Confocal Imaging

CEF cells cultured in 24-well culture plates and 15-mm culture dishes were infected and coinfected with MDV and REV. For immunofluorescence assay (IFA), cells were first fixed with 4% paraformaldehyde for 30 min and permeabilized with 0.1% Triton X-100 in phosphate-buffered saline (PBS) for 15 min, followed by blocking with 5% bovine serum albumin in PBS for 1 h. Whereafter, the cells were incubated with mouse anti-gp90 and fluorescein isothiocyanate (FITC)-labeled goat anti-mouse IgG (for REV) or rabbit anti-pp38 and Cy3-labeled goat anti-rabbit IgG (for MDV) diluted in PBS for 1 h. For confocal imaging, the above cells were examined using an SP8 confocal laser scanning microscope (CLSM) (Leica, Wetzlar, Germany). The overlap of the two colors of fluorescent markers appears yellow. The nuclei of all the infected cells were stained by DAPI.

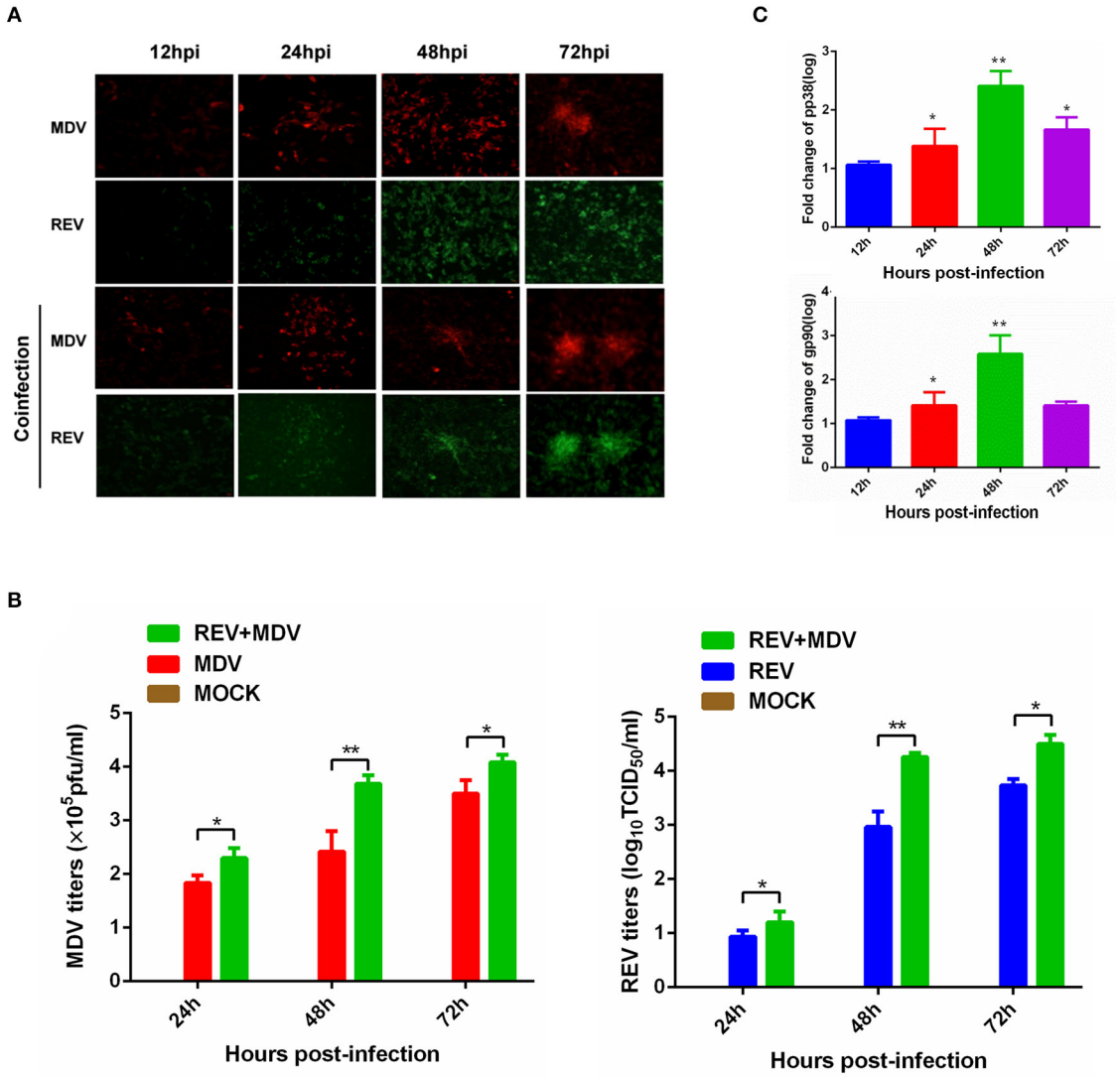

FIGURE 1 | Synergistic infection of MDV and REV increases the two viruses' replication in CEF. **(A)** Detection of MDV-pp38 and REV-gp90 in infected CEFs was visualized by IFA from 24 to 72 hpi. FITC-labeled goat anti-mouse IgG (for REV) (green) and Cy3-labeled goat anti-rabbit IgG (for MDV) (red) were used as the secondary antibodies in the assay. **(B)** The MDV and REV viral titers were tested from 24 to 72 hpi. **(C)** Differential expression fold change of MDV pp38 and REV gp90 genes in the MDV and REV coinfected cells compared to the single-infected control group. The fold change between both groups is shown using a logarithmic scale. Data are presented as the mean ± SD from three independent experiments. $^{*}p < 0.05$; $^{**}p < 0.01$. MDV, Marek's disease virus; REV, reticuloendotheliosis virus; CEF, chicken embryo fibroblast; IFA, immunofluorescence assay; FITC, fluorescein isothiocyanate.

Western Blotting

Total protein lysates were isolated from treated CEF cells using a lysis buffer [pH 7.6, 0.1 mmol/L of NaCl, 0.01 mmol/L of Tris-HCl, 0.001 mol/L of ethylene diamine tetraacetic acid (EDTA), pH 8.0, 1 μg/ml of aprotinin, 100 μg/ml of phenylmethylsulfonyl fluoride (PMSF)]. The protein concentrations were measured by BCA Protein Assay Kit (PIERCE, Rockford, IL, USA). The proteins were separated by 10% sodium dodecyl sulfate–polyacrylamide gel electrophoresis (SDS-PAGE) and transferred to polyvinylidene fluoride membranes (Millipore, Billerica, USA), which were blocked for 2 h in 5% defatted milk in Tris-buffered saline containing Tween-20. The membranes were incubated at 37°C for 60 min with rabbit polyclonal antibody to TIMP3 (Abcam, Cambridge, UK), rabbit polyclonal antibody to AKT1 (BIOSS, Beijing, China), rabbit polyclonal antibody to MX1 (ProteinTech Group, Chicago, IL, USA), rabbit polyclonal antibody to IRF7 (BIOSS, Beijing, China), mouse monoclonal antibody anti-REV gp90, and rabbit polyclonal anti-MDV pp38. After being washed three times with 0.05% TBST, the membranes were incubated at 37°C for 60 min with horseradish peroxidase

(HRP)-conjugated goat anti-rabbit IgG or goat anti-mouse IgG (BIOSS, Beijing, China). The results were detected using the ECL Detection Kit (Vazyme, Nanjing, China). β-Actin was used as an internal control.

Protein Sample Preparation, Trypsin Digestion, and Tandem Mass Tag Labeling

The MDV-infected, REV-infected, MDV/REV coinfected, and mock-infected CEF cells were washed with PBS and collected in lysis buffer (8 M of urea, 1% Protease Inhibitor Cocktail). Three biological replicates of the sample were sonicated on ice using a high-intensity ultrasonic processor (Scientz, Ningbo, China) and then centrifuged at 4°C for 10 min at 12,000 *g*. The supernatant was collected, and total protein concentration was determined using a BCA kit (Beyotime, Shanghai, China).

For digestion, the dithiothreitol (5 mM) was added to reduce protein solution at 56°C for 30 min, and iodoacetamide was used to alkylate for 15 min at room temperature. After that, trypsin was added overnight for the first digestion, 1:50 trypsin-to-protein mass ratio; then for the second digestion, trypsin was added at 4 h, 1:100 trypsin-to-protein mass ratio.

After trypsin digestion, the peptide was desalted and then processed with a TMT kit (Thermo Fisher Scientific, Waltham, MA, USA) according to the manufacturer's protocol.

High-Performance Liquid Chromatography Fractionation and Liquid Chromatography–Tandem Mass Spectrometry Analysis

The tryptic peptides were fractionated by Agilent 300 Extend C18 column (Agilent, Santa Clara, CA, USA) using a high-performance liquid chromatography (HPLC) system (Thermo Fisher Scientific). For LC-MS/MS analysis, the tryptic peptides were dissolved and analyzed on an EASY-nLC 1000 UPLC system (Thermo Fisher Scientific, Waltham, MA, USA) at a constant flow rate of 450 nl/min. Solvent A (0.1% formic acid) was used to dissolve tryptic peptides, held at solvent B, and increased gradient from 8 to 23% with 0.1% formic acid in 90% acetonitrile.

MS/MS was performed on Q Exactive™ HF-X system (Thermo Fisher Scientific, Waltham, MA, USA). MS1 spectra were collected in the 2.0 kV electrospray voltage and in the range 350–1,600 *m*/*z*. For MS/MS, noise-contrastive estimation (NCE) setting as 28, the selected peptides were detected in the Orbitrap at a resolution of 17,500. A data-dependent procedure that alternated between one MS scan followed by 20 MS/MS scans with 15.0 s dynamic exclusion. Automatic gain control (AGC) was set at 5E4. Fixed first mass was set as 100 *m*/*z*. The HPLC fractionation and LC-MS/MS analysis in our research are supported by Jingjie PTM BioLabs (Hangzhou, China).

Database Search

The MS/MS data were submitted to the Maxquant search engine (v.1.5.2.8) for data analysis. MS/MS spectra were searched against the Uniprot Gallus database (27535 sequences, downloaded on May 30, 2021) concatenated with reverse decoy database. Two missing cleavages were allowed in Trypsin/P with 20-ppm first search and 5-ppm main search, and the fragment ion mass tolerance was 0.02 Da. The false discovery rate (FDR) calculation was adjusted to <1%, and the minimum score was set to >40. For quantification, the unused value was >1.2, and the proteins had at least one unique peptide.

Bioinformatics Analysis

The biological interpretation and function of identified proteins were analyzed using Gene Ontology (GO) annotation (www.http://www.ebi.ac.uk/GOA/) and Kyoto Encyclopedia of Genes and Genomes (KEGG) pathway mapping through KEGG mapper web server (http://www.genome.jp/kegg/tool/map_pathway2.html). GO enrichment and KEGG pathway enrichment were performed using a double-tailed Fisher's precision test. The GO and KEGG pathways with a corrected *p*-value <0.05 were considered significant. The protein–protein interaction network was analyzed by the STRING database (http://string.embl.de/).

Statistical Analysis

Data were analyzed by one-way repeated-measures ANOVA and least significance difference (LSD), which was considered statistically significant when $p < 0.05$.

RESULTS

Coinfection of Marek's Disease Virus and Reticuloendotheliosis Virus Increases the Virus Replication in Chicken Embryo Fibroblasts

MDV and REV infections were confirmed using IFA, as REV does not induce cytopathic effects (CPEs) in CEFs. In MDV-infected (MOI = 1) cells, fluorescence intensity was observed obviously at 24 and 48 hpi. However, the cell death was present at 72 hpi (**Supplementary Figure 1**). In REV (MOI = 1) infected cells, weak fluorescence was observed beginning at 48 hpi (**Supplementary Figure 1**). To understand the effect of coinfection on MDV and REV replication, according to the above experimental results, the CEFs were first infected with REV (MOI = 1) or mock-infected for 24 h and then infected with the MDV (MOI = 0.1) for 12, 24, 48, and 72 h. The results of IFA showed that the fluorescence signal was more intense in MDV and REV coinfected cells compared to MDV/REV-infected cells. Meanwhile, in MDV and REV coinfected cells, the CPE was observed earlier and more severe than that of MDV-infected cells. The viral titers of MDV and REV were quantified by plaque assay and the $TCID_{50}$ assay. As the results show, the replication rate of MDV or REV was higher at 24 hpi ($p < 0.05$), 48 hpi ($p < 0.01$), and 72 hpi ($p < 0.05$) in the MDV and REV coinfected group compared to the MDV/REV-infected control group (**Figure 1B**). Consistently, the results of qRT-PCR showed that MDV pp38 and REV gp90 mRNA expressed levels increased gradually and reached a peak at 48 h in MDV and REV coinfected cells (**Figure 1C**). All the results suggested

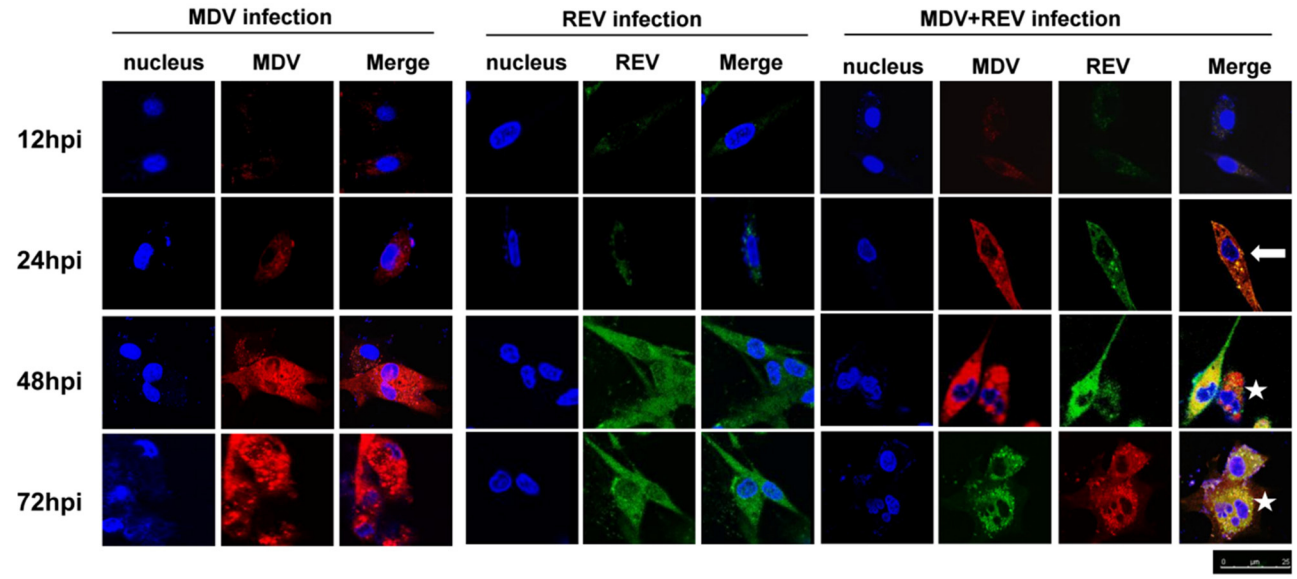

FIGURE 2 | Protein expression and localization of MDV and REV examined by confocal laser scanning microscope (CLSM). The proteins of MDV and REV were co-localized in cytoplasm (arrowhead). The coinfected cells showed more cytopathy (CPE) (star) than single-infected cells. Samples stained with pp38 or gp90 antibodies as well as Cy3-labeled goat anti-rabbit IgG (for MDV) (red) or FITC-labeled goat anti-mouse IgG (for REV) (green) antibody in the assay. The areas of colocalization are shown in yellow. Cell nuclei (blue) were stained with DAPI. MDV, Marek's disease virus; REV, reticuloendotheliosis virus; CLSM, confocal laser scanning microscope; CPE, cytopathic effect; FITC, fluorescein isothiocyanate.

that MDV and REV synergistically increase viral replication in CEF cells.

Marek's Disease Virus and Reticuloendotheliosis Virus Are Localized in the Same Cell

CLSM was performed to assess whether MDV and REV can replicate in the same CEF cell and whether MDV and REV coinfection could affect the subcellular localization of MDV or REV proteins using MDV pp38-specific and REV gp90-specific antibodies. The results of the CLSM assay showed that the MDV and REV signals could be detected simultaneously in the same cells, indicating that MDV and REV could coexist in or coinfect a cell. Dynamic fluorescent signal analysis showed that MDV pp38 protein and REV gp90 protein accumulated significantly higher and that the CPE appeared earlier in coinfected cells than that of single-infected cells (**Figure 2**). The data indicated that MDV and REV could replicate in the same cells and throw light on the possible synergistic mechanism of MDV and REV.

For further proteomic analysis, a higher proportion of infected cells and avoiding an excessive CPE are necessary. We selected 48 hpi as the time point to prepare samples under our infection conditions according to the results of **Figure 1**. In addition, a significant difference ($p < 0.01$) in titers of the MDV/REV progeny between MDV-REV coinfected cells and MDV/REV-infected cells may indicate significant changes in the patterns of expression of host cells at 48 hpi (**Figure 1B**).

Global Proteome Analysis Upon Single and Coinfection of Marek's Disease Virus and Reticuloendotheliosis Virus

Extraction of total proteins from mock-infected CEF cells (N), REV-infected CEF cells (R), MDV-infected CEF cells (M), and REV and MDV coinfected CEF cells (RM) at 48 hpi. A total of 3,515 proteins were obtained from LC-MS/MS proteomic analysis, and 2407 proteins were identified (**Supplementary Table 1**). A total of 1,043, 483, and 881 detected proteins were identified in comparing R versus N (459 and 584 proteins were upregulated and downregulated, respectively), M vs. N (203 and 280 proteins were upregulated and downregulated, respectively), and RM vs. N (404 and 477 proteins were upregulated and downregulated, respectively). The results indicated that infection with MDV resulted in fewer changes in the global proteome of CEF cells than did infection with REV. Further, in RM compared with R (RM/R), 1,023 proteins that were differentially accumulated were identified, 547 of which were upregulated and 476 of which were downregulated. Of the 362 proteins identified between RM and M (RM/M), 188 and 174 proteins were upregulated and downregulated in RM, respectively (**Figure 3A**; **Supplementary Table 1**). The results showed that coinfection with MDV and REV significantly altered the abundance of proteins. To identify the common and specifically changed proteins between RM and M, between RM and R, or between M and R, a Venn diagram was generated (**Figure 3B**; **Supplementary Table 2**). It clearly showed that differentially abundant proteins (DAPs) were divided into

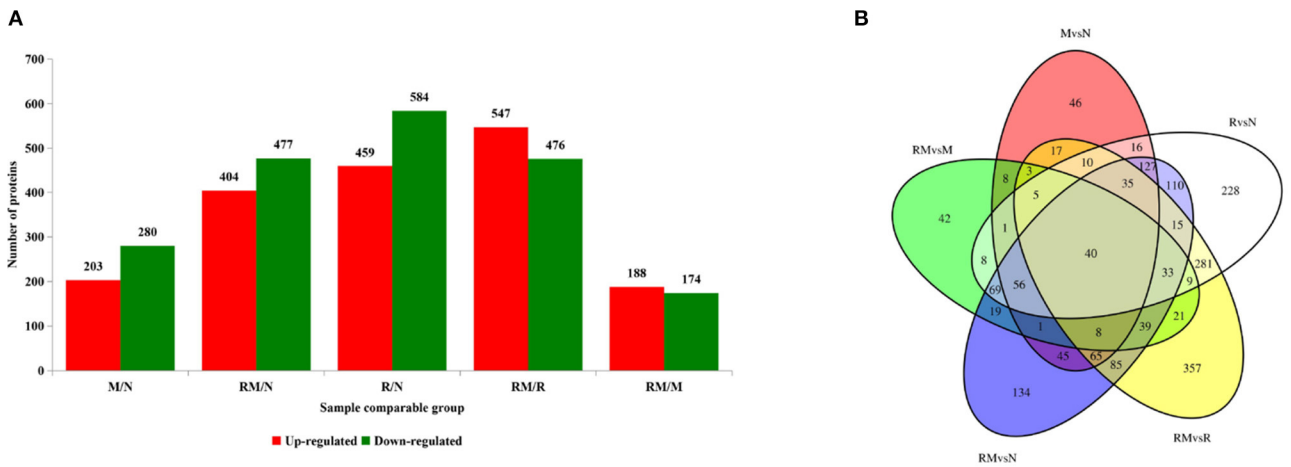

FIGURE 3 | Distribution of differentially accumulated proteins (DAPs). **(A)** Number of upregulated (red) and downregulated (green) DAPs in M vs. N, R vs. N, RM vs. N, RM vs. M, and RM vs. R. **(B)** Venn diagram to show the distribution of DAPs between RM vs. N (blue circle), RM vs. R (yellow circle), RM vs. M (green circle), R vs. N (white circle), and M vs. N (red circle). N, mock-infected CEF cells; R, REV-infected CEF cells; M, MDV-infected CEF cells; RM, REV and MDV coinfected CEF cells. CEF, chicken embryo fibroblast; REV, reticuloendotheliosis virus; MDV, Marek's disease virus.

11 clusters obtained across all groups and divided into 11 clusters. These proteins were annotated using the GO database: molecular functions, biological processes, and cellular components (**Supplementary Table 1**).

The DAPs between the sample groups were defined as those with a $\geq$1.2-fold or $\leq$0.83-fold change in relative abundance ($p < 0.05$). An average protein ratio <1 represented downregulated proteins, and an average proteins ratio >1 represented upregulated proteins.

Gene Ontology Enrichment Analysis

To determine the DAP expression trends in the different GO functional classifications, comparative cluster analysis was performed in RM vs. M and RM vs. R. For DAPs in RM vs. M (**Figure 4A**; **Supplementary Table 3**), extracellular matrix (ECM) structural constituent was highly represented in molecular function. Consistently, most DAPs were clustered in the ECM in the cellular component category. Furthermore, in terms of biological process annotation, biological adhesion process, cell adhesion, and cell migration process were enriched. Other proteins involved in immune response and immune system process were also enriched. For DAPs in RM versus R (**Figure 4B**; **Supplementary Table 4**), monovalent inorganic cation and monovalent inorganic cation transmembrane transporter activity were highly represented in molecular function. The mitochondrial membrane and organelle inner membrane were enriched in the cellular component category. ATP metabolic process, hydrogen transport, and proton transport showed significant enrichment.

Kyoto Encyclopedia of Genes and Genomes Pathway Analysis

To further investigate the function of DAPs between the sample groups, we analyzed the changes of rich clustering classes in KEGG pathways. In RM vs. M, the upregulated proteins identified were mapped to a total of 8 KEGG pathways, and the downregulated proteins participated in 5 pathways (**Figure 5A**; **Supplementary Table 5**). Upregulated DAPs in RM vs. R were involved in 3 pathways, and the downregulated proteins participated in 21 pathways (**Figure 5B**; **Supplementary Table 6**). The results showed that the AGE-RAGE signaling pathway in diabetic complications, ECM–receptor interaction, and PPAR signaling pathway was enriched in RM vs. M and RM vs. R, indicating the above pathway's possible involvement in MDV and REV coinfection.

String Analysis of the Relationships Between Selected Differentially Accumulated Proteins

To further investigate, STRING tool was used to explore the potential protein network connections for the differentially regulated proteins in detail (21). In **Figure 3B**, of the 158 DAPs identified between RM vs. M and RM vs. R, 98 DAPs in co-expression trends were selected (**Supplementary Table 7**). Of these, 60 proteins were upregulated and 38 proteins were downregulated. The DAPs were mainly mapped to two functional networks by STRING software analysis (**Figure 6**). A specific network was focused on IRF7, IFIT5, TRAF2, MX1, TRIM25, STAT2, EIF2AK2, IFIH1, ZNFX1, CMPK2, PARP12, and USP18. These proteins were involved in innate immune pathways like the NOD-like receptor signaling pathway, RIG-I-like receptor signaling pathway, and AGE-RAGE signaling pathway. Another specific network contains AKT1, MMP2, CTGF, CTR61, LTBP1, CTHRC1, COMP, TGFβ1, LAMC1, TIMP3, POSTN, COL1A1, and COL1A2, of which ECM–receptor interaction and PPAR signaling pathway were enriched.

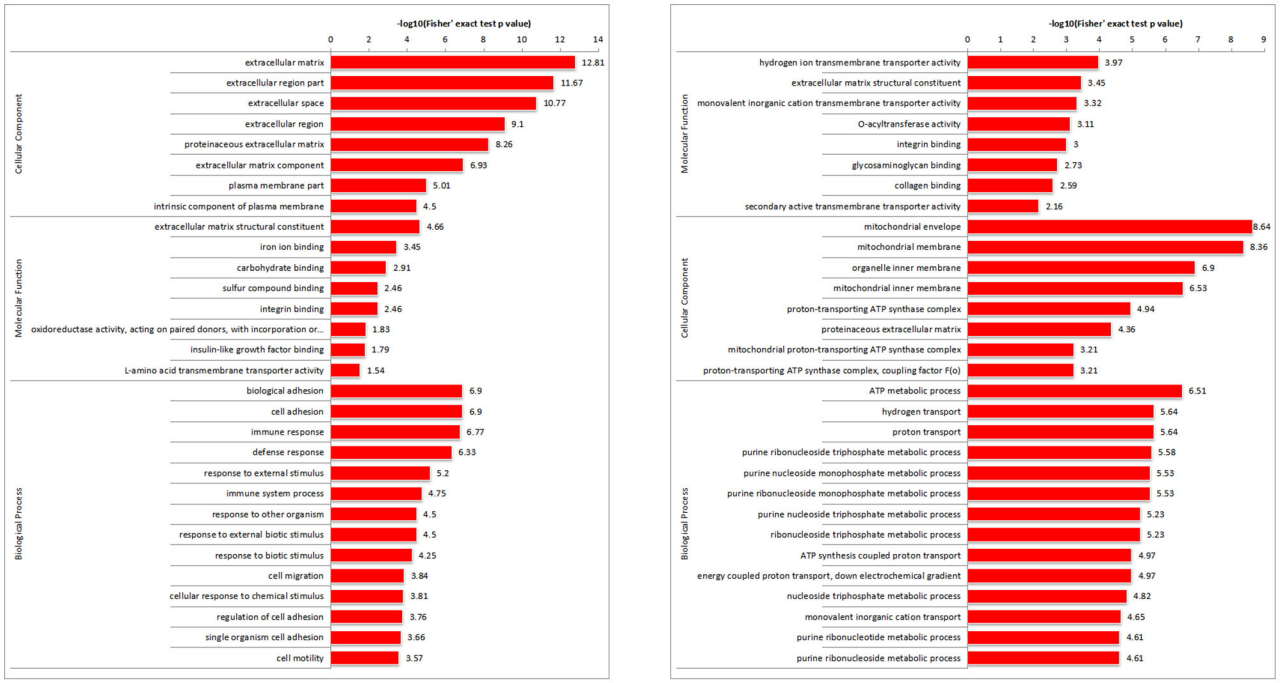

FIGURE 4 | GO enriched histogram of DAPs. Statistics of GO enrichment in RM vs. M **(A)** and RM vs. R **(B)**. Each column in the figure is a GO term, the vertical axis text indicates the name and classification of GO, and the height of the column indicates the enrichment rate. R, REV-infected CEF cells; M, MDV-infected CEF cells; RM, REV and MDV coinfected CEF cells. GO, Gene Ontology; DAPs, differentially accumulated proteins; REV, reticuloendotheliosis virus; CEF, chicken embryo fibroblast; MDV, Marek's disease virus.

Confirmation of Proteomic Data by qRT-PCR and Western Blotting Analysis

In order to further validate the differentially expressed proteins identified by the proteomic analysis, we selected the representative proteins IRF7, MX1, AKT1, and TIMP3 for Western blotting analysis. IRF7, a crucial transcription factor to trigger innate immune responses, and Mx1, an important IFN-stimulated gene (ISG), play a pivotal role against viral infection (22, 23). It is known that activation of Akt, an important protein kinase, is crucial for the replication of many viruses (24). Furthermore, TIMPs can regulate ECM degradation and then regulate cell migration and proliferation (25). As shown in **Figure 7**, the expressions of IRF7, MX1, and AKT1 were obviously increased, and the expressions of TIMP3 were decreased in MDV and REV coinfected CEF cells when compared with MDV/REV-infected CEF cells. The results were consistent with those in proteomic analysis. Next, the protein expression levels of MDV and REV were quantified by Western blotting at 48 hpi. The expressions of the pp38 and gp90 proteins were significantly upregulated in the MDV and REV coinfected group.

DISCUSSION

Coinfection of viruses generally influences the disease pattern compared with a single infection (11, 25, 26). The outcome of coinfection usually is viral interference (27, 28). Besides interference, coinfections of viruses may also enhance viral replication and virulence (29, 30). To support virus replication, viruses can interact with a major number of cellular proteins (virus–host interactome) (31). Proteomic techniques have become significant methodologies for determining host cellular pathophysiological processes and cellular protein interactions following virus infection (32, 33). In the present study, we reported that coinfection of MDV and REV significantly increased the expression levels of both the viral gene transcript and virus titers (**Figure 1**). Furthermore, MDV and REV could infect in same cells and synergistically induce cytopathy (**Figure 2**). Taking this substantial evidence into consideration, cell samples at 48 hpi were chosen for further proteomic analysis. Based on our study, the expression levels of 98 co-regulated DAPs were found to be significantly altered upon a single infection and coinfections of MDV and REV. The results of GO, KEGG pathway, and STRING analysis predicted that these DAP pertaining to different types of functional categories and signal pathways (**Supplementary Table 1**). Our data may provide an overview of the proteins altered in expression during the host response to coinfection with MDV and REV may provide insight into the process of synergistic pathogenesis between two viruses.

The production of type I interferons (IFNs) is one of the most immediate responses upon infection, such as IFN-α and IFN-β (34). These secreted IFNs induce the expression of a

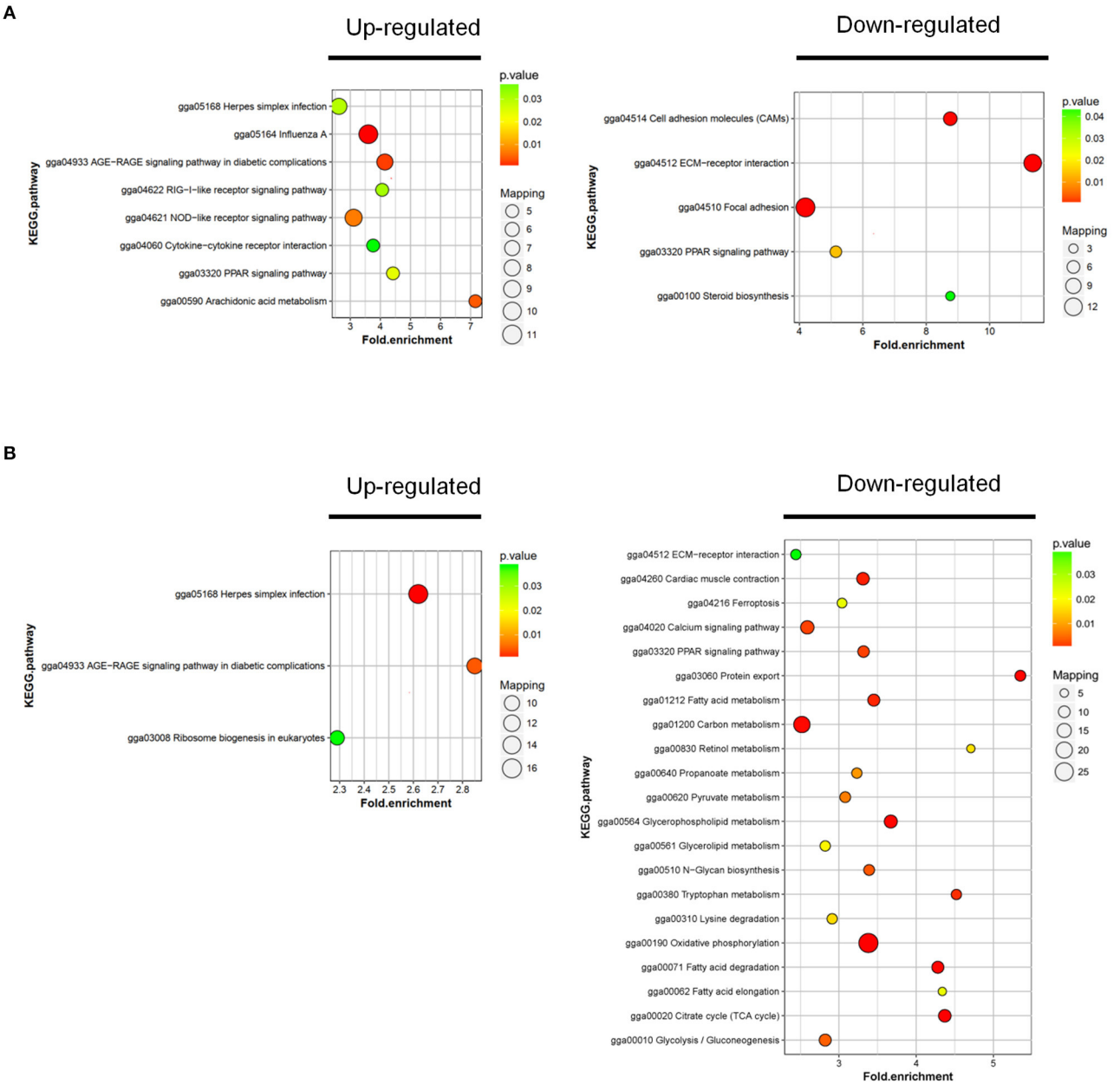

FIGURE 5 | KEGG cluster and pathway enrichment analysis of DAPs. Statistics of KEGG enrichment in RM vs. M **(A)** and RM vs. R **(B)**. The pathway enrichment statistical analysis was performed by Fisher's exact test. The x-axis is folded enrichment; the y-axis is enrichment pathway. The mapping is the protein number. The color indicates the significance of the enrichment (*p*-value). The darker the color, the more significant the enrichment of the pathway. R, REV-infected CEF cells; M, MDV-infected CEF cells; RM, REV and MDV coinfected CEF cells. KEGG, Kyoto Encyclopedia of Genes and Genomes; DAPs, differentially accumulated proteins; REV, reticuloendotheliosis virus; MDV, Marek's disease virus.

wide range of ISGs, which collectively mediate the inhibition of viruses (35). IRF7 is an interferon regulatory factor, inducing the production of IFN-β and is crucial in the establishment of innate immunity in response to viral infection in chickens (22, 36, 37). In this study, IRF7 and MX1 were upregulated in coinfected cells (**Figure 6**), which indicated that MDV and REV coinfection in CEF cells leads to pronounced induction of innate immune responses in comparison to a single infection. Interestingly, some expression increased factors such as CTHRC1 (**Supplementary Table 1**) could be hijacked by the virus to evade host immunity and maintain replication (38, 39).

The results of this study have shown that coinfection of MDV and REV upregulated cell-adhesion molecules (CAMs) compared to a single infection (**Supplementary Table 1**). CAMs, a group

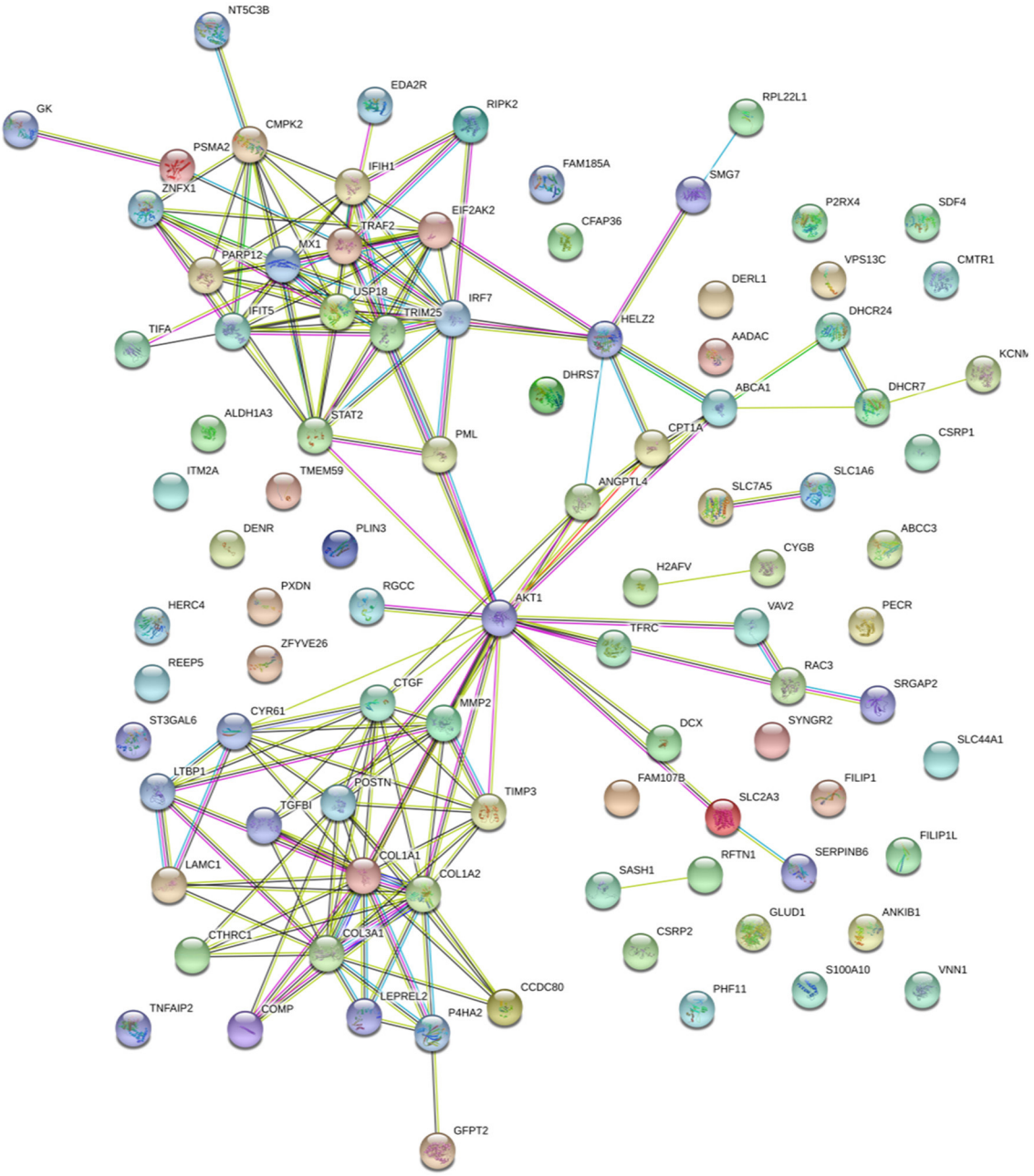

FIGURE 6 | Specific network analysis of proteins significantly altered in both RM/R and RM/M. The network of DAPs with STRING analysis. Each node represents a protein in the graph, each line represents the interaction between proteins, and the wider the line, the closer the relationship. REV-infected CEF cells; M, MDV-infected CEF cells; RM, REV and MDV coinfected CEF cells. DAPs, differentially accumulated proteins; REV, reticuloendotheliosis virus; CEF, chicken embryo fibroblast; MDV, Marek's disease virus.

of membrane glycoprotein and carbohydrate molecules, mediate the adhesion of cells to cells or of cells to the ECM. Virus-activated cells regulate the expression of adhesion molecules on cells in sites of infection enhanced by virus replication (40, 41). TIMP3 plays a key role in cell adhesion and migration at the cellular level and correlates with the severity of virus infection (25, 40). AKT1 upregulated upon virus infection enhances cell adhesion and decreases cell migration (42). The PI3K/Akt signal pathway is a classical phosphorylation cascade to transduce external signals to internal responses. Some viruses benefit from more than one signaling arm of the PI3K/Akt pathway (24, 43). In the present study, AKT1 was upregulated and TIMP3 downregulated at 48 hpi to various degrees following MDV and REV coinfection comparison to a single infection. This may

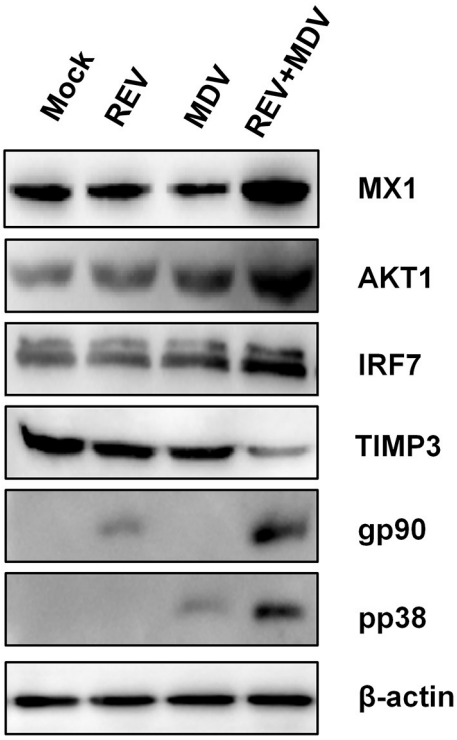

FIGURE 7 | Confirmation of four differentially expressed proteins (IRF7, MX1, AKT1, and TIMP3) in MDV and REV coinfected and single infected, and mock-infected CEF cells by Western blotting. β-Actin was used as an internal control to normalize the quantitative data. MDV, Marek's disease virus; REV, reticuloendotheliosis virus; CEF, chicken embryo fibroblast.

indicate that AKT1 and TIMP3 affect the synergistic replication of MDV and REV coinfection.

The results of our proteomics assay, the large scale of proteins associated with MDV and REV single infection and coinfection, indicates that two virus synergistic replication *in vitro* interact with the innate immune pathway, Akt pathway, and cell adhesion and migration pathway, but the detailed mechanism remains unclear.

CONCLUSIONS

Our study has provided insights into the differential manner in which the host cell proteome is regulated during single and coinfections of MDV and REV. The proteomic changes were analyzed using TMT combined with LC-MS/MS. To the best of our knowledge, this is the first time that proteomics has been used to explore the virus–host protein interaction network in MDV and REV coinfected CEF cells. The results revealed that 98 DAPs be may be associated with increased pathogenicity of MDV and REV coinfection, among which 60 were upregulated and 38 were downregulated. In addition, four DAPs were validated by Western blotting analysis. Our analyses of the DAPs were descriptive, and further functional investigations are required to elucidate the synergistic replication mechanisms and cellular responses to MDV and REV coinfection.

DATA AVAILABILITY STATEMENT

The mass spectrometry proteomics data have been deposited to the ProteomeXchange Consortium (http://proteomecentral.proteomexchange.org) *via* the iProX partner repository with the dataset identifier PXD031291. The link is https://www.iprox.cn/page/project.html?id=IPX0003983000.

AUTHOR CONTRIBUTIONS

ZC and XD took part in all the experiments and wrote the manuscript. ZC helped to design the whole project and draft the manuscript. DZ and JZ conducted cell culture and sample processing for sequencing and conducted data analysis. All authors read and approved the final manuscript.

FUNDING

This work was supported by grants from the Shandong Modern Agricultural Technology and Industry System (No. SDAIT-11-04), the Key Research and Development Program of Shandong Province (Important Science and Technology Innovation Project) (2019JZZY010735), and the Natural Science Foundation of China (No. 32072816).

ACKNOWLEDGMENTS

We are grateful to Dr. Libo Huang and Ms. Li Zhang for their technical assistance. We thank Dr. Guihua Wang and Dr. Chengui Li for their helpful discussion and manuscript revision.

SUPPLEMENTARY MATERIAL

The Supplementary Material for this article can be found online at: https://www.frontiersin.org/articles/10.3389/fvets.2022.854007/full#supplementary-material

REFERENCES

1. Osterrieder N, Kamil J, Schumacher D, Tischer B, Trapp S. Marek's disease virus: from miasma to model. *Nat Rev Microbiol.* (2006) 4:283–94. doi: 10.1038/nrmicro1382
2. Niewiadomska AM, Gifford RJ, Sugden B. The extraordinary evolutionary history of the reticuloendotheliosis. *Viruses.* (2013) 11:e1001642. doi: 10.1371/journal.pbio.1001642
3. Buscaglia C. Mixed infections of Marek's disease and reticuloendotheliosis viruses in layer flocks in Argentina. *Avian Dis.* (2013) 57:569–71. doi: 10.1637/10398-100112-Case.1
4. Chacón RD, Astolfi-Ferreira CS, Guimarães MB, Torres LN, De la Torre DI, de Sá LR, et al. Detection and molecular characterization of a natural co-infection of Marek's disease virus and reticuloendotheliosis virus in brazilian backyard chicken flock. Veterinary sciences (2019) 6(4). doi: 10.3390/vetsci6040092

5. Zhang Y, Yu Z, Lan X, Zhang F, Wang Q, Li K, et al. A high frequency of Gallid herpesvirus-2 co-infection with Reticuloendotheliosis virusis associated with high tumor rates in Chinese chicken farms. *Vet Microbiol.* (2019) 237:108418. doi: 10.1016/j.vetmic.2019.108418
6. Sun G-R, Zhang Y-P, Zhou L-Y, Lv H-C, Zhang F, Li K, et al. Co-Infection with Marek's disease virus and reticuloendotheliosis virus increases illness severity and reduces marek's disease vaccine efficacy. *Viruses.* (2017) 9:158. doi: 10.3390/v9060158
7. Zheng YS, Cui ZZ, Zhao P, Li HM, Liu CY, Tian ZJ, et al. Effects of reticuloendotheliosis virus and Marek's disease virus infection and co-infection on IFN-gamma production in SPF chickens. *J Vet Med Sci.* (2007) 69:213–6. doi: 10.1292/jvms.69.213
8. Wozniakowski G, Mamczur A, Samorek-Salamonowicz E. Common occurrence of Gallid herpesvirus-2 with reticuloendotheliosis virus in chickens caused by possible contamination of vaccine stocks. *J Appl Microbiol.* (2015) 118:803–8. doi: 10.1111/jam.12734
9. Zhang YP, Bao KY, Sun GR, Lv HC, Cui HY, Gao YL. Characterization of a Gallid herpesvirus 2 strain with novel reticuloendotheliosis virus long terminal repeat inserts. *Virus Genes.* (2017) 53:386–91. doi: 10.1007/s11262-017-1427-1
10. Zhou Z, Cui N, Su S, Sun S, Cui Z. The molecular basis for host responses to Marek's disease viruses integrated with different retro-viral long terminal repeat. *Poultry Sci.* (2018) 97:3015–22. doi: 10.3382/ps/pey135
11. Kumar N, Sharma S, Barua S, Tripathi BN, Rouse BT. Virological and immunological outcomes of co-infections. *Clin Microbiol Rev.* (2018) 31:e00111. doi: 10.1128/CMR.00111-17
12. Zheng J, Sugrue RJ, Tang K. Mass spectrometry based proteomic studies on viruses and hosts–a review. *Anal Chim Acta.* (2011) 702:149–59. doi: 10.1016/j.aca.2011.06.045
13. Scholle F, Li K, Bodola F, Ikeda M, Luxon BA, Lemon SM. Virus-host cell interactions during hepatitis C virus RNA replication: impact of polyprotein expression on the cellular transcriptome and cell cycle association with viral RNA synthesis. *J Virol.* (2004) 78:1513–24. doi: 10.1128/JVI.78.3.1513-1524.2004
14. Li H, Minarovits J. Host cell-dependent expression of latent Epstein-Barr virus genomes: regulation by DNA methylation. *Adv Cancer Res.* (2003) 89:133–56. doi: 10.1016/S0065-230X(03)01004-2
15. Hartlova A, Krocova Z, Cerveny L, Stulik J, A. proteomic view of the host-pathogen interaction: the host perspective. *Proteomics.* (2011) 11:3212–20. doi: 10.1002/pmic.201000767
16. Chien KY, Blackburn K, Liu HC, Goshe MB. Proteomic and phosphoproteomic analysis of chicken embryo fibroblasts infected with cell culture-attenuated and vaccine strains of Marek's disease virus. *J Proteome Res.* (2012) 11:5663–77. doi: 10.1021/pr300471y
17. Hu F, Li Y, Yu K, Ma X, Liu C, Guo X, et al. Proteome analysis of reticuloendotheliosis-virus-infected chicken embryo fibroblast cells through iTRAQ-based quantitative proteomics. *Arch Virol.* (2019) 164:2995–3006. doi: 10.1007/s00705-019-04409-4
18. Chen M, Li X, Zhu A, Storey KB, Sun L, Gao T, et al. Understanding mechanism of sea cucumber Apostichopus japonicus aestivation: Insights from TMT-based proteomic study. *Comp Biochem Physiol Part D Genom Proteom.* (2016) 19:78–89. doi: 10.1016/j.cbd.2016.06.005
19. Zhou D, Xue J, He S, Du X, Zhou J, Li C, et al. Reticuloendotheliosis virus and avian leukosis virus subgroup J synergistically increase the accumulation of exosomal miRNAs. *Retrovirology.* (2018) 15:45. doi: 10.1186/s12977-018-0427-0
20. Zhou J, Zhao GL, Wang XM, Du XS, Su S. Synergistic viral replication of Marek's disease virus and avian leukosis virus subgroup J is responsible for the enhanced pathogenicity in the superinfection of chickens. *Viruses.* (2018) 10:271. doi: 10.3390/v10050271
21. Szklarczyk D, Gable AL, Lyon D, Junge A, Wyder S, Huerta-Cepas J, et al. STRING v11: protein-protein association networks with increased coverage, supporting functional discovery in genome-wide experimental datasets. *Nucleic Acids Res.* (2019) 47:D607–d613. doi: 10.1093/nar/gky1131
22. Honda K, Taniguchi T. IRFs: master regulators of signalling by Toll-like receptors and cytosolic pattern-recognition receptors. *Nat Rev Immunol.* (2006) 6:644–58. doi: 10.1038/nri1900
23. Spitaels J, Van Hoecke L, Roose K, Kochs G, Saelens X, et al. Mx1 in hematopoietic cells protects against thogoto virus infection. *J Virol.* (2019) 93:e00193–19. doi: 10.1128/JVI.00193-19
24. Phosphatidylinositol-3-kinase-Akt pathway in negative-stranded RNA virus infection: a minireview. *Arch Virol.* (2020) 165(10), 2165–2176 doi: 10.1007/s00705-020-04740-1
25. Han J, Jing Y, Han F, Sun P. Comprehensive analysis of expression, prognosis and immune infiltration for TIMPs in glioblastoma. *BMC Neurol.* (2021) 21:447. doi: 10.1186/s12883-021-02477-1
26. Ghedin E, Fitch A, Boyne A, Griesemer S, DePasse J, Bera J, et al. Mixed infection and the genesis of influenza virus diversity. *J Virol.* (2009) 83:8832–41. doi: 10.1128/JVI.00773-09
27. Potiwat R, Komalamisra N, Thavara U, Tawatsin A, Siriyasatien P. Competitive suppression between chikungunya and dengue virus in Aedes albopictus c6/36 cell line. *Southeast Asian J Trop Med Public Health.* (2011) 42:1388–94.
28. Kumar N, Barua S, Riyesh T, Chaubey KK, Rawat KD, Khandelwal N, et al. Complexities in isolation and purification of multiple viruses from mixed viral infections: viral interference, persistence and exclusion. *PloS ONE.* (2016) 11:e0156110. doi: 10.1371/journal.pone.0156110
29. Gonzalez Alvarez DA, Lopez Cortes LF, Cordero E. Impact of HIV on the severity of influenza. *Exp Rev Resp Med.* (2016) 10:463–72. doi: 10.1586/17476348.2016.1157474
30. Goto H, Ihira H, Morishita K, Tsuchiya M, Ohta K, Yumine N, et al. Enhanced growth of influenza A virus by co-infection with human parainfluenza virus type 2. *Med Microbiol Immunol.* (2016) 205:209–18. doi: 10.1007/s00430-015-0441-y
31. Mendez-Rios J, Uetz P. Global approaches to study protein-protein interactions among viruses and hosts. *Fut Microbiol.* (2010) 5:289–301. doi: 10.2217/fmb.10.7
32. Kunec D. Proteomics applied to avian herpesviruses. *Avian Dis.* (2013) 57(2 Suppl):351–9. doi: 10.1637/10483-010413-Reg.1
33. Xiao Y, Wu W, Gao J, Smith N, Burkard C, Xia D, et al. Characterization of the interactome of the porcine reproductive and respiratory syndrome virus nonstructural protein 2 reveals the hyper variable region as a binding platform for association with 14-3-3 proteins. *J Proteome Res.* (2016) 15:1388–401. doi: 10.1021/acs.jproteome.5b00396
34. Levy DE, Garcia-Sastre A. The virus battles: IFN induction of the antiviral state and mechanisms of viral evasion. *Cytokine Growth Factor Rev.* (2001) 12:143–56. doi: 10.1016/S1359-6101(00)00027-7
35. Brennan K, O'Leary BD, Mc Laughlin D, Breen EP, Connolly E, Ali N, et al. Type 1 IFN induction by cytosolic nucleic acid is intact in neonatal mononuclear cells, contrasting starkly with neonatal hyporesponsiveness to TLR ligation due to independence from endosome-mediated IRF3 activation. *J Immunol.* (2018) 201:1131–43. doi: 10.4049/jimmunol.1700956
36. Diwakar S, Dennis R, Luis MS, Muhammad M. Avian interferons and their antiviral effectors. *Front Immunol.* (2017) 8:49.
37. Wu J, Chen ZJ. Innate immune sensing and signaling of cytosolic nucleic acids. *Annu Rev Immunol.* (2014) 32:461–88. doi: 10.1146/annurev-immunol-032713-120156
38. Bai L, Zhang W, Tan L, Yang H, Ge M, Zhu C, et al. Hepatitis B virus hijacks CTHRC1 to evade host immunity and maintain replication. *J Mol Cell Biol.* (2015) 7:543–56. doi: 10.1093/jmcb/mjv048
39. Pang Y, Zhou D, Xue J, Zhou J, Zhang Y, Zheng G, et al. Interplay between CTHRC1 and the SU protein of avian leukosis virus subgroup J (ALV-J) facilitates viral replication. *Virus Res.* (2019) 264:32–9. doi: 10.1016/j.virusres.2019.02.014
40. Liao B, Tang Y, Hu F, Zhou W, Yao X, Hong W, et al. Serum levels of soluble vascular cell adhesion molecules may correlate with the severity of dengue virus-1 infection in adults. *Emerg Microb Infect.* (2015) 4:1–17. doi: 10.1038/emi.2015.24
41. Marker O, Scheynius A, Christensen JP, Thomsen AR. Virus-activated T cells regulate expression of adhesion molecules on endothelial cells in sites of infection. *J Neuroimmunol.* (1995) 62:35–42. doi: 10.1016/0165-5728(95)00099-N
42. Ma WL, Jeng LB, Lai HC, Liao PY, Chang C. Androgen receptor enhances cell adhesion and decreases cell migration via modulating β1-integrin-AKT signaling in hepatocellular carcinoma cells. *Cancer Lett.* (2014) 351:64–71. doi: 10.1016/j.canlet.2014.05.017

43. Dunn EF, Connor JH. HijAkt: the PI3K/Akt pathway in virus replication and pathogenesis. *Prog Mol Biol Transl ENCE.* (2012) 106:223–50. doi: 10.1016/B978-0-12-396456-4.00002-X

Conflict of Interest: The authors declare that the research was conducted in the absence of any commercial or financial relationships that could be construed as a potential conflict of interest.

Publisher's Note: All claims expressed in this article are solely those of the authors and do not necessarily represent those of their affiliated organizations, or those of the publisher, the editors and the reviewers. Any product that may be evaluated in this article, or claim that may be made by its manufacturer, is not guaranteed or endorsed by the publisher.

frontiers in Veterinary Science

ORIGINAL RESEARCH
published: 28 March 2022
doi: 10.3389/fvets.2022.871826

Molecular Epidemiology and Pathogenic Characterization of Novel Chicken Infectious Anemia Viruses in Henan Province of China

Xin-Wei Wang[1†], Jie Feng[1†], Jia-Xin Jin[1], Xiao-Jing Zhu[1], Ai-Jun Sun[1], Hua-Yuan Liu[2], Jing-Jing Wang[1], Rui Wang[1], Xia Yang[1], Lu Chen[1], Yi-Fei Liao[3] and Guo-Qing Zhuang[1]*

[1] College of Veterinary Medicine, Henan Agricultural University, Zhengzhou, China, [2] Wolong Animal's Sanitation Administration, Nanyang, China, [3] Division of Infectious Disease, Department of Medicine, Brigham and Women's Hospital and Harvard Medical School, Boston, MA, United States

OPEN ACCESS

Edited by:
Aijian Qin,
Yangzhou University, China

Reviewed by:
Tongling Shan,
Shanghai Veterinary Research Institute (CAAS), China
Yani Sun,
Northwest A&F University, China

***Correspondence:**
Guo-Qing Zhuang
gqzhuang2008@163.com

[†] These authors have contributed equally to this work

Specialty section:
This article was submitted to Veterinary Infectious Diseases, a section of the journal Frontiers in Veterinary Science

Received: 08 February 2022
Accepted: 07 March 2022
Published: 28 March 2022

Citation:
Wang X-W, Feng J, Jin J-X, Zhu X-J, Sun A-J, Liu H-Y, Wang J-J, Wang R, Yang X, Chen L, Liao Y-F and Zhuang G-Q (2022) Molecular Epidemiology and Pathogenic Characterization of Novel Chicken Infectious Anemia Viruses in Henan Province of China. Front. Vet. Sci. 9:871826. doi: 10.3389/fvets.2022.871826

Chicken infectious anemia (CIA) is an immunosuppressive disease caused by the chicken infectious anemia virus (CIAV) resulting in heavy economic losses once an outbreak is established. This study conducted a systematic analysis of the epidemiology and pathology of CIA in Henan province, China. A total of 437 clinical tissue samples and 120 poultry disease-related live attenuated vaccines were collected during 2017–2020; of which 45 were positive for CIAV nucleic acid, with a positive rate of 8.08%. Our results showed that genome sequence similarity among a total of 12 CIAV isolates was high, and ranged from 97.1 to 99.3%, and their similarity to the vaccine strains Cux-1 and Del-Ros ranged from 97.8 to 98.6%. However, There were mutations in the locus of the major capsid proteins VP1, VP2, and VP3 among all isolates. The subsequent sequence analysis indicated that the isolates of HN-4 and HN-8 showed genetic recombination and follow up animal experiments revealed that HN-4 might be a pathogenic strain. Our results reveal that both field infection and non-CIAV vaccines contamination promote the epidemiology of CIAV in China and some dominant epidemic viruses have undergone recombination and evolution. This study provides important information to help with the prevention and control of CIAV in the poultry industry.

Keywords: epidemiology, immunosuppressive disease, live attenuated vaccine, recombination, chicken infectious anemia

INTRODUCTION

Chicken infectious anemia (CIA) is a viral disease caused by the chicken infectious anemia virus (CIAV). The disease is characterized by aplastic anemia and lymphatic atrophy (1). CIAV is a non-encapsulated, symmetrical icosahedral virus particle, with an average diameter of 25 nm. The genome of CIAV is single-stranded, circular, negative-stranded covalently closed DNA, of ∼2 kb, which contains three partially overlapping open reading frames (ORF) encoding VP1, VP2, and VP3, respectively (2). VP1 represents the nucleocapsid protein of CIAV and is the main immunogen, which encodes an arginine-rich polypeptide with a molecular weight of approximately

50 Ka (3). VP2 is an auxiliary scaffold protein required for CIAV assembly, which helps VP1 to form the correct conformation (4), and both VP1 and VP2 can cooperate with each other to induce an immune response. VP3 represents a functional protein of the virus, which is also known as apoptin (5) and studies have found that transfection of the *VP3* gene into chicken monocyte cultures, can induce apoptosis, highlighting its importance in CIAV infection (6).

CIAV mainly invades the bone marrow and thymus of the central immune organ, leading to yellowing of the bone marrow and atrophy of the thymus, and can also cause aplastic anemia and immunosuppression (7). As one of the important poultry diseases, CIAV infection can either directly reduce the protective efficacy of certain vaccines, or enhance pathogenicity of attenuated vaccines, leading to immune failure (8, 9). The natural mortality rates from CIAV infection in the clinic is approximately 10–20%. Due to the low mortality rates and masked infectivity, CIAV has often been neglected in clinical settings (10). However, the latent infection causes chicken immunosuppression, which enhances the invasion of other opportunist pathogens including bacteria and viruses, which ultimately lead to chicken growth and development disorders (11). Significantly, CIAV can transmit both horizontally and vertically. Horizontal transmission occurs in the flock usually from the feces, danders or feathers, mainly through oral infection. More importantly however, vertical infection is derived from breeding eggs, which can easily result in an outbreak of CIA in the offspring. Furthermore, previous studies have highlighted the fact that vertical transmission still exists, even if there is an immune response in infected hens (12).

CIAV infection has recently spread globally causing severe economic losses. For example, 32 CIAV sequences were identified in 2010 in South Korea (13). In India, 351 serum samples were positive out of 404 (86.88%) collected from chicken flocks in 11 poultry farms (14), and in northern Vietnam, there were 74 positive tests from 119 samples (62.2%) collected from 64 farms (15). In China, CIAV has been detected in poultry farms from most provinces, and has been successfully isolated both from live non-CIAV vaccines and specific pathogen free (SPF) chickens (16), which may explain the reason for the CIAV contamination found in the field. Interestingly, co-infection of four immunosuppressive pathogens including CIAV has been detected in Shandong Province (17, 18). Recently, 1,187 clinical samples from major poultry farms nationwide from 2017 to 2020, have been tested for co-infection with six immunosuppressive pathogens including CIAV (19). These surveys have confirmed the widespread nature of CIAV in China, which has seriously affected the development of the poultry industry. However, there is a paucity of information relating to CIAV infection in the central region of China. Therefore, an epidemiological investigation of CIA was carried out on samples collected from chicken farms and live attenuated non-CIAV vaccines in the markets of Henan Province, and the genomes of CIAV epidemic strains in this region were systematically analyzed. Furthermore, the pathogenesis of one recombinant strain has been investigated further.

Abbreviations: CIA, Chicken infectious anemia; CIAV, Chicken infectious anemia virus; NDV, Newcastle disease virus; IB, Infectious bronchitis; FPV, Feline parvovirus; MS, Multiple sclerosis; ILTV, Infectious laryngotracheitis virus; ORF, Open Reading Frame; MSB1, Marek's disease lymphoblastoid cell; PBS, Phosphate-buffered saline; SPF, Specific pathogen free; PCR, Polymerase chain reaction; NCBI, National Center for Biotechnology Information; H&E, Hematoxylin-eosin.

MATERIALS AND METHODS

Sample Collection

During 2017–2020, the spleen samples were collected from 5–10 weeks old sick chicken of 437 flocks produced throughout Henan province, China, diagnosed by the Poultry Disease Research Institute of Henan Agricultural University. In brief, spleens from suspected chickens containing CIAV were cut into small pieces and place into a sterile tube. Samples were then homogenized three times in phosphate buffer saline (PBS) using small steel balls in an automated tissue grinder. Next, the samples were freeze/thawed three times to encourage the release of the virus. The viral supernatant was isolated by centrifugation at 8,000 rpm and then transferred into a new sterile tube. A total of 120 non-CIAV live attenuated vaccines were collected from 24 manufacturers and five different batches for CIAV detection.

Virus Amplification

Marek's disease lymphoblastoid cells (MSB1), a kind gift from Professor Jun Ji, Nanyang Normal University, Henan province were cultured in 1640 culture medium with 10% fetal bovine serum (Solarbio, Beijing, China). When the cells reached confluency at 5×10^5 cells/cm^3, they were centrifuged at 1000 rpm for 5 min and washed twice with sterile PBS to remove residual serum. Then the CIAV containing supernatant was added for virus adsorption for 1 h. After this step, MSB1 cells were cultured in 5 mL of 1640 medium containing 2% fetal bovine serum and when visible enlarged and broken CIAV infected cells could be seen, the infected cells were passaged blind five times with fresh MSB1 cells, for viral amplification.

Nucleic Acid Extraction and CIAV Detection

Genomic DNA was extracted from the chicken samples using a commercial kit (TIANamp Genomic DNA Kit, Tiangen, Beijing, China) and used according to the manufacturer's instructions. Three pairs of primers for amplification of the CIAV genome were designed and synthesized by Primer Premier 5.0 (Sangon Biotech, Shanghai, China). The primers for gene amplification were designed based on CUX-1 sequence (accession number M55918). The first primer pair were as follows: forward primer 5′-GCATTCCGAGTGGTTACTATTCC-3′, reverse primer 5′-CGTCTTGCCATCTTACAGTCTTAT-3′; and these primers were expected to produce a predicted amplicon size of 842 bp. The second primer pair were as follows: forward primer 5′-CGA GTACAGGGTAAGCGAGCTAAA-3′, reverse primer 5′-TGC TATTCATGCAGCGGACTT-3′; and these primers produced a predicted amplicon size of 990 bp. The final set of primers were as follows: forward primer 5′-GAAAATGAGACCCGACGAGCA

ACAG-3′, reverse primer 5′-GATTCGTCCATCTTGACTTTCT GTG-3′, and these primers produced a predicted amplicon size of 736 bp. There three pairs of primers are used for CIAV detection and sequencing analysis. The polymerase chain reaction (PCR) was performed in a total volume of 50 μL, containing 18 μL of 2 x Taq Master Mix, 1 μL (10 μm/L) of each primer, 27 μL of distilled water, and 3 μL of template DNA. The PCR cycling conditions for amplification were as follows: 95°C pre-denaturation for 5 min; 95°C denaturation for 30 s, 60°C annealing for 30 s, and 72°C extension for 30 s. Amplification was performed over 35 cycles with a final extension at 72°C for 10 min. The PCR products were then resolved using 1% agarose gel electrophoresis, and included both positive and negative controls.

Sequencing Analysis

The PCR products were purified with a PCR gel recovery kit and cloned into PMD18-T vectors and sent to Sangon Biotech for sequencing. The sequencing results were analyzed by the DNASTAR7.1 (DNASTAR, Inc., WI, USA), and then aligned using the BLAST program on the National Center for Biotechnology Information (NCBI) website (www.ncbi.nlm.nih.gov) to reference strains (**Supplementary Table 1**). Next, the MEGA 6.0 software (https://www.megasoftware.net) was used for phylogenetic analysis. The RDP 4.0 software was used for recombination analysis of the isolates. The positive recombinant isolate was determined by at least five methods of RDP, GENECONV, BootScan, MaxChi, Chimera, SiScan, Phyl-Pro, LARD And 3Seq (20).

Animal Experiments

SPF chickens (Qian yuan hao biotechnology Co, Zhengzhou, China) were used for all animal experiments. Forty one-day-old SPF white broilers were wing-banded upon hatching, and housed in isolators, and randomly sorted into experimental groups. An additional group was used as control. To determine the pathogenic properties of the NH-4 isolate, experimental groups from one-day-old SPF chickens were inoculated with 0.1 ml of HN-4 in the muscle tissue, whereas the chickens in the control group were inoculated with an identical volume of physiological saline. All chickens that had died during the experiment (21 days), or were euthanized at the end of the experiment, were necropsied and examined for CIAV-related pathology.

To evaluate the effect of HN-4 on body weight and lymphoid organs, three chickens in each group were euthanized at 7, 14, and 21 days post-infection, and their body weight and lymphoid organ weights (thymus and bursa) were measured. The ratio of the lymphoid organs was expressed as the weight of lymphoid organ divided by the body weight for each chicken, multiplied by one hundred.

For hematoxylin-eosin (H&E) staining, tissues were formalin fixed and paraffin embedded and 6–8 μm-thick sections were prepared. H&E staining was carried out following regular procedures and sections were examined under a microscope.

Data Analysis

The ratio of the lymphoid organs and survival rates were analyzed using GraphPad Prism version 8.0.1 software (GraphPad Software, Inc. La Jolla, CA). Statistical *t*-test analysis was used for each data point, which represented a triplicate average and a value of $P < 0.05$ was considered statistically significant.

RESULTS

Complete Gene Sequence Analysis of Isolated CIAVs

A total of 41 spleen samples were detected to be CIAV positive from 437 sick chickens collected from June 2017 to January 2020 in Henan province. The overall positive rate was 9.4% (95% CI: 6.8–12.5%). Four CIAV positive vaccines in 120 non-CIAV live attenuated vaccines were detected, and the overall positive rate was 3.33% (95% CI: 0.9–8.3%) (**Table 1**). A total of 12 CIAV strains were isolated and identified by PCR from chicken samples and as shown in **Supplementary Figure 1**, the amplicon sizes were 842 bp, 990 bp, and 736 bp, respectively, and this was consistent with prediction.

The whole genome sequences of 12 isolates were amplified and aligned to the reference strain. Four strains of CIAV virus (HN-1, HN-8, HN-9, HN-12) had a similarity between 98.1 and 99.7%, of which, HN-1 and HN-9 had the highest similarity. These four isolates are more closely related to the American strain L14767.1, with a similarity of over 98%. Compared to the vaccine strains that have been widely used worldwide, the 12 isolates had high sequence similarity with the Del-Ros vaccine strain ranged from 97.8 to 98.6%, but was less than 98% with Cux-1 vaccine strain (**Supplementary Figure 2**).

A phylogenetic tree, represented by two large branches, was constructed based on the complete genome sequence of 44 reference strains and 12 isolates. All of the isolates were on the same large branch, which was closely related to the CIAV strains derived from Asia. After subdivision, the isolates became located

TABLE 1 | CIAV test from collected spleens and attenuated vaccine circulating in the market.

Sample type	Number of samples tested	Number of positive samples	Positive rate (%)
Spleen	437	41	9.4
NDV + IB vaccine strain	53	3	5.66
FPV vaccine strain	31	1	3.23
NDV vaccine strain	34	0	0
MS vaccine strain	1	0	0
FPV + ILTV vaccine strain	1	0	0

NDV, Newcastle disease virus; IB, Infectious bronchitis; FPV, Feline parvovirus; MS, Multiple sclerosis; ILTV, Infectious laryngotracheitis virus.

to three different small branches. The four strains HN-3, HN-5, HN-7, HN-10, and HN-11 were on the same branch as the CIAV strains isolated from Shandong and Liaoning, and closely related to the classical attenuated strain C369 and CIAVV89-69. Another three strains HN-2, HN-4, and HN-6 appeared on the same branch as the HN1405 strain isolated from Shandong. HN-1, HN-8, HN-9, and HN-12 are on the same branch as the HN1504 strain. All of the CIAV strains isolated in Henan are far removed from the internationally prevalent vaccine strain Cux-1, and are not on the small branch with the Del-Ros vaccine strain (**Figure 1A**).

Amino Acid Sequence Analysis of the VP1 and VP2 Proteins

Amino acid sequence analysis based on the VP1 sequence (450 aa) showed that the overall variation in VP1 protein from all of the isolates was 0–3.4%. The similarity in the VP1 amino acid sequence for the HN-1 and HN-12 strains reached 100% (**Supplementary Figure 3**). When comparing the VP1 protein amino acid evolutionary tree (**Figure 1B**), and the nucleotide sequence evolutionary tree (**Figure 1C**), we found that the VP1 nucleotide tree was roughly the same as the whole genome nucleotide evolutionary tree. When we compared the amino acid trees, we found HN-3, HN-4, and HN-7 were on the same branch as GD-1-12, while the HN-3 and HN-7 isolates were on the same branch as the HN-5 and HN-10 isolates. Finally, the HN-4 isolate was on the same branch as the HN-2 and HN-6 isolates. Therefore, it can be inferred that there may exist site mutations, or sequence recombinations in these strains at the amino acid level.

VP2 is the most conserved CIAV protein and there are no significant differences at the amino acid level between the isolates and the reference strain, and the co-efficient of variance was less than 2.3% **Supplementary Figure 4**. The VP2 nucleotide phylogenetic tree (**Figure 1D**) and amino acid phylogenetic tree (**Figure 1E**) displayed no obvious phylogenetic pattern. The VP3 protein from the isolates and reference strain, are more conservative at the amino acid level with a difference co-efficient of 0–1.7% (**Supplementary Figure 5**). The nucleotide phylogenetic tree (**Figure 1F**) and the amino acid phylogenetic tree (**Figure 1G**) of VP3 had no obvious phylogenetic pattern.

Analysis of Major Amino Acid Sites in VP1, VP2, and VP3 Proteins

Previous studies have confirmed that the hypervariable region in the VP1 sequence is at amino acid position 13, in which amino acids 139 and 144 have an effect on the replication rate and infection efficiency of the virus in infected cells (21). When the 139 th and 144 th amino acids of the strain were glutamine

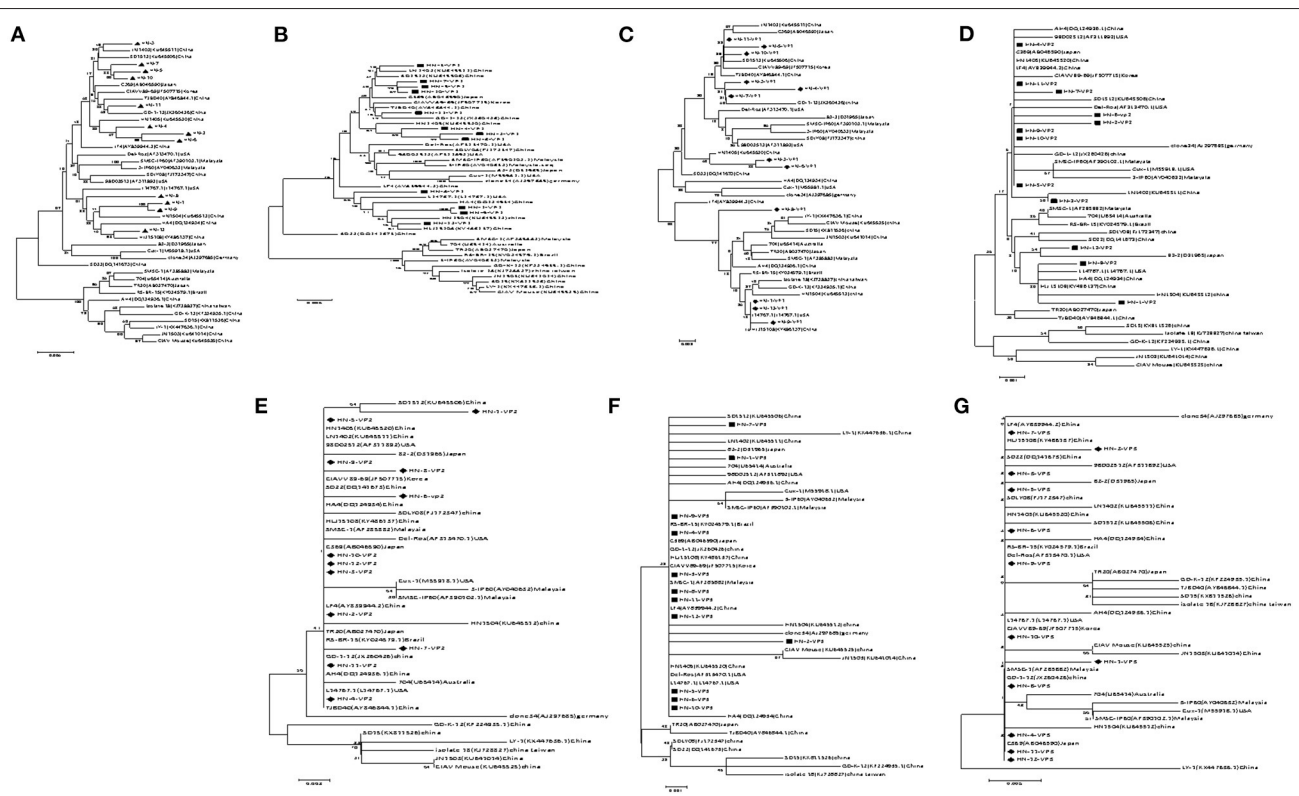

FIGURE 1 | Evolutionary tree analysis of **(A)** Whole genome sequence evolutionary tree analysis; **(B)** Nucleotides of VP1; **(C)** Amino acids of VP1; **(D)** Nucleotides of VP2; **(E)** Amino acids of VP2; **(F)** Nucleotides of VP3; **(G)** Amino acids of VP3.

TABLE 2 | Main amino acid positions in the VP1 protein.

Virus strain	VP1 amino acid site												
	22	75	97	125	139	144	157	287	290	370	376	413	446
Cux-1	H	V	M	I	K	D	V	A	A	S	L	A	T
Del-Ros	.	.	.	.	.	E	.	S	.	G	.	S	G
C369	.	.	.	L	.	E	.	S	.	G	I	S	S
GD-1-12	.	.	.	L	.	E	M	S	.	G	I	S	S
HN1405	.	.	.	L	.	E	.	S	.	A	.	.	S
HN1504	N	I	L	.	Q	Q	.	.	.	.	.	.	S
SMSC-IP60	.	.	.	.	.	E	M	S	.	G	.	.	.
SDLY08	N	.	.	.	.	E	.	S	.	G	.	S	.
HN-1	N	I	L	.	Q	Q	.	.	.	.	.	.	S
HN-2	.	.	L	L	.	E	M	S	.	A	.	.	S
HN-3	.	.	.	L	.	E	M	S	.	G	I	.	S
HN-4	.	.	L	L	.	E	M	N	P	G	I	S	S
HN-5	.	.	.	L	.	E	.	S	.	G	I	S	S
HN-6	.	.	L	L	.	E	M	T	P	A	.	.	S
HN-7	.	.	.	L	.	E	M	S	.	G	I	S	S
HN-8	N	I	L	.	Q	Q	.	.	P	G	I	.	S
HN-9	N	I	L	.	Q	Q	.	.	.	.	.	.	S
HN-10	.	.	.	L	.	E	.	S	.	G	I	S	S
HN-11	.	.	.	L	.	E	.	S	.	G	I	S	S
HN-12	N	I	L	.	Q	Q	.	.	.	.	.	.	S

(Q), the proliferation rate was significantly slower. In this study, the amino acid sites for the VP1 protein in the 12 isolates and previously isolated strains from Henan were all analyzed. Among these, HN-1, HN-8, HN-9, and HN-12 strains all carried Q139 and Q144, the same as those of the HN1504 strain. The other eight CIAV isolates (HN-2, HN-3, HN-4, HN-5, HN-6, HN-7, HN-10, and HN-11) carried the amino acid lysine (K) at position 139 and glutamate (E) at position 144. All the viruses isolated from Henan contained Q, at position 394, suggesting that the isolates from Henan had pathogenicity. HN-4, HN-6, and HN-8 had an A290P mutation, which has never been previously reported. In addition, there is a S287N mutation in the HN-4 strain and an S287T mutation in the HN-6 strain. However, whether this mutation influences its pathogenicity, needs further investigation (**Table 2**).

The amino acid sites of the VP2 and VP3 proteins were relatively conserved with only a few mutated amino acid positions. In VP2, five alternative amino acid mutations were observed: G31E, A53V in the HN-1 isolate, S13R in HN-6 isolate, K102E in HN-7 isolate, and G24E in the HN-8 isolate. In VP3, P18S was observed in HN-1 isolates, and A54G was observed in HN-2 isolates (**Table 3**).

TABLE 3 | Main amino acid positions in the VP2 and VP3 proteins.

Virus strain	VP2 amino acid site				VP3 amino acid site		
	13	24	31	53	102	18	54
Cux-1	S	G	G	A	K	P	A
Del-Ros	.	.	.	.	.	.	.
C369	.	.	.	.	.	.	.
GD-1-12	.	.	.	.	.	.	.
HN1405	.	.	.	.	.	.	.
HN1504	.	.	.	.	.	.	.
SMSC-IP60	.	.	.	.	.	.	.
SDLY08	.	.	.	.	.	.	.
HN-1	.	.	E	V	.	S	.
HN-2	.	.	.	.	.	.	G
HN-3	.	.	.	.	.	.	.
HN-4	.	.	.	.	.	.	.
HN-5	.	.	.	.	.	.	.
HN-6	R	.	.	.	.	.	.
HN-7	.	.		.	E	.	.
HN-8	.	E	.	.	.	.	.
HN-9	.	.	.	.	.	.	.
HN-10	.	.	.	.	.	.	.
HN-11	.	.	.	.	.	.	.
HN-12	.	.	.	.	.	.	.

Recombination Sequence Analysis

Recombination analysis between all isolates and reference strains using RDP 4 software showed that recombination events occurred between different strains. Among them, HN-4 and HN-8 strains may be two potential recombinant strains. The isolate HN-4 may be a potential recombinant strain between the Korean isolate CIAVV89-69 and the Henan isolate HN-2. Bootscan analysis of the sequence of the HN-4 strain and its major and minor parental strains was conducted. The Korean strain CIAVV89-69 was found to be the major parental strain, while the

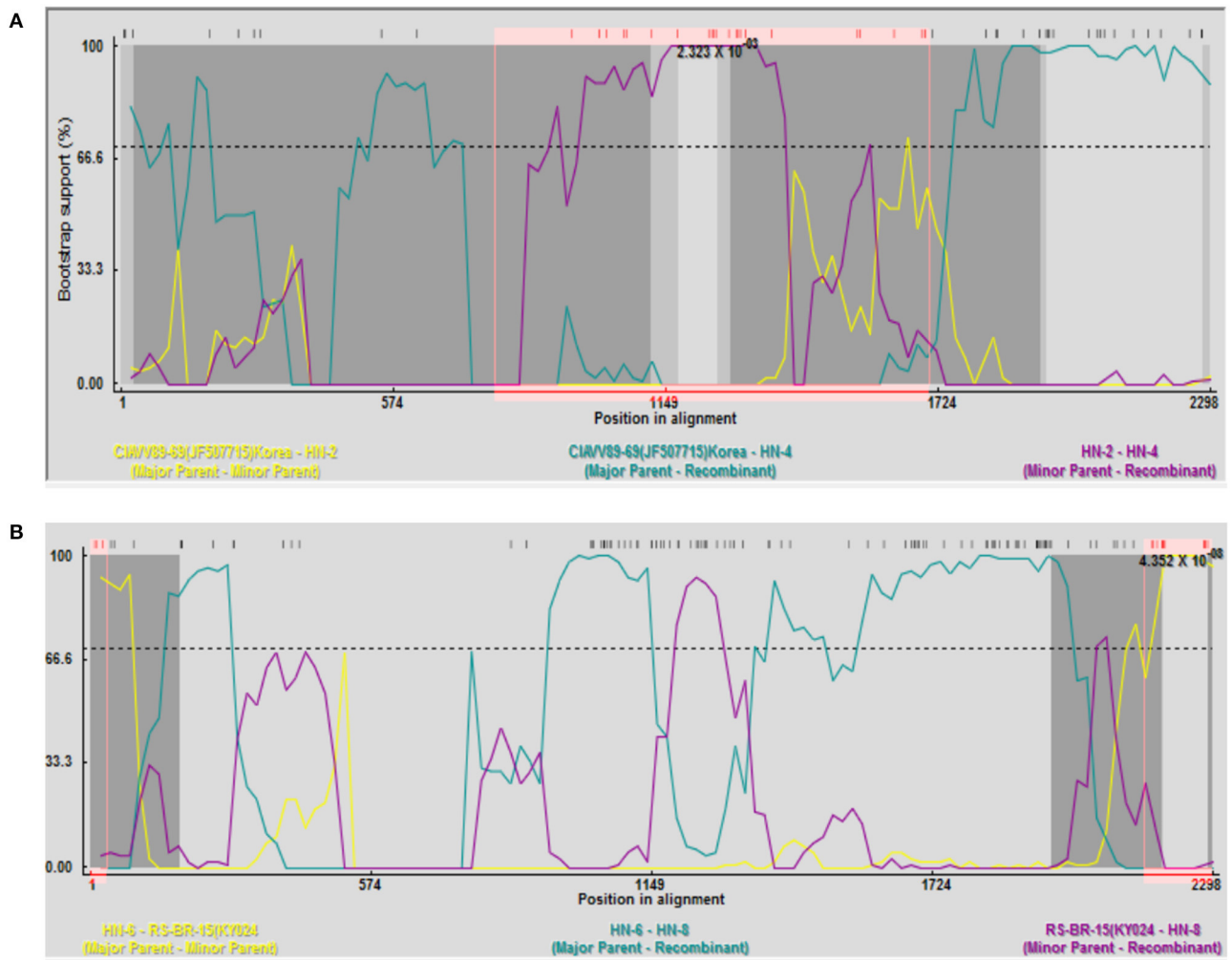

FIGURE 2 | Recombination analysis of the **(A)** HN-4 strain; and **(B)** HN-8 strain. **(A)** Bootscan analysis of HN-4 strain and sequences of primary and secondary parents. Korean strain CIAVV89-69 was the main parent, and Henan strain HN-2 was the secondary parent, whose recombinant breakpoints were mapped to sites 787 and 1707. Bootscan analysis of HN-8 strain and sequence of primary and secondary parents. Henan strain HN-6 was the main parent, and Brazilian strain RS-BR-15 was the secondary parent, whose recombinant breakpoints were mapped to sites 36 and 2155.

Henan strain HN-2 represented the minor parental strain, and its recombination breakpoint was mapped to position 787 (initial breakpoint) and 1,707 (termination breakpoint) (**Figure 2A**).

Isolate HN-8 may represent a potential recombinant strain between the Brazilian isolate RS-BR-15 and the Henan isolate HN-6. Here, we used Bootscan analysis of the sequence of the HN-8 strain and its major and minor parental strains. We found that the Henan isolate HN-6 was the major parental strain, while the Brazilian isolate RS-BR-15 was the minor parental strain, and its recombination breakpoint was mapped to position 36 (initial breakpoint) and 2,155 (termination breakpoint) (**Figure 2B**).

Pathogenesis of HN-4

It has been found that CIAV could be isolated using MSB1 cells, but different strains have great differences in susceptibility infection (22). We found that only HN-4 strains and HN-6 strains could be propagated on MSB1 cells. Sequence analysis showed that only HN-4 has gene recombination. To examine the biological characteristics of the CIAV field isolates, we conducted analyses of their pathogenicity by infecting one-day-old SPF chickens with the HN-4 strain. As expected, there were no pathogenic symptoms in the control group. In the experimental group, however, no death was seen from day 1 to day 13, but chickens showed depression, were somnolent, displayed abnormal development and had a significantly lower body weight ($P < 0.001$) (**Figure 3A**). Chickens in the experiment group died continuously from 14 days post infection, with a total of 10 in 20 deaths seen up until the end of the experiment (21 days) (**Figure 3B**). At necropsy, no obvious pathological changes were seen in their livers and kidneys, but significant atrophy was seen in the spleen, bursa, and thymus, when compared to the control group (**Figure 3C**). The tibia of chickens infected with HN-4

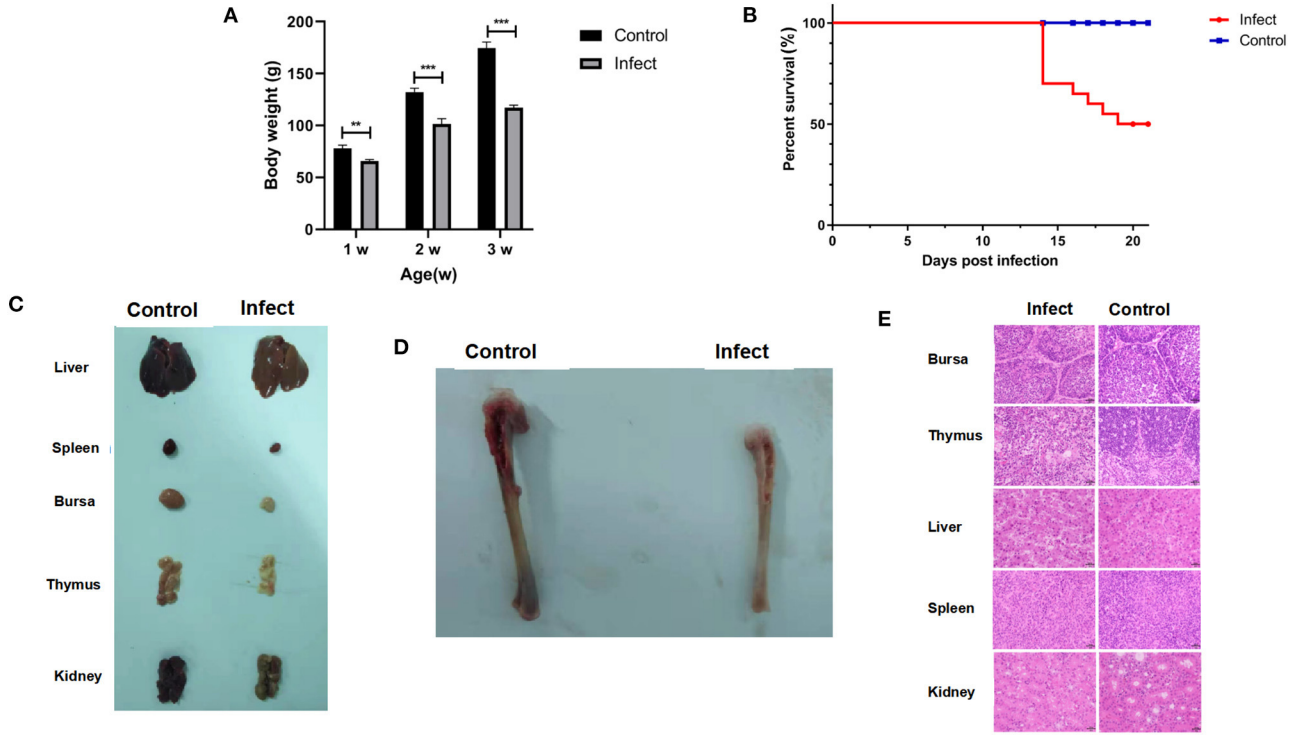

FIGURE 3 | Pathogenic characterization of HN-4. **(A)** Body weight changes in chickens of different ages (weeks) after HN-4 infection; The statistical differences between groups were examined by student *t*-test. ** and *** represent $p < 0.001$. **(B)** Survival rate of chickens infected with HN-4. **(C)** Bone marrow changes in chickens infected with HN-4 after 16 days, Compared with the control group, there were no obvious pathological changes in liver and kidney, but obvious atrophy of spleen, bursa of Fabricius and thymus. **(D)** Pathological changes in various organs from chickens infected with HN-4 after 16 days, The tibia of the chicken infected with HN-4 is thin and fragile, and the bone marrow is yellow. **(E)** Histopathology in different tissues at day 16 post infection (H&E staining, original magnification × 400). The number of lymphocytes decreased significantly in bursa of Fabricius, thymus, spleen and kidney. Compared with the control group, the hepatocytes atrophied, the thymocytes edema and degeneration appeared "vacuole-like," and the inclusion bodies in the virus nucleus could be seen. Among of the figures, infect means CIAV infection.

was thin and fragile and had yellowish colored bone marrow (**Figure 3D**).

To further evaluate the pathogenicity of the HN-4 strain, histological lesions were examined on day 16 in the bursa, thymus, liver, spleen, and kidney. Our findings revealed that there was a significantly reduced number of lymphocytes in the Bursa, Thymus, spleen, and kidney. Whereas liver cells displayed metatropy when compared to the control group (**Figure 3E**). These results revealed that HN-4 is a pathogenic strain.

DISCUSSION

CIAV infection of its natural host, the chicken, results in a low mortality rate, however, CIAV infection does cause important symptoms such as a poor immune response and even immune failure in its host, resulting in invasion of secondary pathogens, which can then induce a huge economic loss to the poultry industry (23). Therefore, it is vital to perform epidemiological and pathological investigations to help control the spread of CIA. We performed a PCR survey of CIAV infection, which was carried out on 437 samples collected from September 2017 to January 2020, with a positive rate of 9.4% (95% CI: 6.8–12.5%), confirming the prevalence of CIA in the field, in the Henan province region of China.

In addition, the safety of a potential vaccine is closely related to the health of chickens (24). Here, we investigated the extent of CIAV contamination in the live attenuated non-CIAV vaccines sold at market in Henan Province. A molecular epidemiological survey was conducted on vaccine samples from 24 manufacturers, with a total of 120 attenuated non-CIAV vaccines. The results showed that the overall positive rate was 3.3% (95%CI: 0.9–8.3%), indicating that the necessity for biological product quality control. In the present study, CIAV was mainly tested in the Newcastle disease vaccine, bivalent live attenuated vaccine of Newcastle disease, Avian infectious bronchitis, and Fowlpox live vaccines. Possible CIAV contamination in other important avian diseases, also needs to be further investigated. Unfortunately, we did not isolate or identify live CIAV from these non-CIAV vaccines.

We did however, isolate and identify 12 CIAV strains from chicken samples, and then analyzed their genome sequences. The nucleotide variations among all the isolates ranged from 0.75 to 3.9%, indicating little difference between these strains and the

reference strains. The high identity seen in the Henan isolates suggested that these strains are highly conserved. Phylogenetic results revealed that the 12 CIAV strains were in one large branch, most of which were Asian isolates. These isolates were further divided into three branches, where HN-3, HN-5, HN-7, HN-10, and HN-11 were all on the same branch as the Japanese classical attenuated strain C369 and the Korean attenuated strain CIAV 89-69 (25). Among them, HN-11 was on the same small branch as Guangdong isolate GD-1-12 (26). The three strains HN-2, HN-4, and HN-6 were on the same branch as the former Henan HN1405 strain, whereas the HN-1, HN-8, HN-9, and HN-12 strains were on the same branch as the former Henan HN1504 strain, indicating that these strains might be the dominant strains in Henan province. However, there were no similar branches seen for the international vaccine strains Cux-1 and Del-Ros (27). These results indicate that the Henan isolates may be epidemic strains, after a natural recombination and evolutionary event in Asia.

Of the three intact proteins found in the isolates, VP1 protein had the most amino acid site variations. Previous studies have confirmed that higher virulence strains are seen when position 394 in VP1 protein is Q, which represents the main genetic determinant of CIAV virulence (28). In this study, all isolates had Q at this position, indicating that the viral strains have strong virulence. HN-4, HN-6, and HN-8 have A 290 to P mutations at position 290, which has never been previously reported. However, VP2 and VP3 were relatively conserved, which may not affect their basic functions. These results suggested that the antigenic variation seen in VP1 may be important for virulence.

Recombination is the main source of mutation and the driving force for virus evolution (26). We tested the 12 isolated CIAV strains and found that there were genetic recombination events in the HN-4 and HN-8 strains. Recombination occurred both in the coding region and the non-coding region, suggesting a higher level of adaptability and epidemic transmission. Importantly, HN-4 infection induced 50% death and significant pathological symptoms after inoculation of one-day-old chickens in a 21-day long experiment. These results suggest that HN-4 might be a pathogenic epidemic strain induced by recombination.

In conclusion, our study has focused on the isolation, identification and analysis of different CIAV strains prevalent in Henan province, and found that there were specific amino acid site variations and gene recombinations. These recombination events may be responsible for the evolution of virulence in the epidemic strains, whose biological characteristics need further investigation.

DATA AVAILABILITY STATEMENT

The original contributions presented in the study are included in the article/**Supplementary Material**, further inquiries can be directed to the corresponding author.

ETHICS STATEMENT

The animal study was reviewed and approved by Animal Ethics Committee of Henan Agricultural University.

AUTHOR CONTRIBUTIONS

X-WW, JF, and G-QZ conceived and designed the study. H-YL and J-JW performed the experiments. J-XJ, X-JZ, RW, XY, and LC analyzed the data. X-WW, JF, Y-FL, A-JS, and G-QZ wrote and revised the manuscript. All authors read and approved the final version.

FUNDING

This work was supported by the National Natural Science Foundation of China (Nos. U21A20260 and U21A201577), the Starting Foundation for Outstanding Young Scientists of Henan Agricultural University (No. 30500690), the Advanced program of 2020 for returned overseas scholar (No. 30602136), the Key Scientific Research program of 2022 for Colleges and Universities in Henan Province (No. 22A230011), and Henan Fengyuan poultry Co., Ltd (Poultry farm disease control and eradication program).

SUPPLEMENTARY MATERIAL

The Supplementary Material for this article can be found online at: https://www.frontiersin.org/articles/10.3389/fvets.2022.871826/full#supplementary-material

REFERENCES

1. Vaziry A, Silim A, Bleau C, Frenette D, Lamontagne L. Chicken infectious anaemia vaccinal strain persists in the spleen and thymus of young chicks and induces thymic lymphoid cell disorders. *Avian Pathol.* (2011) 40:377–85. doi: 10.1080/03079457.2011.586330
2. Eltahir YM, Qian K, Jin W, Qin A. Analysis of chicken anemia virus genome: evidence of intersubtype recombination. *Virol J.* (2011) 8:512. doi: 10.1186/1743-422X-8-512
3. Lien YY, Huang CH, Sun FC, Sheu SC, Lu TC, Lee MS, et al. Development and characterization of a potential diagnostic monoclonal antibody against capsid protein VP1 of the chicken anemia virus. *J Vet Sci.* (2012) 13:73–9. doi: 10.4142/jvs.2012.13.1.73
4. Peters MA, Jackson DC, Crabb BS, Browning GF. Chicken anemia virus VP2 is a novel dual specificity protein phosphatase. *J Biol Chem.* (2002) 277:39566–73. doi: 10.1074/jbc.M201752200
5. Feng C, Liang Y, Teodoro JG. The role of apoptin in chicken anemia virus replication. *Pathogens.* (2020) 9:294. doi: 10.3390/pathogens9040294
6. Brown AC, Reddy V, Lee J, Nair V. Marek's disease virus oncoprotein meq physically interacts with the chicken infectious anemia virus-encoded apoptotic protein apoptin. *Oncotarget.* (2018) 9:28910–20. doi: 10.18632/oncotarget.25628
7. Haridy M, Goryo M, Sasaki J, Okada K. Pathological and immunohistochemical study of chickens with co-infection of marek's disease virus and chicken anaemia virus. *Avian Pathol.* (2009) 38:469–83. doi: 10.1080/03079450903349162

8. Zhang Y, Cui N, Han N, Wu J, Cui Z, Su S. Depression of vaccinal immunity to marek's disease by infection with chicken infectious anemia virus. *Front Microbiol*. (2017) 8:1863. doi: 10.3389/fmicb.2017.01863
9. Su Q, Meng F, Li Y, Zhang Y, Zhang Z, Cui Z, et al. Chicken infectious anemia virus helps fowl adenovirus break the protection of maternal antibody and cause inclusion body hepatitis-hydropericardium syndrome in layers after using co-contaminated newcastle disease virus-attenuated vaccine. *Poult Sci*. (2019) 98:621–8. doi: 10.3382/ps/pey153
10. Hoerr FJ. Clinical aspects of immunosuppression in poultry. *Avian Dis*. (2010) 54:2–15. doi: 10.1637/8909-043009-Review.1
11. Erfan AM, Selim AA, Helmy SA, Eriksson P, Naguib MM. Chicken anaemia virus enhances and prolongs subsequent avian influenza (H9N2) and infectious bronchitis viral infections. *Vet Microbiol*. (2019) 230:123–9. doi: 10.1016/j.vetmic.2019.01.024
12. Gimeno IM, Schat KA. Virus-induced immunosuppression in chickens. *Avian Dis*. (2018) 62:272–85. doi: 10.1637/11841-041318-Review.1
13. Kim HR, Kwon YK, Bae YC, Oem JK, Lee OS. Molecular characterization of chicken infectious anemia viruses detected from breeder and broiler chickens in South Korea. *Poult Sci*. (2010) 89:2426–31. doi: 10.3382/ps.2010-00911
14. Bhatt P, Shukla SK, Mahendran M, Dhama K, Chawak MM, Kataria JM. Prevalence of chicken infectious anaemia virus (CIAV) in commercial poultry flocks of northern India: a serological survey. *Transbound Emerg Dis*. (2011) 58:458–60. doi: 10.1111/j.1865-1682.2011.01215.x
15. Huynh LTM, Nguyen GV, Do LD, Dao TD, Le TV, Vu NT, et al. Chicken infectious anaemia virus infections in chickens in northern Vietnam: epidemiological features and genetic characterization of the causative agent. *Avian Pathol*. (2020) 49:5–14. doi: 10.1080/03079457.2019.1637821
16. Li Y, Wang Y, Fang L, Fu J, Cui S, Zhao Y, et al. Genomic analysis of the chicken infectious anemia virus in a specific pathogen-free chicken population in China. *Biomed Res Int*. (2016) 2016:4275718. doi: 10.1155/2016/4275718
17. Meng F, Dong G, Zhang Y, Tian S, Cui Z, Chang S, et al. Co-infection of fowl adenovirus with different immunosuppressive viruses in a chicken flock. *Poult Sci*. (2018) 97:1699–705. doi: 10.3382/ps/pex414
18. Su Q, Wang T, Meng F, Cui Z, Chang S, Zhao P. Synergetic pathogenicity of newcastle disease vaccines LaSota strain and contaminated chicken infectious anemia virus. *Poult Sci*. (2019) 98:1985–92. doi: 10.3382/ps/pey555
19. Li X, Zhang K, Pei Y, Xue J, Ruan S, Zhang G. Development and application of an MRT-qPCR assay for detecting coinfection of six vertically transmitted or immunosuppressive avian viruses. *Front Microbiol*. (2020) 11:1581. doi: 10.3389/fmicb.2020.01581
20. Martin DP, Murrell B, Golden M, Khoosal A, Muhire B. RDP4: Detection and analysis of recombination patterns in virus genomes. *Virus Evol*. (2015) 26:1. doi: 10.1093/ve/vev003
21. Renshaw RW, Soine C, Weinkle T, O'Connell PH, Ohashi K, Watson S, et al. A hypervariable region in VP1 of chicken infectious anemia virus mediates rate of spread and cell tropism in tissue culture. *J Virol*. (1996) 70:8872–8. doi: 10.1128/jvi.70.12.8872-8878.1996
22. Tan J, Tannock GA. Role of viral load in the pathogenesis of chicken anemia virus. *J Gen Virol*. (2005) 86:1327–33. doi: 10.1099/vir.0.80599-0
23. Wanganurakkul S, Smith DR, Chintapitaksakul L, Assavalapsakul W. Effective production of recombinant Delta60VP1 chicken anemia virus protein in escherichia coli and its application to a serodiagnostic indirect ELISA. *J Virol Methods*. (2020) 282:113887. doi: 10.1016/j.jviromet.2020.113887
24. Tseng TY, Liu YC, Hsu YC, Chang PC, Hsieh MK, Shien JH, et al. Preparation of chicken anemia virus (CAV) virus-like particles and chicken interleukin-12 for vaccine development using a baculovirus expression system. *Pathogens*. (2019) 8:262. doi: 10.3390/pathogens8040262
25. Nakamura K, Mase M, Yamamoto Y, Takizawa K, Kabeya M, Wakuda T, et al. Inclusion body hepatitis caused by fowl adenovirus in broiler chickens in Japan, 2009–2010. *Avian Dis*. (2011) 55:719–23. doi: 10.1637/9813-052511-Case.1
26. Tan C, Wang Z, Lei X, Lu J, Yan Z, Qin J, et al. Epidemiology, molecular characterization, and recombination analysis of chicken anemia virus in Guangdong province, China. *Arch Virol*. (2020) 165:1409–17. doi: 10.1007/s00705-020-04604-8
27. Van Dong H, Tran GTH, Van Nguyen G, Dao TD, Bui VN, Huynh LTM, et al. Chicken anemia virus in northern Vietnam: molecular characterization reveals multiple genotypes and evidence of recombination. *Virus Genes*. (2019) 55:643–53. doi: 10.1007/s11262-019-01686-8
28. Yamaguchi S, Imada T, Kaji N, Mase M, Tsukamoto K, Tanimura N, et al. Identification of a genetic determinant of pathogenicity in chicken anaemia virus. *J Gen Virol*. (2001) 82:1233–8. doi: 10.1099/0022-1317-82-5-1233

Conflict of Interest: The authors declare that the research was conducted in the absence of any commercial or financial relationships that could be construed as a potential conflict of interest.

Publisher's Note: All claims expressed in this article are solely those of the authors and do not necessarily represent those of their affiliated organizations, or those of the publisher, the editors and the reviewers. Any product that may be evaluated in this article, or claim that may be made by its manufacturer, is not guaranteed or endorsed by the publisher.

frontiers | Frontiers in Veterinary Science

ORIGINAL RESEARCH
published: 25 April 2022
doi: 10.3389/fvets.2022.871549

Blood B Cell Depletion Reflects Immunosuppression Induced by Live-Attenuated Infectious Bursal Disease Vaccines

Céline Courtillon[1], Chantal Allée[1], Michel Amelot[2], Alassane Keita[2], Stéphanie Bougeard[3], Sonja Härtle[4], Jean-Claude Rouby[5], Nicolas Eterradossi[6] and Sebastien Mathieu Soubies[1†]*

[1] Ploufragan-Plouzané-Niort Laboratory, OIE Reference Laboratory for Infectious Bursal Disease, French Agency for Food, Environmental and Occupational Health & Safety (ANSES), VIPAC Unit, Ploufragan, France, [2] Ploufragan-Plouzané-Niort Laboratory, French Agency for Food, Environmental and Occupational Health & Safety (ANSES), SELEAC Service, Ploufragan, France, [3] Ploufragan-Plouzané-Niort Laboratory, French Agency for Food, Environmental and Occupational Health & Safety (ANSES), EPISABE Unit, Ploufragan, France, [4] Ludwig-Maximilians-Universität München, Veterinärwissenschaftliches Department, München, Germany, [5] French Agency for Veterinary Medicinal Products (ANMV), French Agency for Food, Environmental and Occupational Health & Safety (ANSES), Javené, France, [6] Ploufragan-Plouzané-Niort Laboratory, French Agency for Food, Environmental and Occupational Health & Safety (ANSES), Management Department, Ploufragan, France

OPEN ACCESS

Edited by:
Yulong Gao,
Harbin Veterinary Research Institute (CAAS), China

Reviewed by:
Ping Wei,
Guangxi University, China
Venugopal Nair,
The Pirbright Institute, United Kingdom

***Correspondence:**
Céline Courtillon
celine.courtillon@anses.fr

†Present address:
Sebastien Mathieu Soubies,
UMR 1225 IHAP, Toulouse, France

Specialty section:
This article was submitted to Veterinary Infectious Diseases, a section of the journal Frontiers in Veterinary Science

Received: *08 February 2022*
Accepted: *08 March 2022*
Published: *25 April 2022*

Citation:
Courtillon C, Allée C, Amelot M, Keita A, Bougeard S, Härtle S, Rouby J-C, Eterradossi N and Soubies SM (2022) Blood B Cell Depletion Reflects Immunosuppression Induced by Live-Attenuated Infectious Bursal Disease Vaccines. Front. Vet. Sci. 9:871549. doi: 10.3389/fvets.2022.871549

Immunosuppression in poultry production is a recurrent problem worldwide, and one of the major viral immunosuppressive agents is Infectious Bursal Disease Virus (IBDV). IBDV infections are mostly controlled by using live-attenuated vaccines. Live-attenuated Infectious Bursal Disease (IBD) vaccine candidates are classified as "mild," "intermediate," "intermediate-plus" or "hot" based on their residual immunosuppressive properties. The immunosuppression protocol described by the European Pharmacopoeia (Ph. Eur.) uses a lethal Newcastle Disease Virus (NDV) infectious challenge to measure the interference of a given IBDV vaccine candidate on NDV vaccine immune response. A Ph. Eur.-derived protocol was thus implemented to quantify immunosuppression induced by one mild, two intermediate, and four intermediate-plus live-attenuated IBD vaccines as well as a pathogenic viral strain. This protocol confirmed the respective immunosuppressive properties of those vaccines and virus. In the search for a more ethical alternative to Ph. Eur.-based protocols, two strategies were explored. First, *ex vivo* viral replication of those vaccines and the pathogenic strain in stimulated chicken primary bursal cells was assessed. Replication levels were not strictly correlated to immunosuppression observed *in vivo*. Second, changes in blood leukocyte counts in chicks were monitored using a Ph. Eur. - type protocol prior to lethal NDV challenge. In case of intermediate-plus vaccines, the drop in B cells counts was more severe. Counting blood B cells may thus represent a highly quantitative, faster, and ethical strategy than NDV challenge to assess the immunosuppression induced in chickens by live-attenuated IBD vaccines.

Keywords: IBDV, live-attenuated vaccine, vaccine safety, immunosuppression, B cells, replication

INTRODUCTION

Immunosuppression is, as defined by Gimeno and Schat (1), "A state of temporary or permanent dysfunction of the immune response resulting from insults to the immune system with suboptimal antibody production and/or suboptimal innate and/or suboptimal cell-mediated responses leading to increased susceptibility to disease." In poultry production, immunosuppression is a multifactorial and recurrent problem worldwide.

Infection with the *Birnaviridae* family's infectious bursal disease virus (IBDV) is one of many possible causes of immunosuppression (2). This virus mainly replicates in immature B cells found in the bursa of Fabricius (BF), a bird-specific immune organ responsible for the development and selection of B cells during the first month of life (3). Infection by this agent may result in the destruction of the organ (3). Depending on the viral pathotype, the age of chickens, their genetics, and their IBDV immune status, infection can induce an acute and sometimes lethal disease called Infectious Bursal Disease (IBD), also known as Gumboro disease, or be asymptomatic. In both cases, surviving birds, due to BF atrophy, will undergo a transient or permanent immunosuppression, in turn resulting in secondary infections and vaccination failures (4).

Infectious bursal disease control is achieved by a combination of biosecurity and medical prophylaxis (vaccination). Several vaccination strategies exist. These include the use of live-attenuated vaccines, inactivated vaccines, immune complexes, and vectored vaccines (4). Live-attenuated IBD vaccines are particularly adapted to mass vaccination due to low costs and to an easy distribution in the drinking water. Several types have been developed based on their residual virulence. Hence, live-attenuated vaccines are classified as mild, intermediate (further abbreviated as "I"), intermediate-plus ("I+"), and hot. The higher the residual virulence of an attenuated IBD vaccine, the earlier it can be administered to chicks to break through maternal antibodies and induce an immune response. I+ and hot vaccines can be used in epidemiological contexts (for instance circulation of very virulent strains of IBDV) in which chicks are particularly at risk. Those vaccines can nevertheless induce significant B cell depletion in the bursa and cause immunosuppression by themselves.

Vaccine challenge strategies, which are used to check vaccine safety during licensing processes, can demonstrate this immunosuppression. In those strategies, specific pathogen-free chicks, after receiving IBDV vaccination, are immunized with a model antigen (e.g., killed *Brucella abortus*) or a live-attenuated vaccine [e.g., Hitchner B1 strain of Newcastle disease virus (NDV)] (5). The ability of the chicks to mount an immune response to those immunogens is then evaluated through their humoral response and/or an infectious challenge.

In particular, the assessment of immunosuppressive properties of IBD vaccine candidates following the European Pharmacopeia (Ph. Eur.) protocol requires administering IBD vaccine candidate to specific pathogen-free (SPF) chicks. After 15 days, around the time when IBDV-induced bursal lesions peak, chicks are immunized with live-attenuated Newcastle Disease (ND) vaccine. A lethal NDV infectious challenge is performed 15 days after the NDV vaccination. For the vaccine candidate to be considered as safe both NDV serology and clinical protection results are expected to be similar in chicks vaccinated against IBD or not (6). Still according to the Ph. Eur., vaccine candidates that induce a significant degree of bursal microscopic damages in preliminary studies fall into the category of I+ vaccines candidates. Therefore, the standards retained by the Ph. Eur. monograph with regard to the immunosuppression testing are not applicable for licensing. However, a special warning is introduced in the Summary of Product Characteristics to describe how these vaccines are subjected to additional precautions for use.

The aim of this study was to explore, in the interest of improving ethics and cost, alternatives to challenge-based protocols to quantify immunosuppression induced by IBD vaccine candidates. First, a Ph. Eur. —derived protocol was implemented to confirm the immunosuppressive properties of mild, I, and I+ live-attenuated IBD vaccines as well as a pathogenic viral strain. Next, two alternative strategies were then explored, namely (i) comparing the replicative capacity of vaccine viruses *ex vivo* using bursal B cells and (ii) measuring blood leucocyte counts after IBDV vaccination in SPF chicks.

MATERIALS AND METHODS

Ethic Statements

All animal trials were conducted in an animal facility approved for animal experiments (n°C-22–745–1). They were approved by Anses Ploufragan ethical committee (committee number C2EA-016/ ComEth ANSES/ENVA/UPEC) and authorized by French Ministry for higher education and research (permit number APAFiS#3925-2016020310538529, application number 16-016, statement number 08/03/16-1). Chickens were raised and humanely euthanized in agreement with EU directive number 2010/63/UE.

Viruses

Vaccine viruses used in this study were obtained from a local veterinary practice, reconstituted, and administered according to the manufacturer's instructions. To avoid any conflict of interest, currently distributed IBD vaccines used in this study were anonymized. All IBD I+ vaccines (coded as I+1, I+2, I+3, and I+4) marketed in France as of 2016 were included. As representative intermediate vaccines, two intermediate vaccines (I1 and I2) were also included. The NDV Poulvac Hitchner B1

Abbreviations: BF, Bursa of Fabricius; EDTA, Ethylene Diamine Tetra Acetic acid; EID_{50}, 50% Embryo Infective Dose; EU, European Union; HI, Hemagglutination Inhibition; h.p.i., hours post-infection; I, Intermediate; I+, Intermediate-plus; IBD, Infectious Bursal Disease; IBDV, Infectious Bursal Disease Virus; ND, Newcastle Disease; NDV, Newcastle Disease Virus; Ph. Eur., European Pharmacopeia; SPF, Specific Pathogen-Free; $TCID_{50}$, 50% Tissue Culture Infective Dose.

strain (Zoetis) was used for NDV vaccination and the velogenic NDV strain "Herts33" (Anses Ploufragan laboratory) was used to challenge the birds. The classical IBDV virulent strain "F52/70" and the mild IBD vaccine strain "PBG98" (no longer marketed in France; passaged twice on chicken fibroblasts) were obtained from the collection of IBDV strains maintained by the OIE reference Laboratory (Anses, Ploufragan, France).

Animal Experiments

In total three experiments were performed. The layouts of the experiments are presented in **Figure 1A** (experiments 1 and 2) and **Figure 3A** (experiment 3), respectively. For each experiment, six groups of 10 1-day-old SPF chicks (Anses, Ploufragan, France) were housed in negative-pressure filtered-air isolators and were administered (or not, in case of controls) one dose of IBD vaccine by the eye-drop route. In the case of PBG98 or F52/70, chicks received 100 tissue culture median infectious doses ($TCID_{50}$) or 100 embryo median infectious doses (EID_{50}, corresponding for this virus to 740 $TCID_{50}$), respectively. Chicks received (or not, in case of the non-vaccinated controls) one dose of ND vaccine by the eye-drop route after 14 days of IBDV vaccination. Controls included a group that received neither IBD nor ND vaccine ("no vaccine control"), and a group that received only the ND vaccine ("NDV vaccine control"). In the case of experiment 3, prior to ND vaccination, chicks were blood-sampled at the occipital sinus with EDTA-coated tubes (S-Monovette EDTA K2 2.7 mL, Sarstedt, reference 04.1915.100) for blood cell quantification. For all experiments, chickens were blood-sampled at the occipital sinus 2 weeks post-NDV vaccination, either in serology tubes (S-Monovette serum-gel, 2.6 mL, Sarstedt, reference 04.1904) for serological analyses only (experiments 1 and 2) or in EDTA-coated tubes for blood cell quantification as well as serological analyses (experiment 3). On the same day, chicks were inoculated intra-muscularly with 10^5 EID_{50} of NDV strain Herts33. A clinical follow-up was performed for 14 days following the challenge. Birds were rated as "clinically protected" when no clinical sign was observed or "non-protected" when they displayed neurological, respiratory signs, or prostration. Animals showing clinical signs clearly unrelated to the NDV challenge were excluded from the clinical follow-up. Animals exhibiting neurological signs and/or prostration reached the ethical endpoint of the experiment and were consequently humanely euthanized.

NDV Serological Analyses

In all experiments, serum (experiments 1 and 2) or plasma (experiment 3) obtained after blood sampling were analyzed by hemagglutination inhibition (HI) to quantify levels of anti-NDV antibodies according to Agence Française de Normalisation Norm U 47-011. Four hemagglutination units of NDV LaSota strain were used as antigen. Results were expressed as the reciprocal of the highest dilution of serum able to completely inhibit the hemagglutination of 4 units of NDV antigen in $\log_2$. In this assay, titers equal to or below 2 $\log_2$ are considered negative. To exclude any impact of EDTA from the blood-collection tube on HI titers, plasmas from experiment 3 were treated with $CaCl_2$ (to a final concentration of 2.5 mM) to induce fibrin precipitation (7). After 2 h of incubation at room temperature, the fibrin clot was mechanically disrupted by stirring with micropipette tips, the tubes were centrifuged at room temperature for 10 min at 14 000 $\times$ g and supernatants were collected.

Blood Leukocytes Quantification

In the case of experiment 3, collected blood was analyzed by flow cytometry to quantify leukocytes following the approach developed by Seliger et al. (8) with the few modifications already described (9). Accordingly, blood thrombocytes (defined as $K1^+$ cells), blood monocytes (defined as $K1^+$, $Kul01^+$ and $CD45^+$ cells), blood T cells (defined as $CD45^+$ cells that are additionally either $CD4^+$ or $CD8^+$ or $TCR\gamma\delta^+$), and blood B cells (defined as $CD45^+$ and $Bu1^+$ cells) were quantified.

Ex vivo Bursal Cell Infection

Bursal cells were isolated from 9 to 15 week-old SPF chickens as previously described (10). Cells were maintained at 40°C, 5% CO_2 in a lymphocyte culture medium consisting of Iscove's Modified Dulbecco's Medium (IMDM) with L-glutamine and HEPES (reference 21980–032, Gibco, Thermo Fisher), supplemented with 8% FBS, 2% SPF chicken serum (ANSES, Ploufragan, France), 1X Insulin Transferrin Selenium (reference 41400–045, Gibco, Thermo Fisher), 50 µM beta-mercaptoethanol, 1 µg/mL Phorbol 12-myristate 13-acetate (reference tlrl-pma, Invivogen), penicillin (200 IU/mL), streptomycin (0.2 mg/mL), and fungizone (2 µg/mL).

For infection, one million bursal cells per well seeded in 96-well plates were inoculated at a target multiplicity of infection of 5×10^{-4}. Inocula were titrated and titers are presented as the 0 h post-infection (h.p.i.) time-point in **Figure 2A**. Supernatants were collected at 16, 23, and 48 h.p.i. and were frozen at −70°C until titration. Additionally, at 16 and 23 h.p.i., cells were collected for immunolabeling and flow cytometry analyses. A total of 5 biological replicates (consisting of cells from distinct birds) were analyzed during two distinct experiments.

Immunolabeling and Flow Cytometry

Bursal cells collected at 16 and 23 h.p.i. were labeled as previously described (10). Briefly, viability was evaluated using the Fixable Viability Dye eFluor 750 (Thermofisher, reference 65-0865-14) and cells were immunostained using an anti-VP3 monoclonal antibody [mAb 18, (11)] followed by a goat anti-mouse IgG2a Alexa Fluor 546 antibody (Thermofisher, reference A21133). Cells were analyzed on a FC500 MPL flow cytometer (Beckman Coulter).

Virus Titration

Virus titration of inocula and supernatants at 16, 23, and 48 h.p.i. was carried out as previously described (10). Briefly, serial dilutions of viral suspensions were incubated into 96-well plates with chicken bursal cells in lymphocyte culture medium at 40°C for 48 h in a humidified 5% CO_2 incubator. Cells were then subjected to immunocytochemistry using the IBDV VP3 specific mAb 18, a horse-radish peroxidase coupled anti-mouse IgG serum and KPL Trueblue peroxidase substrate (Seracare,

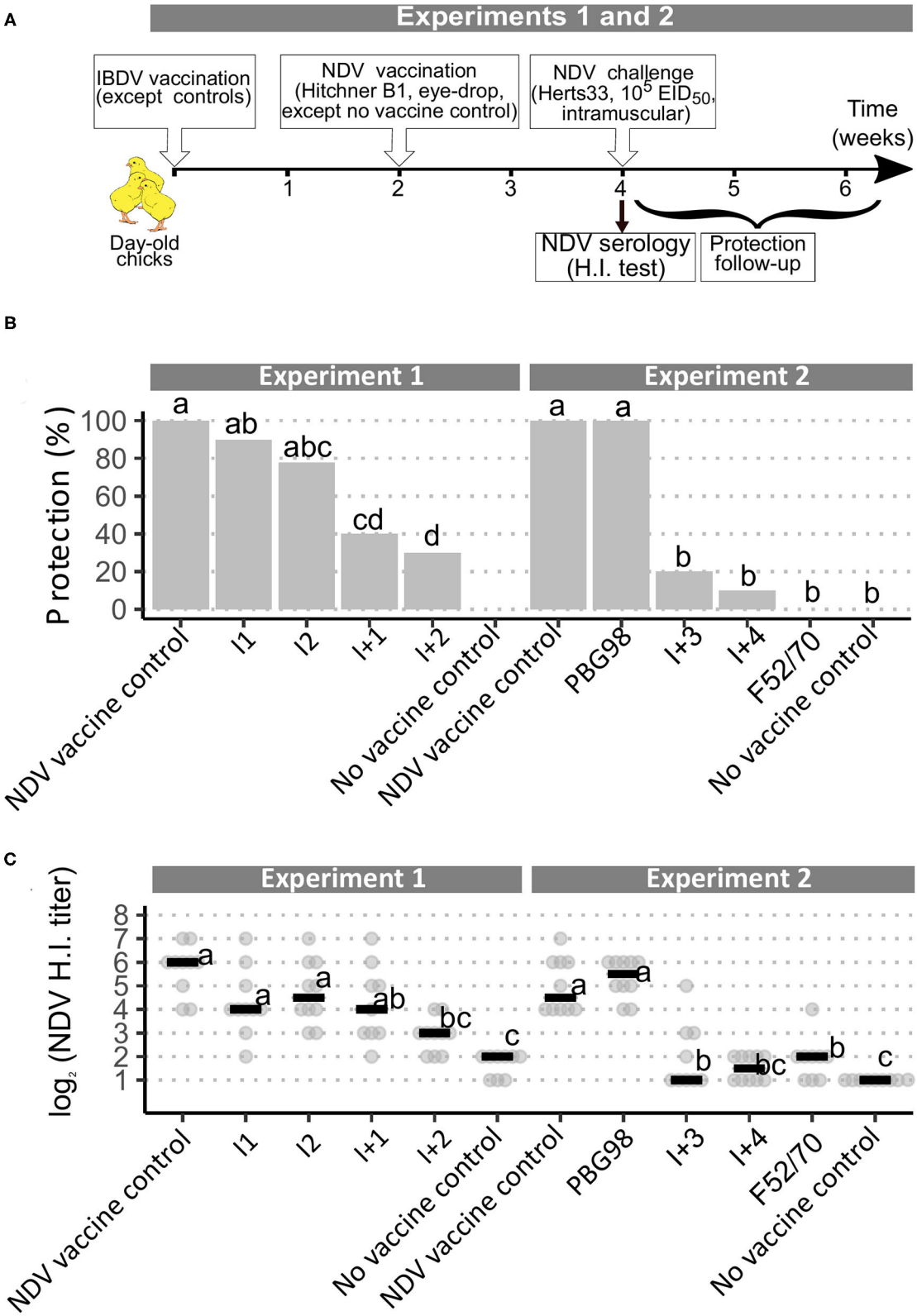

FIGURE 1 | Implementation of a European Pharmacopoeia-derived protocol for IBDV immunosuppression testing. **(A)** Layout of animal experiments 1 and 2. **(B)** Percentage of clinically protected chicks observed after velogenic Newcastle Disease Virus Challenge. Different letters indicate statistically significant differences ($p < 0.05$) between groups (within one given experiment) using Fisher's exact test with FDR adjustment method for multiple pairwise comparisons. **(C)** Serological response to NDV vaccination during experiments 1 and 2. Horizontal bars indicate the median of each group. Different letters indicate statistically significant differences ($p < 0.05$) between groups (within one given experiment) using Kruskal-Wallis test.

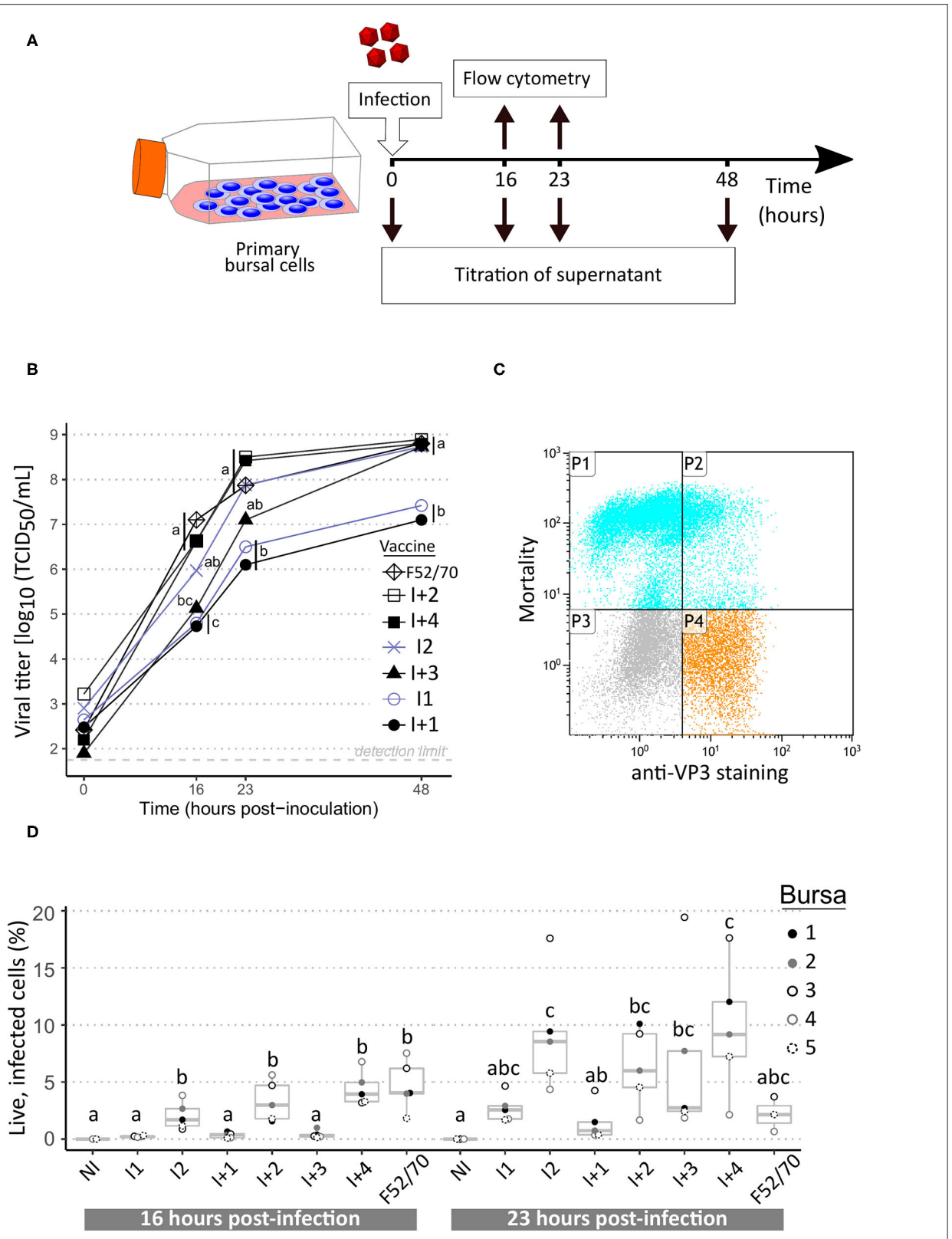

FIGURE 2 | Replication curves of IBDV vaccine and pathogenic strains in *ex vivo* chicken bursal cells. **(A)** Layout of the experiment. **(B)** Viral growth kinetics of IBDV vaccine and pathogenic strains. Intermediate vaccine strains appear in blue grey while intermediate-plus and pathogenic strains are in black. Supernatants collected

(Continued)

FIGURE 2 | at the indicated time-points were titrated on freshly isolated bursal cells. Viral titers, expressed as median tissue culture infective doses ($TCID_{50}$) were calculated using the Read and Muench formula. Icons at each time-point indicate the median value obtained from a total of five biological replicates. Different letters indicate statistically significant differences ($p < 0.05$) between groups using Kruskall-Wallis test. **(C)** Example of flow cytometry dot-plot. P1: IBDV-negative dead cells; P2: IBDV-positive dead cells; P3: IBDV-negative live cells; P4: IBDV-positive live cells. **(D)** Percentages of live infected cells at 16 and 23 h post-infection. Dots indicate values for cells from individual bursae (color-coded). Box-plots indicate extreme values, quartiles and median. Different letters indicate statistically significant differences ($p < 0.05$) between groups using Kruskal-Wallis test.

reference 5510-0030). Viral titers, expressed as $TCID_{50}$/mL, were determined using Reed and Muench formula (12).

Statistical Analyses

Statistical analyses were performed using R version 4.0.3 (13). Differences in percentages of protection were analyzed using the Fisher's exact test followed by pair-wise comparisons using the "fisher.multcomp" function from RVAideMemoire package version 0.9-79 (14). All other quantitative parameters were analyzed using Kruskal-Wallis test followed by Fisher's least significant difference test with Holm adjustment method for multiple comparisons using the "kruskal" function from the package "Agricolae" version 1.3-2 (15).

RESULTS

The Ph. Eur. IBDV Immunosuppression Protocol Confirms the Expected Immunosuppressive Properties of the Selected IBDV Strains

In both experiments 1 and 2, following challenge with the virulent NDV strain Herts 33, all the NDV non-vaccinated control birds rapidly exhibited intense prostration and died or were euthanized within 72 h post-inoculation. All the NDV vaccine control birds showed complete clinical protection, without any sign of disease. Chicks that received both IBD and ND vaccines showed varying degrees of protection from the NDV challenge. Chicks from the PBG98-treated group showed 100% clinical protection. Those that received I vaccines had 80–90% protection, which did not differ statistically from those who received NDV vaccine controls. In contrast, protection in chicks that received I+ vaccines was significantly lower than that received NDV vaccine controls, with only 10–40% protection (**Figure 1B**). Finally, no animals from the F52/70 group were protected. HI testing for anti-NDV antibodies revealed expected background levels (1–2 $\log_2$) for non-vaccinated controls and high titers for NDV-vaccinated controls, with median values of 6 and 4.5 $\log_2$ in experiments 1 and 2, respectively (**Figure 1C**). Chicks vaccinated with PBG98 or I vaccines did not show any statistically significant difference in HI titers compared with NDV vaccine controls. In contrast, birds that received I+2, I+3, I+4, and F52/70 showed severe reduction in HI titers, almost reaching the background levels of non-vaccinated controls. Interestingly, chicks that received I+1 vaccine showed a numerically mild and statistically non-significant reduction in HI titers in spite of a statistically reduced clinical protection (only 40% birds protected).

Ex vivo Replicative Fitness in Chicken Primary Bursal Cells Does Not Accurately Reflect Immunosuppression *in vivo*

Primary bursal cells obtained from SPF chickens were infected with various IBDV strains to determine whether replication parameters (e.g., replicative fitness or cytopathogenicity) could mirror immunosuppressive properties. Strain F52/70 as well as the six vaccines tested *in vivo* were included in this approach. Since the PBG98 vaccine does not replicate in bursal B cells (data not shown), it was not included in the panel. For each of the tested strains, a dramatic increase in viral titers measured from bursal cells supernatants was visible as early as 16 h.p.i. and viral titers increased until 48 h.p.i. (**Figure 2B**). Interestingly, two trends in replication curves could be observed. On the one hand, I2, I+2, I+3, I+4, and strain F52/70 reached a viral titer higher than 10^7 $TCID_{50}$/mL at 23 h.p.i. and then reached almost 10^9 $TCID_{50}$/mL at 48 h.p.i. On the other hand, I1 and I+1 presented viral titers of about 10^6 $TCID_{50}$/mL at 23 h.p.i. and then reached a plateau phase of about 10^7 $TCID_{50}$/mL at 48 h.p.i., which was statistically lower compared with the first trend for this time point. In parallel of these infectious titrations, both the percentages of viable and IBDV-infected cells were analyzed by flow cytometry (example of dot-plot in **Figure 2C**). Significant differences in the percentage of live infected cells were detected at 16 h.p.i. with higher values for I2, I+2, I+4, and F52/70 (**Figure 2D**). At 23 h.p.i., a high variability in percentages between cells originating from distinct birds was observed, and differences between viruses were no longer significant. It is noteworthy that a bursa-specific trend was observed: for instance, at least 3 fold-higher percentages of infected cells were observed for bursa number 3 compared with bursa 4 for almost all viruses at 23 h.p.i.

Intermediate-Plus Vaccines Induce a Dramatic Depletion of Blood B Cells in SPF Chickens

Based on the hypothesis that I+ vaccines, inducing higher bursal damages, may reduce blood B cell concentrations, a third *in vivo* experiment was implemented in which four vaccines were tested (**Figure 3A**): I1 and I+3, for which *ex vivo* replication levels were correlated to the intensity of *in vivo* immunosuppression, and I2 and I+1, for which this correlation was not observed. Clinical protection from NDV challenge was consistent with results from experiments 1 and 2, except for the I+1 treated group, which no longer differed statistically from the NDV vaccine control (**Figure 3B**). Anti-NDV antibody levels were significantly reduced for all vaccines except I1 compared with NDV vaccine controls (**Figure 3C**), unlike in experiment 1 (**Figure 1C**). To check the lack of

interference of the anti-coagulant, HI testing was performed again after adding $CaCl_2$ to the plasmas to induce clotting. No difference in HI titers was observed after this treatment (data not shown). At both time-points, blood leukocyte counts revealed significant differences in B cell concentrations between virus strains. At 15 days of age, prior to NDV vaccination, both control groups exhibited concentrations close to 1,000 B cells/μL (**Figure 3D**, left panel). For I1 vaccinated birds, the median concentration significantly dropped to 143 B cells/μL. For I2 vaccinated birds, the drop was even more pronounced (median of 42 cells/μL, $p < 0.05$). For I+1 and I+3 vaccinated birds, B cell counts were statistically lower than in I vaccine groups, with medians below the detection limit of 8 cells/μL. In addition, no bird in these two groups presented more than 60 B cells/μL. Blood cell counts performed at 29 days of age (prior to NDV challenge) revealed a global increase of B cell counts in all groups compared with 15 days of age (**Figure 3D**, right panel). Both controls groups showed median concentrations above 2,000 B cells/μL. Median B cell concentrations significantly dropped to 956 for I1 vaccinated group. Those median concentrations were lower in I2, I+1, and I+3 vaccinated groups, with 130, 91, and 10 B cells/μL, respectively. Some birds from I+1 and I+3 treated groups still did not show any blood B cell at that time-point. Some milder variations were observed in other blood leukocyte concentrations: for instance, at 15 days of age, a statistically significant reduction in both monocytes and T cell concentrations were seen for I2 and I+3 groups compared with control groups (**Supplementary Figure 1**).

DISCUSSION

Evaluating the immunosuppressive properties of live-attenuated IBD vaccines is crucial for a precise assessment of their risk-benefit ratio. In this study, alternative strategies to the Ph. Eur. protocol, which is based on lethal viral challenges, were explored to quantify IBDV immunosuppressive properties in the interest of improving ethics and cost. The Ph. Eur. derived *in vivo* immunosuppression protocol that was implemented provided results in agreement with the official status (mild, intermediate, or intermediate-plus) of the tested vaccines. Accordingly, only mild and intermediate vaccines gave both protection and HI results not differing from NDV vaccine controls. These results are also in agreement with previous data obtained in the Ploufragan laboratory for some of the tested vaccines (16). NDV HI titer patterns were higher in experiment 1 than in experiments 2 and 3. As the presence of anti-coagulants has been linked to differences in values observed during serological testing (7), $CaCl_2$ was added to plasma samples from experiment 3 to artificially induce fibrinogen precipitation allowing coagulation. The lack of impact of $CaCl_2$ addition on HI titers, combined with the comparable titers of NDV vaccine controls from experiments 2 and 3 argue against an effect of EDTA on HI titers. A more likely hypothesis may thus be that a higher efficacy of NDV vaccination in experiment 1 resulted in higher HI titers.

As a first alternative strategy to the current *in vivo* testing scheme, *ex vivo* infections of primary bursal cells were performed. This strategy was based on the assumption that the varying degrees of immunosuppression were caused by differences in IBDV replicative fitness in the BF (with higher replication levels producing higher immunosuppression) (17, 18) and that those differences may persist during *ex vivo* infection. Among the seven viruses tested, two of them (I2 and I+1) went against that assumption: while I+1 mimicked I1 replication curve, I2 replicated as well as I+ vaccines. Flow cytometry analyzes of live-infected cells, although revealing virus-specific differences at 16 h.p.i., did not allow differentiating I from I+ vaccines. Those differences were no longer visible at 23 h.p.i., partly due to high inter-individual differences. It was a surprise to see that cells from some individuals presented consistently high percentages of infection irrespective of the infecting viral strain. Higher numbers of biological replicates would be necessary to ascertain those tendencies in the flow cytometry analyses. Similarly, analysis of virus-induced cell death by flow cytometry did not reveal any difference between viral strains (data not shown). Thus, flow cytometry analyses, alone or in combination with *ex vivo* viral replication studies, did not allow discrimination of IBDV immunosuppressive properties.

B cells continuously exit the BF to reach the bloodstream during the first weeks post-hatching, resulting in a steady increase in blood B cells during this period (8). Early studies have shown that IBDV infection at 1 day of age with a pathogenic strain results in a dramatic and durable reduction of blood B cell concentrations (19). Based on these studies, the second alternative strategy consisted in checking whether the reduction in blood B cell concentration would be more severe in the case of I+ vaccines, and if other leukocyte populations could be modified. This strategy revealed striking differences for blood B cells, in particular at 15 days of age. All IBDV-infected groups showed a significant reduction relative to controls, and I+ infected groups showed a significantly more severe reduction than I infected groups, with some birds without any detectable blood B cells. Noteworthy, I1 and I2 infections, which had no effect on NDV HI titers or protection results of experiment 1, induced significant 8- and 28-fold reductions in B cell counts, respectively, when compared to controls. Furthermore, the approximate 3.4-fold reduction between I2 and I1 also appeared significant, making it possible to differentiate the impact of those two vaccines. At 29 days of age, a global increase in blood B cell concentration was observed. Apart from the increase normally observed in control birds, these higher values may reflect, in IBDV-infected groups, the recovery of the BF from IBDV-induced lesions (20, 21). Although all IBDV-infected groups still showed a significant blood B cell depletion compared with control birds, it was no longer possible to completely differentiate I+ from I infected groups. It is worth mentioning that some birds from I+ infected groups still lacked any detectable blood B cell at that time-point.

In summary, following circulating B cell counts may help to accurately quantify the impact of IBDV vaccination on the B cell compartment and to distinguish intermediate from intermediate-plus vaccines. It therefore represents an attractive potential

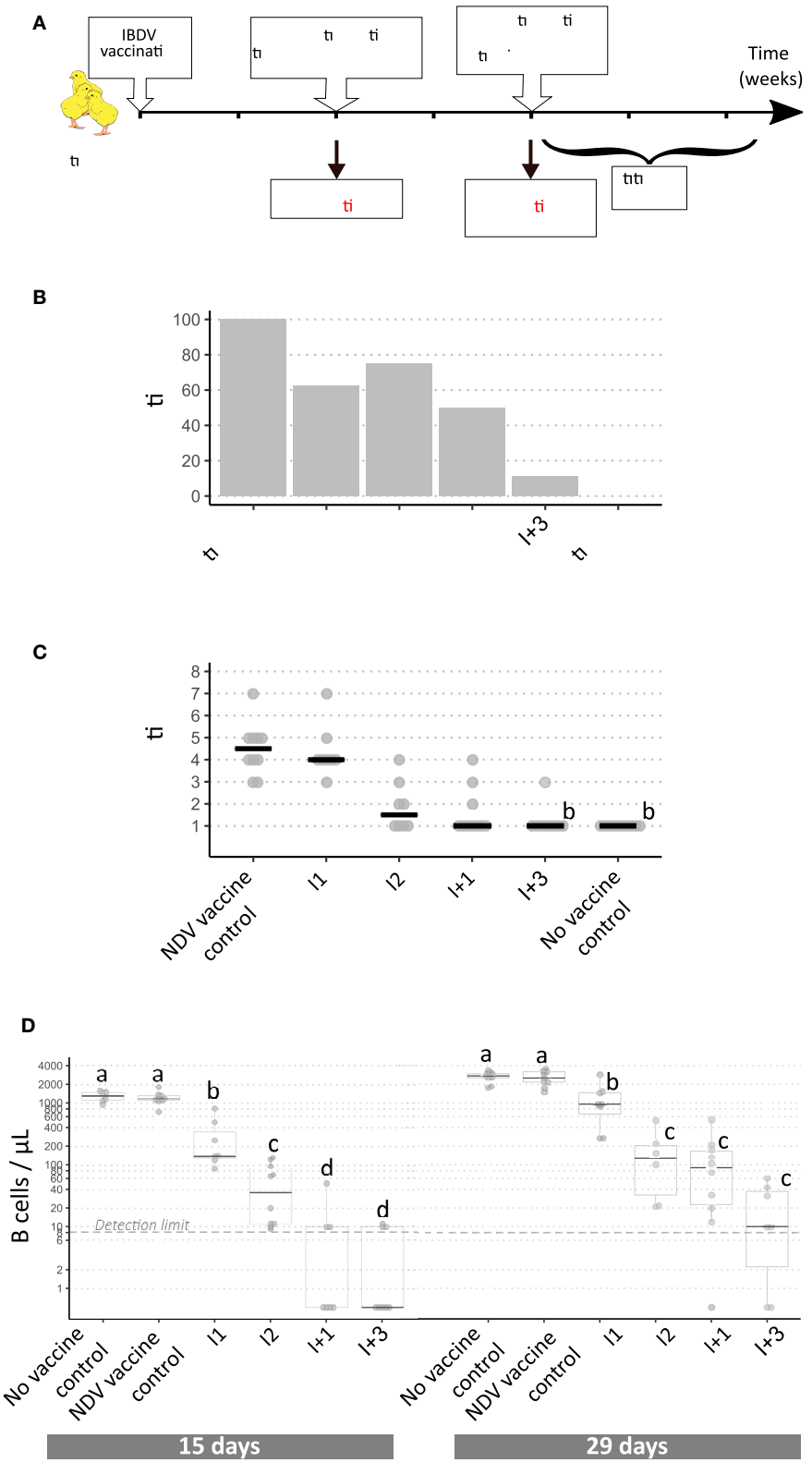

FIGURE 3 | Implementation of a modified European Pharmacopoeia-derived protocol for IBDV immunosuppression testing. **(A)** Layout of animal experiment 3. Extra analyses compared to animal experiments 1 and 2 appear in red text. **(B)** Percentage of clinically protected chicks observed after velogenic Newcastle Disease Virus

(Continued)

FIGURE 3 | challenge. Different letters indicate statistically significant differences ($p < 0.05$) between groups using Fisher's exact test with FDR adjustment method for multiple pairwise comparisons. **(C)** Serological response to NDV vaccination during experiment 3. Horizontal bars indicate the median of each group. Different letters indicate statistically significant differences ($p < 0.05$) between groups using Kruskal-Wallis test. **(D)** Blood B cell concentrations prior to NDV vaccination ("15 days," left panel), and prior to NDV challenge ("29 days," right panel). Different letters indicate statistically significant differences ($p < 0.05$) between groups using Kruskal-Wallis test.

strategy, alone or in combination with NDV HI testing, to assess the immunosuppressive properties of IBDV vaccine candidates or field strains in a faster and more ethical way to the current Ph.Eur. procedure, which relies on a lethal NDV infectious challenge. Further investigations, using other IBDV vaccines and IBDV strains with varying degree of pathogenicity are required to establish the threshold of this technique in differentiating intermediate from intermediate-plus vaccines.

DATA AVAILABILITY STATEMENT

Inquiries concerning raw data availability can be directed to the corresponding author.

ETHICS STATEMENT

The animal study was reviewed and approved by Anses Ploufragan Ethical Committee (Committee Number C2EA-016/ComEth ANSES/ENVA/UPEC) and French Ministry for higher education and research.

AUTHOR CONTRIBUTIONS

NE and SS proposed the original idea. SH, J-CR, NE, and SS participated in the design of the study. SS supervised the experiments. CC, CA, MA, AK, SB, and SS participated to experiments and/or to their analysis. CC and SS wrote the manuscript. All authors read, improved, and approved the final manuscript.

FUNDING

This work was supported by the French Agency for Veterinary Medicinal Products (CRD number 2015-112). Anses Ploufragan research was supported by Département des Côtes d'Armor and Saint Brieuc Armor Agglomération.

ACKNOWLEDGMENTS

The authors thank Mélissa Sizorn for her contribution on some *ex vivo* experiments, and Paul Alun Brown for his advices and the reading of the manuscript.

SUPPLEMENTARY MATERIAL

The Supplementary Material for this article can be found online at: https://www.frontiersin.org/articles/10.3389/fvets.2022.871549/full#supplementary-material

REFERENCES

1. Gimeno IM, Schat KA. Virus-induced immunosuppression in chickens. *Avian Dis.* (2018) 62:272–85. doi: 10.1637/11841-041318-Review.1
2. Delmas B, Attoui H, Ghosh S, Malik YS, Mundt E, Vakharia VN, et al. ICTV virus taxonomy profile: Birnaviridae. *J Gen Virol.* (2019) 100:5–6. doi: 10.1099/jgv.0.001185
3. Ratcliffe MJH, Härtle S. Chapter 4 - B cells, the bursa of fabricius and the generation of antibody repertoires. In: Schat KA, Kaspers B, Kaiser P, editors. *Avian Immunology*. 2nd ed. Boston, MA: Academic Press (2014). p. 65–89.
4. Eterradossi N, Saif YM. Infectious bursal disease. In: Swayne DE, Boulianne M, Logue CM, McDougald LR, Nair V, Suarez DL, editors. *Diseases of Poultry*. Hoboken: Wiley-Blackwell (2020). p. 257–83.
5. Infectious Bursal disease (Gumboro disease). In: *Manual of Diagnostic Tests and Vaccines for Terrestrial Animals*. Paris: Organisation mondiale de la santé animale (2021). p. 931–51.
6. Avian infectious bursal disease vaccine (live). In: *European Pharmacopoeia (Ph Eur)*. 10th ed. p. 1217–9.
7. Nilson E, Ekholm B, Rees Smith B, Törn C, Hillman M. Calcium addition to EDTA plasma eliminates falsely positive results in the RSR GADAb ELISA. *Clin Chim Acta.* (2008) 388:130–4. doi: 10.1016/j.cca.2007.10.021
8. Seliger C, Schaerer B, Kohn M, Pendl H, Weigend S, Kaspers B, et al. A rapid high-precision flow cytometry based technique for total white blood cell counting in chickens. *Vet Immunol Immunopathol.* (2012) 145:86–99. doi: 10.1016/j.vetimm.2011.10.010
9. Cubas-Gaona LL, Flageul A, Courtillon C, Briand FX, Contrant M, Bougeard S, et al. Genome evolution of two genetically homogeneous infectious bursal disease virus strains during passages *in vitro* and *ex vivo* in the presence of a mutagenic nucleoside analog. *Front Microbiol.* (2021) 12:678563. doi: 10.3389/fmicb.2021.678563
10. Soubies SM, Courtillon C, Abed M, Amelot M, Keita A, Broadbent A, et al. Propagation and titration of infectious bursal disease virus, including non-cell-culture-adapted strains, using *ex vivo*-stimulated chicken bursal cells. *Avian Pathol.* (2018) 47:179–88. doi: 10.1080/03079457.2017.1393044
11. Eterradossi N, Toquin D, Rivallan G, Guittet M. Modified activity of a VP2-located neutralizing epitope on various vaccine, pathogenic and hypervirulent strains of infectious bursal disease virus. *Arch Virol.* (1997) 142:255–70. doi: 10.1007/s007050050075
12. Reed LJ, Muench H. A simple method of estimating fifty per cent endpoints. *Am J Epidemiol.* (1938) 27:493–7. doi: 10.1093/oxfordjournals.aje.a118408
13. R Core Team. *R: A Language and Environment for Statistical Computing*. 4.0.3 ed. Vienna: R Foundation for Statistical Computing (2020).
14. Hervé M. *RVAideMemoire: Testing and Plotting Procedures for Biostatistics*. R package version 0.9-79. ed (2021).
15. Mendiburu Fd. *agricolae: Statistical Procedures for Agricultural Research*. R package version 1.3-3. ed (2020).

16. Guittet M, Le Coq H, Picault JP, Eterradossi N, Bennejean G. Safety of infectious bursal disease vaccines: assessment of an acceptability threshold. *Dev Biol Standard.* (1992) 79:147–52.
17. Wang W, Huang Y, Ji Z, Chen G, Zhang Y, Qiao Y, et al. The full region of n-terminal in polymerase of ibdv plays an important role in viral replication and pathogenicity: either partial region or single amino acid V4I substitution does not completely lead to the virus attenuation to three-yellow chickens. *Viruses.* (2021) 13:107. doi: 10.3390/v13010107
18. Wang W, Huang Y, Zhang Y, Qiao Y, Deng Q, Chen R, et al. The emerging naturally reassortant strain of IBDV (genotype A2dB3) having segment A from Chinese novel variant strain and segment B from HLJ 0504-like very virulent strain showed enhanced pathogenicity to three-yellow chickens. *Transbound Emerg Dis.* (2021). doi: 10.1111/tbed.14336. [Epub ahead of print].
19. Sivanandan V, Maheswaran SK. Immune profile of infectious bursal disease: I. Effect of infectious bursal disease virus on peripheral blood T and B lymphocytes of chickens. *Avian Dis.* (1980) 24:715–25. doi: 10.2307/1589807
20. Withers DR, Davison TF, Young JR. Diversified bursal medullary B cells survive and expand independently after depletion following neonatal infectious bursal disease virus infection. *Immunology.* (2006) 117:558–65. doi: 10.1111/j.1365-2567.2006.02332.x
21. Kim IJ, Gagic M, Sharma JM. Recovery of antibody-producing ability and lymphocyte repopulation of bursal follicles in chickens exposed to infectious bursal disease virus. *Avian Dis.* (1999) 43:401–13. doi: 10.2307/1592637

Conflict of Interest: The authors declare that the research was conducted in the absence of any commercial or financial relationships that could be construed as a potential conflict of interest.

Publisher's Note: All claims expressed in this article are solely those of the authors and do not necessarily represent those of their affiliated organizations, or those of the publisher, the editors and the reviewers. Any product that may be evaluated in this article, or claim that may be made by its manufacturer, is not guaranteed or endorsed by the publisher.

frontiers | Frontiers in Microbiology

ORIGINAL RESEARCH
published: 27 April 2022
doi: 10.3389/fmicb.2022.868377

Residues 140–142, 199–200, 222–223, and 262 in the Surface Glycoprotein of Subgroup A Avian Leukosis Virus Are the Key Sites Determining Tva Receptor Binding Affinity and Infectivity

*Jinqun Li[1†], Jian Chen[1†], Xinyi Dong[1], Canxin Liang[1], Yanyan Guo[1], Xiang Chen[1], Mengyu Huang[1], Ming Liao[1,2,3,4,5] and Weisheng Cao[1,2,3,4,5]**

[1] College of Veterinary Medicine, South China Agricultural University, Guangzhou, China, [2] Key Laboratory of Zoonosis Prevention and Control of Guangdong Province, Guangzhou, China, [3] National and Regional Joint Engineering Laboratory for Medicament of Zoonosis Prevention and Control, South China Agricultural University, Guangzhou, China, [4] Key Laboratory of Veterinary Vaccine Innovation of the Ministry of Agriculture, Guangzhou, China, [5] Key Laboratory of Zoonosis of Ministry of Agriculture and Rural Affairs, Guangzhou, China

OPEN ACCESS

Edited by:
Aijian Qin,
Yangzhou University, China

Reviewed by:
Qi Wang,
National Agricultural Science and Technology Center (CAAS), China
Jianqiang Ye,
Yangzhou University, China

***Correspondence:**
Weisheng Cao
caoweish@scau.edu.cn

[†] These authors have contributed equally to this work

Specialty section:
This article was submitted to Virology, a section of the journal Frontiers in Microbiology

Received: 02 February 2022
Accepted: 05 April 2022
Published: 27 April 2022

Citation:
Li J, Chen J, Dong X, Liang C, Guo Y, Chen X, Huang M, Liao M and Cao W (2022) Residues 140–142, 199–200, 222–223, and 262 in the Surface Glycoprotein of Subgroup A Avian Leukosis Virus Are the Key Sites Determining Tva Receptor Binding Affinity and Infectivity. Front. Microbiol. 13:868377. doi: 10.3389/fmicb.2022.868377

Subgroup A avian leukosis virus (ALV-A) invades cells through *gp85*-encoded surface glycoprotein (SU) *via* specifically recognizing the cellular receptor Tva. To identify the key residues of ALV-A SU that determine the Tva binding affinity and infectivity in DF-1 cells, a strategy of substituting corresponding residues of SU between ALV-A RSA and ALV-E ev-1 (using Tvb as the receptor) was adopted. A series of chimeric soluble gp85 proteins were expressed for co-immunoprecipitation (co-IP) analysis and blocking analysis of viral entry, and various recombinant viruses based on replication-competent avian retrovirus vectors containing Bryan polymerase (RCASBP) were constructed for transfection into DF-1 cells and measurement of the percentage of GFP-positive cells. The results revealed that the substitution of residues V138, W140, Y141, L142, S145, and L154 of host range region 1 (hr1), residues V199, G200, Q202, R222, and R223 of host range region 2 (hr2), and residue G262 of variable region 3 (vr3) reduced the viral infectivity and Tva binding affinity, which was similar to the effects of the −139S, −151N, −155PWVNPF, −201NFD, Δ214–215, and −266S mutations. Our study indicated that hr1 and hr2 contain the principal receptor interaction determinants, with new identified-vr3 also playing a key role in the receptor binding affinity of ALV-A.

Keywords: avian leukosis viruses, Tva, surface glycoprotein, binding affinity, infectivity

INTRODUCTION

Avian leukosis virus (ALV), a member of the genus *Alpharetrovirus* and the family *Retroviridae*, has been classified into 11 subgroups from A to K based on the host range, antibody neutralization, and interference in superinfection experiments (Chesters et al., 2002; Zhang et al., 2014; Prikryl et al., 2019). Subgroup A of ALV (ALV-A), an exogenous ALV subgroup associated with neoplastic and

immunosuppressive diseases, could cause serious economic losses to the poultry industry, as there is no effective vaccine or drug to control infection (Wang et al., 2020; Lipsick, 2021).

Like most retroviruses, ALV initially synthesizes its envelope glycoprotein (Env) as a precursor that is subsequently processed into two subunits: *gp85*-encoded surface glycoprotein (SU), which contains the main domains that interact with the host receptor, and transmembrane glycoprotein (TM), which anchors SU on the membrane with a stable covalent disulfide bond (Smith and Cunningham, 2007; Li et al., 2020; Deng et al., 2021). The SU glycoproteins of ALV-A through ALV-E are highly conserved except for two host range regions (hr1 and hr2) and three variable regions (vr1, vr2, and vr3) (Federspiel, 2019). Previous studies have revealed that the hr1 and hr2 domains contain the principal determinants of receptor interaction, while the vr3 domain contributes to the specificity of receptor recognition for initiating effective infection but not to receptor binding affinity (Holmen et al., 2001; Melder et al., 2003; Federspiel, 2019; Munguia and Federspiel, 2019). The variable regions of vr1 and vr2 did not appear to be required for binding affinity or receptor specificity (Dorner et al., 1985; Melder et al., 2003).

For ALVs to invade cells, their envelope proteins must primarily bind to cell surface receptor proteins (Federspiel, 2019). Unlike human immunodeficiency virus (HIV), which needs dual coreceptors to invade cells (Weichseldorfer et al., 2022), ALVs, a group of simple retroviruses similar to mouse leukemia virus (MLV; Bova et al., 1988), require only a single functional receptor to infect target cells. Members of different families of proteins have been identified as receptors of ALV: Tva for ALV-A/K (Prikryl et al., 2019), Tvb for ALV-B/D/E (Adkins et al., 2000; Brojatsch et al., 2000), Tvc for ALV-C (Elleder et al., 2005), and chicken Na^+/H^+ exchanger type 1 for ALV-J (Chai and Bates, 2006). Some studies on the functional domain of ALV receptor have confirmed that a few specific amino acid residues play a key role in binding to ALV Env proteins and mediating viral infection (Rong and Bates, 1995; Klucking and Young, 2004; Guan et al., 2018; Kheimar et al., 2021). However, under the selective pressure of entry competitors, ALVs have the ability to evolve the structure of their Env proteins to use different cellular proteins as receptors (Munguia and Federspiel, 2019).

The SU glycoproteins of ALV-A RSA (GenBank: M37980.1) and the endogenous virus ALV-E ev-1 (GenBank: AY013303.1) used in this study show high homology, and the regions with differences are mainly located in hr1, hr2, and vr3. However, different receptors are involved in the invasion and sensitivity of DF-1 cells, a permanent, non-transformed cell line derived from Line 0 chicken embryo fibroblasts, which is insensitive to ALV-E (Federspiel et al., 1991). Therefore, the differences between the binding sites of ALV-A and ALV-E determine the mechanism of cell invasion. In other words, hr1, hr2, and vr3 may be the key regions determining the Tva receptor binding affinity and infectivity in DF-1 cells.

To verify this conjecture, a series of chimeric gp85 proteins and recombinant viruses were evaluated by replacing the residues corresponding to ALV-E ev-1 for Tva binding and viral infectivity. Our results indicated that hr1 and hr2 contain the principal binding domains between SU and the Tva receptor, with vr3 playing a key role in the receptor binding affinity of ALV-A.

MATERIALS AND METHODS

Cell Cultures and Antibodies

DF-1 cells (from ATCC, kept in our lab) were grown in Dulbecco's Modified Eagle's Medium (DMEM; Gibco, Carlsbad, CA, United States) supplemented with 10% fetal bovine serum (FBS; Gibco, Australia), 100 units/ml of penicillin, and 100 mg/ml of streptomycin (Gibco, Carlsbad, CA, United States) in the presence of 5% CO_2 at 39°C. 293T cells were cultured in DMEM supplemented with 10% FBS at 37°C in a 5% CO_2 atmosphere. The mouse anti-HA tag antibody was purchased from Thermo Fisher Scientific Inc. (Rockford, IL, United States), whereas the mouse anti-flag M2 tag antibody and the rabbit anti-GAPDH antibodies were purchased from Sigma (Sigma-Aldrich, St. Louis, MO, United States). IRDye 680RD goat anti-mouse IgG (H + L) antibody was purchased from LI-COR Biosciences (Lincoln, NE, United States).

Construction of Recombinant RCASBP Retroviral Vector With ALV-A RSA and ALV-E ev-1

The construction of the RCASBP (A)-EGFP retroviral vector [the ALV-based replication-competent RCASBP vector with the ALV-A RSA *env* gene and the enhanced green fluorescent protein (EGFP) gene] and the RCASBP (E)-EGFP retroviral vector has been described previously (Chen et al., 2020). Similar to the method of constructing RCASBP (K/E)-EGFP described previously (Chen et al., 2020), a series of fragments containing the 3′ end of *pol*, mutant SU regions, and complete TM regions were amplified by overlapping PCR with corresponding primers (**Supplementary Table 1**) and cloned into the unique *KpnI* and *StuI* sites of RCASBP (A)-EGFP to construct various recombinant RCASBP (A/E)-EGFP vectors.

Construction of Plasmids Expressing the Tva Receptor and Various Chimeric Soluble gp85 Proteins

The eukaryotic plasmid pCAGGS-Tva-HA-Fc, encoding chicken Tva, HA tag, and the human IgG-Fc fragment, which specifically binds to the protein A/G (Lexington, MA, United States), has been described previously (Chen et al., 2020). To express gp85 protein in a soluble form and facilitate identification, a signal peptide designated "s" and 3 × flag tags were fused to its N-terminus and C-terminus, respectively. The *s-gp85-flag* sequence was subsequently cloned into the *EcoRI* and *BglII* sites of pCAGGS to construct a eukaryotic plasmid (pCAGGS-s-RSA-gp85-flag). Similar to the method of constructing RCASBP (A/E)-EGFP, the residues of RSA SU were replaced with the corresponding ev-1 residues by overlapping PCR with corresponding primers (**Supplementary Table 2**), and various recombinant pCAGGS-s-gp85-flag plasmids

encoding chimeric soluble gp85 proteins were constructed by homologous recombination.

Fluorescence-Activated Cell Sorting Analysis of Recombinant Virus Infecting DF-1 Cells

Virus propagation was initiated by the transfection of plasmid DNA that contained the retroviral vector in proviral form. DF-1 cells in 6-well plates were transfected with 1 μg of RCASBP (A/E)-EGFP vector using Lipofectamine 3000 reagent (Shanghai, China) and passaged at 48 h posttransfection. The cells were then visualized under a Leica DMI 4000B fluorescence microscope (Leica, Wetzlar, Germany) and collected to determine the percentage of GFP-positive cells by FACS using an LSRII analyzer (Becton, Dickinson and Company, United States) at 5 or 7 days posttransfection.

Blocking Analysis of gp85 Protein Binding to Receptor

Using PolyJet DNA transfection reagent (Rockville, MD, United States), 4 μg optimal transfection amount (**Supplementary Figure 1**) of the respective recombinant pCAGGS-s-gp85-flag plasmid was transfected into 293T cells with 95% confluence in a 60 mm culture dish. At 8 h posttransfection, the cell supernatant with transfection mixtures was replaced by 3 mL of fresh DMEM with 1% FBS. The supernatant was subsequently collected at 48 h posttransfection as the source of recombinant gp85 proteins. DF-1 cells with 75% confluence in 24-well plates were washed with phosphate-buffered saline (PBS) and incubated with chimeric gp85 proteins for 1 h at 4°C. After discarding the supernatant, DF-1 cells were incubated with 0.1 multiplicity of infection (MOI) ALV-A RSA obtained by RCASBP (A)-EGFP transfection for 2 h at 39°C. The cells were then washed 5 times with PBS and cultured in 1% FBS DMEM for 5 days to measure the percentage of GFP-positive cells by FACS. The higher the binding affinity of the gp85 protein to the Tva receptor was, the lower the percentage of GFP-positive cells.

Co-immunoprecipitation and Pull-Down Assay

To express chimeric soluble gp85 proteins, 4 μg of pCAGGS-s-gp85-flag plasmid was transfected into 293T cells in a 60 mm culture dish using PolyJet DNA transfection reagent. At 48 h posttransfection, the culture supernatant was collected and the cells were lysed with NP-40 buffer (Beyotime Biotechnology, Shanghai, China) for the next experiment. Cleared supernatant harvested from 293T cells transfected with pCAGGS-Tva-HA-Fc was concentrated to 1/10 volume through a 10 kDa molecular weight cutoff ultrafiltration spin columns (Merck Millipore, Darmstadt, Germany) and the Tva proteins were purified using 60 μL of Protein A/G agarose for 2 h at 4°C with gentle agitation. After washing 5 times with ice-cold PBS, the Protein A/G agarose was incubated with recombinant soluble gp85 proteins for 5 h at 4°C. After washing again with ice-cold PBS, the bound proteins were denatured by heating for 5 min at 100°C with SDS–PAGE sample loading buffer.

Western Blotting

The denatured protein was separated by 10% SDS–PAGE (Beyotime Biotechnology, Shanghai, China) and transferred to nitrocellulose membranes (Merck Millipore, Darmstadt, Germany). After blocking with 5% non-fat powdered milk for 1 h at room temperature and washing 3 times with TBST (Tris-buffered saline containing 0.1% Tween 20), the membranes were incubated with anti-FLAG or anti-HA monoclonal antibody at 4°C overnight. After washing again with TBST, the membranes were incubated with IRDye 680RD goat anti-mouse IgG (H + L) antibody for 1 h at room temperature. Finally, an Odyssey Infrared Imaging System (LI-COR Biosciences, Lincoln, NE, United States) was used to scan the membrane spots.

Statistical Analysis

Data are shown as the means ± standard deviations in triplicate from a representative experiment and were analyzed by Student's *t*-test using GraphPad Prism 7. A P value of <0.05 was considered significant. *, **, ***, and **** indicate P values less than 0.05, 0.01, 0.001, and 0.0001, respectively. These experiments were performed independently at least three times with similar results.

RESULTS

Low Homology Between ALV-A and ALV-E in the hr1, hr2, and vr3 Regions

The SU glycoproteins of ALV-A RSA and ALV-E ev-1 were highly conserved, exhibiting 83.5% homology at the amino acid level according to the ClustalW method in the MegAlign program, with the greatest degree of variability in the hr1, hr2, and vr3 regions. The vr1 and vr2 regions were relatively stable, with changes of only two amino acids and one amino acid, respectively. The residues from hr1 to hr2 and the vr3 region were divided into 12 segments (designated s1–s12) for subsequent research (**Figure 1**).

Substitution of Residues s2–s6 of ALV-A With ALV-E Reduced Tva Binding Affinity and Infectivity in DF-1 Cells

To determine the role of hr1 in the infection and receptor binding of ALV-A, hr1 was divided into six segments and replaced with the corresponding regions of ev-1 to construct a series of chimeric gp85 proteins s1–s6 and recombinant virus vectors RCASBP (A/E)-s1-s6-EGFP (**Figure 2A**). DF-1 cells were separately incubated with s1–s6 chimeric gp85 protein and subsequently infected with RCASBP (A)-EGFP recombinant virus. As expected, the entry of RCASBP (A)-EGFP was blocked by wild-type (wt) A-gp85, and the GFP-positive signal was not present at experimentally detectable levels, in contrast to E-gp85 wt (**Figure 2B**). The chimeric gp85 proteins s1 completely blocked viral entry, whereas s2–s6 significantly reduced the blocking effect, showing higher percentages of GFP-positive cells

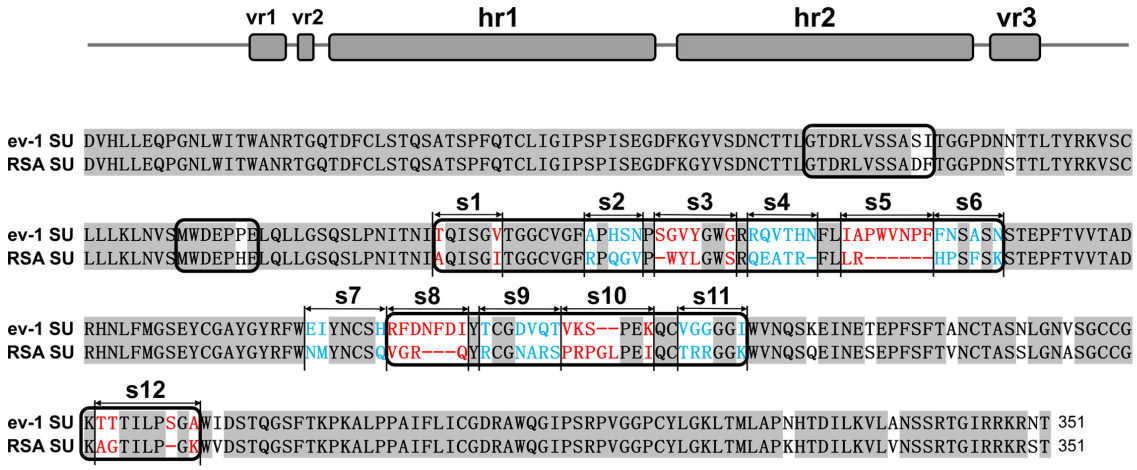

FIGURE 1 | Schematic representations of the replacement fragments and comparison between the amino acid sequences of RSA and ev-1 SU. The amino acid sequences were aligned by using the ClustalW method in the MegAlign program (DNASTAR, Madison, WI, United States). The residues from hr1 to hr2 and the vr3 region were divided into 12 segments (designated s1–s12). ev-1, Subgroup E of avian leukosis virus strain ev-1, GenBank AY013303.1; RSA, Subgroup A of avian leukosis virus strain RSA, GenBank M37980.1. Red and blue letters indicated substitutions of residues in different fragments.

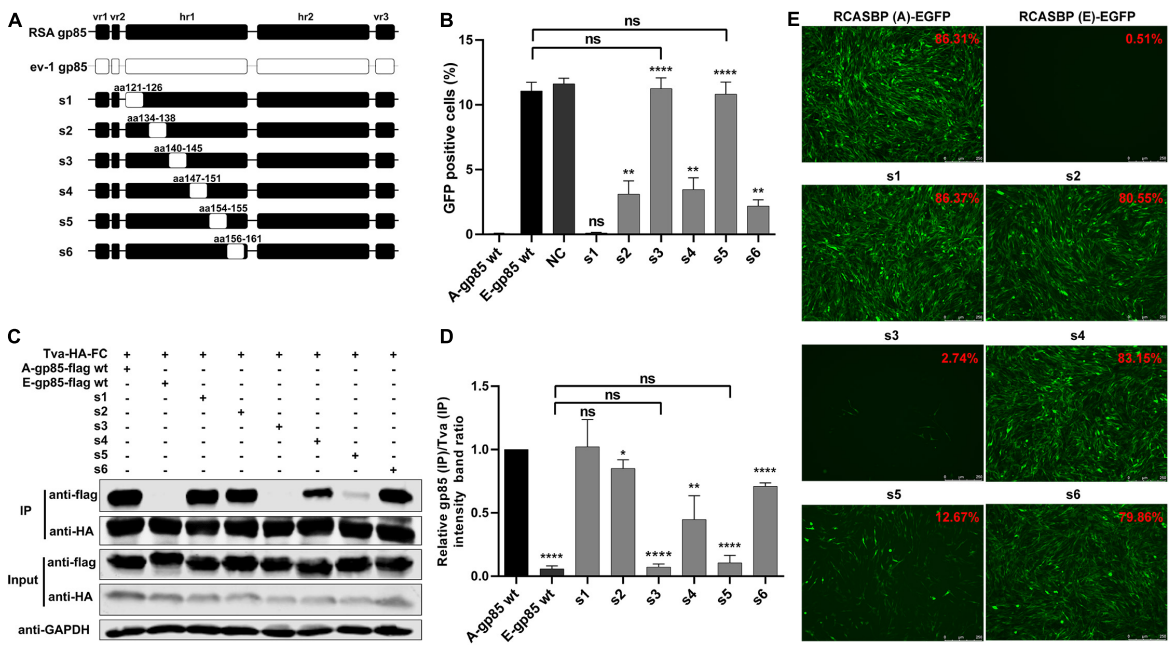

FIGURE 2 | Substitution of residues s1–s6 of ALV-A with ALV-E reduced the Tva binding affinity and infectivity of DF-1 cells. **(A)** Schematic representations of the replacement fragments s1–s6 in hr1. **(B)** DF-1 cells were incubated with chimeric gp85 protein s1–s6 and subsequently infected with RCASBP (A)-EGFP supernatants. The percentage of GFP-positive cells was measured by FACS for blocking analysis of the binding of chimeric gp85 protein to Tva. **(C)** The interaction of chimeric gp85 proteins s1–s6 with Tva-HA-Fc. **(D)** The gray scale value of the protein band was quantified using Image Studio Lite Version 5.2, and gp85 (IP)/Tva (IP) was calculated. **(E)** DF-1 cells transfected with recombinant RCASBP (A/E)-s1-s6-EGFP vectors were visualized under a fluorescence microscope, and the percentage of GFP-positive cells (indicated with red color letters) was detected by FACS 7 days posttransfection. *$P < 0.05$, **$P < 0.01$, ****$P < 0.0001$.

than A-gp85 wt ($p < 0.01$). Moreover, the substitution of residues s3 and s5 showed the maximum reduction in the blocking effect ($p < 0.0001$), which was not statistically different from the result of E-gp85 wt (**Figure 2B**).

Since the blocking effect of gp85 proteins depends on competitive binding to the Tva receptor on the surface of DF-1 cells, the above results suggested that the substitution of residues s2–s6 reduced the binding affinity to the Tva receptor. For further verification, the chimeric soluble gp85 proteins s1–s6 were used for co-IP (**Figure 2C**). The gray values of s2, s3, s4, s5, and s6 were significantly lower than that of A-gp85 wt ($P < 0.05$). In particular, the substitution of residue s3 eliminated

the interaction with Tva, with almost no gray signal detected (**Figures 2C,D**).

Furthermore, DF-1 cells separately transfected with recombinant RCASBP (A/E)-s1-s6-EGFP vectors were visualized under a fluorescence microscope and collected to determine the percentage of GFP-positive cells by FACS. As expected, the substitution of residues s2–s6 reduced the percentage of GFP-positive cells. Moreover, the substitution of s3 almost eliminated the ability to infect DF-1 cells, exhibiting only 2.74% GFP-positive cells (**Figure 2E**).

Substitution of Residues s7–s12 of ALV-A With ALV-E Reduced the Tva Binding Affinity and Infectivity in DF-1 Cells

To further investigate the effects of the region between hr1 and hr2, hr2, and vr3 on the receptor binding affinity and infectivity in DF-1 cells, a series of chimeric gp85 proteins s7–s12 were expressed for co-IP and blocking analysis and various recombinant virus vectors RCASBP (A/E)-s7-s12-EGFP were constructed for viral entry assays (**Figure 3A**). The blocking analysis showed that the percentages of GFP-positive cells of chimeric proteins s7–s12 were significantly higher than those of A-gp85 wt ($p < 0.05$). In particular, the substitution of the vr3 region (s12) exhibited no blocking effect on viral entry ($p < 0.0001$), similar to E-gp85 wt (**Figure 3B**). The results of protein interactions revealed that chimeric proteins s7–s12 all had significantly reduced Tva binding affinity ($p < 0.05$). In particular, the substitution of vr3 eliminated the interaction with Tva (**Figures 3C,D**). To further verify the influence of these residues on infectivity, wild-type and mutant virus vectors RCASBP (A/E)-s7-s12-EGFP were transfected into DF-1 cells, and the percentage of GFP-positive cells was monitored. As expected, all six mutant ALVs had a replication disadvantage over wild-type ALV-A in DF-1 cells, in which the substitution of the vr3 region basically eliminated the ability to infect DF-1 cells, resulting in only 2.61% GFP-positive cells (**Figure 3E**).

Identification of the Key Residues in the s3, s5, s8, and vr3 Regions for ALV-A Binding Receptor and Invading Cells

In the above experiment, substitution of the s3, s5, s8, and s12 regions showed the maximum reduction in receptor binding affinity and infectivity in DF-1 cells. To identify which amino acid residues in s3 and s5 of hr1 determine the interaction of gp85 and Tva, various mutant gp85 proteins with amino acid substitutions in s3 and s5 were expressed for competitive blocking analysis and co-IP assay (**Figure 4A**). While R155A did not, the mutant gp85 proteins −139S, W140G, Y141V, L142Y, S145G, L154I, and −155PWVNPF all reduced but not eliminated the blocking effect of viral entry, as their percentages of GFP-positive cells were significantly higher than that of A-gp85 wt ($p < 0.05$) but lower than that of E-gp85 wt, of which W140G, Y141V, L142Y, and −155PWVNPF had the maximum reduction ($p < 0.0001$, **Figure 4B**). As expected, the co-IP assay showed a similar result: the mutant gp85 protein with amino acid substitutions in s3 and s5 all significantly reduced the binding affinity with Tva except R155A ($p < 0.05$, **Figures 4C,D**).

Similarly, a series of recombinant gp85 proteins targeting single residue mutations in S8 of hr2 and s12 of vr3 were also constructed for blocking analysis and co-IP assay (**Figure 4E**). The percentage of GFP-positive cells suggested that the V199R, G200F, −201NFD, Q202I, G262T, and −266S mutations significantly inhibited interaction with the Tva receptor ($p < 0.05$). In particular, the G262T mutation in vr3 had the maximum reduction in Tva binding affinity (**Figure 4F**). The co-IP assay also showed a similar result (**Figures 4G,H**).

For further verification, the corresponding recombinant RCASBP (A/E)-EGFP vectors with amino acid substitutions in s3, s5, s8, and s12 were transfected into DF-1 cells, and the infection ability was detected by FACS (**Figure 4I**). As expected, the percentages of GFP-positive cells for the R155A, R201D, A261T, and K268A mutations were not statistically different from that of RCASBP (A)-EGFP, whereas the mutations −139S, W140G, Y141V, L142Y, S145G, L154I, −155PWVNPF, V199R, G200F, −201NFD, Q202I, G262T, and −266S significantly reduced the level of virus replication in DF-1 cells ($p < 0.001$, **Figure 4I**). These results suggested that the residues of W140, Y141N, L142, S145, and L154 in hr1; V199, G200, and Q202 in hr2; and G262 in vr3 play key roles in determining receptor binding affinity and infectivity of DF-1 cells.

Identification of the Key Residues in the s2, s4, s6, s7, s9, and s11 Regions for ALV-A Binding Receptor and Invading Cells

In addition to s3, s5, s8, and s12, the substitution of residues s2, s4, s6, s7, s9, s10, or s11 of ALV-A RSA with ALV-E ev-1 also reduced the receptor binding affinity and infectivity in DF-1. To further determine which amino acid residue in these regions plays a key role, a series of mutant gp85 proteins with amino acid substitutions in s2, s4, s6, s7, s9, s10, and s11 were expressed and divided into three groups for the competitive blocking test (**Figures 5A,C,E**). The results showed that the blocking effect of the mutations R134A, G137S, V138N in s2, and H156F, P157N, F159A in s6 was statistically reduced ($p < 0.05$, **Figure 5B**), which was similar to the effect of the mutations −151N in s4 and Δ214–215 in s10 ($p < 0.0001$, **Figure 5D**), as well as N192E, Q198H in s7, N207D, A208V, R209Q in s9, and R222G, R223G, K226I in s11 ($p < 0.05$, **Figure 5F**). For further confirmation, five recombinant RCASBP (A/E)-EGFP vectors with the mutations V138N, −151N, P157N, Δ214–215, R222G, and R223G, which had the maximum reduction in receptor binding affinity above, were transfected into DF-1 cells, and the percentage of GFP-positive cells was detected by FACS. As expected, all five mutations inhibited virus replication in DF-1 cells ($p < 0.001$, **Figure 5G**).

Back Mutation Restored the Interaction Between gp85 and Tva

To verify the identified key amino acid residues determining the binding affinity of ALV-A SU to Tva, using ALV-E ev-1

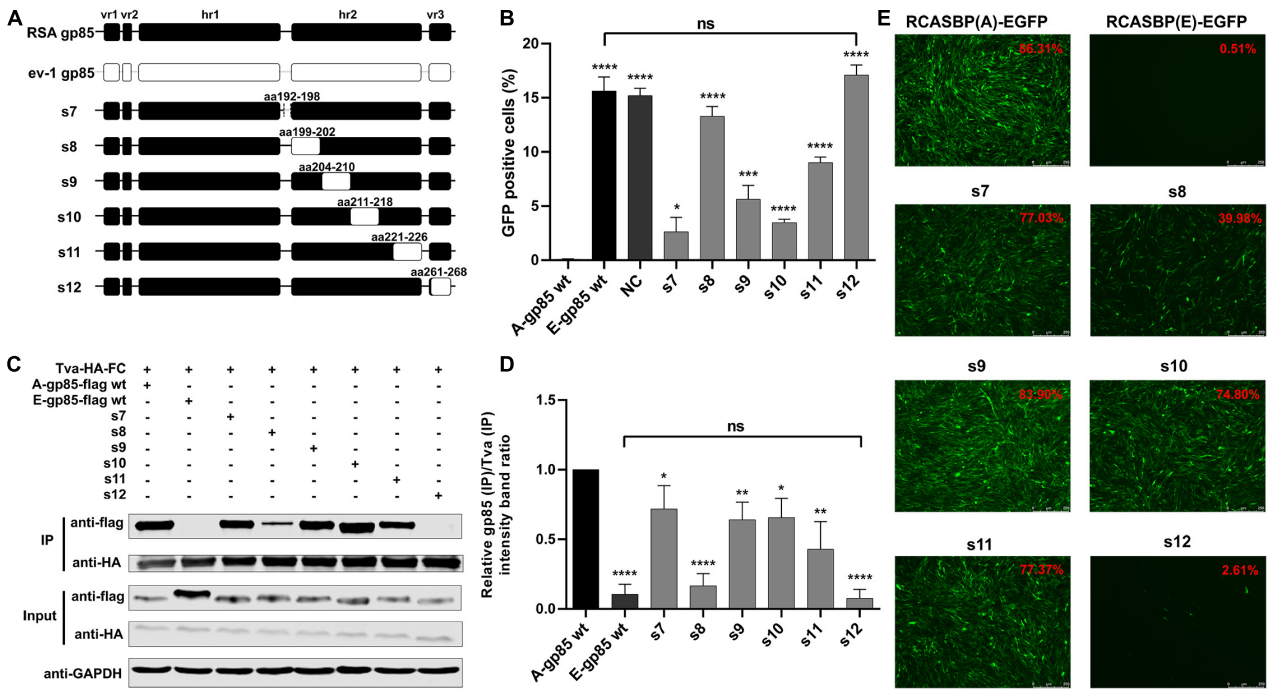

FIGURE 3 | Substitution of residues s7–s12 of ALV-A with ALV-E reduced the Tva binding affinity and infectivity in DF-1 cells. **(A)** Schematic representations of the replacement fragments s7–s12. **(B)** DF-1 cells were incubated with chimeric gp85 protein s7–s12 and subsequently infected with RCASBP (A)-EGFP supernatants. The percentage of GFP-positive cells was measured by FACS for blocking analysis of the binding of chimeric gp85 proteins to Tva. **(C)** The interaction of chimeric gp85 protein s1–s6 with Tva-HA-Fc. **(D)** The gray scale value level of gp85 (IP)/Tva (IP) was calculated. **(E)** DF-1 cells transfected with recombinant RCASBP (A/E)-s1-s6-EGFP vectors were visualized under a fluorescence microscope and the percentage of GFP-positive cells (indicated with red color letters) was detected by FACS 7 days posttransfection. *$P < 0.05$, **$P < 0.01$, ***$P < 0.001$, ****$P < 0.0001$.

SU as the skeleton, the gp85 protein was replaced with the corresponding regions of ALV-A RSA (A134R, G137S, N138V, S140-, G141W, V142Y, Y143L, G146S, N153-, I156L, Δ158–163, F164H, N165P, A167F, R207V, F208G, Δ209–211, I213Q, −224GL, G231R, G232R, T272G, and S277-) to construct a back mutant protein E/A-gp85 (**Figure 6A**). As expected, co-IP and pull-down assays showed that the back mutant E/A-gp85 protein could interact with Tva protein (**Figure 6B**). Moreover, the back mutation partially restored the blocking effect of RCASBP (A)-EGFP in the infection of DF-1 cells, exhibiting only 12.97% GFP-positive cells (**Figure 6C**), which was lower than that of E-gp85 wt (30.96%) but higher than that of A-gp85 wt (0.21%). Therefore, the corresponding residues R134, G137, V138, W140, Y141, L142, S145, L154, H156, P157, and F159 in hr1; V199, G200, Q202, G214, L215, R222, and R223 in hr2; and G262 in vr3 were the key sites for ALV-A SU binding to the Tva receptor.

DISCUSSION

Subgroup A-E avian leukosis viruses are a group of highly related retroviruses that evolved their env genes encoding viral envelope glycoproteins from a common ancestor to use very different members of the host protein families as receptors, enabling efficient viral entry (Federspiel, 2019). Among them, ALV-A shares Tva as a receptor with ALV-K (Prikryl et al., 2019), while ALV-E shares the tumor necrosis factor receptor encoded by three alleles (tvbs^1, tvbs^3, and tvbst) as a receptor with ALV-B/D (Adkins et al., 2000). The amino acid differences of Env between ALV-A and ALV-E are concentrated in three regions (hr1, hr2, and vr3) of the SU glycoprotein (**Figure 1**). Therefore, hr1, hr2, and vr3 may be the key regions determining Tva receptor binding affinity and infectivity in DF-1 cells, a permanent cell line that is sensitive to exogenous ALV but insensitive to ALV-E (Federspiel et al., 1991). To verify this hypothesis, using a strategy of substituting corresponding residues of SU between ALV-A RSA and ALV-E ev-1, a series of chimeric gp85 proteins were expressed for blocking analysis and co-IP assay, while various recombinant virus vectors based on RCASBP were transfected into DF-1 cells for infectivity analysis. The results revealed that the substitution of residues s2 (aa134–138) to s12 (aa261–268) all reduced the blocking effect against RCASBP (A)-EGFP, the binding affinity of Tva, and replication in DF-1 cells (**Figures 2**, **3**), and residues 138, 140, 141, 142, 145, 154 in hr1, residues 199, 200, 222, 223 in hr2, and residue 262 in vr3 were the key sites determining receptor binding affinity and infectivity in DF-1 cells (**Figures 4–6**). In particular, the substitution of residues 140–142, 199–200, 222–223, and 262 of ALV-A with ALV-E exhibited no blocking effect on viral entry (**Supplementary Figure 2**). Our study indicates that hr1 and hr2 contain the principal receptor interaction determinants, with vr3 also playing a key role in the receptor binding affinity in ALV-A.

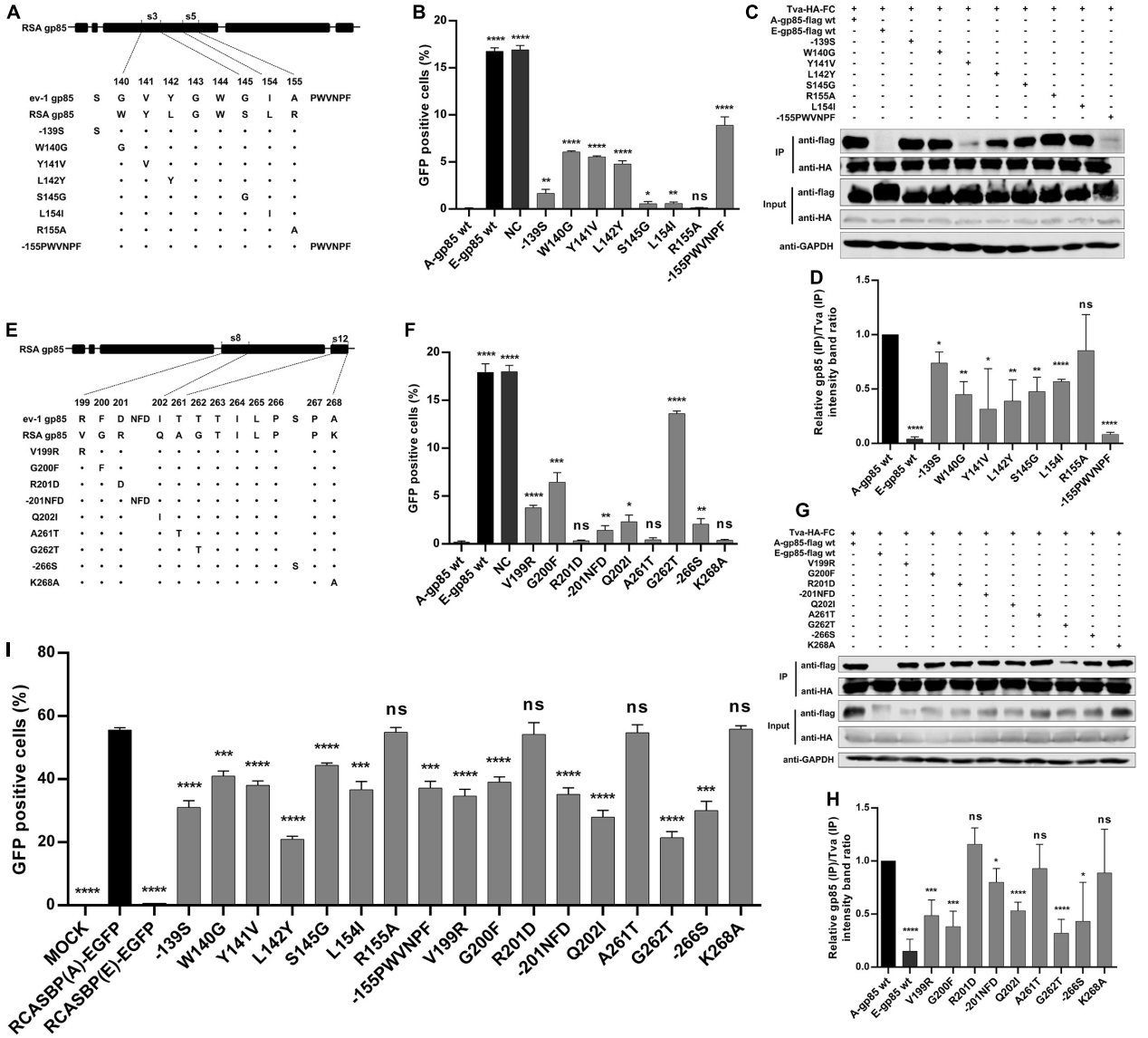

FIGURE 4 | Identification of the key residues in the s3, s5, s8, and vr3 regions for the ALV-A binding receptor and invading cells. **(A,E)** Schematic representation of amino acid substitutions in s3 and s5 or s8 and s12. **(B,F)** DF-1 cells were incubated with mutant gp85 proteins with amino acid substitutions in s3 and s5 or s8 and s12 and subsequently infected with RCASBP (A)-EGFP. The percentage of GFP-positive cells was measured by FACS for blocking analysis. **(C,G)** The interaction of the mutant gp85 protein with amino acid substitutions in s3 and s5 or s8 and s12 with Tva-HA-Fc. **(D,H)** The gray scale value level of gp85 (IP)/Tva (IP) was calculated. **(I)** DF-1 cells transfected with recombinant RCASBP (A/E)-EGFP vectors with mutations V138N, −151N, Δ214–215, R222G, or R223G were detected for the percentage of GFP-positive cells by FACS 5 days posttransfection. *$P < 0.05$, **$P < 0.01$, ***$P < 0.001$, ****$P < 0.0001$.

In previous studies on retroviruses, the domain of SU glycoprotein that binds to host cell receptors can be classified into two types: one is concentrated in the highly variable region in SU, as in mouse leukemia virus and ALV-A/B/C/D/E/K (Battini et al., 1995; Federspiel, 2019; Chen et al., 2020); the other is composed of a complex of discontinuous and multivariate segments of the SU protein, as in human immunodeficiency virus, equine infectious anemia virus, and ALV-J (Kwong et al., 1998; Sun et al., 2008; Zhang et al., 2020). Previous studies have determined that hr1 and hr2 are the principal binding domains between the viral glycoprotein trimer and the host protein receptor (Tsichlis et al., 1980; Federspiel, 2019). Consistently our research showed that the substitution of residues s2–s6 (aa134–161) in hr1 (**Figure 2**) and s8–s11 (aa192–216) in hr2 (**Figure 3**) of ALV-A all had a negative influence on the infectivity of DF-1 cells and the interaction between SU and the receptor. Specifically, residues R134, G137, V138, W140, Y141, L142, S145, L154, H156, P157, and F159 in hr1 and V199, G200, Q202, G214, L215, R222, and R223 in hr2 were the key sites for ALV-A SU binding to the Tva receptor (**Figures 4**, **5**). Moreover, in our previous studies, we replaced the residues between hr1 and hr2 of ALV-K with those of ALV-E and found that the mutant SU retained its binding affinity

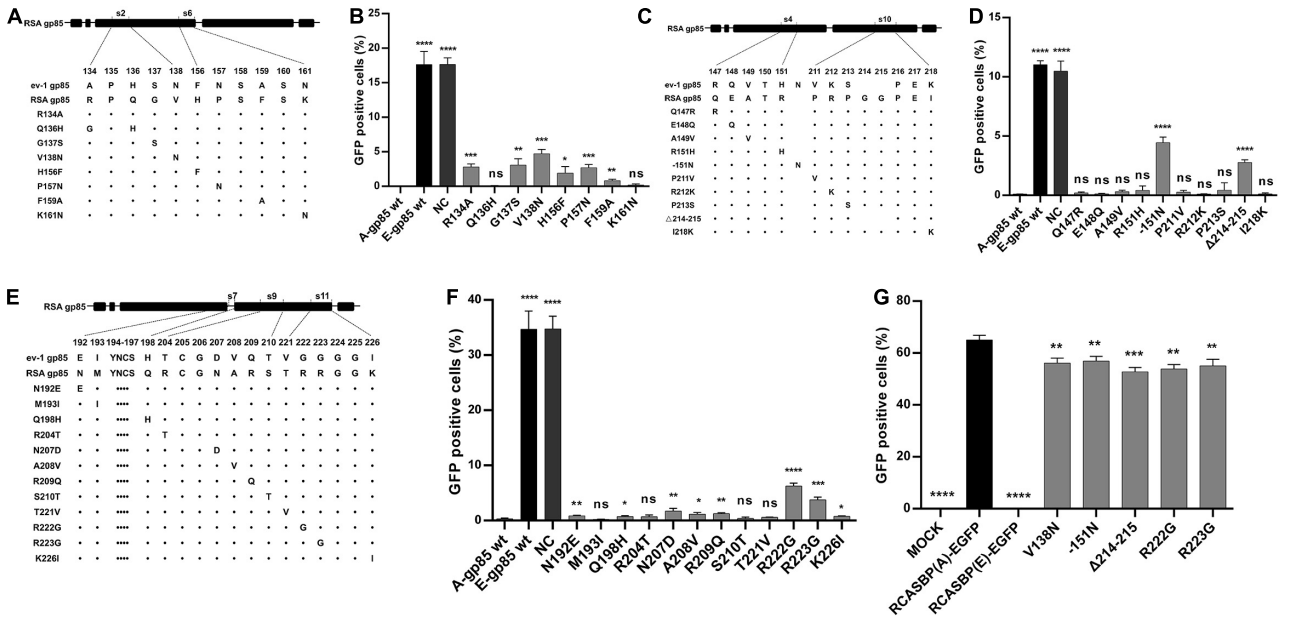

FIGURE 5 | Identification of the key residues in the s2, s4, s6, s7, s9, s10, and s11 regions for the ALV-A binding receptor and invading cells. **(A,C,E)** Schematic representation of amino acid substitutions in s2 and s6, s4 and s10, or s7, s9, and s11. **(B,D,F)** DF-1 cells were incubated with mutant gp85 proteins with amino acid substitutions in s2 and s6 or s4 and s10 or s7, s9, and s12 and subsequently infected with RCASBP (A)-EGFP. The percentage of GFP-positive cells was measured by FACS for blocking analysis. **(G)** DF-1 cells transfected with recombinant RCASBP (A/E)-EGFP vectors with amino acid substitutions in s3, s5, s8, and s12 were detected for the percentage of GFP-positive cells by FACS 5 days posttransfection. **P* < 0.05, ***P* < 0.01, ****P* < 0.001, *****P* < 0.0001.

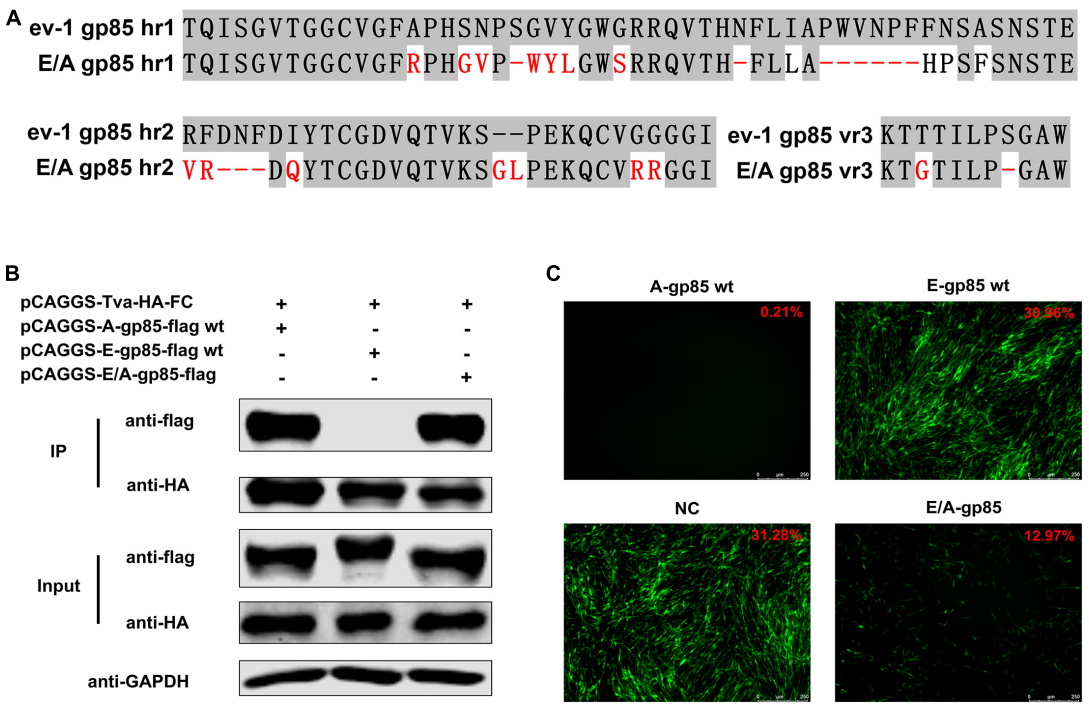

FIGURE 6 | Back mutation restored the interaction between gp85 and Tva. **(A)** Schematic representation of back mutation. **(B)** The interaction of A-gp85-flag wt, E-gp85-flag wt, and back mutant protein E/A-gp85-flag with Tva-HA-Fc. **(C)** DF-1 cells were incubated with A-gp85 wt, E-gp85 wt, and back mutant E/A-gp85 protein and subsequently infected with RCASBP (A)-EGFP. The cells were visualized under a fluorescence microscope and the percentage of GFP-positive cells (indicated with red color letters) was detected by FACS for blocking analysis.

to Tva, but the infectivity of the recombinant virus was almost completely negated (Chen et al., 2020). However, this study revealed that the domain between hr1 and hr2 of ALV-A could affect not only the infectivity in DF-1 cells but also the binding affinity of SU and Tva to a certain extent (**Figure 3**), although it did not appear to be required for restoring the interaction between the back mutant SU and the Tva receptor (**Figure 6**).

It is worth noting that although previous studies have revealed that the vr3 domain contributes to the specificity of receptor recognition for initiating effective infection but not to receptor binding affinity (Federspiel, 2019), our results indicated that the vr3 region plays an essential role in the direct binding affinity between ALV-A SU and Tva receptor. After we replaced the vr3 domain of ALV-A with ALV-E, the recombinant virus hardly infected DF-1 cells and the recombinant gp85 protein appeared to lose its binding affinity to Tva (**Figures 3B–D**). Further single amino acid substitution demonstrated that residue G262 is essential for the binding of SU to Tva, mutation of G262 significantly reduced the blocking effect of viral entry, the Tva receptor binding affinity, and infectivity of the recombinant virus (**Figures 4F–I**).

The cellular receptor of ALV-A, Tva, utilizes a 40-residue, acidic domain to mediate viral entry (Rong and Bates, 1995). This domain of Tva is closely related to the ligand-binding domain of the low-density lipoprotein receptor (LDLR), which binds ligand *via* the interaction between acidic amino acids in the receptor and clustered basic residues in the ligand (Wilson et al., 1991). Analysis of the env sequence of ALV-A revealed a cluster of unique basic residues in hr2, suggesting a potential role of these residues in receptor recognition. Previous studies have shown that residues 210, 213, 223, 224, and 227 of the ALV-A SR-A isolate are important for effective infection (Rong et al., 1997). In addition, the alanine substitution of amino acids R213 or K227 reduced the receptor binding affinity by approximately 50%, while the alanine substitution of R210, R223, or R224 had no effect, suggesting that the effect of the basic residue mutations on envelope-mediated infection did not parallel the effect on receptor binding. However, our research showed an interesting result: the mutation R209Q, R222G, R223G, or K226I of the ALV-A RSA isolate (corresponding to residues R210, R223, R224, and K227 of SR-A) diminished the blocking effect against RCASBP (A)-EGFP (**Figure 5F**), suggesting a lower receptor binding affinity of these mutations, while the mutation R212K (corresponding to residue R213 of SR-A) had no effect (**Figure 5D**). This may be related to the basicity of L-lysine, as receptor binding was diminished significantly by alanine substitution but not by L-lysine substitution at R213 (Rong et al., 1997). In addition, although alanine substitution on R223 or R224 had no effect on receptor binding in a previous study, our research found that glycine substitution at the corresponding residue of ALV-A RSA could significantly reduce the blocking effect of viral entry (**Figure 5F**) and infectivity of DF-1 cells (**Figure 5G**), indicating that residues R222 and R223 of ALV-A RSA play an important role in receptor interaction. A similar result also appeared at residue Y141 (corresponding to residue Y142 of the ALV-A SR-A isolate) in hr1. Previous studies have revealed that the Y142N mutation of SR-A reduced the binding affinity of the env glycoproteins for quail but not chicken sTva-mIgG and the infectivity in cells expressing quail but not chicken Tva (Holmen et al., 2001). However, the chicken Tva receptor binding affinity and the infectivity in DF-1 cells were both significantly inhibited by mutating Y141 of ALV-A RSA to valine in our research (**Figures 4B–D,I**). Therefore, different amino acid mutations at the same site of SU may have different results on receptor interaction and virus invasion.

Due to the low fidelity in the reverse transcription process, ALV replicates with an extremely high mutation rate and exhibits huge genetic diversity, allowing the virus to quickly adapt to the external environment and develop resistance to the host immune response and antiviral drugs (Dong et al., 2017). Under external selection pressure, ALVs have the ability to change their cell invasion mechanism by evolving the structure of their Env proteins (Yin et al., 2019). ALV-A, in the presence of a competitive inhibitor, sTva-mIgG, evolved three variants (Y142N, W141G K261E, and W145R K261E) that may expand viral receptor usage while retaining wt levels of binding affinity for the chicken Tva receptor (Melder et al., 2003). In addition, the selected ALV-A variant had a six-amino acid deletion in residues 155–160 of hr1 in the presence of the subgroup A SU immune adhesin, expanding the use of Tvb and Tvc receptors and possibly other cell surface proteins for entry, while maintaining the ability to use the Tva receptor (Munguia and Federspiel, 2019). Our results showed that the substitutions W140 (corresponding to residue W141 of SR-A), Y141 (corresponding to residue Y142 of SR-A), s5 (aa153–155), and s6 (156–163) all had negative effects on receptor binding and viral infectivity (**Figures 2**, **4**), suggesting a potential role of these residues in receptor recognition and viral invasion. In this study, utilizing a strategy of site-directed mutagenesis to substitute ALV-A SU with the corresponding sequence of ALV-E, a series of key amino acid positions that determine receptor interaction and virus invasion were systematically identified without excessively affecting the spatial conformation of the SU glycoprotein. However, this strategy cannot truly simulate the evolutionary mutation of ALV-A under the pressure of natural selection. Since ALV-A shares the Tva receptor with ALV-K, ALV-A SU could possibly evolve under selection pressure in the presence of ALV-K glycoprotein immune adhesins. Therefore, the evolutionary direction of ALV-A SU in the presence of ALV-K SU immune adhesins would be an interesting field to explore.

CONCLUSION

The substitutions of residues s2 (aa134–139) to s12 (aa261–268) of ALV-A RSA with those of ALV-E ev-1 all reduced the blocking effect of viral entry, Tva binding affinity and the infectivity in DF-1 cells, and the substitutions of s3 (aa140–145), s5 (aa153–155), s8 (aa199–202), and s12 (aa261–268) had the most significant reduction. In addition, the substitutions of residues V138, W140, Y141, L142, S145, and L154 in hr1; residues V199, G200, Q202, R222, and R223 in hr2; or residue G262 in vr3 reduced the viral infectivity and the binding affinity of gp85 to Tva, similar to the results of the −139S, −151N,

−155PWVNPF, −201NFD, Δ214–215, and −266S mutations. Our research has proven that the hr1 and hr2 domains of ALV-A contain principal receptor interaction determinants. However, in contrast to previous studies, here the vr3 domain was revealed to play a key role in the receptor binding affinity of ALV-A. This study will help to further clarify the infection mechanism of ALV-A.

DATA AVAILABILITY STATEMENT

The original contributions presented in the study are included in the article/**Supplementary Material**, further inquiries can be directed to the corresponding author.

AUTHOR CONTRIBUTIONS

JL, JC, ML, and WC designed the study, performed the experiments, and analyzed the data. CL, XD, XC, and MH helped to construct a series of RCASBP-based recombinant viruses and pCAGGS-based recombinant gp85 proteins. YG participated in the collection of literature and statistical analysis. All authors contributed to the article and approved the submitted version.

FUNDING

This work was supported by the Key-Area Research and Development Program of Guangdong Province (2020B020222001), National Natural Science Foundation of China (31672552), Poultry Industry Technology System of Guangdong (2021KJ128), and Earmarked Fund for the China Agriculture Research System (CARS-41-G16).

SUPPLEMENTARY MATERIAL

The Supplementary Material for this article can be found online at: https://www.frontiersin.org/articles/10.3389/fmicb.2022.868377/full#supplementary-material

REFERENCES

Adkins, H. B., Brojatsch, J., and Young, J. A. (2000). Identification and characterization of a shared TNFR-related receptor for subgroup B, D, and E *Avian leukosis* viruses reveal cysteine residues required specifically for subgroup E viral entry. *J. Virol.* 74, 3572–3578. doi: 10.1128/jvi.74.8.3572-3578.2000

Battini, J. L., Danos, O., and Heard, J. M. (1995). Receptor-binding domain of murine leukemia virus envelope glycoproteins. *J. Virol.* 69, 713–719. doi: 10.1128/JVI.69.2.713-719.1995

Bova, C. A., Olsen, J. C., and Swanstrom, R. (1988). The avian retrovirus ENV gene family: molecular analysis of host range and antigenic variants. *J. Virol.* 62, 75–83. doi: 10.1128/JVI.62.1.75-83.1988

Brojatsch, J., Naughton, J., Adkins, H. B., and Young, J. A. (2000). TVB receptors for cytopathic and noncytopathic subgroups of *Avian leukosis* viruses are functional death receptors. *J. Virol.* 74, 11490–11494. doi: 10.1128/jvi.74.24.11490-11494.2000

Chai, N., and Bates, P. (2006). Na^+/H^+ exchanger type 1 is a receptor for pathogenic subgroup J *Avian leukosis* virus. *Proc. Natl. Acad. Sci. U.S.A.* 103, 5531–5536. doi: 10.1073/pnas.0509785103

Chen, J., Li, J., Li, L., Liu, P., Xiang, Y., and Cao, W. (2020). Single amino acids G196 and R198 in hr1 of subgroup K *Avian leukosis* virus glycoprotein are critical for Tva receptor binding. *Front. Microbiol.* 11:596586. doi: 10.3389/fmicb.2020.596586

Chesters, P. M., Howes, K., Petherbridge, L., Evans, S., Payne, L. N., and Venugopal, K. (2002). The viral envelope is a major determinant for the induction of lymphoid and myeloid tumours by *Avian leukosis* virus subgroups A and J, respectively. *J. Gen. Virol.* 83, 2553–2561. doi: 10.1099/0022-1317-83-10-2553

Deng, Q., Li, M., He, C., Lu, Q., Gao, Y., Li, Q., et al. (2021). Genetic diversity of *Avian leukosis* virus subgroup J (ALV-J): toward a unified phylogenetic classification and nomenclature system. *Virus. Evol.* 7:veab037. doi: 10.1093/ve/veab037

Dong, X., Meng, F., Hu, T., Ju, S., Li, Y., Sun, P., et al. (2017). Dynamic Co-evolution and interaction of *Avian leukosis* virus genetic variants and host immune responses. *Front. Microbiol.* 8:1168. doi: 10.3389/fmicb.2017.01168

Dorner, A. J., Stoye, J. P., and Coffin, J. M. (1985). Molecular basis of host range variation in avian retroviruses. *J. Virol.* 53, 32–39. doi: 10.1128/JVI.53.1.32-39.1985

Elleder, D., Stepanets, V., Melder, D. C., Senigl, F., Geryk, J., Pajer, P., et al. (2005). The receptor for the subgroup C avian sarcoma and *leukosis* viruses, Tvc, is related to mammalian butyrophilins, members of the immunoglobulin superfamily. *J. Virol.* 79, 10408–10419. doi: 10.1128/JVI.79.16.10408-10419.2005

Federspiel, M. J. (2019). Reverse engineering provides insights on the evolution of subgroups A to E *Avian* sarcoma and *Leukosis* virus receptor specificity. *Viruses* 11:497. doi: 10.3390/v11060497

Federspiel, M. J., Crittenden, L. B., Provencher, L. P., and Hughes, S. H. (1991). Experimentally introduced defective endogenous proviruses are highly expressed in chickens. *J. Virol.* 65, 313–319. doi: 10.1128/JVI.65.1.313-319.1991

Guan, X., Zhang, Y., Yu, M., Ren, C., Gao, Y., Yun, B., et al. (2018). Residues 28 to 39 of the extracellular loop 1 of chicken Na^+/H^+ exchanger type I mediate cell binding and entry of subgroup J *Avian leukosis* virus. *J. Virol.* 92, 1617–1627. doi: 10.1128/JVI.01627-17

Holmen, S. L., Melder, D. C., and Federspiel, M. J. (2001). Identification of key residues in subgroup A *Avian leukosis* virus envelope determining receptor binding affinity and infectivity of cells expressing chicken or quail Tva receptor. *J. Virol.* 75, 726–737. doi: 10.1128/JVI.75.2.726-737.2001

Kheimar, A., Klinger, R., Bertzbach, L. D., Sid, H., Yu, Y., Conradie, A. M., et al. (2021). A genetically engineered commercial chicken line is resistant to highly pathogenic *Avian leukosis* virus subgroup J. *Microorganisms* 9:1066. doi: 10.3390/microorganisms9051066

Klucking, S., and Young, J. A. (2004). Amino acid residues Tyr-67, Asn-72, and Asp-73 of the TVB receptor are important for subgroup E *Avian* sarcoma and *leukosis* virus interaction. *Virology* 318, 371–380. doi: 10.1016/j.virol.2003.09.024

Kwong, P. D., Wyatt, R., Robinson, J., Sweet, R. W., Sodroski, J., and Hendrickson, W. A. (1998). Structure of an HIV gp120 envelope glycoprotein in complex with the CD4 receptor and a neutralizing human antibody. *Nature* 393, 648–659. doi: 10.1038/31405

Li, T., Yao, X., Li, C., Zhang, J., Xie, Q., Wang, W., et al. (2020). Gp37 regulates the pathogenesis of *Avian leukosis* virus subgroup J *via* Its C terminus. *J. Virol.* 94, e2180–e2119. doi: 10.1128/JVI.02180-19

Lipsick, J. (2021). A history of cancer research: tumor viruses. *Cold Spring Harb. Perspect. Biol.* 13:a035774. doi: 10.1101/cshperspect.a035774

Melder, D. C., Pankratz, V. S., and Federspiel, M. J. (2003). Evolutionary pressure of a receptor competitor selects different subgroup A *Avian leukosis* virus escape variants with altered receptor interactions. *J. Virol.* 77, 10504–10514. doi: 10.1128/jvi.77.19.10504-10514.2003

Munguia, A., and Federspiel, M. J. (2019). Avian sarcoma and *leukosis* virus envelope glycoproteins evolve to broaden receptor usage under pressure from entry competitors (dagger). *Viruses* 11:519. doi: 10.3390/v11060519

Prikryl, D., Plachy, J., Kucerova, D., Koslova, A., Reinisova, M., Senigl, F., et al. (2019). The novel *Avian leukosis* virus subgroup K shares its cellular receptor with subgroup A. *J. Virol.* 93, e519–e580. doi: 10.1128/JVI.00580-19

Rong, L., and Bates, P. (1995). Analysis of the subgroup *Aavian* sarcoma and *leukosis* virus receptor: the 40-residue, cysteine-rich, low-density lipoprotein receptor repeat motif of Tva is sufficient to mediate viral entry. *J. Virol.* 69, 4847–4853. doi: 10.1128/JVI.69.8.4847-4853.1995

Rong, L., Edinger, A., and Bates, P. (1997). Role of basic residues in the subgroup-determining region of the subgroup A *Avian* sarcoma and *leukosis* virus envelope in receptor binding and infection. *J. Virol.* 71, 3458–3465. doi: 10.1128/JVI.71.5.3458-3465.1997

Smith, J. G., and Cunningham, J. M. (2007). Receptor-induced thiolate couples Env activation to retrovirus fusion and infection. *PLoS Pathog* 3:e198. doi: 10.1371/journal.ppat.0030198

Sun, C., Zhang, B., Jin, J., and Montelaro, R. C. (2008). Binding of equine infectious anemia virus to the equine lentivirus receptor-1 is mediated by complex discontinuous sequences in the viral envelope gp90 protein. *J. Gen. Virol.* 89, 2011–2019. doi: 10.1099/vir.0.83646-0

Tsichlis, P. N., Conklin, K. F., and Coffin, J. M. (1980). Mutant and recombinant avian retroviruses with extended host range. *Proc Natl Acad Sci U.S.A.* 77, 536–540. doi: 10.1073/pnas.77.1.536

Wang, P., Lin, L., Shi, M., Li, H., Gu, Z., Li, M., et al. (2020). Vertical transmission of ALV from ALV-J positive parents caused severe immunosuppression and significantly reduced marek's disease vaccine efficacy in three-yellow chickens. *Vet. Microbiol.* 244:108683. doi: 10.1016/j.vetmic.2020.108683

Weichseldorfer, M., Tagaya, Y., Reitz, M., DeVico, A. L., and Latinovic, O. S. (2022). Identifying CCR5 coreceptor populations permissive for HIV-1 entry and productive infection: implications for *in vivo* studies. *J. Transl. Med.* 20:39. doi: 10.1186/s12967-022-03243-8

Wilson, C., Wardell, M. R., Weisgraber, K. H., Mahley, R. W., and Agard, D. A. (1991). Three-dimensional structure of the LDL receptor-binding domain of human apolipoprotein E. *Science* 252, 1817–1822. doi: 10.1126/science.2063194

Yin, X., Melder, D. C., Payne, W. S., Dodgson, J. B., and Federspiel, M. J. (2019). Mutations in both the surface and transmembrane envelope glycoproteins of the RAV-2 subgroup B *Avian* sarcoma and *leukosis* virus are required to escape the antiviral effect of a secreted form of the Tvb(S3) receptor dagger. *Viruses* 11:500. doi: 10.3390/v11060500

Zhang, L., Cai, D., Zhao, X., Cheng, Z., Guo, H., Qi, C., et al. (2014). Liposomes containing recombinant gp85 protein vaccine against ALV-J in chickens. *Vaccine* 32, 2452–2456. doi: 10.1016/j.vaccine.2014.02.091

Zhang, Y., Yu, M., Xing, L., Liu, P., Chen, Y., Chang, F., et al. (2020). The bipartite sequence motif in the N and C termini of gp85 of subgroup J *Avian leukosis* virus plays a crucial role in receptor binding and viral entry. *J. Virol.* 94, e1232–e1220. doi: 10.1128/JVI.01232-20

Conflict of Interest: The authors declare that the research was conducted in the absence of any commercial or financial relationships that could be construed as a potential conflict of interest.

Publisher's Note: All claims expressed in this article are solely those of the authors and do not necessarily represent those of their affiliated organizations, or those of the publisher, the editors and the reviewers. Any product that may be evaluated in this article, or claim that may be made by its manufacturer, is not guaranteed or endorsed by the publisher.

frontiers | Frontiers in Veterinary Science

ORIGINAL RESEARCH
published: 27 May 2022
doi: 10.3389/fvets.2022.890657

Amino Acid Mutations in Hemagglutinin-Neuraminidase Enhance the Virulence and Pathogenicity of the Genotype III Newcastle Disease Vaccine Strain After Intravenous Inoculation

Xiaolong Lu[1†], *Xiaowen Liu*[1,2†], *Qingqing Song*[1], *Xiaoquan Wang*[1], *Shunlin Hu*[1*] and *Xiufan Liu*[1,2,3*]

[1] *Animal Infectious Disease Laboratory, College of Veterinary Medicine, Yangzhou University, Yangzhou, China,* [2] *Jiangsu Co-innovation Center for Prevention and Control of Important Animal Infectious Diseases and Zoonosis, Yangzhou University, Yangzhou, China,* [3] *Jiangsu Key Laboratory of Zoonosis, Yangzhou University, Yangzhou, China*

Newcastle disease virus (NDV), the causative agent that generally causes severe disease in poultry, continues to mutate and has thus evolved into 21 genotypes. We previously isolated a velogenic genotype III NDV JS/7/05/Ch that evolved from the vaccine strain Mukteswar, accompanying by amino acid mutations in Hemagglutinin-Neuraminidase (HN). Here, we sought to investigate the role of the mutant HN protein in NDV virulence. The HN genes of Mukteswar and JS/7/05/Ch were replaced reciprocally via reverse genetics, yielding two recombinant viruses rJS/MHN and rMu/JHN, respectively. rMu/JHN, in which the endogenous HN protein was replaced with the HN protein of JS/7/05/Ch, had a higher intravenous pathogenicity index (IVPI) value in chickens. Moreover, dual aa mutations (A494D and E495K from JS/7/05/Ch-type HN) were introduced into the HN protein of Mukteswar to generate the recombinant virus rMukHN494+495^{JS}. This virus showed an equivalent IVPI value to that of rJS/7/05/Ch (generated from parental JS/7/05/Ch via reverse genetics). *In vitro* and *in vivo* assays further showed that A494D and E495K in HN induced antigenic changes, a higher replication level and a more intense inflammatory response. Taken together, these findings indicate that aa mutations in HN are crucial for the virulence of the genotype III Newcastle disease (ND) vaccine strain after intravenous inoculation. Our study further highlights that close surveillance is needed to monitor the genetic variation of ND vaccine strains.

Keywords: Newcastle disease virus, vaccine strain, virulence, HN, intravenous inoculation, reverse genetics technology

OPEN ACCESS

Edited by:
Yulong Gao,
Harbin Veterinary Research Institute (CAAS), China

Reviewed by:
Guoyuan Wen,
Hubei Academy of Agricultural Sciences, China
Xusheng Qiu,
Shanghai Veterinary Research Institute (CAAS), China

***Correspondence:**
Shunlin Hu
slhu@yzu.edu.cn
Xiufan Liu
xfliu@yzu.edu.cn

†These authors have contributed equally to this work

Specialty section:
This article was submitted to Veterinary Infectious Diseases, a section of the journal Frontiers in Veterinary Science

Received: *06 March 2022*
Accepted: *05 May 2022*
Published: *27 May 2022*

Citation:
Lu X, Liu X, Song Q, Wang X, Hu S and Liu X (2022) Amino Acid Mutations in Hemagglutinin-Neuraminidase Enhance the Virulence and Pathogenicity of the Genotype III Newcastle Disease Vaccine Strain After Intravenous Inoculation. Front. Vet. Sci. 9:890657. doi: 10.3389/fvets.2022.890657

INTRODUCTION

Virulent Newcastle disease virus (NDV) strains generally cause the highly infectious and devastating disease in poultry (1). NDV, termed as avian paramyxovirus type 1 (APMV-1), is assigned as a member of the genus *Orthoavulavirus*, family *Paramyxoviridae* (2). NDV also belongs to the enveloped virus and contains a non-segmented, single-stranded, and negative-sense Ribonucleic Acid (RNA) (3). The substantial antigenic and genetic diversity of NDV has been widely recognized, although NDV has only one serotype. The latest classification criteria reveals that NDV consists of two subdivisions (class I and class II) classified into more than 20 genotypes. NDV can be divided into the avirulent, low (lentogenic), intermediate (mesogenic), and highly (velogenic) virulent strain via a range of virulence tests (4). Prior works have confirmed that the amino acid (aa) sequence at the fusion protein (F) cleavage site is a determining factor for NDV virulence. Generally, the cleavage site of mesogenic and velogenic NDVs is ^{112}R/K-R-Q-R/K-R↓F^{117}, while that of lentogenic NDVs is ^{112}G/E-K/R-Q-G/E-R↓L^{117} (5). However, factors other than the F protein can also affect NDV virulence. Previous researches have explored the crucial effects of the hemagglutinin-neuraminidase protein (HN) on virulence and have demonstrated that NDVs carrying the identical F protein cleavage site can have different virulence (6–8). HN, a type II membrane glycoprotein, involves in regulating virulence, replication, and tissue tropism of NDV (9–11). Besides, the HN protein takes a main position in antigen recognition that carries seven important antigenic sites including site 1 to site 4, site 12, site 14, and site 23 (12).

ND has been an intractable problem since the first isolation of NDV in China in 1946 (13). Vaccination is the primarily method for controlling ND (14); live vaccines are widely used because of their strong immunogenicity. Common live ND vaccines used in China include La Sota, VGGA, and Mukteswar. The former two vaccines are lentogenic genotype II NDVs, while Mukteswar is a mesogenic genotype III NDV that is suitable for administration after 2 months of age. Vaccination has been extremely successful in controlling ND outbreaks; however, immune pressure imposed by frequent vaccination leads to emergence of viral variants. Although some countries have banned administration of mesogenic ND vaccines because of their potential pathogenicity, the attenuated Mukteswar clone is still used in China for its strong immunogenicity. In 2005, a virulent genotype III NDV (JS/7/05/Ch) with a high intravenous pathogenicity index (IVPI) was isolated, which shared more than 99% genomic identity with Mukteswar (15). This finding suggested that Mukteswar had evolved into a virulent NDV during vaccination.

To elucidate the molecular mechanisms responsible for the increased virulence of the genotype III NDV vaccine strain, we analyzed genomic differences between Mukteswar and JS/7/05/Ch and identified the critical protein and aa associated with NDV virulence.

TABLE 1 | Primer sequences used to construct full-length cDNAs.

Primer	Sequence (5′-3′)
NPS	**CGTCTC**GTATAGGGACCAAACAGAGAATCCGTGAGA **(*Bsm*B I)**
NPA	TCTGAATGTCTCTCTTCTACCC– – – – ***Bgl II***
PMS	**GGATCC**AGATCTTAGAAAAAAATACGGG **(*Bam*H I)**
PMA	AA**TGCGCA**CAGAAGGATGTTGC**ACCGGT**TG **(*Fsp*A I+*Age* I)**
MFS	CTCAATAAACTCTCGCA**ACCGGT**GCAAC **(*Age* I)**
MFA	**GTATAC**CCAAGAGTTGAGTCTGTGAGTCGTAAAAAATAGGGTTGC CGGTG **(*Bst*Z17 I)**
FHS	GACTCACAGACTCAACTCTTGGGTA——— ***BstZ*17 I**
FHA	GTTGACACCTTGATGGATAGGATGGhbox——— ***Mlu* I**
HLS	TAAGTCATCGTATAAGCCTGGGhbox——— ***Mlu* I**
HLA	ATACCTGGAGGATCATATCAAAGTChbox——— ***Fsp*A I**
L1S	ATGTTGTGCCTGTTGCGTCTGThbox——— ***Hpa* I**
L1A	GAAATTATCACTGGCTTGATGChbox——— ***Hpa* I**
L2S	ATGACTCCCCAGAGATGGTGTThbox——— ***Hpa* I**
L2A	ATTCCCTGCATGTAAACCTGAGhbox——— ***Mlu* I**
L3S	AACTGCTAGTCTCTTGCACTCGhbox——— ***Mlu* I**
L3A	**CGTCTC**TACCCACCAAACAAAGATTTGGTGAATG (***Bsm*B I**)

The added restriction sites are marked in bold italics.

MATERIALS AND METHODS

Animals, Viruses, Cells, and Plasmids

Specific-pathogen-free (SPF) chickens and embryonated eggs were supplied by Merial Vital Laboratory Animal Technology Co., Ltd. (Beijing, China) and Zhejiang Lihua Agricultural Technology Co., Ltd (Zhejiang, China), respectively. The genotype III velogenic NDV JS/7/05/Ch isolated from a diseased chicken flock and the vaccine strain Mukteswar were kept by our lab. The viruses were amplified in allantoic fluid, collected under sterile conditions, and then stored at −70°C. The BSR-T7/5 cell line was provided by Dr. Zhigao Bu (Harbin Veterinary Institute, China). Peripheral blood mononuclear cells (PBMCs) were isolated from the whole blood of healthy SPF chickens using chicken PBMC separation medium (TBDscience, Tianjing, China). Three helper plasmids expressing the nucleocapsid (NP), phosphoprotein (P), and large polymerase (L) genes of NDV (pCI-NP, pCI-P, and pCI-L) were kept by our lab. The transcription vector TVT7R (0.0) was gifted from Dr. Andrew Ball (Alabama University, USA). pCR2.1 vector was purchased from Invitrogen (Carlsbad, CA, USA).

RNA Extraction, Reverse Transcription-Polymerase Chain Reaction (RT-PCR), and Sequencing

Viral RNA from fresh allantoic fluid was extracted by RNA purification kit (TransGen Biotech, Beijing, China) according

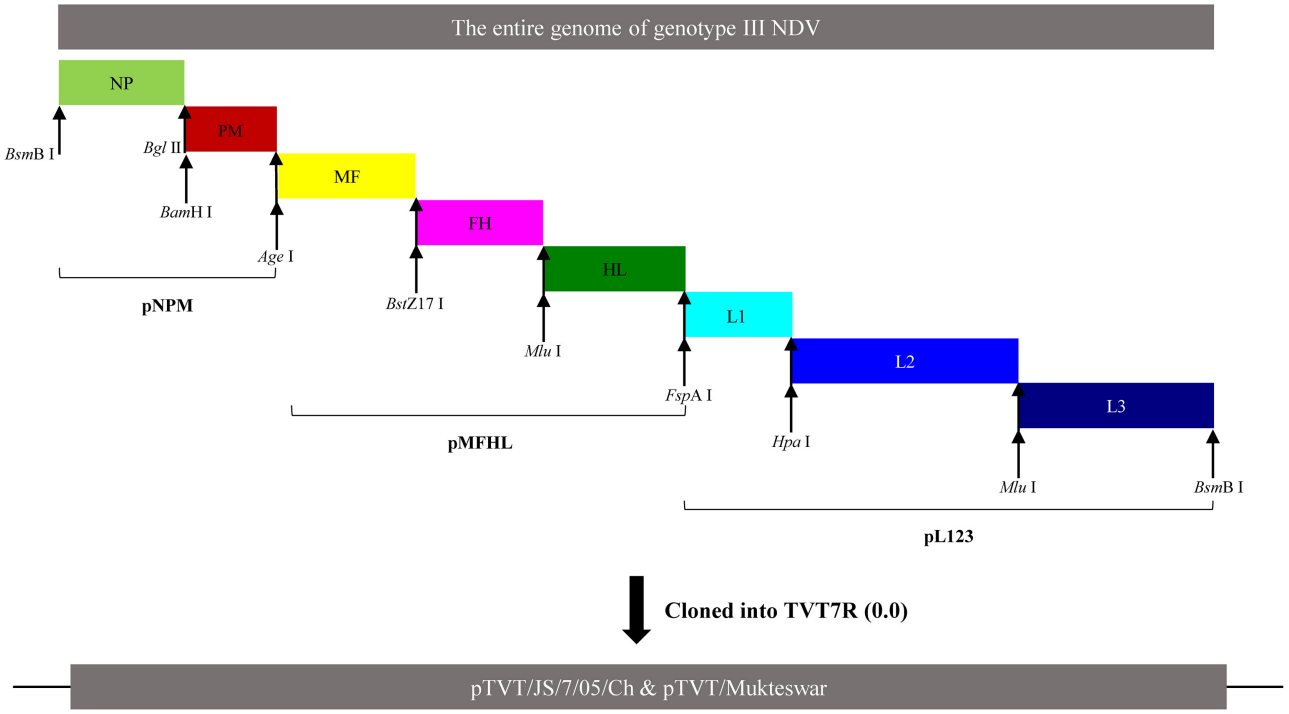

FIGURE 1 | Construction of full-length cDNAs of Mukteswar and JS/7/05/Ch. The NDV genome was divided into eight fragments marked by various colors, including NP, PM, MF, FH, HL, L1, L2, and L3. cDNA fragments were joined at shared restriction sites marked with arrows and then cloned into transcription vectors. The intermediate cDNAs (pNPM, pMFHL, and pL123) and full-length cDNAs of each genotype III NDV were successfully constructed. The full-length cDNAs were thereafter acquired by cloning into the pTVT7R(0.0) vector and named as pTVT/Mukteswar and pTVT/JS/7/05/Ch.

to the product manual. RT-PCR was conducted with One-Step RT-PCR SuperMix (TransGen Biotech, Beijing, China). Target PCR products were thereafter sequenced by Sangon Biotech Co., Ltd (Shanghai, China) following the purification using DNA Gel Extraction Kit (Axygen Biosciences, Union City, CA, USA).

Genome Sequence Analysis and Homology Modeling

Nucleotide sequence editing and aa sequence prediction were conducted using BioEdit 7.2.5 and MEGA 7.0 software. To determine the spatial positions of aa mutations, a homology model of NDV HN protein was constructed using the Automated Mode of Swiss-Model software (16). Protein Data Bank (PDB) files with high quality were screened out as previously reported (17). Next, Swiss-Model chose a suitable template (PDB ID: 1e8v.1.A) as the structural basis for homology modeling after automatic filtering. The three-dimensional (3D) structure and positions of hydrogen bond (H-bond) were computed and displayed using the RasMol and PyMol 2.4.0 softwares (18, 19).

Construction of Genotype III NDV Full-Length CDNAs

The full-length cDNA clones of genotype III NDVs were amplified using eight pairs of primers (**Table 1**). As shown in **Figure 1**, the complete NDV genome was divided into eight fragments including NP, PM, MF, FH, HL, L1, L2, and L3. The eight amplicons were purified and ligated to obtain the full-length tandem genome in the pCR 2.1 vector. The full-length cDNAs were then cloned into the TVT7R (0.0) vector, generating two infectious full-length clones (pTVT/JS/7/05/Ch and pTVT/Mukteswar). These full-length cDNAs were identified by digestion with an *Eco*R I restriction site.

HN gene swapping using the Mukteswar and JS/7/05/Ch genomes as backbones was performed using two restriction enzymes (*Age* I and *Fsp*A I) (**Figure 2A**). Two chimeric NDV cDNAs (pTVT/JS/MHN and pTVT/Mu/JHN) were further characterized by restriction digestion with *Eco*R I. Additionally, the sequence of Mukteswar was altered by replacement of positions 7,892 and 7,894 with the dual-site mutations of JS/7/05/Ch, yielding the recombinant cDNA pTVT/MukHN494+495^{JS}. The cDNA sequence was confirmed by DNA sequencing (**Figure 2B**).

Recovery and Characterization of Virus Produced From CDNA

As described previously, the recombinant NDVs were rescued by co-transfecting each full-length cDNA clone with three helper cDNA clones into BSR cells (20). The harvested cell culture supernatants and cell monolayers were injected into the allantoic cavities of SPF embryonated eggs 96 h post-transfection. Allantoic fluid was harvested following embryo death and subjected to hemagglutination and hemagglutination inhibition

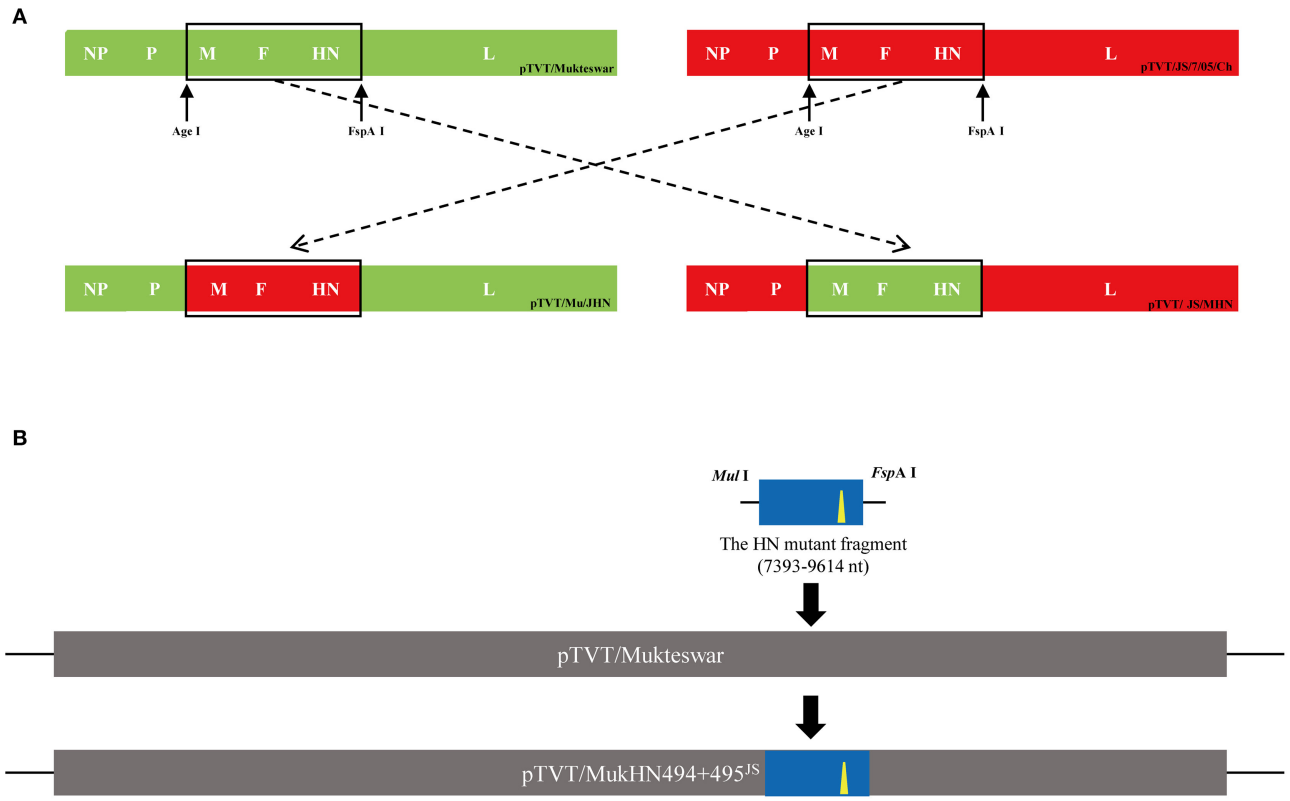

FIGURE 2 | Construction of chimeric NDV cDNAs. **(A)** Schematic representation showed a protocol for the HN exchange between Mukteswar and JS/7/05/Ch. Two restriction sites *Age* I and *Fsp*A I, introduced into the intergenic region, were used to swap the HN gene. The replacement segment included the M, F, HN, and partial L genes. Two HN-replacement chimeric cDNAs were constructed and named as pTVT/Mu/JHN and pTVT/JS/MHN. The locations of the restriction sites were indicated by black arrows. **(B)** Schematic representation of the dual-site mutant cDNA pTVT/MukHN494+495^{JS} construction. The HN mutant fragment was obtained using a fast mutagenesis system, in which dual positions 7,892 and 7,894 of Mukteswar were mutated into those of JS/7/05/Ch. The corresponding DNA segment of pTVT/Mukteswar was then replaced with the dual-site mutant fragment, resulting in the recombinant cDNA pTVT/MukHN494+495^{JS}. Restriction sites were shown in the mutant fragment. The nucleotide mutations at positions 7,892 and 7,894 of HN were shown as yellow triangles.

TABLE 2 | The qPCR primers utilized in this study.

Gene name	Primer sequence (5′-3′)	Length (bp)
β-actin F	ATTGTCCACCGCAAATGCTTC	113
β-actin R	AAATAAAGCCATGCCAATCTCGTC	
IL-18 F	AGGTGAAATCTGGCAGTGGAAT	125
IL-18 R	ACCTGGACGCTGAATGCAA	
IL-1β F	GCTCTACATGTCGTGTGTGATGAG	187
IL-1β R	TGTCGATGTCCCGCATGA	
IL-6 F	TTCGCCTTTCAGACCTACCT	213
IL-6 R	TGGTGATTTTCTCTATCCAGTCC	
M-gene F	GCTTGTGAAGGCGAGAGGTG	99
M-gene R	AACCTGGGGAGAGGCATTTG	

assays according to standard procedures (21). The rescued viruses were characterized by viral RNA extraction, RT-PCR, and sequencing after passaging in SPF embryonated eggs three times. Finally, the recombinant parental and chimeric viruses were named as rMukteswar, rJS/7/05/Ch, rJS/MHN, rMu/JHN, and rMukHN494+495^{JS}, respectively.

The virulence of rescued viruses were determined according to standard procedures, including the intravenous pathogenicity index (IVPI), intracerebral pathogenicity index (ICPI), and mean death time (MDT) tests (21). The 50% embryo infectious doses (EID_{50}) of these viruses were determined following the Reed and Muench method.

Growth Curves

The growth kinetics of recombinant viruses were evaluated in PBMCs. The recombinant viruses were inoculated into cells with an MOI of 0.1 and 1. Cells were thereafter washed three times with PBS to remove unattached viruses and cultured in complete medium at 37°C with 5% CO_2. The cell supernatant was collected and determined by the 50% tissue culture infective dose ($TCID_{50}$) for indicated time points. The growth curves of NDVs were presented as the line charts drawn by GraphPad Prism 7.00 (Graph Pad Software, Inc., USA).

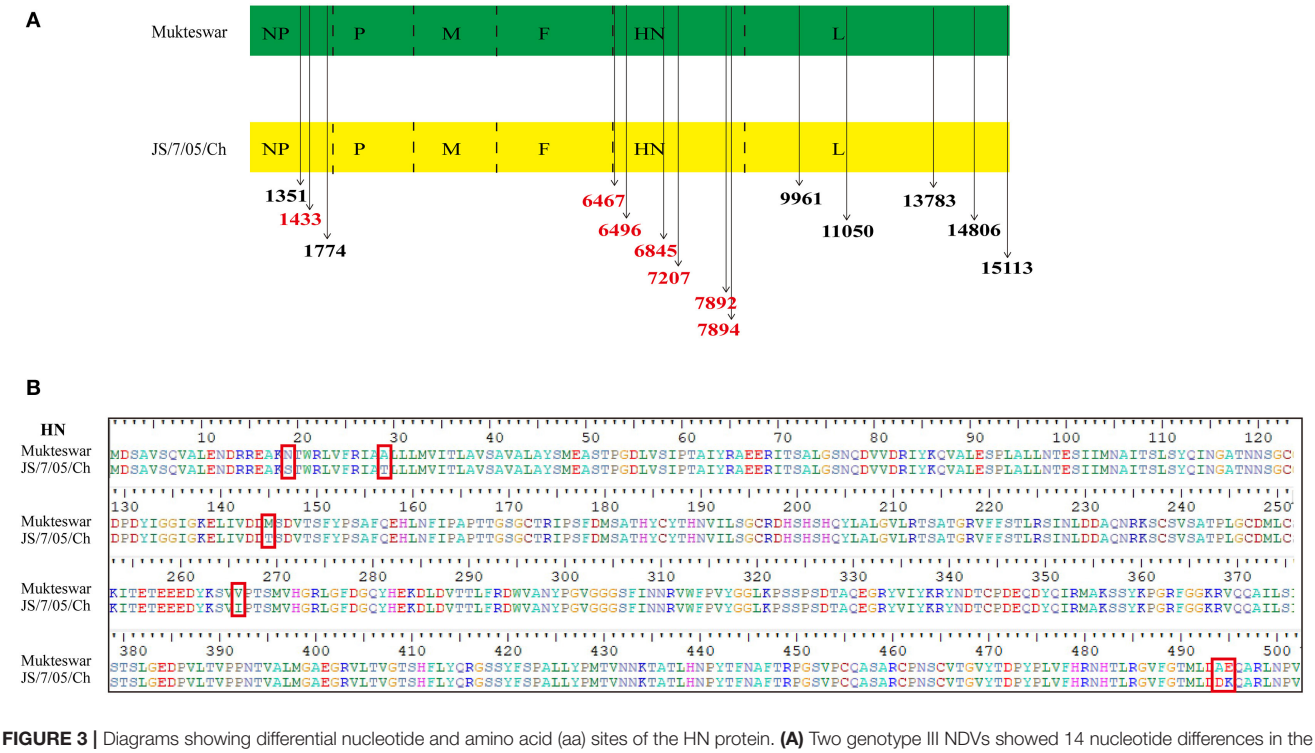

FIGURE 3 | Diagrams showing differential nucleotide and amino acid (aa) sites of the HN protein. **(A)** Two genotype III NDVs showed 14 nucleotide differences in the encoded structural proteins, including NP, HN, and L. The differential nucleotide sites that cause aa variations were marked in red, and others were drawn in black. **(B)** There were six aa mutations in HN proteins between Mukteswar and JS/7/05/Ch, including 19, 29, 145, 266, 494, and 495 aa. The aa mutations in red frames were displayed using BioEdit 7.2.5 software.

Cross Virus-Neutralization (VN) Assay

To investigate whether dual aa mutations A494D and E495K in HN caused antigenic changes of NDV, we carried out the cross-VN test as described by Liu et al. (22). Antisera used in this study were inactivated and provided by our lab. The antisera were prepared from SPF chickens vaccinated with inactivated oil-emulsion rMukteswar, rJS/7/05/Ch and rMukHN494+495^{JS}, respectively. These antisera were then serially diluted multiplicatively with PBS and mixed, respectively, with each virus at 100 EID_{50}/100μl. The mixtures were incubated at 37°C for 1 h and then injected into SPF embryonated chicken eggs to determine neutralization levels. The 50% endpoints were calculated according to the Reed and Muench method (23). The R value was calculated using the formula of Archetti and Horsfall (24).

Animal Experiments

To determine the effects of A494D and E495K on pathogenicity *in vivo*, we measured viral loads and inflammatory cytokine expression post-infection. First, groups of 60 1-month-old SPF chickens (20 for each rMukteswar-, rJS/7/05/Ch-, and rMukHN494+495^{JS}-infection) were intravenously infected with 10^7 EID_{50} of virus per chicken. Mock-infected chickens (as negative control) were injected intravenously with an equal amount of phosphate-buffered saline (PBS). Each group was observed twice daily for 10 days. At 12, 24, and 48 h post-infection (hpi), and at 4 and 6 days post-infection (dpi), three chickens from each group were randomly dissected and the spleen, lung, bursa, and thymus were harvested. Duplicate samples were taken from each organ: 0.3 g each for the viral load measurement, and 0.02 g each for the measurement of cytokine levels. These collected organ samples were stored at −70°C until use.

Total RNA of chicken organs was extracted with Trizol reagent (TransGen Biotech, Beijing, China), then synthesizing the cDNA fragments by PrimeScript^{TM} RT Master Mix (Takara, Shiga, Japan) according to product manuals. As for the determination of viral loads, the conserved region of the NDV M gene was amplified using the primers (M-gene F and M-gene R) as shown in **Table 2**. The amplified M gene was next cloned into the pCMV-vector to serve as the standard plasmid. The copy number was calculated as described previously (25). The cDNA was next subjected to the viral load detection using SYBR Premix reagent (Takara, Shiga, Japan) according to the product manual. The PCR program was set to 30 s at 95°C (pre-denaturation), followed by 40 cycles consisting of 5 s at 95°C and 31 s at 60°C. The ddH_2O and standard plasmid were used as negative and positive controls for quantitative real-time PCR (qPCR), respectively. As for the detection of cytokine expression, an equal quantity of cDNA (2 μl) of each sample was used for examining the amplification of various cytokines. Real-time PCR was detected by SYBR Color Master Mix for qPCR (Vazyme, Nanjing, China) following the

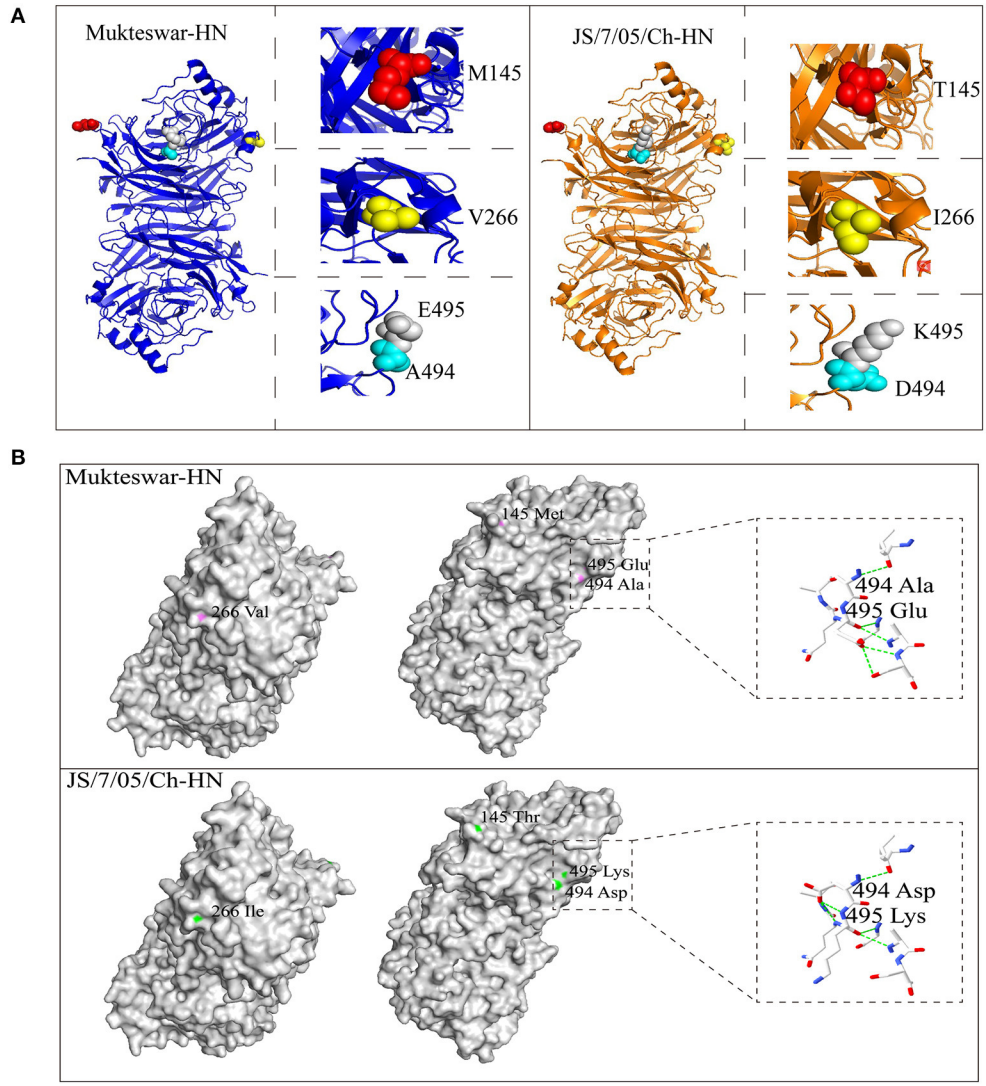

FIGURE 4 | Positions of differential amino acid (aa) residues at the three-dimensional (3D) structure of the HN protein. Homology modeling showed spatial positions of four aa mutations, including 145, 266, 494, and 495 aa. **(A)** The monomer of the HN protein was represented by cartoon mode, including Mukteswar in blue and JS/7/05/Ch in orange. The residues were shown by spheres model in the zoom-in picture, involving 145 aa in red, 266 aa in yellow, 494 aa in cyan, and 495 aa in gray. **(B)** Differential aa residues in the HN protein between Mukteswar and JS/7/05/Ch were marked with violet and green, respectively. Among these aa mutations, A494D and E495K caused H-bond variations drawn by dotted lines in the zoom-in picture. Color coding: blue, nitrogen; red, oxygen; white, carbon. Based on the crystal structure of the HN protein, homology models were carried out using PyMOL 2.4.0 software (PDB ID: 1e8v.1.A).

product manual. The expression level of house-keeping gene β-actin was employed for data normalization. Relative gene expression levels were calculated using the $2^{-\Delta\Delta CT}$ method (26).

Statistical Analysis

All data are presented as the means ± standard deviations (SD) of three independent replicates from a representative experiment. Statistically significant differences were determined by two-way analysis of variance (ANOVA). All statistics were evaluated using GraphPad Prism 7.00 software (San Diego, CA, USA). *P*-values, <0.05, were considered statistically significant.

RESULTS

Analysis of Differential Amino Acid Sites and 3D Protein Structures

Fourteen nucleotide differences in the *NP*, *HN*, and *L* genes were identified (**Figure 3A**). Seven nucleotide mutations resulted in aa mutations: proline (P) to serine (S) at position 438 (P438S) in NP, and asparagine (N) to S at position 19 (N19S), S to threonine (T) at position 29 (S29T), methionine (M) to T at position 145 (M145T), valine (V) to isoleucine (I) at position 266 (V266I), alanine (A) to aspartic acid (D) at position 494 (A494D), and glutamic acid (E) to lysine (K)

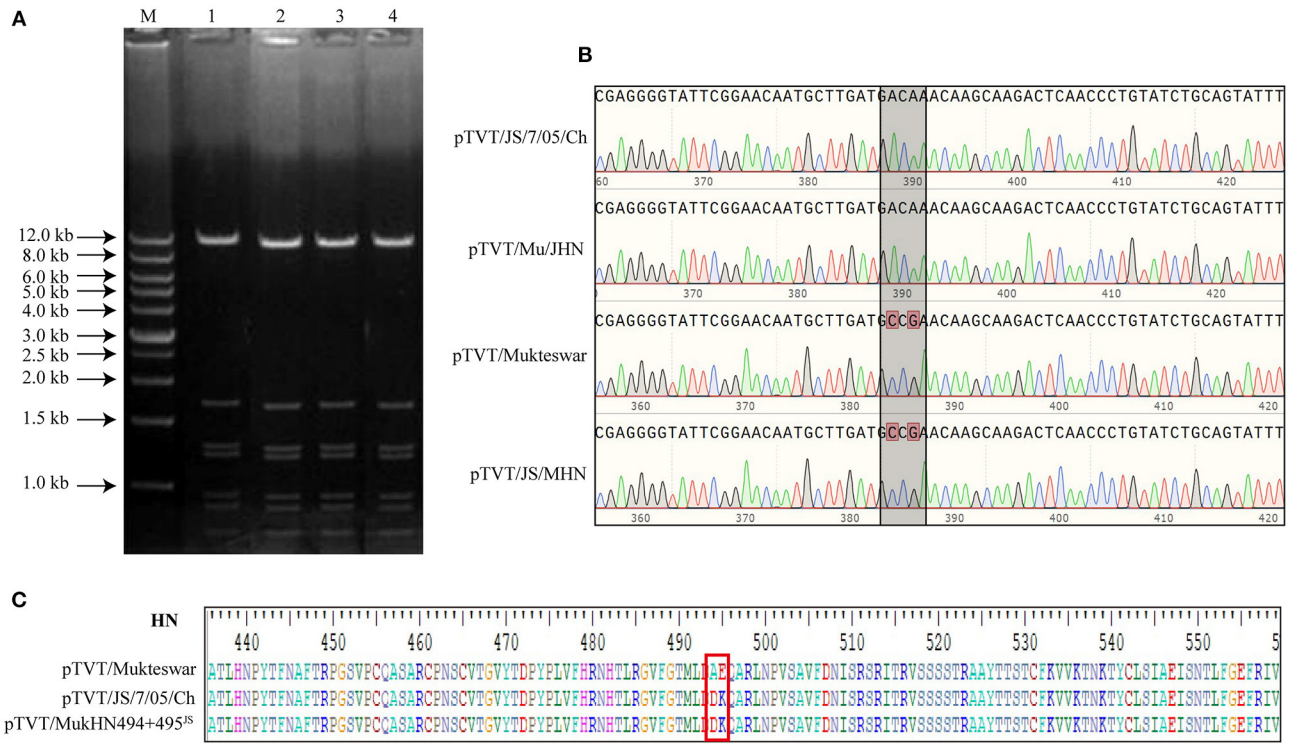

FIGURE 5 | Identification of constructed cDNAs. **(A)** Constructed cDNAs were digested with *Eco*R I. 1: pTVT/JS/7/05/Ch; 2: pTVT/JS/MHN; 3: pTVT/Mukteswar; 4: pTVT/Mu/JHN; M: DNA marker. **(B)** Constructed cDNAs were identified by DNA sequencing. Sequences of RT-PCR products amplified by HLS and HLA were analyzed using BioEdit 7.2.5 software. **(C)** pTVT/MukHN494+495^{JS} showed two aa mutations at positions 494 and 495 compared with pTVT/Mukteswar. Amino acids in NDV HN protein were analyzed by BioEdit 7.2.5 software. The 494 and 495 aa were marked in a red box.

at position 495 (E495K) in HN (**Figure 3B**). Because most aa differences were located in the HN protein, we conducted homology modeling of the 3D structure of HN. The sequence identities between the template (PDB ID: 1e8v.1.A) and the HN protein were higher than 90% and thus suitable for homology modeling. Differential amino acids were marked with various colors in the HN molecular structure as illustrated in **Figure 4**. Four aa mutations (positions 145, 266, 494, and 495) were shown; positions 19 and 29 were not shown because of the incomplete HN crystal structure. These four aa were differentially distributed at the periphery of the HN dimer. Notably, A494D and E495K changed the positions of H-bonds near these mutations as shown in **Figure 4B**, which might impact structural stability.

Generation and Characterization of Recombinant Parental and Chimeric NDVs

Four full-length NDV cDNAs were successfully constructed and characterized by restriction digestion. As expected, the complete full-length cDNAs were digested into seven bands (0.76, 0.9, 0.95, 1.2, 1.3, 1.7, and 11.0 kb) (**Figure 5A**). Amplified sequences from pTVT/Mu/JHN and pTVT/JS/MHN using primers of HLS and HLA were identical to the sequences of pTVT/JS/7/05/Ch and pTVT/Mukteswar, respectively (**Figure 5B**). Four recombinant NDVs (rMukteswar, rJS/7/05/Ch, rMu/JHN, and rJS/MHN) were rescued after the inoculation of cell culture supernatants and cell monolayers into SPF embryonated chicken eggs. Additionally, the recombinant cDNA pTVT/MukHN494+495^{JS} was successfully constructed and confirmed by DNA sequencing (**Figure 5C**). The dual-site mutant NDV (rMukHN494+495^{JS}) was thereafter rescued as described above.

TABLE 3 | Characterization of the recombinant viruses.

Virus	IVPI score[a]	ICPI score[b]	MDT (h)[c]	EID_{50} (0.1ml)[d]
rMukteswar	0.16	1.44	46.4	$10^{8.17}$
rJS/7/05/Ch	1.89	1.88	46.4	$10^{7.69}$
rMu/JHN	1.77	1.80	48	$10^{7.72}$
rJS/MHN	0.12	1.46	46.4	$10^{7.83}$
rMukHN494+495^{JS}	1.20	1.78	46.8	$10^{7.6}$

[a] *Intravenous pathogenicity index (IVPI) tests were determined by intravenously infecting 6-week-old SPF chickens with fresh infective allantoic fluid. The IVPI values of highly virulent strains could reach up to 2.0, while avirulent strains only had IVPI values of 0.0.* [b] *Intracerebral pathogenicity index (ICPI) tests were determined by intracerebrally infecting 1-day-old SPF chicks with fresh infective allantoic fluid. The pathotype definitions by the ICPI: velogenic strains (1.5–2.0), mesogenic strains (0.7–1.5), and lentogenic strains (0.0 to 0.7).* [c] *Mean death time (MDT) tests, the mean time (hours) for the minimum lethal dose to kill all the inoculated embryos, were determined by inoculating fresh allantoic fluid into the allantoic cavities. The pathotype definitions by the MDT: velogenic strains (<60 h), mesogenic strains (60–90 h), and lentogenic strains (>90 h).* [d] *egg 50% infective dose.*

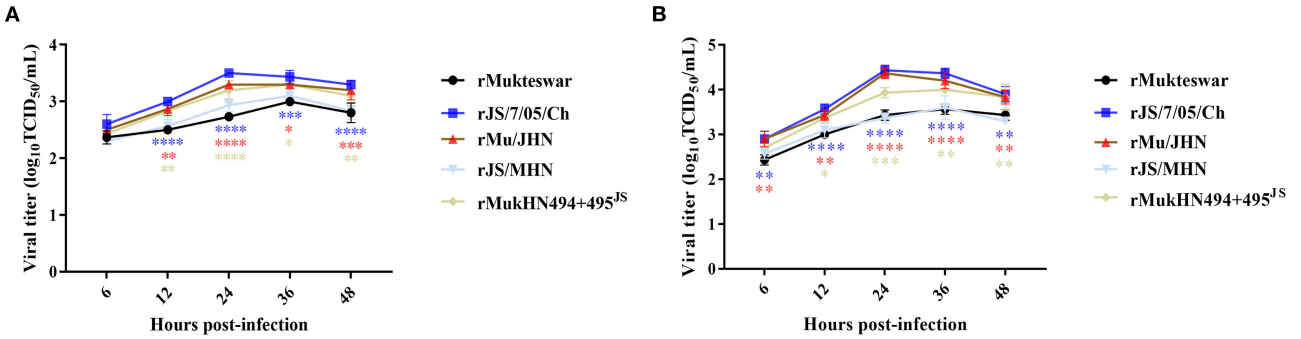

FIGURE 6 | Analyses of growth kinetics of recombinant viruses. The chicken PBMCs were infected with NDVs at an MOI of 0.1 **(A)** and 1 **(B)**. Growth characteristics were evaluated at 6, 12, 24, 36, and 48 hpi. All values of each group were compared with that of rMukteswar. *$P < 0.05$; **$P < 0.01$; ***$P < 0.001$; ****$P < 0.0001$.

TABLE 4 | Cross virus-neutralization titers for antisera against rMukteswar, rJS/7/05/Ch and rMukHN494+495^{JS}.

Antisera	Strains		
	rMukteswar	rJS/7/05/Ch	rMukHN494+495^{JS}
Anti-rMukteswar	1:286	1:91	1:102
Anti-rJS/7/05/Ch	1:45	1:205	1:172
Anti- rMukHN494+495^{JS}	1:57	1:181	1:228

These rescued viruses were subjected to IVPI, ICPI, and MDT assays. As shown in **Table 3**, genotype III NDVs bearing the mutant HN protein showed significantly elevated IVPI values. The IVPI value for rJS/7/05/Ch was 1.89, significantly higher than that of rMukteswar (0.16). Two HN swapped recombinant viruses (rMu/JHN and rJS/MHN) showed virulence comparable with the parental virus carrying the same HN gene. Briefly, rMu/JHN bearing JS/7/05/Ch-type HN had an IVPI value of 1.77, significantly higher than that of rJS/MHN bearing Mukteswar-type HN (0.12). Moreover, rMukHN494+495^{JS} had a higher IVPI value (1.20) than that of its backbone virus rMukteswar and was more similar in this respect to rJS/7/05/Ch carrying the same mutations at 494 and 495 aa of HN. Furthermore, these recombinant viruses also showed some differential ICPI values. The ICPI values for rJS/7/05/Ch (1.88) and rMu/JHN (1.80) were higher than rMukteswar (1.44) and rJS/MHN (1.46). rMukHN494+495^{JS} also exhibited a higher ICPI value (1.78) than rMukteswar and was closer in this respect to rJS/7/05/Ch. Thus, the mutant HN protein, especially dual aa mutations A494D and E495K in HN, was required for viral virulence, especially after intravenous infection.

Evaluation of Virus Replication *in vitro*

To determine whether the mutant HN protein affected virus replication *in vitro*, we next compared growth curves of the recombinant viruses in chicken cells. Because these genotype III NDVs exhibit significant virulence differences after intravenous inoculation, we further selected chicken PBMCs to determine virus replication. As shown in **Figure 6**, all of these viruses could grow in PBMCs successfully and showed differential replication abilities. Briefly, rJS/7/05/Ch replicated more efficiently than rMukteswar in PBMCs throughout the infection at multiple MOIs. Similarly, rMu/JHN bearing JS/7/05/Ch-type HN showed the stronger replication ability compared with rJS/MHN bearing Mukteswar-type HN. Notably, the dual-site mutant NDV rMukHN494+495^{JS} exhibited a higher replication level than rMukteswar and was closer to rJS/7/05/Ch in PBMCs. These results demonstrated that dual aa mutations A494D and E495K in HN significantly enhanced NDV replication *in vitro*.

Evaluation of Effects of A494D and E495K on Antigenic Changes

The cross-VN assay was conducted to evaluate the effects of dual aa mutations A494D and E495K on antigenic diversity. As shown in **Table 4**, against rNDVs bearing A494D and E495K (rJS/7/05/Ch and rMukHN494+495^{JS}), neutralization titers of anti-rMukteswar serum were 1:91 and 1:102, respectively. In addition, the R values between rMukteswar and the two rNDVs bearing A494D and E495K were <0.5 (rMukteswar-rJS/7/05/Ch: 0.26; rMukteswar-rMukHN494+495JS: 0.30). Meanwhile, the R value between rJS/7/05/Ch and rMukHN494+495^{JS} was up to 0.82, indicating no significant antigenic difference between these two viruses. These results suggested that dual aa mutations A494D and E495K in HN induced an obvious significant antigenic difference of NDV.

Assessment of Viral Loads and Inflammatory Responses in NDV-Infected Chickens

rJS/7/05/Ch induced more severe symptoms and higher mortality compared with rMukteswar. Specifically, rJS/7/05/Ch-infected chickens showed clinical symptoms at 3 dpi, and death occurred at 4 dpi. In contrast, rMukteswar-infected chickens showed only mild lethargy and no deaths were observed. Moreover, rMukHN494+495^{JS}-infected chickens exhibited severe clinical signs and mortality similar to those caused by rJS/7/05/Ch-infection.

To examine whether the A494D and E495K mutations in HN were essential for virus replication *in vivo*, we assessed

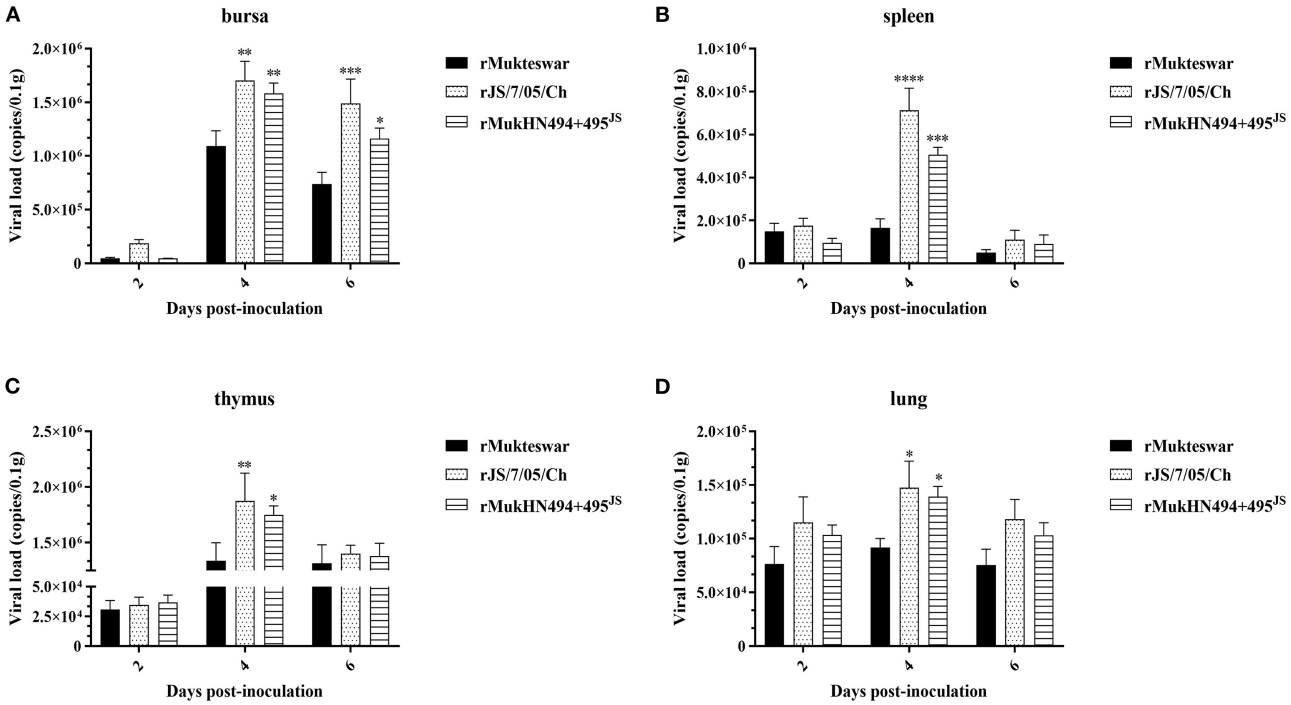

FIGURE 7 | Viral loads in parental and site-mutant rNDV-infected chicken organs. Following infection intravenously with rMukteswar, rJS/7/05/Ch, and rMukHN494+495^{JS}, the bursa **(A)**, spleen **(B)**, thymus **(C)**, and lung **(D)** of infected chickens were selected to measure viral loads using real-time PCR. The viral loads in rJS/7/05/Ch- and rMukHN494+495^{JS}-infected chickens were compared with that in rMukteswar-infected chickens. *$P < 0.05$; **$P < 0.01$; ***$P < 0.001$; ****$P < 0.0001$.

viral loads in sampled organs of infected chickens (**Figure 7**). Real-time PCR results showed higher viral loads in rJS/7/05/Ch-infected chickens compared with those in rMukteswar-infected chickens, significantly in the bursa at 4 and 6 dpi and in the spleen, thymus, and lung at 4 dpi. Furthermore, viral loads in all sampled organs were elevated in rMukHN494+495^{JS}-infected chickens compared with those in rMukteswar-infected chickens and were similar to those in rJS/7/05/Ch-infected chickens. Besides, rMukHN494+495^{JS} infection exhibited the similar statistical differences to rJS/7/05/Ch infection compared with rMukteswar infection.

To evaluate the effects of the A494D and E495K mutations on inflammatory responses, we further detected the expression of inflammatory cytokines in rNDV-infected chickens (**Figure 8**). In the spleen, rJS/7/05/Ch significantly enhanced the mRNA levels of IL-1β, IL-6, and IL-18 in the spleen at 12 and 24 hpi compared with rMukteswar. In the thymus, rJS/7/05/Ch remarkedly strengthened the expression of IL-1β at 24 hpi and IL-6 at 12 and 24 hpi compared with rMukteswar. Additionally, rJS/7/05/Ch induced higher levels of IL-18 than rMukteswar in the thymus throughout the infection. Notably, rMukHN494+495^{JS} induced the similar expression of inflammatory cytokines compared with rJS/7/05/Ch. In brief, rMukHN494+495^{JS} infection significantly upregulated the IL-1β level at 24 hpi and the IL-6 level at 12 and 24 hpi compared with rMukteswar infection in the spleen and thymus. Meanwhile, rMukHN494+495^{JS} also induced higher levels of IL-18 both in the spleen and thymus than rMukteswar throughout the infection, especially at 24 and 48 hpi in the thymus. Overall, these results indicated that dual mutations A494D and E495K in HN enhanced NDV replication and inflammatory responses *in vivo* after intravenous infection.

DISCUSSION

To control the ND epidemic, vaccination measures are widely applied in China, such as the live vaccine strains La Sota and Mukteswar. The mesogenic vaccine strain Mukteswar was first isolated in India and then attenuated by several passages in chicken embryos (27). Although mesogenic ND vaccines have been abandoned in some countries, Mukteswar is still used for emergency immunization in China because of its strong immunogenicity. RNA viruses are susceptible to mutation and changes in virulence during passaging because RNA polymerases lack proofreading ability. It was previously reported that NDV virulence can be enhanced during serial passage in chickens (28). Moreover, a chicken-derived NDV acquired high pathogenicity during serial passaging in ducks because of the occurrence of aa mutations (29). One virulent genotype III NDV JS/7/05/Ch was isolated from diseased chickens and showed high genomic similarity with Mukteswar (15), suggesting that virulent NDV JS/7/05/Ch may have emerged from Mukteswar during vaccination of poultry. Prior studies of NDV virulence were often performed using lentogenic and mesogenic NDVs, such as La

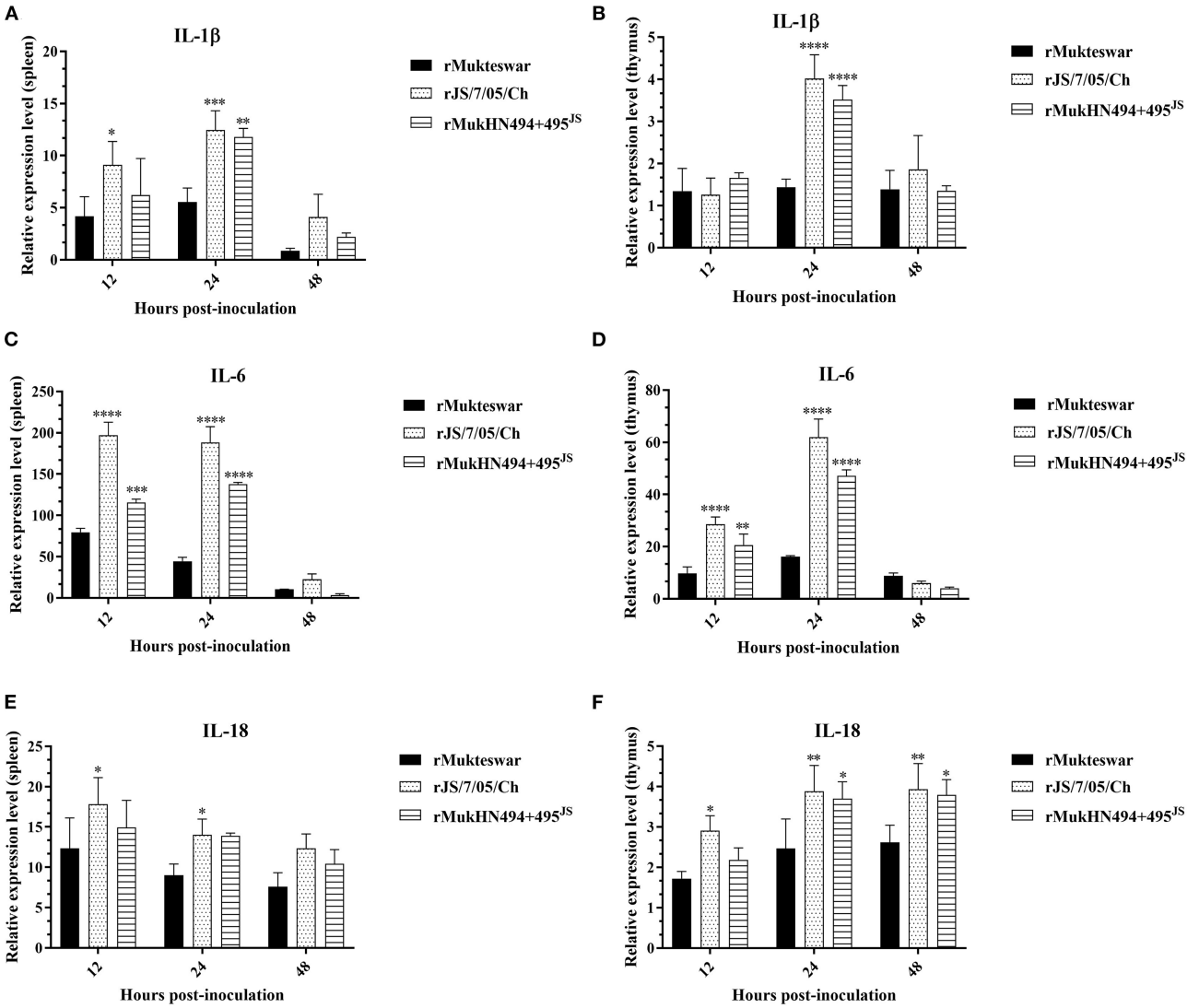

FIGURE 8 | Relative expression of inflammatory cytokine genes in parental and site-mutant rNDV-infected chicken organs. Chickens were infected with rMukteswar, rJS/7/05/Ch, and rMukHN494+495^{JS} through the intravenous route, after which the spleen **(A,C,E)** and thymus **(B,D,F)** were subjected to determine inflammatory cytokine expression using qPCR. The mRNA levels of inflammatory cytokine genes in rJS/7/05/Ch- and rMukHN494+495^{JS}-infected chickens were compared with that in rMukteswar-infected chickens. *$P < 0.05$; **$P < 0.01$; ***$P < 0.001$; ****$P < 0.0001$.

Sota and BC (30). However, ND is commonly caused by virulent NDVs (31), so it is necessary to conduct studies using virulent NDVs as well.

The virulent field strain JS/7/05/Ch shared high identity with the vaccine strain Mukteswar according to whole-genome sequencing. Only 14 nucleotide differences were observed in the NP, HN, and L genes, which caused only seven aa mutations: one in the NP protein and six in the HN protein. HN is made up of four domains: The cytoplasmic domain, the transmembrane region, the stalk region, and the globular head (32, 33). In this study, the aa substitutions in HN between Mukteswar and JS/7/05/Ch were located at positions 19, 29, 145, 266, 494, and 495, which were scattered around various domains of HN. Four aa mutations (positions 145, 266, 494, and 495) were predicted to alter the crystal structure of HN. Structural differences in the HN protein have been reported to affect viral biological activities and virulence (6). Additionally, two aa mutations A494D and E495K in JS/7/05/Ch altered H-bond formation in the HN protein. H-bonds are some of the most important non-covalent interactions in biology and plays roles in stabilizing protein 3D structures and molecular interactions (34). Changes in H-bonding patterns in viral proteins could affect the process of host adaptation (35). Accordingly, we speculate that HN mutations that impact H-bonding may lead to differences in virulence between genotype III NDVs. An increasing number of researches have concentrated on the effects of HN on NDV virulence using reverse genetics technology (6, 10, 36, 37). In this study, two HN-replacement chimeric NDVs (rMu/JHN and rJS/MHN)

were generated using a reverse genetics system. rJS/7/05/Ch and rMu/JHN both showed higher IVPI values than rMukteswar and rJS/MHN, indicating that JS/7/05/Ch-type HN enhanced viral virulence during intravenous infection. These findings agree well with previous data suggesting that HN plays a prominent role in NDV virulence following intravenous inoculation (9). NDV HN protein involves in inducing immune protection against virus infection, and thus is more easily to generate antigenic variation under immune pressure (22, 38). Moreover, the 494 and 495 aa of HN have been demonstrated to be located in the antigen epitope and involve in receptor recognition (12, 39, 40). To verify this hypothesis, we conducted the cross-VN test to determine the effects of A494D and E495K on antigenic variation. The results indicated that a significant antigenic difference was observed between rMukteswar and the rNDVs bearing A494D and E495K, while the antigenic difference was not detected between rJS/7/05/Ch and rMukHN494+495^{JS}. Therefore, dual mutations A494D and E495K from JS/7/05/Ch-type HN likely cause a significant change in NDV antigenicity. Generally, the antigenic variation probably results in the inefficiency of the vaccine and changes of viral virulence (41, 42). Therefore, we further focused on effects of these two aa mutations on the virulence of the genotype III NDV. As we expected, the dual-site mutant virus bearing A494D and E495K in HN mediated a higher IVPI value. This finding suggests that dual aa mutations A494D and E495K in HN can enhance the virulence phenotype of NDV after intravenous infection. Additionally, PBMCs, distributed in peripheral blood, are widely used as a standard *in vitro* model to study virus infection (43). In this study, A494D and E495K in HN enhanced virus replication in chicken PBMCs, which can be responsible for the increased virulence of NDV after intravenous infection.

To better understand the mechanisms underlying the increased virulence of the genotype III NDV, we selected 1-month-old chickens as models to infect intravenously with recombinant NDVs. Dual aa mutations A494D and E495K in HN significantly boosted NDV replication and pathogenicity *in vivo* following intravenous inoculation. In general, the pathogenicity of virus in animals is thought to be associated with the virus replication level (44). Thus, differential *in vivo* replication abilities of these genotype III NDVs can lead to distinct symptoms and pathogenicity in chickens. Additionally, the host response against NDV infection can influence the pathogenicity of virus (45). In this study, rNDVs bearing D494 and K495 activated inflammatory responses more strongly compared with rMukteswar, which can further explain their severe symptoms and pathogenicity in chickens. Previous researches suggested that efficient viral proliferation can result in severe organ damage and pathogenicity (8), and the strong inflammatory response can contribute to pathogen infection (46, 47). Here, combination of higher viral loads and hyper inflammatory responses may be responsible for the enhanced pathogenicity of the genotype III NDV. Taken together, dual aa mutations A494D and E495K in HN facilitate virus infection and result in higher virulence of the genotype III NDV after intravenous infection. However, the precise mechanism how these aa mutations modulate viral virulence remains to be further investigated.

CONCLUSION

Taken together, our study illuminated the molecular mechanisms responsible for increased virulence of the genotype III ND vaccine strain at levels of virus and host. The mutant HN protein of the vaccine strain was identified as the crucial factor in the virulence of NDV after intravenous infection, in which dual aa mutations A494D and E495K in HN played an important role. These findings can be of benefit to the scientific development and application of ND vaccines.

DATA AVAILABILITY STATEMENT

The datasets presented in this study can be found in online repositories. The names of the repository/repositories and accession number(s) can be found in the article/supplementary material.

ETHICS STATEMENT

The animal study was reviewed and approved by Jiangsu Administrative Committee for Laboratory Animals (Permission number: SYXK-SU-2007-0005).

AUTHOR CONTRIBUTIONS

XiuL and SH designed the study. XiaolL and QS performed experiments. XiaolL drafted the manuscript. XiaowL and XW contributed to the revision of the manuscript. All authors read and approved the final manuscript.

FUNDING

This work was supported by the National Natural Science Foundation of China: 31873021; by the Earmarked Fund for China Agriculture Research System: CARS-40 and by the Priority Academic Program Development of Jiangsu Higher Education Institutions (PAPD).

REFERENCES

1. Habib M, Yaqub T, Nazir J, Shehzad W, Aziz Ul R, Sohail T, et al. Genomic and biological characterization of newcastle disease viruses isolated from migratory mallards (Anas Platyrhynchos). *Arch Virol.* (2018) 163:2179–88. doi: 10.1007/s00705-018-3840-8
2. Amarasinghe GK, Ayllon MA, Bao Y, Basler CF, Bavari S, Blasdell KR, et al. Taxonomy of the order mononegavirales: update 2019. *Arch Virol.* (2019) 164:1967–80. doi: 10.1007/s00705-019-04247-4
3. Chen L, Song J, Liu H, Cai J, Lin Q, Xu C, et al. Phylodynamic analyses of class i newcastle disease virus isolated in China. *Transbound Emerg Dis.* (2020) 68:1294–304. doi: 10.1111/tbed.13785

4. Alexander DJ. Newcastle disease and other avian paramyxoviruses. *Rev Sci Tech.* (2000) 19:443–62. doi: 10.20506/rst.19.2.1231
5. Dortmans JC, Koch G, Rottier PJ, Peeters BP. Virulence of newcastle disease virus: what is known so far? *Vet Res.* (2011) 42:122. doi: 10.1186/1297-9716-42-122
6. Yan C, Liu H, Jia Y, Prince-Theodore DW, Yang M, Addoma Adam FE, et al. Screening and mechanistic study of key sites of the hemagglutinin-neuraminidase protein related to the virulence of newcastle disease virus. *Poult Sci.* (2020) 99:3374–84. doi: 10.1016/j.psj.2020.04.014
7. Kim SH, Yan Y, Samal SK. Role of the cytoplasmic tail amino acid sequences of newcastle disease virus hemagglutinin-neuraminidase protein in virion incorporation, cell fusion, and pathogenicity. *J Virol.* (2009) 83:10250–5. doi: 10.1128/JVI.01038-09
8. Jin JH, Cheng JL, He ZR, Ren YC, Yu XH, Song Y, et al. Different origins of newcastle disease virus hemagglutinin-neuraminidase protein modulate the replication efficiency and pathogenicity of the virus. *Front Microbiol.* (2017) 8:1607. doi: 10.3389/fmicb.2017.01607
9. de Leeuw OS, Koch G, Hartog L, Ravenshorst N, Peeters BP. Virulence of newcastle disease virus is determined by the cleavage site of the fusion protein and by both the stem region and globular head of the haemagglutinin-neuraminidase protein. *J Gen Virol.* (2005) 86:1759–69. doi: 10.1099/vir.0.80822-0
10. Huang Z, Panda A, Elankumaran S, Govindarajan D, Rockemann DD, Samal SK. The hemagglutinin-neuraminidase protein of newcastle disease virus determines tropism and virulence. *J Virol.* (2004) 78:4176–84. doi: 10.1128/jvi.78.8.4176-4184.2004
11. Kim SH, Subbiah M, Samuel AS, Collins PL, Samal SK. Roles of the fusion and hemagglutinin-neuraminidase proteins in replication, tropism, and pathogenicity of avian paramyxoviruses. *J Virol.* (2011) 85:8582–96. doi: 10.1128/JVI.00652-11
12. Iorio RM, Syddall RJ, Sheehan JP, Bratt MA, Glickman RL, Riel AM. Neutralization map of the hemagglutinin-neuraminidase glycoprotein of newcastle disease virus: domains recognized by monoclonal antibodies that prevent receptor recognition. *J Virol.* (1991) 65:4999–5006. doi: 10.1128/JVI.65.9.4999-5006.1991
13. Hualei, Liu, Zhiliang, Wang, Cuiping, Son, et al. Characterization of pigeon-origin newcastle disease virus isolated in China. *Avian Dis.* (2006) 50:636–40. doi: 10.1637/7618-042606R1.1
14. Amoia C, Nnadi PA, Ezema C, Couacy-Hymann E. Epidemiology of newcastle disease in africa with emphasis on cote d'ivoire: a review. *Vet World.* (2021) 14:1727–40. doi: 10.14202/vetworld.2021.1727-1740
15. Qiu X, Sun Q, Yao C, Dong L, Wu Y, Hu S, et al. Full-Length genome analysis of two genotype iii velogenic newcastle diseases virus strains reveals their close relationship with vaccine mukteswar. *Art Chin.* (2009) 49:302–8. doi: 10.3321/j.issn:0001-6209.2009.03.004
16. Waterhouse A, Bertoni M, Bienert S, Studer G, Tauriello G, Gumienny R, et al. Swiss-model: homology modelling of protein structures and complexes. *Nucleic Acids Res.* (2018) 46:W296–303. doi: 10.1093/nar/gky427
17. Cagliani R, Forni D, Clerici M, Sironi M. Computational inference of selection underlying the evolution of the novel coronavirus, severe acute respiratory syndrome coronavirus 2. *J Virol.* (2020) 94:e00411–20. doi: 10.1128/JVI.00411-20
18. Schrodinger, LLC. *The Pymol Molecular Graphics System, Version 1.8*. San Carlos, CA: DeLano Scientific (2015).
19. Goodsell D. Representing structural information with rasmol. *Curr Protoc Bioinform.* (2005) 5:5–4. doi: 10.1002/0471250953.bi0504s11
20. Hu Z, Liu X, Jiao X, Liu X. Newcastle disease virus (NDV) recombinant expressing the hemagglutinin of H7N9 avian influenza virus protects chickens against NDV and highly pathogenic avian influenza a (H7N9) virus challenges. *Vaccine.* (2017) 2017:6585. doi: 10.1016/j.vaccine.2017.10.010
21. Oie A. Manual of diagnostic tests and vaccines for terrestrial animals. *Bull Off Int Epizoot.* (2015) 2015:1092–106.
22. Liu J, Zhu J, Xu H, Li J, Hu Z, Hu S, et al. Effects of the hn antigenic difference between the vaccine strain and the challenge strain of newcastle disease virus on virus shedding and transmission. *Viruses.* (2017) 9:225. doi: 10.3390/v9080225
23. Reed LJ, Muench H. A simple method of estimating fifty per cent endpoints. *Am J Epidemiol.* (1938) 3:3. doi: 10.1093/oxfordjournals.aje.a118408
24. Archetti I, Horsfall Jr FL. Persistent antigenic variation of influenza a viruses after incomplete neutralization in ovo with heterologous immune serum. *J Exp Med.* (1950) 92:441–62. doi: 10.1084/jem.92.5.441
25. Niu X, Hao C, Jing Y, Yu X, Diao Y. Development of a taqman-based real-time PCR assay for the detection of novel GPV. *J Virol Methods.* (2016) 237:32–7. doi: 10.1016/j.jviromet.2016.08.006
26. Xu X, Zhang D, Ding W, Wang W, Jin N, Ding Z. Ndv related exosomes enhance ndv replication through exporting Nlrx1 Mrna. *Vet Microbiol.* (2021) 260:109167. doi: 10.1016/j.vetmic.2021.109167
27. Iyer SG, Dobson N. A successful method of immunization against newcastle disease of fowls. *Vet Record.* (1940) 52:52–889.
28. Yu S, Kishida N, Ito H, Kida H, Otsuki K, Kawaoka Y, et al. Generation of velogenic newcastle disease viruses from a nonpathogenic waterfowl isolate by passaging in chickens. *Virology.* (2002) 301:206–11. doi: 10.1006/viro.2002.1539
29. Hidaka C, Soda K, Nomura F, Kashiwabara Y, Ito H, Ito T. The chicken-derived velogenic newcastle disease virus can acquire high pathogenicity in domestic ducks via serial passaging. *Avian Pathol.* (2021) 2021:1-43. doi: 10.1080/03079457.2021.1889461
30. Paldurai A, Kumar S, Nayak B, Samal SK. Complete genome sequence of highly virulent neurotropic newcastle disease virus strain texas gb. *Virus Genes.* (2010) 41:67–72. doi: 10.1007/s11262-010-0486-3
31. Mohan CM, Dey S, Kumanan K, Manohar BM, Nainar AM. Adaptation of a velogenic newcastle disease virus to vero cells: assessing the molecular changes before and after adaptation. *Vet Res Commun.* (2007) 31:371–83. doi: 10.1007/s11259-006-3502-2
32. Jin Z, Wei Q, Bi Y, Li Y, Huo N, Mou S, et al. Identification of a potential neutralizing linear epitope of hemagglutinin-neuraminidase in newcastle disease virus. *Virol J.* (2021) 18:8. doi: 10.1186/s12985-020-01483-y
33. Ferreira L, Munoz-Barroso I, Marcos F, Shnyrov VL, Villar E. Sialidase, receptor-binding and fusion-promotion activities of newcastle disease virus haemagglutinin-neuraminidase glycoprotein: a mutational and kinetic study. *J Gen Virol.* (2004) 85:1981–8. doi: 10.1099/vir.0.79877-0
34. Stickle DF, Presta LG, Dill KA, Rose GD. Hydrogen bonding in globular proteins. *J Mol Biol.* (1992) 226:1143–59. doi: 10.1016/0022-2836(92)91058-w
35. Luo J, Deng L, Ding X, Quan L, Wu A, Jiang T. Hydrogen bond variations of influenza a viruses during adaptation in human. *Sci Rep.* (2017) 7:14295. doi: 10.1038/s41598-017-14533-3
36. Dortmans J, Koch G, Rottier PJM, Peeters BPH. Virulence of pigeon paramyxovirus type 1 does not always correlate with the cleavability of its fusion protein. *J Gen Virol.* (2009) 90:2746–50. doi: 10.1099/vir.0.014118-0
37. Estevez C, King D, Seal B, Yu Q. Evaluation of newcastle disease virus chimeras expressing the hemagglutinin-neuraminidase protein of velogenic strains in the context of a mesogenic recombinant virus backbone. *Virus Res.* (2007) 129:182–90. doi: 10.1016/j.virusres.2007.07.008
38. Li ZJ, Li Y, Chang S, Ding Z, Mu LZ, Cong YL. Antigenic variation between newcastle disease viruses of goose and chicken origin. *Arch Virol.* (2010) 155:499–505. doi: 10.1007/s00705-010-0610-7
39. Iorio RM, Bratt MA. Monoclonal antibodies to newcastle disease virus: delineation of four epitopes on the hn glycoprotein. *J Virol.* (1983) 48:440–50. doi: 10.1128/JVI.48.2.440-450.1983
40. Iorio RM, Borgman JB, Glickman RL, Bratt MA. Genetic variation within a neutralizing domain on the haemagglutinin-neuraminidase glycoprotein of newcastle disease virus. *J Gen Virol.* (1986) 67:1393–403. doi: 10.1099/0022-1317-67-7-1393
41. Vishnoi A, Roy R, Bhattacharya A. Comparative analysis of bacterial genomes: identification of divergent regions in mycobacterial strains using an anchor-based approach. *Nucleic Acids Res.* (2007) 35:3654–67. doi: 10.1093/nar/gkm209
42. Qiu X, Meng C, Zhan Y, Yu S, Li S, Ren T, et al. Phylogenetic, antigenic and biological characterization of pigeon paramyxovirus type 1 circulating in China. *Virol J.* (2017) 14:186. doi: 10.1186/s12985-017-0857-7
43. Qi X, Wang T, Xue Q, Li Z, Yang B, Wang J. Microrna expression profiling of goat peripheral blood mononuclear cells in response to peste des petits ruminants virus infection. *Vet Res.* (2018) 49:62. doi: 10.1186/s13567-018-0565-3
44. Watanabe T, Tisoncik-Go J, Tchitchek N, Watanabe S, Benecke AG, Katze MG, et al. 1918 influenza virus hemagglutinin (ha) and the viral rna

polymerase complex enhance viral pathogenicity, but only ha induces aberrant host responses in mice. *J Virol.* (2013) 87:5239–54. doi: 10.1128/jvi.02753-12
45. Hu Z, Hu J, Hu S, Song Q, Ding P, Zhu J, et al. High levels of virus replication and an intense inflammatory response contribute to the severe pathology in lymphoid tissues caused by newcastle disease virus genotype viid. *Arch Virol.* (2015) 160:639–48. doi: 10.1007/s00705-014-2301-2
46. Ayres JS. Cooperative microbial tolerance behaviors in host-microbiota mutualism. *Cell.* (2016) 165:1323–31. doi: 10.1016/j.cell.2016.05.049
47. Deng S, Yu K, Wu Q, Li Y, Zhang X, Zhang B, et al. Toll-Like receptor 4 reduces oxidative injury via glutathione activity in sheep. *Oxid Med Cell Longev.* (2016) 2016:9151290. doi: 10.1155/2016/9151290

Conflict of Interest: The authors declare that the research was conducted in the absence of any commercial or financial relationships that could be construed as a potential conflict of interest.

Publisher's Note: All claims expressed in this article are solely those of the authors and do not necessarily represent those of their affiliated organizations, or those of the publisher, the editors and the reviewers. Any product that may be evaluated in this article, or claim that may be made by its manufacturer, is not guaranteed or endorsed by the publisher.

frontiers | Frontiers in Veterinary Science

ORIGINAL RESEARCH
published: 16 June 2022
doi: 10.3389/fvets.2022.925935

Genomic Characteristics of a Chicken Infectious Anemia Virus in Contaminated Attenuated Vaccine

Longfei Chen[1,2,3†], *Qi Su*[1,2,3†], *Yan Li*[1,2,3], *Jinjin Wang*[1,2,3], *Yawen Zhang*[1,2,3], *Shuang Chang*[1,2,3], *Yixin Wang*[1,2,3] *and Peng Zhao*[1,2,3*]

[1] College of Veterinary Medicine, Shandong Agricultural University, Tai'an, China, [2] Shandong Provincial Key Laboratory of Animal Biotechnology and Disease Control and Prevention, Tai'an, China, [3] Shandong Provincial Engineering Technology Research Center of Animal Disease Control and Prevention, Tai'an, China

Chicken infectious anemia virus (CIAV) can be transmitted by contaminated live vaccines, and causes huge economic losses. This study evaluated the contamination status of CIAV in 24 batches of vaccines by recombinase-aided amplification assay (RAA), fluorescence quantitative PCR and dot blot assay, and then found a contaminated attenuated vaccine. The whole genome of the CIAV contaminant was then sequenced and named JS2020-PFV (Genbank accession number: MW234428, 2296bp). It showed 94.5 to 99.9% identities with reference strains and shared the closest evolution relationship with AB1K strain which was isolated from a chicken farm in Turkey. All of these suggested that the use of CIAV contaminated live vaccine may be one of the reason for its epidemic in poultry.

Keywords: chicken infectious anemia virus, recombinase-aided amplification assay, contamination, genome analysis, live vaccines

OPEN ACCESS

Edited by:
Yulong Gao,
Chinese Academy of Agricultural Sciences, China

Reviewed by:
Hualei Liu,
China Animal Health and Epidemiology Center, China
Basavaraj S. Mathapati,
Indian Council of Medical Research (ICMR), India

***Correspondence:**
Peng Zhao
zhaopeng@sdau.edu.cn

†These authors have contributed equally to this work

Specialty section:
This article was submitted to Veterinary Infectious Diseases, a section of the journal Frontiers in Veterinary Science

Received: *22 April 2022*
Accepted: *25 May 2022*
Published: *16 June 2022*

Citation:
Chen L, Su Q, Li Y, Wang J, Zhang Y, Chang S, Wang Y and Zhao P (2022) Genomic Characteristics of a Chicken Infectious Anemia Virus in Contaminated Attenuated Vaccine. Front. Vet. Sci. 9:925935. doi: 10.3389/fvets.2022.925935

INTRODUCTION

Chicken infectious anemia virus (CIAV) induces severe anemia and immunosuppression in poultry (1). After its first report in 1979 (2), CIAV has been detected worldwide and has caused huge economic losses (3). Recently, CIAV infections have also frequently appeared in different chicken farms in China (4–8). The pathogenesis of CIAV has been well understood that it mainly causes the atrophy of bone marrow, hematopoietic tissue, and lymphatic tissues (e.g., thymus) in young chickens (9). CIAV can be transmitted both vertically and horizontally via respiratory and digestive tracts (1), but how it spreads across different regions and even countries remains unclear.

It is worth noting that the first strain of CIAV was isolated from the contaminated attenuated vaccine (2). And, after that, similar reports emerged in a lot of countries (10–12), revealing that the use of contaminated live vaccines is an important way of the transmission of CIAV. Through interactions with attenuated vaccine strains or co-infected viruses, CIAV triggers more serious clinical symptoms with a strong immunosuppressive ability (13–15). More importantly, the attenuated vaccines are usually inoculated at a low age, the CIAV infection caused by it will greatly interfere with the immune responses against vaccines, resulting in a secondary infection (16, 17). Therefore, monitoring the vaccine contaminations is of great significance for preventing CIAV infection in poultry.

This study aims to screen the potential CIAV contamination in live vaccines by recombinase-aided amplification (RAA), fluorescence quantitative PCR assay (qPCR) and dot blot. The whole genome of the contaminated CIAV strain was sequenced for further analysis.

TABLE 1 | Sequence of primers used in this study.

Primers	Sequence	Product length
C-F	CAGTAGGTATACGCAAGGCGGTCCGGGTG	277bp
C-R	CACACAGCGATAGAGTGATTGTAATTCCAG	
C-probe	CAAGTAATTTCAAATGAACGCTCTCCAAGA [FAM-dT]A[THF][BHQ1-dT]CCACCCGGACCATCAAC	
CAV-com-F1	GCATTCCGAGTGGTTACTATTCC	842bp
CAV-com-R1	CGTCTTGCCATCTTACAGTCTTA	
CAV-com-F2	CGAGTACAGGGTAAGCGAGCTAAA	990bp
CAV-com-R2	TGCTATTCATGCAGCGGACTT	
CAV-com-F3	ACGAGCAACAGTACCCTGCTA	802bp
CAV-com-R3	CTGTACATGCTCCACTCGTT	

MATERIALS AND METHODS

Vaccine Collection

Twenty-four batches of live vaccines against Newcastle disease virus ($n = 6$), infectious bronchitis ($n = 5$), infectious laryngotracheitis encephalomyelitis ($n = 4$), fowl pox ($n = 4$), Marek disease virus ($n = 3$), mycoplasma gallisepticum ($n = 1$), viral arthritis ($n = 1$), were collected from a layer chicken farm in Heibei province from Jun 2020 to Jun 2021. All these vaccines were selected randomly from the same batch of vaccines purchased by this chicken farm before vaccination for detecting potential exogenous virus contaminations. All vaccines were not opened before testing. All these vaccines were diluted with normal saline according to the instructions, and 200 μl of the dilute was used for DNA extraction.

DNA Extraction

DNA was extracted using the DNA extraction kit (Omega, Bio-Tek, USA) according to the manufacturer's instructions as the template for RAA, qPCR and dot blot.

RAA

The primers and probe were designed according to the published CIAV genome (**Tables 1**, **2**). The RAA fluorescence kit and RAA amplification instrument were provided by Hangzhou ZC Bio-Sci & Tech Co., Ltd. (Hangzhou, China). ddH_2O was used as the negative control and standard plasmid containing full-length CIAV genomes was constructed by our lab and used as a positive control (7). RAA detection methods and primer probes are shown in **Table 1**.

Fluorescent Quantitative PCR

With the fluorescent quantitative PCR kit produced by TaKaRa Biotechnology (Takara, Dalian, Chian), the sample DNA was detected and verified by the fluorescent quantitative PCR method according to the references (7).

Dot Blot Hybridization

The samples were tested by PCR combined with dot blot hybridization (18), and the nitrocellulose membrane was purchased from Boehringer Millipore (Merck, Germany).

Amplification and Sequencing of the Whole Genome of Samples

According to the sequence published in the GenBank, three primers were designed to amplify the sample DNA using DNAStar 6.0 application. The primers are shown in **Table 1**. The amplification procedure was as follows: 94°C for 5 min; 94°C for 30 s, 55°C for 30 s, and 72°C for 30 s (34 cycles); 72°C for 10 min (35 cycles); and 4°C. The PCR products were identified using 1% agarose gel electrophoresis and stained with ethidium bromide. The bands were purified with an Omega gel recovery and purification kit (Omega Bio-Tek, Norcross, GA, USA), and the recovered target fragments were attached to the pMD18-T vector (Takara, Dalian, Chian). After overnight ligation at 16°C, the ligation products were transformed into competent cells of E. coli DH5α (Takara, Japan), and the positive clones were screened. Finally, the bacterial liquid identified as positive by PCR was sent to Shanghai Bioengineering Co., Ltd. for sequencing.

Sequence Analysis

The DNA sequences were assembled using DNAStar (version 6.0). Multiple sequence alignment was performed using the Clustal W (BioEdit version 7.0) program, and the comparison of sequence identity was performed using MegAlign software (DNAStar). Phylogenetic analysis was performed using the maximum likelihood (ML) method on RAxML.

RESULTS

Results of CIAV Nucleic Acid Test in Vaccines

RAA, qPCR assay, and dot blot were employed to detect CIAV contamination in live vaccines. Results showed that a fowlpox attenuated vaccine sample was determined as CIAV positive in all three methods (**Figure 1**).

Whole-Genome Sequencing

To further reveal the molecular characteristics of the CIAV contaminants, the whole genome of this strain was sequenced using three pairs of primers. The electrophoretic analysis confirmed the positive amplification by PCR, and the three segments were 842bp, 990bp and 802bp, respectively (**Figure 2**), which was consistent with the expected band size. Furthermore, the whole genome of this isolate was 2296 bp, covering three open-reading-frame (ORF), namely VP1, VP2, and VP3.

The lengths of VP1, VP2 and VP3 were 1350 bp, 651 bp and 366 bp, respectively. The isolate was named JS2020-PFV and its sequence was uploaded to the GenBank gene library with the accession number of MW234428.

Genome Analysis of JS2020-PFV

The whole genome of the JS2020-PFV strain was compared with that of 56 other CIAV strains. Results showed that JS2020-PFV shared 94.5 to 99.9% of identities with other reference strains. Among them, JS2020-PFV had the highest identity (99%) with the AB1K strain (MT259319) isolated from a chicken farm in Turkey. A phylogenetic tree was constructed based on the whole genome sequence of JS2020-PFV and reference strains, and

TABLE 2 | CIAV strains were used as reference strains in this study.

Strains	Country and Time	Host	Accession No.	Whole length
SDLY08	2008 China	Chicken	FJ172347	2298 bp
3711	2007 Australia	Chicken	EF683159	2279 bp
CAV-6	2014 China	Chicken	KJ728817	2298 bp
CAV-14	2014 China	Chicken	KJ728824	2298 bp
E51057	2000 Japan	Chicken	E51057	2298 bp
SC-MZ	2014 China	Chicken	KM496306	2298 bp
CAT-CA V	2014 China	Chicken	KC414026	2295 bp
CIA V89-69	2013 Korea	Chicken	JF507715	2298 bp
GD-1-12	2012 China	Chicken	JX260426	2298 bp
LF4	2005 China	Chicken	AY839944	2298 bp
HH982173	2006 USA	Chicken	HH982173	2298 bp
AB031296	2000 Japan	Chicken	AB031296	2298 bp
AGV2	2012 China	Human	JQ690762	2316 bp
L14767	1999 USA	Chicken	L14767	2298 bp
3-1	2003 Malaysia	Chicken	AF390038	2298 bp
A48606	1996 USA	Chicken	A48606	2298 bp
CAU66304	1997 UK	Chicken	U66304	2319 bp
clone 33	2002 Germany	Chicken	AJ297684	2298 bp
NC001427	2015 USA	Chicken	NC001427	2319 bp
Cux-1	2008 Netherlands	Chicken	M55918	2319 bp
DI072479	1990 USA	Chicken	DI072479	2298 bp
CAV-4	2014 China	Chicken	KJ728816	2298 bp
CAV-18	2014 China	Chicken	KJ728827	2298 bp
GD-K-12	2013 China	Chicken	KF224935	2298 bp
AH4	2005 China	Chicken	DQ124936	2298 bp
AB119448	2009 Japan	Chicken	AB119448	2298 bp
TR20	1999 Japan	Chicken	AB027470	2298 bp
Cuxhaven	1992 Germany	Chicken	M81223	2298 bp
AB1K	2020 Turkey	Chicken	MT259319	2296 bp
M81223	1993 Germany	Chicken	M81223	2298 bp
CAU65414	1996 Australia	Chicken	CAU65414	2298 bp
A2	2000 Japan	Chicken	AB031296	2298 bp
AF313470	2000 USA	Chicken	AF313470	2294 bp
AF227982	2001 Australia	Chicken	AF227982	2286 bp
AB046590	2001 Japan	Chicken	AB046590	2298 bp
AF475908	2002 China	Chicken	AF475908	2298 bp
clone 34	2002 Germany	Chicken	AJ297685	2297 bp
SMSC-1P60	2003 Malaysia	Chicken	AF390102	2298 bp
SMSC-1	2003 Malaysia	Chicken	AF285882	2298 bp
BD-3	2004 Bangladesh	Chicken	AF395114	2298 bp
C14	2004 China	Chicken	EF176599	2298 bp
SD22	2005 China	Chicken	DQ141673	2298 bp
DQ217401	2005 Malaysia	Chicken	SMSC-1P123	2298 bp
CAE26P4	2007 Netherlands	Chicken	D10068	2298 bp
01-4201	2007 USA	Chicken	DQ991394	2298 bp
Cuxhaven-1	2008 Netherlands	Chicken	M55918	2319 bp
CAECA123	2008 Japan	Chicken	D31965	2319 bp
98D02152	2010 USA	Chicken	AF311892	2298 bp
GXC060821	2012 China	Chicken	JX964755	2292 bp
CAV-10	2014 Argentina	Chicken	KJ872513	2298 bp
KM496307	2014 China	Chicken	SC-MZ42A	2298 bp
Isolate 18	2014 Taiwan	Chicken	KJ728827	2298 bp
SD15	2015 China	Chicken	KX811526	2298 bp
JS2020-PFV	2020 China	Chicken	MW234428	2296 bp
GX1804	2018 China	Chicken	MK484615	2298 bp
SD1510	2016 China	Chicken	KU598851	2298 bp
HN1405	2016 China	Chicken	KU645520	2298 bp

the results further confirmed the closest evolution relationship between JS2020-PFV and AB1K (**Figure 3**).

Analysis of VP1 Gene Variation in JS2020-PFV Strain

The VP1 gene of the JS2020-PFV strain shared 94.0 to 99.9% identities with the reference strains, with the highest identity (99.9%) with AB1K. The genetic evolution relationship between the VP1 gene of the JS2020-PFV strain and reference strains was consistent with the whole genome sequence (**Figure 3**). Further analysis of the VP1 gene of JS2020-PFV strain revealed that there are two amino acid mutations within which had never been found before, namely threonine at position 89 of VP1 protein changed to lysine and glutamine at position 448 changed to lysine (**Table 3**).

TABLE 3 | Position of mutational VP1 amino acid of JS2020-PFV.

Strains	Position of VP1 amino acid										
	89	**92**	**125**	**139**	**141**	**144**	**157**	**254**	**370**	**447**	**448**
Cux-1	T	G	I	K	Q	D	V	G	S	T	Q
GD-F-1	T	G	L	K	Q	E	M	E	G	S	Q
SDLY08	T	G	I	K	R	E	V	E	G	T	Q
SD15	T	G	I	K	Q	Q	V	E	T	S	P
AB1K	T	D	I	K	Q	E	M	G	S	T	Q
JS2020-PFV	**K**	D	I	K	Q	E	M	G	S	T	**H**

Difference Analysis of Transcriptional Regulatory Elements in Non-coding Regions

The Clustal W method was used for multiple alignment analysis of the non-coding regions of JS2020-PFV with 9 reference strains. Compared with the reference strains, the motif in non-coding regions of CIAV was highly conserved (**Figure 4**). Softberry's Nsite online service analysis showed that four CREB sites

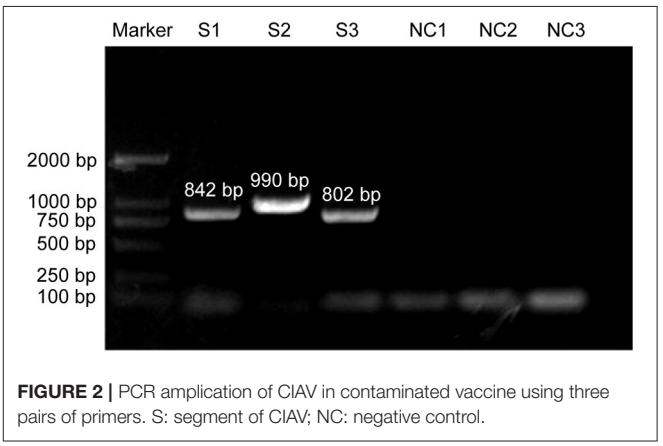

FIGURE 2 | PCR amplication of CIAV in contaminated vaccine using three pairs of primers. S: segment of CIAV; NC: negative control.

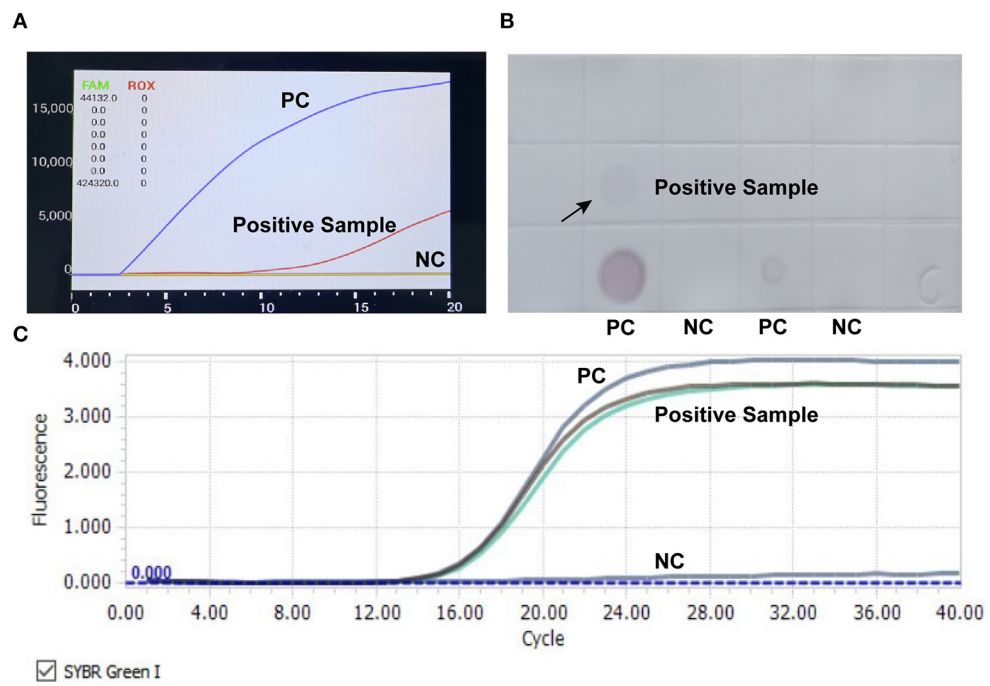

FIGURE 1 | Detection of CIAV nucleic acid in attenuated chicken pox vaccine. RAA rapid assay **(A)**, nucleic acid dot hybridization **(B)**, and fluorescence quantitative PCR assay **(C)** were simultaneously employed to detect CIAV contamination in vaccine samples, and all the methods showed positive results. PC, positive control; NC, negative control.

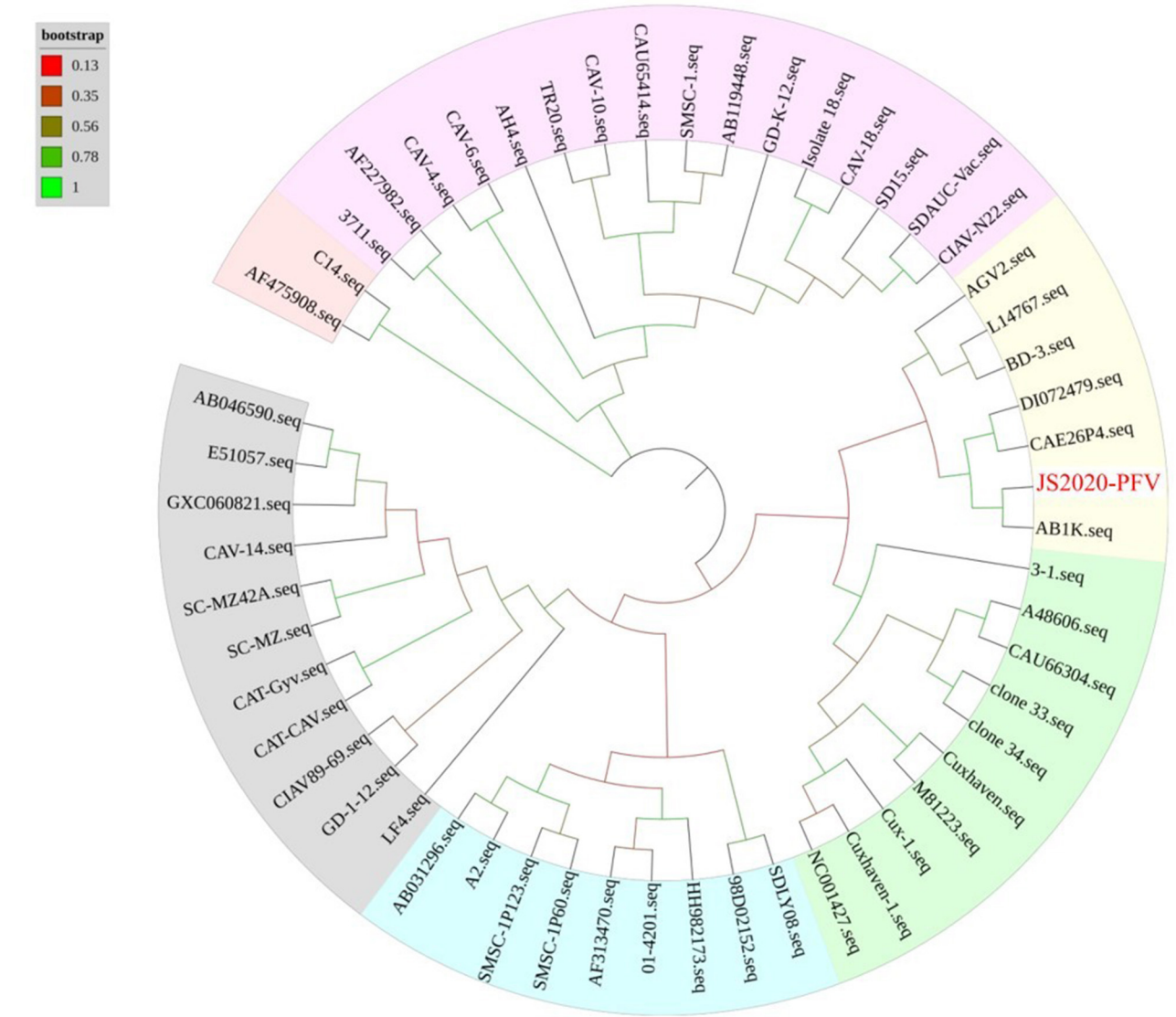

FIGURE 3 | Phylogenetic tree of full-length viral genome of JS2020-PFV and reference strains. The isolated strain in this study has been highlighted in red. The tree was constructed by the maximum likelihood method with 1,000 bootstrap replicates using MEGA 5.0.

associated with viral apoptotic capacity were also conserved in the new isolate. The JS2020-PFV and most of the reference strains all had four DR regions in the non-coding region, except for one additional DR region in the CUX-1 strain.

DISCUSSION

Over the past two decades, many live vaccines have been proved to be contaminated with exogenous viruses, including avian leukosis virus (19), fowl adenovirus (20), reticuloendotheliosis virus (26), CIAV (6) and others. All these viruses share the common feature of being able to vertically propagate through the chicken embryo, suggesting such contamination is mainly caused by the use of SPF chicken embryos infected with exogenous viruses during vaccine production. Several studies have reported the infection of the above viruses in SPF chicken farms, which further confirmed the above hypothesis (21). The use of contaminated vaccines will not only cause the spread of the virus but also cause serious clinical symptoms, especially vaccines contaminated with CIAV that induce strong immunosuppression. Previous studies demonstrated that the co-infection with CIAV can significantly improve the pathogenicity of the LaSota strain in NDV vaccines, and decrease the antibody titer, which makes the vaccinated chickens vulnerable to wild NDV strains (7). Therefore, monitoring the exogenous virus

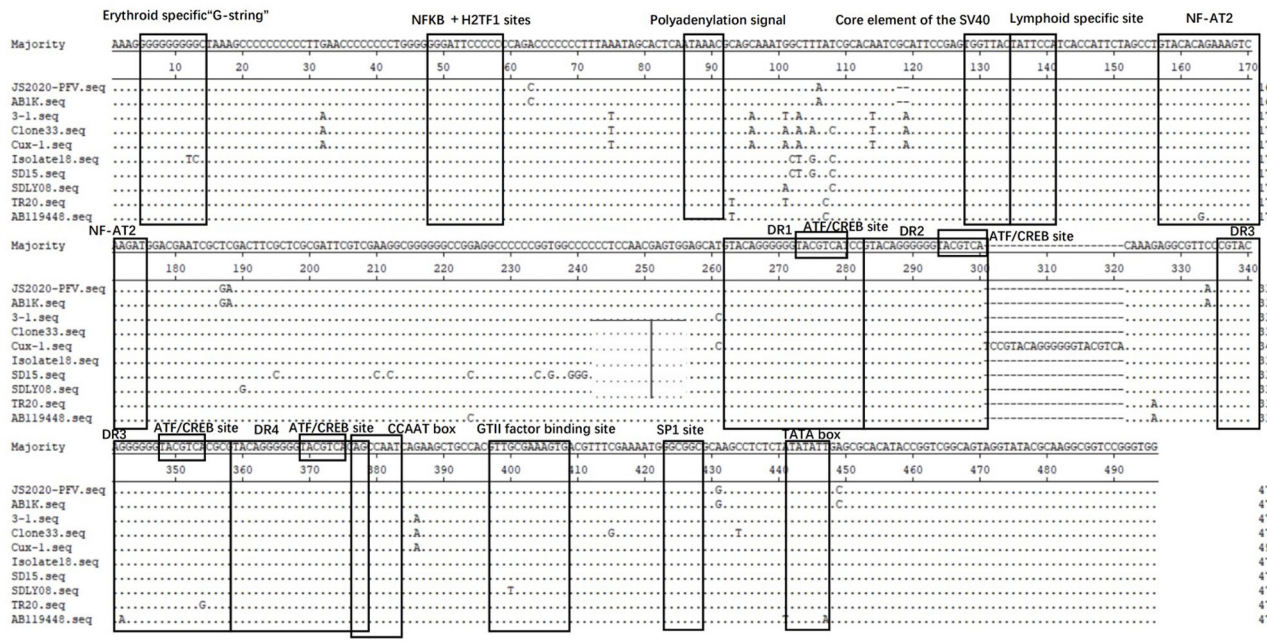

FIGURE 4 | Structural analysis of the non-coding region of JS2020-PFV strain and reference strains. The sequences in black frames are the motifs of transcriptional regulatory elements in this study.

contamination in live vaccination is of great significance for poultry farms.

In this study, RAA assay, the traditional qPCR and dot blot were used at the same time to screen the potential contamination of CIAV in live vaccines. Results found that one fowl pox vaccine was positive for CIAV in all these three methods, indicating that the detection results were true and reliable. It should be noted that RAA completed the whole detection process in only 15 min, while qPCR and dot blot took 1.5 and 14 h respectively. Now, there are also several handheld devices for RAA. Therefore, the RAA method is more suitable for monitoring vaccine contamination in farms because of its flexibility and convenience.

Furthermore, the whole genome sequence of CIAV was sequenced and named JS2020-PFV. It was found that JS2020-PFV had extremely high identities (99%) and the closest evolution relationship with the AB1K strain (MT259319) that was isolated from a chicken farm in Turkey. Besides, JS2020-PFV shared a close relationship with American isolate (DI072479) and Netherland isolate (CAE26P4), while it was relatively unrelated to Chinese isolates, including SDLY18 (FJ172347), GD-K-12 (KF224935) and SD15 (KX811526). These results are consistent with the fact that the vaccine was imported from a foreign company, suggesting that the transnational trade of vaccines may be an important way for some strains to spread across countries and regions.

The amino acid positions of VP1 protein are closely related to CIAV pathogenicity and cell proliferation (5). Previous studies have shown that amino acid positions 139 and 144 on VP1 were associated with the efficiency of virus proliferation and transmission in MSB1 cells (22). The amino acid positions 139 and 144 on the VP1 protein of JS2020-PFV are lysine (K) and glutamic acid (E), which are consistent with the strain with high replication ability (22). Besides, glutamine (Q) at position 394 was associated with higher pathogenicity, while histidine (H) at position 394 was related to lower pathogenicity (22). In this study, the amino acid at position 394 of VP1 protein of JS2020-PFV is glutamine (Q), suggesting that this strain may also be highly pathogenic. There are more than ten motifs related to transcriptional regulation in the non-coding region of CAV, which are closely related to viral replication and transcriptional regulation. After comparing and analyzing the non-coding regions of the selected strains in this paper, it was found that these motifs were very conservative. We speculate that these related motifs may be necessary for the replication of the virus itself.

Overall, CIAV contamination was detected from a fowlpox vaccine, and genome analysis suggested that it may be a highly pathogenic strain, which reminded us to pay close attention to the possible contamination of exogenous virus in live poultry vaccine. To prevent the recurrence of this phenomenon, SPF chicken farms, vaccine factories and farmers all should take reasonable countermeasures. First of all, SPF chicken farms should strengthen the daily monitoring of viruses, regularly detect the viruses with vertical transmission ability that have been reported in contaminated vaccines, and strictly eradicate their breeding chicken flocks. After purchasing chicken embryos, vaccine factories should also conduct viral detections of chicken embryos to eliminate the possibility of exogenous virus infection.

In the last link, farmers should conduct a spot check on each batch of vaccines before using, to eliminate the possibility of exogenous virus contamination. The convenient and fast RAA method applies to the above three links, which is very conducive for on-site detection.

DATA AVAILABILITY STATEMENT

The datasets presented in this study can be found in online repositories. The names of the repository/repositories and accession number(s) can be found below: https://www.ncbi.nlm.nih.gov/, MW234428.

AUTHOR CONTRIBUTIONS

LC and QS conceived and performed the experiments, analyzed the data, and drafted the manuscript. PZ supervised the project and edited the manuscript. YL, JW, YZ, SC, and YW performed part of the experiments. All authors contributed to the article and approved the submitted version.

FUNDING

This work was supported by the National Key Research and Development Program of China (2018YFD0500106).

REFERENCES

1. Rosenberger JK, Cloud SS. Chicken anemia virus. *Poult Sci.* (1998) 77:1190–2. doi: 10.1093/ps/77.8.1190
2. Yuasa N, Taniguchi T, Yoshida I. Isolation and some characteristics of an agent inducing anemia in chicks. *Avian Dis.* (1979) 366–85. doi: 10.2307/1589567
3. Fatoba AJ, Adeleke A. Chicken anemia virus: A deadly pathogen of poultry. *Acta Virol.* (2019) 63:19–25. doi: 10.4149/av_2019_110
4. Zhang X, Liu Y, Wu B, Sun B, Chen F, Ji J, et al. Phylogenetic and molecular characterization of chicken anemia virus in southern China from 2011 to 2012. *Sci Rep.* (2013) 3:3519. doi: 10.1038/srep03519
5. Fang L, Li Y, Wang Y, Fu J, Cui S, Li X, et al. Genetic Analysis of Two Chicken Infectious Anemia Virus Variants-Related Gyrovirus in Stray Mice and Dogs: The First Report in China, 2015. *Biomed Res Int*. (2017) 2017:6707868. doi: 10.1155/2017/6707868
6. Li Y, Fang L, Cui S, Fu J, Li X, Zhang H, et al. Genomic characterization of recent chicken anemia virus isolates in China. *Front Microbiol*. (2017) 8:401. doi: 10.3389/fmicb.2017.00401
7. Su Q, Meng F, Li Y, Zhang Y, Zhang Z, Cui Z, et al. Chicken infectious anemia virus helps fowl adenovirus break the protection of maternal antibody and cause inclusion body hepatitis-hydropericardium syndrome in layers after using co-contaminated Newcastle disease virus-attenuated vaccine. *Poult Sci.* (2019) 98:621–8. doi: 10.3382/ps/pey153
8. Tan C, Wang Z, Lei X, Lu J, Yan Z, Qin J, et al. Epidemiology, molecular characterization, and recombination analysis of chicken anemia virus in Guangdong province, China. *Arch Virol.* (2020) 165:1409–17. doi: 10.1007/s00705-020-04604-8
9. Adair BM. Immunopathogenesis of chicken anemia virus infection. *Dev Comp Immunol.* (2000) 24:247–55. doi: 10.1016/S0145-305X(99)00076-2
10. Marin SY, Barrios PR, Rios RL, Resende M, Resende JS, Santos BM, et al. Molecular characterization of contaminating infectious anemia virus of chickens in live commercial vaccines produced in the 1990s. *Avian Dis*. (2013) 57:15–21. doi: 10.1637/10056-011212-Reg.1
11. Varela APM, Dos Santos HF, Cibulski SP, Scheffer CM, Schmidt C, Lima FES, et al. Chicken anemia virus and avian gyrovirus 2 as contaminants in poultry vaccines. *Biologicals*. (2014) 42:346–50. doi: 10.1016/j.biologicals.2014.08.002
12. Li Y, Hu Y, Cui S, Fu J, Wang Y, Cui Z, et al. Molecular characterization of chicken infectious anemia virus from contaminated live-virus vaccines. *Poult Sci.* (2017) 96:1045–51. doi: 10.3382/ps/pew406
13. Su Q, Li Y, Meng F, Cui Z, Chang S, Zhao P. Newcastle disease virus-attenuated vaccine co-contaminated with fowl adenovirus and chicken infectious anemia virus results in inclusion body hepatitis-hydropericardium syndrome in poultry. *Vet Microbiol.* (2018) 218:52–9. doi: 10.1016/j.vetmic.2018.03.019
14. Su Q, Li Y, Zhang Y, Zhang Z, Meng F, Cui Z, et al. Newcastle disease virus-attenuated vaccine LaSota played a key role in the pathogenicity of contaminated exogenous virus. *Vet Res.* (2018) 49:80. doi: 10.1186/s13567-018-0577-z
15. Su Q, Wang T, Meng F, Cui Z, Chang S, Zhao P. Synergetic pathogenicity of Newcastle disease vaccines LaSota strain and contaminated chicken infectious anemia virus. *Poult Sci.* (2019) 98:1985–92. doi: 10.3382/ps/pey555
16. Zhang Y, Cui N, Han N, Wu J, Cui Z, Su S. Depression of Vaccinal Immunity to Marek's Disease by Infection with Chicken Infectious Anemia Virus. *Front Microbiol.* (2017) 8:1863. doi: 10.3389/fmicb.2017.01863
17. Su Q, Zhang Y, Li Y, Cui Z, Chang S, Zhao P. Epidemiological investigation of the novel genotype avian hepatitis E virus and co-infected immunosuppressive viruses in farms with hepatic rupture haemorrhage syndrome, recently emerged in China. *Transbound Emerg Dis.* (2019) 66:776–84. doi: 10.1111/tbed.13082
18. Meng F, Dong G, Zhang Y, Tian S, Cui Z, Chang S, et al. Co-infection of fowl adenovirus with different immunosuppressive viruses in a chicken flock. *Poult Sci.* (2018) 97:1699–705. doi: 10.3382/ps/pex414
19. Mao Y, Su Q, Li J, Jiang T, Wang Y. Avian leukosis virus contamination in live vaccines: a retrospective investigation in China. *Vet Microbiol.* (2020) 246:108712. doi: 10.1016/j.vetmic.2020.108712
20. Su Q, Hou L, Gao Y, Liu X, Cui Z, Chang S, et al. Research Note: Molecular relationship of the fowl adenovirus serotype 4 isolated from the contaminated live vaccine and wild strains isolated in China, 2013-2018. *Poult Sci.* (2020) 99:6643–6. doi: 10.1016/j.psj.2020.08.063
21. Li Y, Wang Y, Fang L, Fu J, Cui S, Zhao Y, et al. Genomic Analysis of the Chicken Infectious Anemia Virus in a Specific Pathogen-Free Chicken Population in China. *Biomed Res Int.* (2016) 2016:4275718. doi: 10.1155/2016/4275718
22. Yamaguchi S, Imada T, Kaji N, Mase M, Tsukamoto K, Tanimura N, et al. Identification of a genetic determinant of pathogenicity in chicken anaemia virus. *J Gen Virol.* (2001) 82:1233–8. doi: 10.1099/0022-1317-82-5-1233

Conflict of Interest: The authors declare that the research was conducted in the absence of any commercial or financial relationships that could be construed as a potential conflict of interest.

Publisher's Note: All claims expressed in this article are solely those of the authors and do not necessarily represent those of their affiliated organizations, or those of the publisher, the editors and the reviewers. Any product that may be evaluated in this article, or claim that may be made by its manufacturer, is not guaranteed or endorsed by the publisher.

frontiers | Frontiers in Veterinary Science

ORIGINAL RESEARCH
published: 23 June 2022
doi: 10.3389/fvets.2022.873163

Rapid, Sensitive, and Species-Specific Detection of Conventional and Recombinant Herpesvirus of Turkeys Vaccines Using Loop-Mediated Isothermal Amplification Coupled With a Lateral Flow Device Readout

Giulia Mescolini[1], *Susan J. Baigent*[2]*, *Elena Catelli*[1] *and Venugopal K. Nair*[2]

[1] Avian Pathology Service, Department of Veterinary Medical Sciences, University of Bologna, Bologna, Italy, [2] Viral Oncogenesis Group, The Pirbright Institute, Woking, United Kingdom

OPEN ACCESS

Edited by:
Aijian Qin,
Yangzhou University, China

Reviewed by:
Muhammad Munir,
Lancaster University, United Kingdom
Bin Zhou,
Nanjing Agricultural University, China

***Correspondence:**
Susan J. Baigent
sue.baigent@pirbright.ac.uk

Specialty section:
This article was submitted to Veterinary Infectious Diseases, a section of the journal Frontiers in Veterinary Science

Received: 10 February 2022
Accepted: 19 April 2022
Published: 23 June 2022

Citation:
Mescolini G, Baigent SJ, Catelli E and Nair VK (2022) Rapid, Sensitive, and Species-Specific Detection of Conventional and Recombinant Herpesvirus of Turkeys Vaccines Using Loop-Mediated Isothermal Amplification Coupled With a Lateral Flow Device Readout. Front. Vet. Sci. 9:873163. doi: 10.3389/fvets.2022.873163

Marek's disease, an economically important disease of chickens caused by virulent serotype 1 strains of the *Mardivirus* Marek's disease virus (MDV-1), is effectively controlled in the field by live attenuated vaccine viruses including herpesvirus of turkeys (HVT)—both conventional HVT (strain FC126) and, in recent years, recombinant HVT viruses carrying foreign genes from other avian viruses to protect against both Marek's disease and other avian viral diseases. Testing to monitor and confirm successful vaccination is important, but any such test must differentiate HVT from MDV-1 and MDV-2, as vaccination does not prevent infection with these serotypes. End-point and real-time PCR tests are widely used to detect and differentiate HVT, MDV-1 and MDV-2 but require expensive specialist laboratory equipment and trained operators. Here, we developed and validated two tube-based loop-mediated isothermal amplification tests coupled with detection by lateral flow device readout (LAMP-LFD): an HVT-specific test to detect both conventional and recombinant HVT strains, and a second test using novel LAMP primers to specifically detect the Vaxxitek® recombinant HVT. Specificity was confirmed using DNA extracted from virus-infected cultured cells, and limit of detection was determined using plasmid DNA carrying either the HVT or Vaxxitek® genome. The LAMP-LFD tests accurately detected all HVT vaccines, or Vaxxitek® only, in crude DNA as well as purified DNA extracted from field samples of organs, feathers, or poultry house dust that were confirmed positive for HVT by real-time PCR. These LAMP-LFD tests have potential for specific, rapid, simple, and inexpensive detection of HVT vaccines in the field.

Keywords: Marek's disease, herpesvirus of turkeys, LAMP-LFD, FC126, Vaxxitek®

INTRODUCTION

Meleagrid alphaherpesvirus 1, the herpesvirus of turkeys (HVT), is a member of the genus *Mardivirus* of the *Alphaherpesvirinae* subfamily (1), together with *Gallid alphaherpesvirus 2*, traditionally referred to as Marek's disease virus serotype 1 (MDV-1), the aetiological agent of Marek's disease (MD), and *Gallid alphaherpesvirus 3*, or Marek's disease virus serotype 2 (MDV-2). HVT was isolated for the first time in 1968 from healthy turkeys by two different research groups (2, 3) and was shown to be apathogenic for chickens, and antigenically related to MDV-1 offering good protection against MD (4, 5). For these reasons HVT has been successfully used worldwide as a vaccine against MD in chickens since it was first licensed in 1971 in the United States (reviewed by 3), either alone or in combination with MD vaccines of other serotypes (i.e., attenuated serotype 1 CVI988/Rispens strain or serotype 2 naturally apathogenic strain SB-1) (6, 7). Conventional HVT vaccines (for example, using the FC126 strain) have been used to successfully protect chickens from MD since the early 1970s (8). Several recombinant vaccines using HVT as a vector (rHVT) to express heterologous immunogenic proteins of chicken viruses that cause major diseases such as Newcastle disease (9, 10), infectious bursal disease (11), and infectious laryngotracheitis (12) have been developed since the 1990s, and are used worldwide in the control of MD and of the abovementioned poultry diseases. The Vaxxitek® range of vaccines (Boehringer Ingelheim) and Innovax® range of vaccines (MSD Animal Health) use HVT as a vector to express single genes from other pathogenic avian viruses: infectious bursal disease virus (IBDV), infectious bronchitis virus (IBV), infectious laryngotracheitis virus (ILTV), and Newcastle disease virus (NDV), or combinations thereof. The Vaxxitek® range includes VAXXITEK® HVT + IBD, VAXXITEK® HVT + IBD + ND, and VAXXITEK® HVT + IBD + ILT. The Innovax® range includes Innovax®-ND-ILT, Innovax®-ND-IBD, Innovax®-ND, and Innovax®-ILT.

The efficacy of HVT vaccination against MD has decreased over time, mainly due to increased virulence of MDV-1 strains (13). Nowadays, the use of HVT vaccine alone is restricted to the vaccination of broilers; long-living birds such as breeders and layers are usually vaccinated with a bivalent HVT and CVI988/Rispens vaccine (14). Cell-free lyophilized HVT vaccine, which is cheaper and easier to handle than cell-associated formulations where liquid nitrogen is needed for storage, is frequently adopted for the protection of valuable ornamental chicken flocks with a history of MD, and also some backyard chicken flocks (15).

Both conventional and recombinant HVT vaccines are live vaccines that actively replicate within the host mimicking natural infection and eliciting a protective immune response. HVT vaccinal viruses replicate in the feather follicle epithelium and are persistently shed into the environment through physiological desquamation of epithelial cells (16). Thus, feather tips taken from vaccinated birds represent a non-invasive sample to confirm HVT vaccine administration and uptake for monitoring success of HVT-based MD vaccination in the field (17). Furthermore, the HVT genome can be detected in dust collected from the poultry house environment (18–20), often in combination with MDV-1 and MDV-2 (21).

MD vaccines have been reported as "imperfect" or "leaky", as they prevent clinical MD but do not impede the infection, replication, and shedding of wild-type MDV-1 into the environment (19, 20, 22–24). Thus, vaccine and field viruses can coexist in the vaccinated host (25) and, in case of mixed infection, molecular tests able to discriminate between MDV-1, MDV-2 and HVT are required.

The full-length genome sequences of the three viral species included in the genus *Mardivirus* are publicly available in online databases (26–31) and many species-specific molecular methods that allow for their differential detection have been developed over time.

Such molecular methods include end-point and real-time PCR assays (17, 18, 25, 32–34) and have one or more of the following drawbacks: they are labor-intensive, require time-consuming post-PCR handling such as gel electrophoresis to visualize the outcome, need expensive specialized equipment, and need to be performed by highly trained personnel. A simple, fast, and accurate test for monitoring of vaccination success in the field could be greatly beneficial for field veterinarians and small laboratories.

Loop-mediated isothermal amplification (LAMP) first described by Notomi et al. (35) and improved by Nagamine et al. (36) is a rapid, extremely specific, and sensitive molecular method that could overcome most of the drawbacks of PCR-based methods. The outstanding specificity is obtained using six primers (two outer primers, two inner primers and two loop primers) that specifically recognize eight different regions in the target genome. A DNA polymerase with strand displacement activity, working under isothermal conditions (temperature between 60 and 65°C) combined with suitably designed primers, enables, starting from the target DNA sequence, the formation of a stem-loop DNA structure, which is the starting point for exponential amplification of the target DNA.

LAMP-based assays for the specific detection of HVT, MDV-1 or MDV-2 genomes have been reported previously (37–43). In all the above-mentioned methods the detection of LAMP products was achieved by sequence-independent methods, such as the utilization of agarose gel electrophoresis or intercalating fluorescent dyes. Sequence-specific detection methods, that enable the exact identification of specific amplicons without being affected by non-specific products (44), are available and, of these, the immunochromatographic lateral flow device (LFD) is one of the most often used. LFDs are designed to specifically detect dual-labeled LAMP DNA amplicons that are captured on a lateral flow test strip, allowing their rapid and direct visualization. Lateral flow tests are low cost, easy to handle, do not require additional equipment, and give an unequivocal positive or negative result that can be interpreted by non-specialist personnel.

The purpose of the current work was to develop HVT-specific LAMP-LFD assays, and to validate these to test field samples in a controlled laboratory setting. Herein, we describe the modification of a previously reported HVT-specific LAMP

assay (37), to allow detection of dual-labeled LAMP products with commercially available LFDs. In addition, a novel LAMP assay able to specifically detect the recombinant HVT vaccine VAXXITEK® HVT + IBD was developed and validated. Finally, crude DNA extracted from samples of chicken organs, feathers and poultry house dust subjected to a heat treatment, bypassing the extraction of genomic DNA with commercial extraction kits, was shown to be suitable for virus-specific detection in HVT LAMP-LFD assays.

MATERIALS AND METHODS

DNA Samples From Virus Stocks and Field Samples

All DNA samples tested in this study were already available within the research group. DNA was prepared from chicken embryo fibroblast cells (CEF) infected with *Mardivirus* stocks of known provenance (HVT strain FC126, MDV-2 strain SB-1, very virulent MDV-1 strain RB-1B, and attenuated MDV-1 vaccine strain CVI988/Rispens). Vaxxitek® DNA and Innovax® DNA was prepared from commercial stocks of cell-associated rHVT vaccine VAXXITEK® HVT + IBD (Boehringer Ingelheim), and rHVT vaccine Innovax®-ND-IBD (MSD Animal Health), respectively.

DNA stocks from field samples of chicken feather tips, organs, tumors, and poultry house dust, submitted to the Marek's Disease Virus Reference Laboratory (MDVRL) of The Pirbright Institute between February and December 2020, were also available. The DNA had been extracted from approximately 20 mg tissue or 5 mg dust. These field samples were predominantly from HVT-vaccinated commercial chickens, some of which had been diagnosed with MD, and all samples had already been tested by serotype-specific MDVRL real-time PCR assays to determine C_T values for HVT, MDV-2 (25), CVI988/Rispens, and virulent MDV-1 (45). DNA extracted from blood samples of experimental chickens vaccinated with Vaxxitek® or Innovax® was available from a study previously conducted at The Pirbright Institute.

DNA From Virus BAC Clones

Bacterial-artificial-chromosome (BAC) clones, stable infectious clones of the whole virus genome, generated in the Viral Oncogenesis Group of The Pirbright Institute, were available for HVT FC126 (46) and VAXXITEK® HVT + IBD (unpublished). These BAC stocks were named pHVT-BAC3, and pVaxxitek-BAC, respectively. The number of viral genome copies in BAC DNA can easily be quantified by determining the mean DNA concentration by spectrophotometry and, subsequently, the number of molecules per µl. Therefore, 10-fold serial dilutions of these BAC DNA stocks (10^0-10^6 virus genome copies/3 µl), were used to determine the limit of detection (LoD) of each assay.

Design of LAMP Primers

Primers for the HVT-specific assay were those previously designed and published by Wozniakowski et al. (38) to target eight distinct regions of the HVT070 gene according to the sequence of HVT strain FC126. This gene is unique to HVT and is conserved between all published wild-type HVT sequences available in the GenBank database, and Vaxxitek® and Innovax® [as the HVT070 gene is intact in these recombinant viruses and is not disrupted by insertion of the exogenous gene(s)]. Basic Local Alignment Search Tool (BLAST) search confirmed the specificity of the six primers for the HVT genome.

Primers for the rHVT (VAXXITEK® HVT + IBD)-specific assay were designed using Primer Explorer V5 online software (Eiken Chemical Co. LTD, Tokyo, Japan) with manual adjustments to sequences to improve specificity or sensitivity of the method. The cloning vector sequence and insertion sites of the foreign genes differ between Vaxxitek® and Innovax®, so these vaccine types can be distinguished based on sequence. VAXXITEK® HVT + IBD expresses the VP2 gene of IBDV which is inserted at a specific site in the HVT genome. A new set of LAMP primers was designed to target a distinctive genomic region encompassing the HVT065 gene and intergenic region plus the cloning vector sequence of Vaxxitek®. The sequence required for the primer design was available from previous studies conducted by the Viral Oncogenesis Group of The Pirbright Institute. Each primer was evaluated for GC content, secondary structures, and 3′ or 5′ end stability. Primer specificity was verified *in silico* by BLAST analysis for both the HVT genome and the inserted cloning vector sequence.

LAMP primers, both unlabelled and 5′-labeled with Biotin (5′-Biosg) or 6-Carboxyfluorescein (5′-6-FAM), were manufactured by Integrated DNA Technologies, Inc. (Leuven, Belgium). The sequences for each specific set of primers are given in **Table 1**. Each primer set consisted of six primers: two outer primers (F3 and B3), two unlabeled or 5′-labeled inner primers (FIP and BIP), and two loop primers (LF and LB).

Real-Time LAMP Assays and Tube LAMP Assays With LFD Readout (LAMP-LFD Assay)

Primer sets were tested in LAMP assays with two different types of result readout, detailed in the following sections. Initially, primers were tested in real-time LAMP as a rapid way to check primer specificity and sensitivity using unlabeled, therefore inexpensive, LAMP primers. Subsequently, 5′-labeled primers were used in LAMP-LFD using in-tube amplification followed by result readout on housed lateral flow test strips.

The real-time LAMP reactions were set up in 96-well PCR plates. Each reaction (total volume of 25 µl) contained the six specific LAMP primers for the virus to be detected (1 µl of 5 µM outer primers, 1 µl of 50 µM inner primers and 1 µl of 25 µM loop primers), 15 µl of GspSSD2.0 Isothermal Mastermix (ISO-004) (OptiGene Limited, Horsham, West Sussex, UK), 4 µl of water and 3 µl of template DNA. An ABI 7500FAST® Real-Time PCR system (Applied Biosystems, Waltham, Massachusetts, USA) was used to amplify and detect the reaction products, under the following thermal cycling conditions: 30 cycles for 1 min at 65°C. The master mix contained a dsDNA-binding dye read by the machine through the SYBR green/FAM detection channel allowing the generation of amplification plots used to identify positive samples. Melt curve analysis was performed at 98°C

TABLE 1 | LAMP primer sets used in this study.

Target	Primer name	Primer sequence and label	References
HVT (HVT070 gene)	HVT-F3	5′-ATAAATTATATCGCTAGGACAGAC-3′	(38)
	HVT-B3	5′-ACGATGTGCTGTCGTCTA-3′	
	HVT-FIP	5′-6-FAM-CCAGGGTATGCATATTCCATAACAGTTTTCCAAACGACCTTTATCCCA-3′	
	HVT-BIP	5′-Biosg-CCAGAAATTGCACGCACGAGTTTTAGAATTTGTGCATTTAGCCTT-3′	
	HVT-LF	5′-TTGAGAAGAGGATCTGACTG-3′	
	HVT-LB	5′-GCGTCATTGGTTTTACATTT-3′	
Vaxxitek® (HVT065 gene and intergenic region + cloning vector)	Vaxxitek-F3	5′-CCGAACAAACTTCATCGCTA-3′	This study
	Vaxxitek-B3	5′-GCTATTGCTTTATTTGTAACCAT-3′	
	Vaxxitek-FIP	5′-6-FAM-CCCAAAGACCTCTATGAACATTTATTTTTGCAAAGAGATGCGTGTG-3′	
	Vaxxitek-BIP	5′-Biosg-TGTCGACTCTAGAGGATCCGAAAATTTTGTTAACAACAACAATTGCATTCA-3′	
	Vaxxitek-LF	5′-TACTCAACGGCGCGTGTA-3′	
	Vaxxitek-LB	5′-CACACCTCCCCCTGAACCTG-3′	

(15 s), 80°C (1 min), 98°C (1 min), 98°C (30 s) and 80°C (15 s), to confirm reaction specificity for positive samples. ABI 7500 v2.3 software was used to analyse the results.

Once the assays in real-time LAMP were validated, 5′-labeled FIP and BIP primers were ordered for each set of virus-specific LAMP primers. FIP primers were labeled with 6-FAM and BIP primers were labeled with Biosg (**Table 1**). The "three-stripe LFD strips" used (Abingdon Health, York, UK) have three lines: Test line 1 (T1), Test line 2 (T2), and Run Control line (C). T1 contains antibodies that specifically bind 6-FAM and Biosg to give a chromogenic product to detect 6-FAM/Biosg-labeled amplicons; T2 contains antibodies that specifically bind Digoxigenin (DigN)/Biosg to give a chromogenic product to detect DigN/Biosg-labeled amplicons; C confirms successful running of the reaction solution through the LFD strip. Only two of the three stripes, T1 (marked with a "T" on the plastic housing cassette) and C, were used in our LAMP-LFD assays. LAMP reactions were run in individual tubes. Each reaction (total volume of 25 μl) contained the six specific LAMP primers for the virus to be detected (1 μl of 5 μM outer primers, 1 μl of 50 μM 5′-labeled inner primers and 1 μl of 25 μM loop primers), 15 μl of GspSSD2.0 Isothermal Mastermix (ISO-004), 4 μl of water and 3 μl template DNA. Reactions were run by placing the tubes in a heating block at 65°C for 30 min. LFD strips were assembled into the plastic housing cassettes. Reaction tubes were only opened in a laminar flow cabinet in a designated laboratory, to avoid the risk of laboratory contamination with LAMP amplicons. The whole volume of the LAMP reaction (25 μl) was mixed with 100 μl running buffer and added to the sample application well of the plastic housing cassette. Results were read after 10 min of incubation at ambient temperature.

Sensitivity and Specificity of the LAMP Assays

The sensitivity of the LAMP assays, tested in triplicate using 10-fold serial dilutions of the BAC DNA stocks, was expressed as limit of detection (LoD) and defined as the lowest amount of analyte in a sample that could be detected by the assay (real-time LAMP or LAMP-LFD) in at least 50% of the replicates. LoD was expressed as absolute copy number of HVT or Vaxxitek® genomes.

To determine the specificity of the assay, DNA from MDV-1 (CVI988/Rispens and RB-1B), MDV-2 (SB-1), HVT (FC126) or rHVT (Vaxxitek® and Innovax®) strains was used as a template for the real-time LAMP and LAMP-LFD assays, and tested in triplicate.

Crude DNA Preparations

Crude DNA preparations were extracted from ∼20 mg samples of chicken organs, feather tips and poultry house dust. The samples were weighed and prepared as 4% (organs and dust) or 8% (feather tips) w/v suspensions in sterile PBS. The suspensions were then vortexed and subjected to a heat treatment in a heating block at 95°C for 10 min, centrifuged at 1,000 ×g for 3 min and the supernatant was tested in LAMP-LFD assay as a crude extract.

RESULTS

HVT-Specific LAMP Assay: Sensitivity and Specificity

Using target DNA from virus-infected CEF cells, the HVT LAMP primer set previously published by Wozniakowski et al. (38), targeting the HVT070 gene of HVT, was confirmed to be specific for the amplification of conventional HVT vaccine (strain FC126) and the recombinant HVT vaccines Vaxxitek® and Innovax® in real-time LAMP (**Figure 1**) and in LAMP-LFD (**Figure 2**). Negative results were obtained using DNA from MDV-2 strain SB-1, MDV-1 vaccine strain CVI988/Rispens, and very virulent MDV-1 strain RB-1B.

The LoD, determined using 10-fold serial dilutions of pHVT-BAC3 DNA, was 10^2 copies of the HVT genome in both the real-time LAMP assay and the LAMP-LFD assay (**Figure 3**). This is 10-fold less sensitive than the HVT-specific real-time PCR assay which targets the HVT sORF1 gene and is an ISO/IEC 17025-accredited assay used by the MDVRL (**Table 2**).

The LAMP-LFD results for DNA extracted by commercial kit from 15 field samples are shown in **Table 3**, and compared

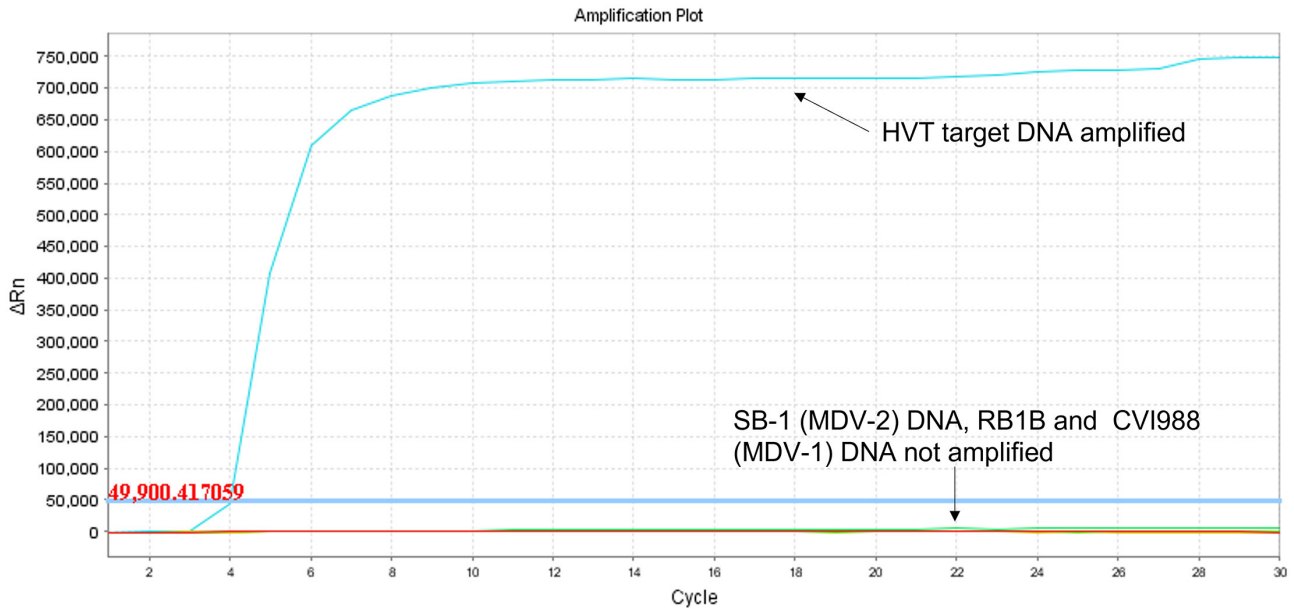

FIGURE 1 | Specificity of HVT LAMP assay in real-time LAMP (amplification plot of fluorescence change vs. cycle number). Specificity of the HVT LAMP primers was tested in real-time LAMP using unlabeled LAMP primers in a 30-cycle assay with SYBR Green readout. *Mardivirus* target DNA was prepared from CEF cells infected with HVT strain FC126, MDV-2 strain SB-1, virulent MDV-1 strain RB-1B, or the MDV-1 vaccine strain CVI988/Rispens. Only HVT DNA was amplified.

FIGURE 2 | HVT-specific LAMP-LFD assay detects conventional HVT FC126, and the rHVT vaccines Vaxxitek® and Innovax®. The HVT-specific LAMP assay was performed in a heating block and using FAM/Biosg-labeled primers. Target DNA was prepared from non-infected CEF cells (negative control), or CEF cells infected with HVT strain FC126, the Vaxxitek® recombinant HVT vaccine virus, or the Innovax® recombinant HVT vaccine virus. The reaction mixture was loaded onto a LFD for readout of results. A band at the test line (T) shows a positive result, and a band at the control line (C) shows a negative result. HVT FC126, Vaxxitek® and Innovax® all gave a positive result.

with C_T values obtained in the MDVRL HVT real-time PCR using the same DNA samples. The sample types included spleens, tumors, feather tips, and poultry house dust. Most samples were from commercial chickens vaccinated with conventional HVT or Innovax®. Thus, all were positive for HVT by real-time PCR, although the C_T values varied from 27 to 38. Samples with a C_T value < 34 were always positive in HVT-specific LAMP-LFD (**Figure 4**). When the C_T value was > 35, some samples tested positive by LAMP-LFD (sample MDVRL067-1) and some negative (samples MDVRL091-1 and MDVRL091-9, result not shown), consistent with the finding that real-time PCR was more sensitive than the LAMP-LFD assay. The latter samples were positive for high levels of MDV-1 and MDV-2 by real-time PCR, so the negative result in HVT LAMP-LFD shows there was no false detection of other *Mardiviruses* in these field samples.

Vaxxitek®-Specific LAMP Assay: Sensitivity and Specificity

Using target DNA from cell-associated vaccine virus stocks, the assay detected only Vaxxitek® (not conventional HVT vaccine or Innovax®) in real-time LAMP (**Figure 5**) and LAMP-LFD (**Figure 6**). The LoD, determined using 10-fold serial dilutions of pVaxxitek-BAC DNA, was 10^2 copies of the HVT genome in both the real-time LAMP assay and the LAMP-LFD assay (**Figure 7**). There is no Vaxxitek®-specific real-time PCR assay for comparison; however, the Vaxxitek®-specific LAMP assays

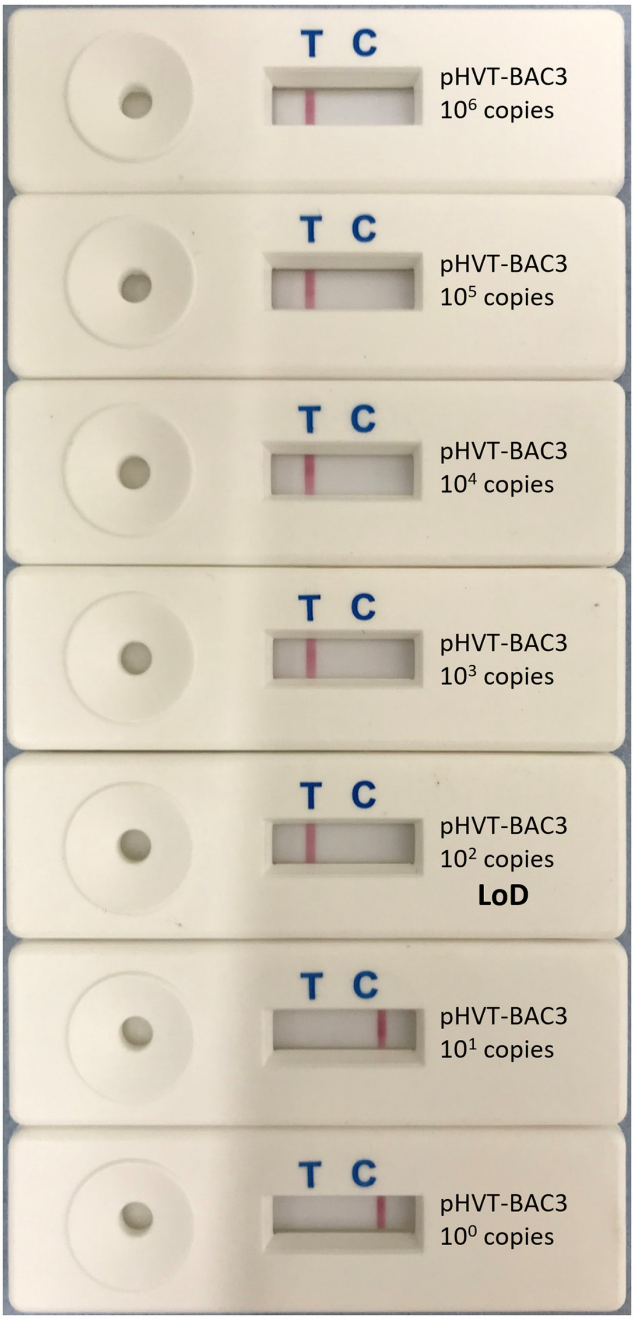

FIGURE 3 | Limit of detection of HVT LAMP-LFD assay. The limit of detection (LoD) was tested using 10-fold serial dilutions of the pHVT-BAC 3 plasmid containing a known number of copies of the HVT genome (10^0-10^6). This was repeated in triplicate (replicates not shown). A band at the test line (T) shows a positive result. A band at the control line (C) shows a negative result. The LoD was 10^2 copies of the HVT genome.

were 10-fold less sensitive than the MDVRL HVT-specific real-time PCR assay (**Table 2**).

No field samples were available from Vaxxitek®-vaccinated flocks. However, DNA samples extracted from blood samples of experimental birds vaccinated with either Vaxxitek® (n = 3 birds), or Innovax®, (n = 3), or from non-vaccinated control birds (n = 3) were tested. The C_T values in the MDVRL HVT-specific real-time PCR assay were similar for the three Vaxxitek®-vaccinated chickens and the three Innovax®-vaccinated chickens (C_T values all in range 28.7–32.1); however, only the Vaxxitek®-vaccinated samples tested positive by Vaxxitek®-specific LAMP-LFD (data not shown), showing that the Vaxxitek®-specific LAMP-LFD does not detect Innovax® in samples from vaccinated birds.

Furthermore, four field samples from chickens vaccinated with conventional HVT (MDVRL60-4, 82-3, 91-1, and 91-9 (**Table 3**) were negative by Vaxxitek®-specific LAMP-LFD (data not shown), showing that the Vaxxitek®-specific LAMP-LFD does not detect wild-type HVT in field samples.

TABLE 2 | Sensitivity of HVT LAMP assays and Vaxxitek®-specific LAMP assays, and comparison with real-time PCR.

Assay and target gene	LoD[a] (number of virus genomes)		
	Real-time LAMP	LAMP-LFD	MDVRL real-time PCR
HVT (HVT070 gene)	10^2	10^2	10^1 (HVT sORF1 gene)
HVT Vaxxitek® (HVT065 gene and intergenic region + cloning vector)	10^2	10^2	No Vaxxitek®-specific real-time PCR available

[a] *Limit of detection.*

Crude DNA Samples as a Substrate for LAMP-LFD Assay

Eight of the 15 field samples, representative of the different sample types (organs, feathers, and poultry house dust) were used to make crude DNA preparations which were then used as template in the HVT-specific LAMP-LFD assay. Six of these eight samples were positive in HVT-specific LAMP-LFD assay when crude DNA preparations were tested, whereas all eight samples were positive when purified DNA was tested (**Table 3**; **Figure 8**). The two crude DNA samples which were negative in LAMP-LFD assay were those containing lower levels of HVT (C_T > 34 in HVT real-time PCR). Thus, crude DNA preparations from chicken tissues or poultry house dust can be used as a substrate for HVT LAMP-LFD assay, but sensitivity is lower compared with purified DNA substrates extracted from the same original sample.

DISCUSSION

The present study reports the development of two LAMP-LFD assays for the rapid, sensitive, and species-specific detection of conventional and recombinant HVT-based vaccines, the most commonly used vaccines, worldwide, to prevent and control MD in commercial poultry flocks (47, 48), expanding the diagnostic

TABLE 3 | Field samples tested in HVT LAMP-LFD assay: comparison of LAMP-LFD and real-time PCR results.

MDVRL sample ref[a]	Sample type	Bird age and type	MD vaccination history and clinical signs[b]	Real-time PCR results[c]	C_T in HVT real-time PCR[d]	HVT LAMP-LFD result	
						Purified DNA	Crude sample
MDVRL060-4	Spleen	30 weeks Commercial layer	Vaccinated (no detail) High mortality, splenomegaly	HVT-pos[e] CVI988-neg vMDV-pos	27.0	Pos	Pos
MDVRL067-1	Poultry dust	33 weeks Commercial layer	Vaccinated with CVI988 + HVT High mortality	HVT-inc CVI988-pos vMDV-neg MDV2-pos	38.6	Pos	Neg
MDVRL067-4	Poultry dust	33 weeks Commercial layer	Vaccinated with CVI988 + HVT High mortality	HVT-pos CVI988-pos vMDV-neg MDV2-pos	33.8	Pos	NT[f]
MDVRL071-2	Poultry dust	20 weeks Breed not recorded	Vaccinated with CVI988 + HVT Outbreak of MD from 18 weeks	HVT-pos CVI988-pos vMDV-pos	30.2	Pos	Pos
MDVRL075-8	Ovary tumor	25 weeks Broiler-breeder	Vaccinated with CVI988 + HVT Visceral tumors from 20 weeks	HVT-pos CVI988-neg vMDV-pos	28.1	Pos	Pos
MDVRL076-3	Feathers	30 weeks Commercial layer	Vaccinated with CVI988 + HVT No clinical signs	HVT-pos CVI988-pos	29.1	Pos	Pos
MDVRL082-3	Feathers	10 weeks Broiler-breeder	Vaccinated with CVI988 + HVT	HVT-pos CVI988-pos vMDV-neg	31.3	Pos	NT
MDVRL083-2	Feathers	30 weeks Broiler-breeder	Vaccinated with Innovax®-ILT + CVI988	HVT-pos CVI988-pos vMDV-neg MDV2-pos	29.1	Pos	Pos
MDVRL088-1	Poultry dust	5 weeks Broiler-breeder	Vaccinated with Innovax®-ILT + CVI988 No clinical signs	HVT-pos CVI988-pos vMDV-neg MDV2-pos	29.9	Pos	NT
MDVRL088-5	Feathers	5 weeks Broiler-breeder	Vaccinated with Innovax®-ILT + CVI988 No clinical signs	HVT-pos CVI988-pos vMDV-neg MDV2-neg	32.2	Pos	Pos
MDVRL091-1	Spleen	29 weeks Broiler-breeder	Vaccinated with CVI988 + HVT Clinical signs of MD	HVT-pos CVI988-neg vMDV-pos MDV2-pos	35.5	Neg	NT
MDVRL091-9	Spleen	29 weeks Broiler-breeder	Vaccinated with CVI988 + HVT Clinical signs of MD	HVT-pos CVI988-neg vMDV-pos MDV2-pos	35.7	Neg	NT
MDVRL102-3	Spleen	60 weeks Commercial layer	Vaccinated with CVI988 + HVT High mortality	HVT-pos CVI988-pos vMDV-neg MDV2-pos	29.9	Pos	NT
MDVRL114	Liver	4 years Pet hen	MD vaccination status unknown Lymphoma	HVT-pos vMDV-neg	34.1	Pos	Neg

(Continued)

TABLE 3 | Continued

MDVRL sample ref[a]	Sample type	Bird age and type	MD vaccination history and clinical signs[b]	Real-time PCR results[c]	C_T in HVT real-time PCR[d]	HVT LAMP-LFD result	
						Purified DNA	Crude sample
MDVRL122-12	Feathers	4 weeks Broiler-breeder	Vaccinated with CVI988 + HVT High mortality at 3–5 days only	HVT-pos CVI988-pos vMDV-neg MDV2-neg	27.0	Pos	NT

[a] *Reference number assigned upon receipt of samples by Marek's Disease Virus Reference Laboratory.*
[b] *Information provided by sender of samples.*
[c] *Any or all of four virus-specific real-time PCR tests performed as requested by sender of sample.*
[d] *Real-time PCR targeting HVT sORF1 gene detects conventional HVT, and the recombinant HVTs Vaxxitek® and Innovax®.*
[e] *pos (positive): $C_T \leq 37$; neg (negative): $C_T = 40$; inc (inconclusive): $C_T > 37$ and < 40.*
[f] *Not tested.*

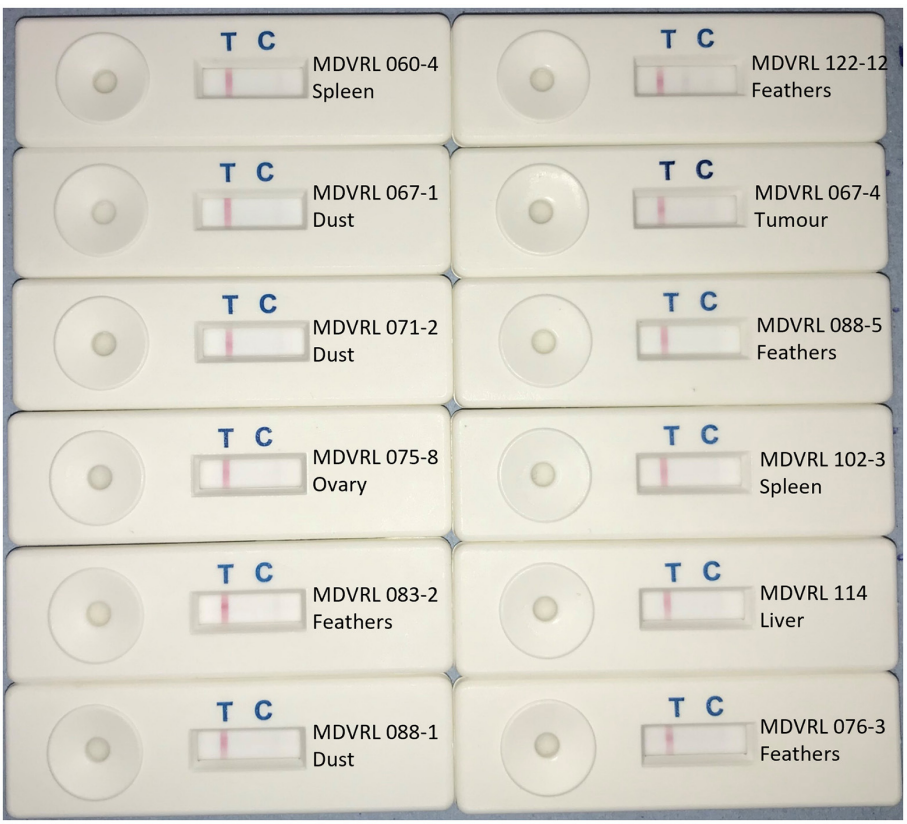

FIGURE 4 | HVT LAMP-LFD assay testing of field samples. DNA was extracted from field samples submitted to the MDV Reference Laboratory for monitoring MD vaccine virus replication and/or presence of virulent MDV field strains. Samples included organs, feather tips, and poultry house dust. A band at the test line (T) shows a positive result. A band at the control line (C) shows a negative result.

capabilities, especially in resource-limited settings. The LAMP-LFD technique has proved to be a valuable alternative to the more complex, expensive, and time-consuming PCR-based molecular methods allowing achievement of reliable results in <60 min.

Prior to developing the LAMP-LFD assay, the primer sets were tested in real-time LAMP with fluorescent detection of the LAMP amplicons through the SYBR green fluorescence acquisition channel of the ABI 7500FAST® system. The dsDNA-binding dye included in the master mix intercalates non-specifically into dsDNA, making this method of detection of LAMP products non-sequence specific. For this reason, post-amplification melting-curve analysis was performed to check real-time LAMP reactions for primer-dimer artifacts and to ensure reaction specificity. The perfected real-time LAMP assays

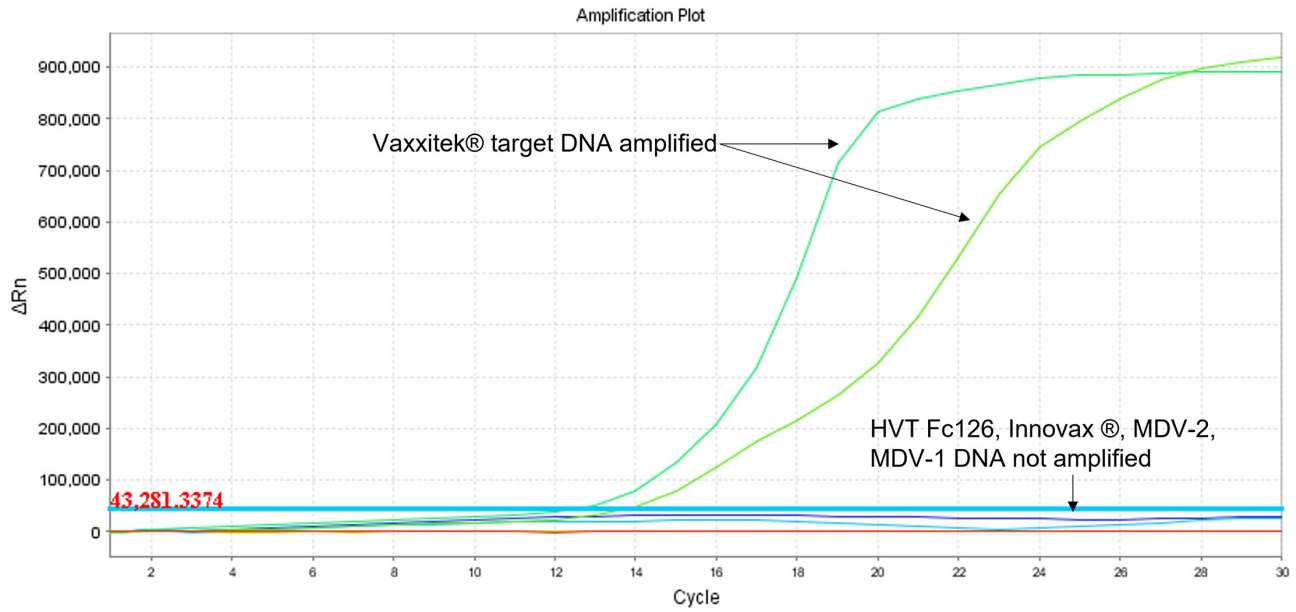

FIGURE 5 | Specificity of Vaxxitek®-specific LAMP assay in real-time LAMP (amplification plot of fluorescence change vs. cycle number). Specificity of the Vaxxitek® LAMP primers was tested in real-time LAMP using unlabeled LAMP primers in a 30-cycle assay with SYBR Green readout. *Mardivirus* target DNA was prepared from CEF cells infected with HVT strain FC126, MDV-2 strain SB-1, virulent MDV-1 strain RB-1B, MDV-1 vaccine strain CVI988/Rispens, Vaxxitek® or Innovax® recombinant HVT vaccine virus. A band at the test line (T) shows a positive result. A band at the control line (C) shows a negative result. Only Vaxxitek® DNA was amplified.

FIGURE 6 | Vaxxitek®-specific LAMP-LFD assay detects Vaxxitek® but not conventional HVT vaccine strain FC126 or rHVT vaccine Innovax®. The Vaxxitek®-specific LAMP assay was performed in a heating block and using FAM/Biosg-labeled primers and target DNA was prepared from non-infected CEF cells (negative control), or CEF cells infected with HVT strain FC126, the Vaxxitek® recombinant HVT vaccine virus, or the Innovax® recombinant HVT vaccine virus. The reaction mixture was loaded onto a LFD for readout of results. A band at the test line (T) shows a positive result. A band at the control line (C) shows a negative result. Only Vaxxitek® gave a positive result.

were then transposed in LAMP-LFD. Methods for sequence-specific detection, such as LAMP assays coupled with LFD readout, have gained increasing importance in the last few years, because, unlike sequence-independent detection methods used in the previously developed LAMP assays for HVT (37, 43), LAMP-LFD assays are highly specific toward the target DNA (44).

The HVT-specific LAMP-LFD assay was proven to be specific for HVT detection alone and did not cross-react with the other two member species of interest included in the *Mardivirus* genus: MDV-1 and MDV-2. The LAMP primer set used in this assay was previously published by Wozniakowski et al. (38) and further tested by Adedeji et al. (43) which demonstrated that LAMP was a successful alternative to end-point PCR for the detection of HVT in vaccinated and unvaccinated poultry, having much higher sensitivity compared with the end-point PCR assays. This study revealed that the newly developed HVT-specific LAMP-LFD assay was 10-fold less sensitive than the MDVRL real-time PCR assay, which detects the HVT sORF1 gene (25). Despite this, the assay reliably detected HVT in all the tested samples (tissues, feathers, and poultry house dust) from HVT-vaccinated chickens when the C_T value (from the ISO/IEC 17025-accredited MDVRL HVT-specific real-time PCR assay) was $\leq$ 34. Results were variable in samples with a $C_T > 34$.

The results of the Vaxxitek®-specific LAMP-LFD assay confirmed that the assay was specific for VAXXITEK® HVT - IBD detection and did not detect MDV-1, MDV-2, and,

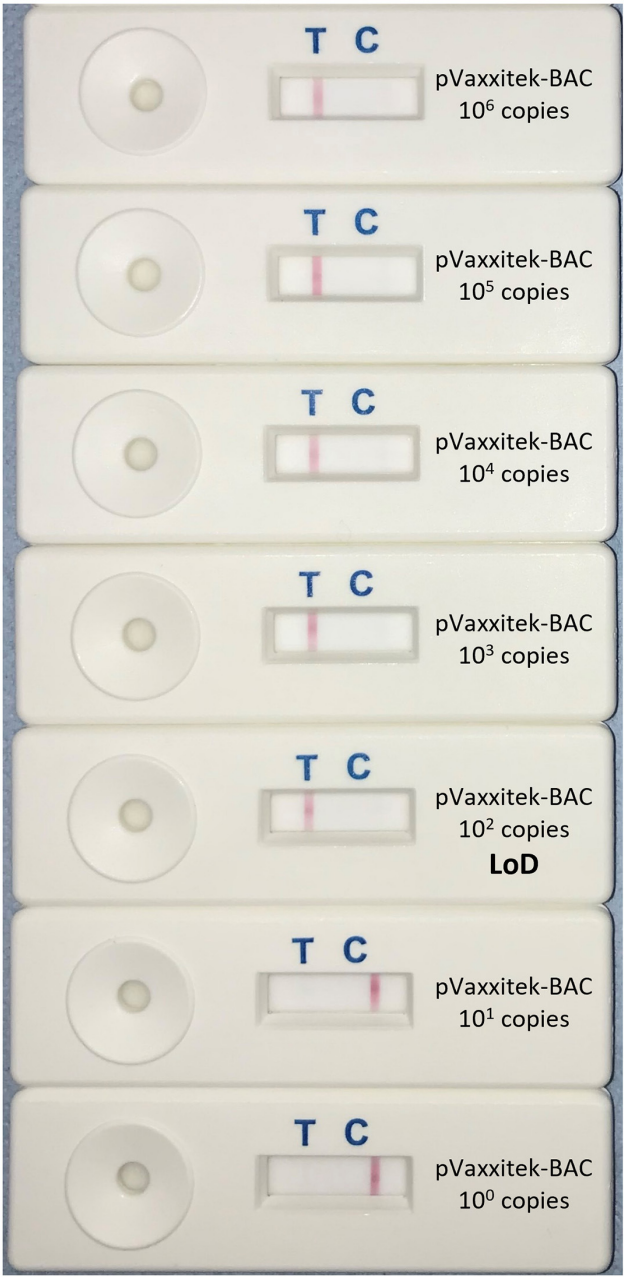

FIGURE 7 | Limit of detection of Vaxxitek®-specific LAMP-LFD assay. The limit of detection (LoD) was tested using 10-fold serial dilutions of the pVaxxitek-BAC plasmid containing a known number of copies of the Vaxxitek® genome (10^0–10^6). This was repeated in triplicate (replicates not shown). A band at the test line (T) shows a positive result. A band at the control line (C) shows a negative result. The LoD was 10^2 copies of the Vaxxitek® genome.

more importantly, conventional HVT vaccines or other rHVT vaccines (e.g., Innovax®). The expression cassettes with foreign genes encoding immunogenic viral proteins inserted in the HVT genome and their sequences differ between recombinant vaccines produced by different pharmaceutical companies and are not present in conventional HVT vaccine strains ensuring the differentiation of the different vaccine strains based on their sequence (49, 50). The three-in-one vaccines recently added to the Vaxxitek® range (VAXXITEK® HVT + IBD + ND, and VAXXITEK® HVT + IBD + ILT) use the same bioengineering platform as VAXXITEK® HVT + IBD, so we predict that our Vaxxitek®-specific LAMP-LFD assay will detect all Vaxxitek® vaccines. The LAMP-LFD assay for the detection of Vaxxitek® reliably detected as few as 100 copies of pVaxxitek-BAC DNA per reaction, and gave a positive result only when samples were from birds vaccinated with Vaxxitek®. Unfortunately, no Vaxxitek®-specific real-time PCR assay was available for comparison of analytical sensitivity.

In negative samples, the control line C was very clear on the LFD strips. However, in positive samples with a clear T line, the C line was not visible: the result was either a T line or a C line but not both (an either/or result). This is likely to be because the colored dye/bead mix is the limiting factor in the reaction; when a sample is highly positive, all the beads are captured at the T line and there are no excess beads to migrate to the C line. If a test sample was only weakly positive, so giving a faint T line, there may be sufficient beads to show the C line. Other users of similar LFDs have shown that the intensity of the C line is weak in samples with an intense T line (51).

LAMP-LFD was found to be an effective, sensitive and 100% specific technique for HVT detection even in field samples harboring mixed *Mardivirus* infections, that are very common in the field. In fact, multiple MD vaccines of different serotypes are frequently administered in combination to achieve optimal protection against MD and, furthermore, these imperfect vaccines are unable to prevent superinfections with field MDV strains (19, 20, 22–25). Therefore, the absolute specificity of these HVT LAMP-LFD assays is crucial for their effective application in the field.

It has previously been shown that LAMP amplification tolerates higher levels of inhibitors present in biological samples than PCR (52–54). For poultry samples, these inhibitors include melanin pigment in feathers from colored birds, and particles of dried litter, feces, and feed in poultry house dust. The HVT-specific LAMP-LFD assay developed in this study efficiently amplified and detected DNA from crude organ, feather, and dust samples processed by direct heating, showing robustness to sample-derived inhibitors, but (compared with use of purified DNA) it was slightly less sensitive for detection in samples having low levels of HVT. This treatment of field samples allows further reduction of the overall procedure time by eliminating the need for nucleic acid extraction with commercial kits and demonstrating LAMP-LFD suitability for field use.

In summary, we developed and validated novel HVT-specific LAMP-LFD assays and demonstrated the utility of these assays in a controlled laboratory setting to detect HVT vaccines in field samples. These assays are simple, cost-effective, specific, and sensitive alternatives to PCR-based methods for the rapid and reliable detection of HVT from chicken tissues and feathers and from poultry dust. To our knowledge, this is the first time that LAMP technology coupled with LFD readout has been used for the rapid detection of HVT and Vaxxitek®.

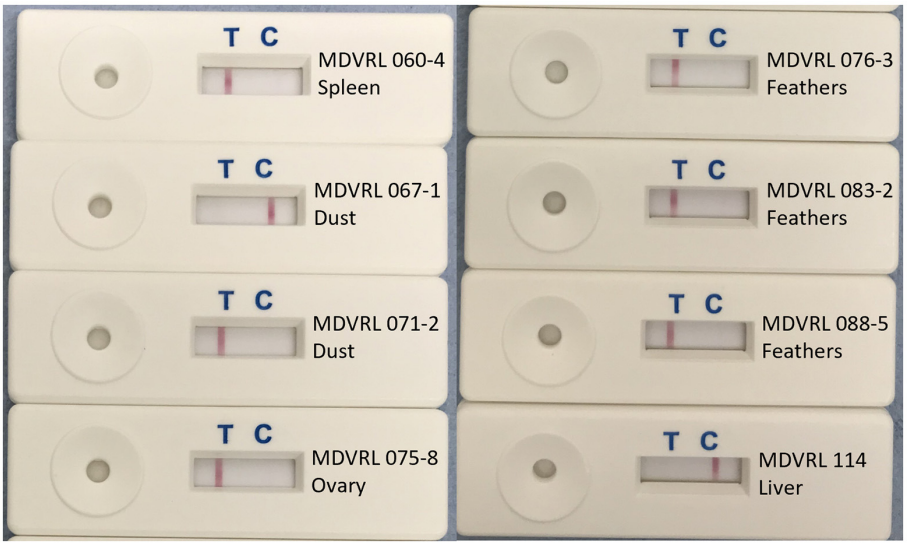

FIGURE 8 | Use of crude DNA to detect HVT in field samples by HVT LAMP-LFD assay. Crude DNA prepared from 20 mg sample material (organs, tumors, feather tips, or poultry house dust) by direct heating was successfully used for detection of HVT by the HVT LAMP-LFD assay. A band at the test line (T) shows a positive result. A band at the control line (C) shows a negative result.

Larger scale testing in the field was not within the scope of this work, but would be required to further validate use of these assays to monitor Marek's disease vaccination directly in the field or in small laboratories with few resources.

Further research will be aimed to develop new LAMP-LFD assays to detect the remaining HVT recombinant vaccines and ultimately to determine the performance of the HVT LAMP-LFD assays in analyzing field samples obtained from poultry flocks vaccinated with different vaccines and vaccination protocols.

DATA AVAILABILITY STATEMENT

The original contributions presented in the study are included in the article/supplementary material, further inquiries can be directed to the corresponding authors.

ETHICS STATEMENT

Ethical review and approval was not required because no samples were collected specifically for use in this study. The majority of samples tested in this study were from commercial or backyard chickens and were submitted to the Marek's Disease Virus Reference Laboratory at The Pirbright Institute by poultry veterinary surgeons for diagnostic testing. Written informed consent for participation was not obtained from the owners because no samples were collected specifically for use in this study. A condition of sample submission is that the submitter accepts that samples may be retained and used (anonymously) for research purposes. Six samples were from a vaccination experiment previously conducted at The Pirbright Institute.

AUTHOR CONTRIBUTIONS

The research project was conceived by VN and SB. The experimental work was conducted by GM (a student from the laboratory of EC) during a 6-month research visit to the Viral Oncogenesis Group at The Pirbright Institute. The manuscript was written by GM and SB, with input from VN and EC. All authors agree to be accountable for the content of the work.

FUNDING

This research was funded by a ISCG Agri-food Technology Seeding Catalyst Award (grant reference BB/SCA/Pirbright/17). Research in this paper was also supported by the BBSRC grants BBS/E/I/00007034 and BBS/E/I/00007039.

ACKNOWLEDGMENTS

We thank Dr. Claudio Busato and Dr. Mar Fernandez de Marco (Business Development Unit, Animal and Plant Health Agency, UK), Dr. Elen Withycombe (Abingdon Health, UK), and Dr. Donald King and Dr. Emma Howson (Vesicular Disease Reference Laboratories, The Pirbright Institute) for their guidance, advice and troubleshooting on LAMP-LFD assays. We also thank Dr. Yaoyao Zhang and Mr. Weicheng Li (Viral Oncogenesis Group, The Pirbright Institute) for provision of DNA samples, and laboratory assistance.

REFERENCES

1. Gatherer D, Depledge DP, Hartley CA, Szpara ML, Vaz PK, Benko M, et al. ICTV virus taxonomy profile: herpesviridae 2021. *J Gen Virol.* (2021) 102:1–2. doi: 10.1099/jgv.0.001673
2. Kawamura H, King DJ Jr, Anderson DP. A herpesvirus isolated from kidney cell culture of normal turkeys. *Avian Dis.* (1969) 13:853–86. doi: 10.2307/1588592
3. Schat KA. History of the first-generation Marek's disease vaccines: the science and little-known facts. *Avian Dis.* (2016) 60:715–24. doi: 10.1637/11429-050216-Hist
4. Witter RL, Nazerian K, Purchase HG, Burgoyne GH. Isolation from turkeys of a cell-associated herpesvirus antigenically related to Marek's disease virus. *Am J Vet Res.* (1970) 31:525–38.
5. Okazaki W, Purchase HG, Burmester BR. Protection against Marek's disease by vaccination with a herpesvirus of turkeys. *Avian Dis.* (1970) 14:413. doi: 10.2307/1588488
6. Gimeno IM, Cortes AL, Witter RL, Pandiri AR. Optimization of the protocols for double vaccination against Marek's disease by using commercially available vaccines: Evaluation of protection, vaccine replication, and activation of T cells. *Avian Dis.* (2012) 56:295–305. doi: 10.1637/9930-091311-Reg.1
7. Witter RL. A new strategy for Marek's disease immunisation - bivalent vaccine. *Avian Pathol.* (1984) 13:133–5. doi: 10.1080/03079458408418517
8. Purchase HG, Okazaki W, Burmester BR. Field trials with the herpes virus of turkeys (HVT) strain FC126 as a vaccine against Marek's disease. *Poult Sci.* (1971) 50:775–83. doi: 10.3382/ps.0500775
9. Morgan RW, Gelb JJ, Schreurs CS, Lutticken D, Rosenberger JK, Sondermeijer PJA. Protection of chickens from Newcastle and Marek' diseases with a recombinant herpesvirus of turkeys vaccine expressing the Newcastle disease virus fusion protein. *Avian Dis.* (1992) 36:858–70. doi: 10.2307/1591544
10. Heckert RA, Riva J, Cook S, McMillen J, Schwartz RD. Onset of protective immunity in chicks after vaccination with a recombinant herpesvirus of turkeys vaccine expressing Newcastle disease virus fusion and hemagglutinin-neuraminidase antigens. *Avian Dis.* (1996) 40:770–7. doi: 10.2307/1592296
11. Darteil R, Bublot M, Laplace E, Bouquet JF, Audonnet JC, Riviè M. Herpesvirus of turkey recombinant viruses expressing infectious bursal disease virus (IBDV) VP2 immunogen induce protection against an IBDV virulent challenge in chickens. *Virology*. (1995) 211:481–90. doi: 10.1006/viro.1995.1430
12. Johnson DI, Vagnozzi A, Dorea F, Riblet SM, Mundt A, Zavala G, et al. Protection against infectious laryngotracheitis by in ovo vaccination with commercially available viral vector recombinant vaccines. *Avian Dis.* (2010) 54:1251–9. doi: 10.1637/9401-052310-Reg.1
13. Witter RL. Increased virulence of Marek's disease virus field isolates. *Avian Dis.* (1997) 41:149–63. doi: 10.2307/1592455
14. Gimeno IM. Marek's disease vaccines: a solution for today but a worry for tomorrow? *Vaccine.* (2008) 26:C31–41. doi: 10.1016/j.vaccine.2008.04.009
15. Mescolini G, Lupini C, Felice V, Guerrini A, Silveira F, Cecchinato M, et al. Molecular characterization of the meq gene of Marek's disease viruses detected in unvaccinated backyard chickens reveals the circulation of low- and high-virulence strains. *Poult Sci.* (2019) 98:3130–7. doi: 10.3382/ps/pez095
16. Rémy S, Le Pape G, Gourichon D, Gardin Y, Denesvre C. Chickens can durably clear herpesvirus vaccine infection in feathers while still carrying vaccine-induced antibodies. *Vet Res.* (2020) 51:24. doi: 10.1186/s13567-020-00749-1
17. Cortes AL, Montiel ER, Lemiere S, Gimeno IM. Comparison of blood and feather pulp samples for the diagnosis of Marek's disease and for monitoring Marek's disease vaccination by real time-PCR. *Avian Dis.* (2011) 55:302–10. doi: 10.1637/9578-101510-ResNote.1
18. Islam A, Cheetham BF, Mahony TJ, Young PL, Walkden-Brown SW. Absolute quantitation of Marek's disease virus and herpesvirus of turkeys in chicken lymphocyte, feather tip and dust samples using real-time PCR. *J Virol Methods.* (2006) 132:127–34. doi: 10.1016/j.jviromet.2005.10.009
19. Fakhrul Islam AFM, Walkden-Brown SW, Groves PJ, Underwood GJ. Kinetics of Marek's disease virus (MDV) infection in broiler chickens 1: effect of varying vaccination to challenge interval on vaccinal protection and load of MDV and herpesvirus of turkey in the spleen and feather dander over time. *Avian Pathol.* (2008) 37:225–35. doi: 10.1080/03079450701802230
20. Islam A, Walkden-Brown SW. Quantitative profiling of the shedding rate of the three Marek's disease virus (MDV) serotypes reveals that challenge with virulent MDV markedly increases shedding of vaccinal viruses. *J Gen Virol.* (2007) 88:2121–8. doi: 10.1099/vir.0.82969-0
21. Walkden-Brown SW, Islam A, Groves PJ, Rubite A, Sharpe SM, Burgess SK. Development, application, and results of routine monitoring of Marek's disease virus in broiler house dust using real-time quantitative PCR. *Avian Dis.* (2013) 57:544–54. doi: 10.1637/10380-92112-REG.1
22. Islam T, Walkden-Brown SW, Renz KG, Fakhrul Islam AFM, Ralapanawe S. Replication kinetics and shedding of very virulent Marek's disease virus and vaccinal Rispens/CVI988 virus during single and mixed infections varying in order and interval between infections. *Vet Microbiol.* (2014) 173:208–23. doi: 10.1016/j.vetmic.2014.07.027
23. Read AF, Baigent SJ, Powers C, Kgosana LB, Blackwell L, Smith LP, et al. Imperfect vaccination can enhance the transmission of highly virulent pathogens. *PLoS Biol.* (2015) 13:e1002198. doi: 10.1371/journal.pbio.1002198
24. Ralapanawe S, Renz KG, Burgess SK, Walkden-Brown SW. Field studies of the detection, persistence and spread of the Rispens CVI988 vaccine virus and the extent of co-infection with Marek's disease virus. *Aust Vet J.* (2016) 94:329–37. doi: 10.1111/avj.12479
25. López-Osorio S, Villar D, Piedrahita D, Ramírez-Nieto G, Nair V, Baigent S, et al. Molecular detection of Marek's disease virus in feather and blood samples from young laying hens in Colombia. *Acta Virol.* (2019) 63:380–91. doi: 10.4149/av_2019_402
26. Afonso CL, Tulman ER, Lu Z, Zsak L, Rock DL, Kutish GF. The genome of turkey herpesvirus. *J Virol.* (2001) 75:971–8. doi: 10.1128/JVI.75.2.971-978.2001
27. Spatz SJ, Petherbridge L, Zhao Y, Nair V. Comparative full-length sequence analysis of oncogenic and vaccine (Rispens) strains of Marek's disease virus. *J Gen Virol.* (2007) 88:1080–96. doi: 10.1099/vir.0.82600-0
28. Spatz SJ, Zhao Y, Petherbridge L, Smith LP, Baigent SJ, Nair V. Comparative sequence analysis of a highly oncogenic but horizontal spread-defective clone of Marek's disease virus. *Virus Genes.* (2007) 35:753–66. doi: 10.1007/s11262-007-0157-1
29. Spatz SJ, Schat KA. Comparative genomic sequence analysis of the Marek's disease vaccine strain SB-1. *Virus Genes.* (2011) 42:331–8. doi: 10.1007/s11262-011-0573-0
30. Trimpert J, Groenke N, Jenckel M, He S, Kunec D, Szpara ML, et al. A phylogenomic analysis of Marek's disease virus reveals independent paths to virulence in Eurasia and North America. *Evol Appl.* (2017) 10:1091–101. doi: 10.1111/eva.12515
31. Kim T, Volkening JD, Spatz SJ. Comparative molecular characterization of three gallid alphaherpesvirus type 3 strains 301B/1, HPRS24, and SB-1. *Avian Dis.* (2020) 64:174–82. doi: 10.1637/0005-2086-64.2.174
32. Handberg KJ, Nielsen OL, Jørgensen PH. The use of serotype 1- and serotype 3-specific polymerase chain reaction for the detection of Marek's disease virus in chickens. *Avian Pathol.* (2001) 30:243–9. doi: 10.1080/03079450120054659
33. Walkden-Brown SW, Groves PJ, Islam AF, Burgess SK, Arzey KE, Mascord L, et al. Differentiation of Marek's diesease virus serotypes using PCR: Research and field experience. *Proc Aust Poult Sci Symp.* (2003) 15:192–6. Available online at: https://hdl.handle.net/1959.11/4327
34. Renz KG, Islam A, Cheetham BF, Walkden-Brown SW. Absolute quantification using real-time polymerase chain reaction of Marek's disease virus serotype 2 in field dust samples, feather tips and spleens. *J Virol Methods.* (2006) 135:186–91. doi: 10.1016/j.jviromet.2006.03.017
35. Notomi T, Okayama H, Masubuchi H, Yonekawa T, Watanabe K, Amino N, et al. Loop-mediated isothermal amplification of DNA. *Nucleic Acids Res.* (2000) 28:E63. doi: 10.1093/nar/28.12.e63
36. Nagamine K, Hase T, Notomi T. Accelerated reaction by loop-mediated isothermal amplification using loop primers. *Mol Cell Probes.* (2002) 16:223–9. doi: 10.1006/mcpr.2002.0415
37. Wozniakowski G, Samorek-Salamonowicz E, Kozdruń W. Rapid detection of Marek's disease virus in feather follicles by loop-mediated amplification. *Avian Dis.* (2011) 55:462–7. doi: 10.1637/9668-012711-ResNote.1
38. Wozniakowski G, Samorek-Salamonowicz E, Kozdruń W. Comparison of loop-mediated isothermal amplification and PCR for the detection and differentiation of Marek's disease virus serotypes 1, 2, and 3. *Avian Dis.* (2013) 57:539–43. doi: 10.1637/10328-082012-ResNote.1

39. Angamuthu R, Baskaran S, Gopal DR, Devarajan J, Kathaperumal K. Rapid detection of the Marek's disease viral genome in chicken feathers by loop-mediated isothermal amplification. *J Clin Microbiol.* (2012) 50:961–5. doi: 10.1128/JCM.05408-11
40. Wei X, Shi X, Zhao Y, Zhang J, Wang M, Liu C, et al. Development of a rapid and specific loop-mediated isothermal amplification detection method that targets Marek's disease virus meq gene. *J Virol Methods.* (2012) 183:196–200. doi: 10.1016/j.jviromet.2012.04.014
41. Wozniakowski G, Samorek-Salamonowicz E. Direct detection of Marek's disease virus in poultry dust by loop-mediated isothermal amplification. *Arch Virol.* (2014) 159:3083–7. doi: 10.1007/s00705-014-2157-5
42. Wozniakowski G, Niczyporuk JS. Detection of specific UL49 sequences of Marek's disease virus CVI988/Rispens strain using loop-mediated isothermal amplification. *J Virol Methods.* (2015) 221:22–8. doi: 10.1016/j.jviromet.2015.04.015
43. Adedeji AJ, Abdu PA, Luka PD, Owoade AA, Joannis TM. Application of loop-mediated isothermal amplification assay in the detection of herpesvirus of turkey (FC 126 strain) from chicken samples in Nigeria. *Vet World.* (2017) 10:1383–8. doi: 10.14202/vetworld.2017.1383-1388
44. Becherer L, Borst N, Bakheit M, Frischmann S, Zengerle R, Von Stetten F. Loop-mediated isothermal amplification (LAMP)-review and classification of methods for sequence-specific detection. *Anal Methods.* (2020) 12:717–46. doi: 10.1039/C9AY02246E
45. Baigent SJ, Nair VK, Le Galludec H. Real-time PCR for differential quantification of CVI988 vaccine virus and virulent strains of Marek's disease virus. *J Virol Methods.* (2016) 233:23–36. doi: 10.1016/j.jviromet.2016.03.002
46. Baigent SJ, Petherbridge LJ, Smith LP, Zhao Y, Chesters PM, Nair VK. Herpesvirus of turkey reconstituted from bacterial artificial chromosome clones induces protection against Marek's disease. *J Gen Virol.* (2006) 87 (Pt 4):769–76. doi: 10.1099/vir.0.81498-0
47. Gimeno IM, Cortes AL, Faiz N, Villalobos T, Badillo H, Barbosa T. Efficacy of various HVT vaccines (conventional and recombinant) against Marek's disease in broiler chickens: effect of dose and age of vaccination. *Avian Dis.* (2016) 60:662–8. doi: 10.1637/11415-040116-Reg.1
48. Dunn JR, Dimitrov KM, Miller PJ, Garcia M, Turner-Alston K, Brown A, et al. Evaluation of protective efficacy when combining turkey herpesvirus-vector vaccines. *Avian Dis.* (2019) 63:75–83. doi: 10.1637/11979-092818-Reg.1
49. Ingrao F, Rauw F, van den Berg T, Lambrecht B. Characterization of two recombinant HVT-IBD vaccines by VP2 insert detection and cell-mediated immunity after vaccination of specific pathogen-free chickens. *Avian Pathol.* (2017) 46:289–99. doi: 10.1080/03079457.2016.1265083
50. Hein R, Koopman R, García M, Armour N, Dunn JR, Barbosa T, et al. Review of poultry recombinant vector vaccines. *Avian Dis.* (2021) 65:438–52. doi: 10.1637/0005-2086-65.3.438
51. James HE, Ebert K, McGonigle R, Reid SM, Boonham N, Tomlinson JA, et al. Detection of African swine fever virus by loop-mediated isothermal amplification. *J Virol Methods.* (2010) 164:68–74. doi: 10.1016/j.jviromet.2009.11.034
52. Curtis KA, Rudolph DL, Owen SM. Rapid detection of HIV-1 by reverse-transcription, loop-mediated isothermal amplification (RT-LAMP). *J Virol Methods.* (2008) 151:264–70. doi: 10.1016/j.jviromet.2008.04.011
53. Francois P, Tangomo M, Hibbs J, Bonetti EJ, Boehme CC, Notomi T, et al. Robustness of a loop-mediated isothermal amplification reaction for diagnostic applications. *FEMS Immunol Med Microbiol.* (2011) 62:41–8. doi: 10.1111/j.1574-695X.2011.00785.x
54. Kiddle G, Hardinge P, Buttigieg N, Gandelman O, Pereira C, McElgunn CJ, et al. GMO detection using a bioluminescent real time reporter (BART) of loop mediated isothermal amplification (LAMP) suitable for field use. *BMC Biotechnol.* (2012) 12:15. doi: 10.1186/1472-6750-12-15

Conflict of Interest: The authors declare that the research was conducted in the absence of any commercial or financial relationships that could be construed as a potential conflict of interest.

Publisher's Note: All claims expressed in this article are solely those of the authors and do not necessarily represent those of their affiliated organizations, or those of the publisher, the editors and the reviewers. Any product that may be evaluated in this article, or claim that may be made by its manufacturer, is not guaranteed or endorsed by the publisher.

frontiers | Frontiers in Veterinary Science

ORIGINAL RESEARCH
published: 06 July 2022
doi: 10.3389/fvets.2022.930887

Genomic Characterization of CIAV Detected in Contaminated Attenuated NDV Vaccine: Epidemiological Evidence of Source and Vertical Transmission From SPF Chicken Embryos in China

*Yan Li, Jinjin Wang, Longfei Chen, Qun Wang, Meng Zhou, Hui Zhao, Zengna Chi, Yixin Wang, Shuang Chang and Peng Zhao**

College of Veterinary Medicine, Shandong Agricultural University, Tai'an, China

OPEN ACCESS

Edited by:
Aijian Qin,
Yangzhou University, China

Reviewed by:
Aman Ullah Khan,
University of Veterinary and Animal Sciences, Pakistan
Hongyu Cui,
Harbin Veterinary Research Institute (CAAS), China

***Correspondence:**
Peng Zhao
zhaopeng@sdau.edu.cn

Specialty section:
This article was submitted to Veterinary Infectious Diseases, a section of the journal Frontiers in Veterinary Science

Received: *28 April 2022*
Accepted: *17 June 2022*
Published: *06 July 2022*

Citation:
Li Y, Wang J, Chen L, Wang Q, Zhou M, Zhao H, Chi Z, Wang Y, Chang S and Zhao P (2022) Genomic Characterization of CIAV Detected in Contaminated Attenuated NDV Vaccine: Epidemiological Evidence of Source and Vertical Transmission From SPF Chicken Embryos in China. Front. Vet. Sci. 9:930887. doi: 10.3389/fvets.2022.930887

Live attenuated vaccines have been extensively used to prevent infectious disease in poultry flocks. Freedom from exogenous virus is a high priority for any veterinary vaccines. Recently, attenuated Newcastle disease virus (NDV) vaccines were detected to be contaminated with chicken infectious anemia virus (CIAV) in a routine screening for exogenous viruses. To investigate the possible source of the contamination, we conducted virological tests on a specific-pathogen-free (SPF) layer breeder flock that provide the raw materials for vaccines in this manufacturer. Firstly, CIAV antibodies in serum and egg yolks samples of the SPF laying hens were detected by ELISA assays. The results showed that CIAV antibodies in serum and egg yolks were 62% positive and 57% positive, respectively. Then, DNA was extracted from the NDV vaccines and SPF chicken embryonated eggs, and detected by molecular virology assays. The results showed that three assays for pathogens in embryonated eggs had similar positive rates (35.8%). And the sequences of CIAV from SPF embryos and NDV vaccines consisted of 2,298 nucleotides (nt) with 100% homology. The new full-length genome of CIAV was designated SDSPF2020 (Genbank accession number: MW660821). Data showed SDSPF2020 had the sequence similarities of 95.8–99.6% with reference strains, and shared the highest homology with the Chinese strain HLJ15125. These results strongly suggested that exogenous CIAV contamination is most likely caused by wild virus infection in SPF flocks and vertical transmission to chicken embryos. Collectively, this study illustrated that vertical transmission of CIAV from a SPF layer breeder flock to embryos was a non-neglible way for exogenous virus contamination in vaccine production.

Keywords: chicken infectious anemia virus, vertical transmission, SPF chicken, vaccine, genome analysis, molecular characterization

INTRODUCTION

Chicken infectious anemia virus (CIAV) can cause infectious anemia disease characterized by growth retardation and immunosuppression in chickens, which brings costly losses in the poultry industry (1, 2). In the 1970 s, CIAV was first isolated from contaminated vaccines in Japan (3), and its epidemiological and pathogenic features have been revealed as research continues (4–6). Previous studies have shown that CIAV can spread through multiple routes and induce immune dysfunction accompanied by severe damage of the hemocytoblast and T cell lineages (7–9). CIAV is highly prevalent in chicken flocks and infects chickens of all ages through horizontal transmission (10–12), but young chicks are more susceptible to CIAV infection and lesions due to the underdeveloped immune system (8, 13, 14). Infection of 2-week-old chickens resulted in classic symptoms of immunosuppressive disease such as aplastic anemia, heterophil decrease, lymphoid depletion and atrophy of bone marrow hematopoietic tissue (8). Cardona et al. reported that viral DNA hidden in the gonadal tissues of SPF breeding flocks could be transferred to newborn eggs without early viral replication (15). In addition, CIAV carried by feather shafts or within the pulp of feathers can be transmitted horizontally to chickens via the mucosal entries causing diseases (16). Even under good biosafety condition, maintaining CIAV seronegative poultry population is highly challenging due to extreme resistance of CIAV to physical and chemical treatments (17, 18). Hence, stricter monitoring and control systems should be established to prevent the infection and transmission of CIAV and reduce economic losses for poultry farming.

The epidemiological characteristics and pathogenicity of CIAV depends on its molecular structure (19, 20). CIAV is a non-enveloped virus with a single-stranded circular DNA genome containing three partially overlapping ORFs, including VP1-, VP2- and VP3-coding regions (5, 21, 22). VP1 (51.6 kDa) is a viral capsid protein related to the formation of neutralizing antibody, and its conformation is affected by VP2 (24.0 kDa), a non-structural scaffold protein (23, 24). VP3 (13.6 kDa), also known as apoptin, induces apoptosis of thymic precursors and hemocytoblasts (4). Notably, amino acids (AAs) of VP1 involved in the pathogenesis of CIAV are prone to variability, while VP2 and VP3 are relatively conserved. However, VP1 nucleotide or amino acid sequences show fine variation (<6%) between different strains separated by time and geographical location (25, 26). Besides, the non-coding region of CIAV genome contains a series of conserved motifs that exhibit promoter activity and play a crucial role in viral replication and transcription (1, 27–29). Thus, phylogenetic analysis of CIAV complete genome and VP1 sequences is a significant step to understand the evolutionary branches and reveal the differences of amino acids and transcription elements between different strains.

Recently, epidemiological investigation reported that CIAV has sporadically emerged in vaccinated and/or unvaccinated commercial chicken flocks in China (30–33), and the use of CIAV-contaminated attenuated vaccines was suspected to be an important route of transmission. Exogenous CIAV as contaminant in commercial attenuated vaccines has been documented in previous investigations (34, 35). However, no evidence was available to confirm the source of exogenous CIAV contamination in vaccines. To address this issue, we investigated the source of re-emerged CIAV contamination in NDV vaccines and conducted systemic experiments to find a complete chain of evidence for the transmission of CIAV from a SPF layer breeder flock to embryos, and eventually, to the live-attenuated NDV vaccines.

MATERIALS AND METHODS

Background of CIAV Contamination in Vaccines

According to the requirements of Ministry of Agriculture and Rural Affairs of the People's Republic of China, all live poultry vaccines must be regularly tested for exogenous virus dissemination before marketing. To identify if the potential threat caused by live vaccines contaminated with any exogenous virus, we investigated commercial live poultry vaccines produced by a vaccine manufacturer with SPF chicken breeder flocks. Three batch of live vaccines against NDV were provided by the vaccine manufacturer, and three bottles were randomly sampled from each batch. SPF chicks were orally vaccinated with the NDV vaccines at 7 days of age, and antibody responses were detected at 6 wk post-inoculation using commercial enzyme-linked immunosorbent assay (ELISA) kits (Avian Leukosis Virus Antibody Test Kit-subgroup A/B, Avian Leukosis Virus Antibody Test Kit-subgroup J, Reticuloendotheliosis virus Antibody Test Kit, Chicken infectious anemia virus Antibody Test Kit, IDEXX, USA). SPF chicks were positive for CIAV antibody after inoculation with NDV vaccines. Subsequently, DNAs were extracted from NDV vaccines to amplify the CIAV genome using commercial TIANamp Genomic DNA Kits (Tiangen Biotechnology Co., Ltd., China). Each experiment was repeated at least three times. According to the published whole genome sequences of CIAVs in GenBank (**Table 1**), a pair of primers (**Table 2**) were designed and synthesized to detect the viral DNA.

Detection of CIAV Antibody in SPF Chickens

To determine the source of CIAV contamination in live NDV vaccines, blood samples (n = 1,000) were collected from a SPF layer breeder flock. Serum was harvested using standard procedures and stored at 4°C until tested in an ELISA assay according to the manufacturer's instructions (Chicken Infectious Anemia Virus Antibody Test Kit, IDEXX, USA). Next, yolks of SPF chicken embryos (n = 200) used for vaccine production were randomly collected, and maternal CIAV antibody was detected with the dilution ratio of 1:20 using commercial ELISA kit (37).

DNA Extraction and CIAV Detection in Chicken Embryos

Fourteen to 18 day old SPF chicken embryos (n = 40) of the same production origin were randomly selected, and samples of pooled organs (liver, spleen and thymus) were excised from each embryo. The tissues were homogenized in phosphate-buffered

TABLE 1 | The sequence information of CIAV reference strains used in this work.

No.	Isolate	Origin	Year	Accession no.
1	01–4201	USA	2001	DQ991394
2	704	Australia	1996	U65414
3	17SY0902	China	2017	MK089243
4	26P4	USA	1991	D10068
5	3–1	Malaysia	2000	AF390038
6	98D02152	USA	1997-1998	AF311892
7	98D06073	USA	1997-1998	AF311900
8	AB1K	Turkey	2016	MT259319
9	AH4	China	2005	DQ124936
10	AH6	China	2005	DQ124935
11	AH-C369	Japan	2000	AB046590
12	BD-3	Bangladesh	2001	AF395114
13	BJ0401	China	2005	DQ124934
14	C14	China	2002	EF176599
15	C140	Japan	2000	AB046587
16	CAA82-2	Japan	1987	D31965
17	CIA-1	USA	1988	L14767
18	CIAV-10	Argentina	2007	KJ872513
19	CIAV-18	Argentina	2007	KJ872514
20	CIAV-4	China	2012	KJ728816
21	CIAV89-69	Korea	1991	JF507715
22	Cloned isolate 10	UK	1996	U66304
23	Cux-1	Germany	1990	M55918
24	Cuxhaven-1	Germany	1983	M81223
25	Del-Ros	USA	2000	AF313470
26	DI072479	USA	1990	DI072479
27	G6	Japan	2003	AB119448
28	GD-101	China	2014	KU050680
29	GD-104	China	2014	KU050679
30	GD-B-12	China	2011	KF224926
31	GD-K-12	China	2012	KF224935
32	GX1804	China	2018	MK484615
33	GX1904B	China	2019	MN103406
34	Harbin	China	2002	AF475908
35	HLJ15125	China	2015	KY486139
36	HN9	China	2005	DQ141672
37	Isolate 1	China	2012	KJ728814
38	Isolate 18	China	2012	KJ728827
39	Isolate 22	China	2012	KJ728830
40	Isolate 6	China	2012	KJ728817
41	LF4	China	2004	AY839944
42	LN15170	China	2015	KY486155
43	N8	China	2016	MK887164
44	SC-SM	China	2014	KM496305
45	SD1403	China	2014	KU221054
46	SD15	China	2015	KX811526
47	SD1509	China	2015	KU645510
48	SD22	China	2005	DQ141673
49	SD24	China	2005	AY999018
50	SDLY08	China	2008	FJ172347
51	SH11	China	2005	DQ141670
52	SH16	China	2005	DQ141671
53	SK4	Egypt	2017	MG827100
54	SMSC-1	Malaysia	2000	AF285882
55	SMSC-1P60	Malaysia	2001	AF390102
56	TJBD33	China	2004	AY843527
57	TJBD40	China	2004	AY846844
58	TR20	Japan	1999	AB027470
59	UT-Zahraee	Iran	2018	MT239353
60	WO9603507	USA	1996	A48606
61	SDSPF2020	China	2020	MW660821

(Continued)

saline (PBS), and DNA was extracted using dna extraction kits (Tiangen, China) according to the manufacturer's instructions. The extracted DNA was stored in TE buffer (10 mM Tris, pH 7.5; 1 mM EDTA, pH 8.0) at −20°C. Based on the CIAV genome sequences published in Genbank, specific primers targeted to the conserved regions of viral genome were designed by using Primer 5.0 (**Table 2**) (38, 39), and used for PCR. PCR products amplified from viral DNA in the samples were detected by a dot blot hybridization assay. PCR products and controls were spotted onto the nitrocellulose membrane as dots, then baked at 80°C in a vacuum oven and hybridized with a Digoxigenin-labeled DNA probe generated by PCR (PCR-DIG Probe Synthesis Kit, Roche Diagnostics, USA) using primers CIAV-FD/RD (**Table 2**). Meanwhile, high-sensitivity nested-PCR and quantitative real-time polymerase chain reactions (qPCR) were parallelly performed for CIAV detection using the previous published methods (36, 40). The primers used are shown in **Table 2**. Three replicates of each sample were tested by each of the three different methods.

Viral Genome Amplification and Sequencing

Three overlapping genomic segments were amplified from DNA extracted from the PCR-positive pooled organs using three pairs of primers (**Table 2**) (41) to establish the full-length nucleotide sequences. The PCR amplification was carried out in a 25μL total PCR reaction volume containing 10 pmol of each primer, 2.5 μL 10 × PCR buffer (Mg^{2+}), 2 μL dNTPs (2.5 mM), 0.5 μL rTaq DNA polymerase (TaKaRa Biotechnology Co. Ltd., Dalian, China), under the following protocol: denaturation at 95°C for 5 min, followed by 34 cycles of 95°C for 30 s, 56°C for 45 s, and 72°C for 1 min, and a final elongation step at 72°C for 7 min. The PCR products were purified by agarose gel electrophoresis and subcloned into the pMD-18T vector (Takara-Bio, Dalian, China). Genomic DNA extracted from the attenuated NDV vaccines was amplified and sequenced simultaneously. Three genomes from different SPF chicken embryos were randomly selected to amplify, and three clones of each PCR product were randomly selected and submitted to Tsingke Biotechnology Co., Ltd. (Qingdao, China) for sequencing by Sanger method.

TABLE 2 | Sequences of primers used for amplification in this study.

Primers	The sequences of the primers (5'→ 3')	Location	Sizes
CIAV-T-F[a]	5′ - CGCTCTCCAAGAAGATACTC - 3′	470–1,150	682bp
CIAV-T-R	5′ - CTGAAATCTTGGCGACTCTC - 3′		
CIAV-F[b]	5′ - GCATTCCGAGTGGTTACTATTCC - 3′	1–942	942bp
CIAV-R	5′ - TCTCCTCCGATGTCGAAATTTATA - 3′		
CIAV-F_D[c]	5′ - GTTACTATTCCATCACCATT - 3′	13–682	670bp
CIAV-R_D	5′ - ACATTCTTGAAACCAGTGCT - 3′		
C-F[d]	5′ - GCATTCCGAGTGGTTACTATTCC - 3′	1–843	843bp
C-R	5′ - CGTCTTGCCATCTTACAGTCTTAT - 3′		
CC-F[d]	5′ - TACGTCACAGCCAATCAGAA - 3′	231–648	418bp
CC-R	5′ - GCATTGCAGATCTTAGCGT - 3′		
CIAV-q-F[e]	5′ - CGGATTGGTATCGCTGGA - 3′	564–718	155bp
CIAV-q-R	5′ - GAGGGAGGCTTGGGTTGAT - 3′		
CIAV-com-F1[f]	5′ - GCATTCCGAGTGGTTACTATTCC - 3′	1–842	842bp
CIAV-com-R1	5′ - CGTCTTGCCATCTTACAGTCTTAT - 3′		
CIAV-com-F2[f]	5′ - CGAGTACAGGGTAAGCGAGCTAAA–3′	743–1,732	990bp
CIAV-com-R2	5′ - TGCTATTCATGCAGCGGACTT - 3′		
CIAV-com-F3[f]	5′ - ACGAGCAACAGTACCCTGCTAT - 3′	1,643–150	802bp
CIAV-com-R3	5′ - CTGTACATGCTCCACTCGTT - 3′		

[a]Primers were used to identify CIAV gene sequence. [b]Primers to generate PCR products for the dot blot hybridization assay. [c]Primers used for Digoxigenin-DNA probe amplification. [d]Outer and inner primers for nested-PCR. [e]Primers for SYBR Green I-based real-time PCR assay. [f]Three pairs of primers were designed to amplify three overlapping fragments (36).

Alignment and Phylogenetic Analysis of Viral Genome Sequence

The complete genome sequences of the new strain were obtained by assembling separated overlapping fragments using DNAstar software (version 7.1), and multiple sequence alignment was performed with the new strain and 60 reference genome sequences downloaded from GenBank (**Table 1**) using Clustal W method. Homology analysis was implemented by MegAlign and BLAST (https://blast.ncbi.nlm.nih.gov/Blast.cgi). The phylogenetic trees were generated by the neighbor-joining (NJ) method using MEGA X based on the full-length genome, VP1, VP2, and VP3 regions. Bootstrap values (1,000 replications) were indicated on each tree. And phylogenetic trees were further displayed, manipulated, and annotated with a web-based tool (Interactive Tree of Life http://itol.embl.de). In addition, transcriptional regulatory elements in non-coding region of the strain were analyzed by the online service system of NSITE (Recognition of Regulatory motifs) of SoftBerry (http://www.softberry.com/berry.phtml).

RESULTS

Detection of CIAV Infection in the SPF Layer Breeder Flock

The results of ELISA detection of CIAV antibodies in serum and egg yolk of SPF laying hens were 62% positive and 47% positive, respectively, indicating that the SPF layer breeder flock was infected with the virus (**Table 3**). CIAV DNA was detected in the pooled organs of embryo samples (35%) by dot blot hybridization assay, while other potential co-infection viruses were negative. In addition, CIAV was detected in 14/40 (35%) embryos by nested PCR and 15/40 (37.5%) embryos by qPCR. All detection methods indicated that embryos from the SPF breeder flock were infected with CIAV.

Genome Amplification and Phylogenetic Analysis of CIAV

The full-length genome sequences of CIAV were obtained from the NDV vaccines and SPF chicken embryos by assembling three overlapping fragments. Both genomes consisted of 2,298 nucleotides (nt) with 100% homology. Therefore, the CIAV genomes from the NDV vaccines and SPF chicken embryos were confirmed to be the same strain, named as SDSPF2020, and submitted to GenBank with accession NO.MW660821. The obtained sequence had a high level of nucleotide identity with references (95.8–99.6%). The phylogenetic tree showed that CIAV genomes could be divided into four major clusters (A, B, C, and D) based on previously proposed nomenclature (32). CIAV-SDSPF2020 fell within the A1 group and had the maximal nucleotide sequence identity (99.6%) with the Chinese wild strain HLJ15125 (KY486139), belonging to the same clade (**Figure 1**). And this new strain was also found to be related to SD1509 and N8 with 99.5% sequence identity, clustered in the same farther branch. These data indicated that the SDSPF2020 strain possessed the typical Asian virus characteristics in the whole genome sequence.

Protein-Coding Sequence Analysis of SDSPF2020

Similar result was observed in phylogenetic analysis based on VP1 nucleotide sequences. All sequences fell into four gene clusters (**Figure 2**). The nucleotide homology and amino acid

TABLE 3 | Detection of chicken infectious anemia virus by antibody assays and molecular biological methods.

No. of samples tested for CIAV			Antibody assays			Molecular biological methods			
Tril no.	No. of birds	No. of embryos	No. of seropositive	ELISA S/N ratios[a]	No. positive/total (% positive)	No. of embryos positive			No. samples positive total[b] (%)
						Nucleic acid dot blots	Real-time quantitative PCR	Nested PCR assay	
1	1000[c]	/	622	≤ 0.6	62%	NT[f]	NT	NT	NT
2	/	200[d]	94	≤ 0.6	47%	NT	NT	NT	NT
3	/	40[e]	NA[f]	NA	NA	14	15	14	35.8%

[a]ELISA S/N ratios≤0.6 positive or high protective titers; S/N > 0.6 negative or low titer. [b]The positive rate of the three methods was averaged. [c]Sera samples were obtained from the SPF layer breeder flock used for vaccine production. [d]SPF egg yolk samples were randomly collected. [e]DNA was extracted from pooled organs of chicken embryos. [f]NT: not tested; NA: not applicable.

homology of VP1 were 94.4–99.6% and 97.1–100% compared with other reference strains. There are a few differences in nucleotide sequence encoding the VP1 HV region (AAs 139-151) of SDSPF2020, but no unique amino acids were found between SDSPF2020 and the reference sequences (**Figure 1**). The amino acid sites of VP1 protein manifested the presence of lysine (K) at site 139 and glutamic acid (E) at site 144 in SDSPF2020 strain, and the amino acid sites 125 (L) and 157 (M) were different from most reference CIAV strains (**Figure 3**). In addition, compared with HLJ15125, synonymous nucleotide substitutions occurred at codons 151 (L), 309 (T), 383 (L), and 420 (Q) in VP1, but codon 447 has a non-synonymous nucleotide difference. However, nucleotide sequences of VP2 and VP3 of SDSPF2020 were relatively conserved. Sequence analysis showed that nucleotide homology of VP2 gene was 99.1–99.8% and amino acid homology was 97.7–100%, while nucleotide identity and amino acid homology in the apoptin gene were 98.9–100% and 96.7–100%, respectively. In addition, no deletion or insertion was found in VP2 and VP3 protein. However, the nucleotides at site 347 and 352 of the VP3 coding sequences were different from the classical reference strain Cux-1, both of which resulted in amino acid differences in the NLS2 domain of VP3 protein.

Molecular Characterization of Non-coding Region of SDSPF2020

The Clustal W method was used to analyze the homology of non-coding region fragments of 10 CIAV reference strains. Like the reference strains, the non-coding sequences of SDSPF2020 contained a conservative region of DNA with high G+C content (nucleotide homology 97.0–99.4%). Most motifs in untranslated region of SDSPF2020 were the same as those of the reference strains, while several obvious differences in individual nucleotides existed in SDSPF2020. Transcription factor binding site analysis by NSITE demonstrated that a tandem array of four DR regions was found 4nt upstream of the "CCAAT" box in the non-coding region of SDSPF2020 and most of the reference strains, except for Cux-1, which contains an additional DR copy (**Figure 4**). The ATF/CREB binding sites ("ACGTCA" consensus sequence) in the DR resembles imperfect hormone response element half-sites (AGGTCA), especially the SP1 recognition site located in close proximity. In addition, it was found that a cluster of GGTCA-like sequences was found downstream of the transcription start point (TSP). In addition, several transcription factor binding sites were all conserved in the non-coding region of SDSPF2020, like GTII factor binding site, TATA box and lymphoid specific transcription factor binding sites.

DISCUSSION

Since the first strain was isolated from chickens with a vaccine accident in 1979, CIAV has attracted worldwide attention in the poultry industry (42, 43). Although exogenous contamination in vaccines or even SPF chickens has been reported, our results provided evidence for the vertical transmission of CIAV. Recently, we discovered exogenous contamination of CIAV during routine vaccine screening, and confirmed that the contamination also existed in a SPF layer breeder flock and embryos. Next, we analyzed the genetic variation of CIAV-SDSPF2020 strain and tracked its possible origin. Shockingly, the new CIAV genome in NDV vaccines and SPF embryos is the same strain, and has high homology with the Chinese strain HLJ15125 or other wild strains (up to 99.5% or more). It suggested that widespread and multiple epidemics of wild strains may cause the prevalence of CIAV in SPF chickens. These data provided new and crucial information toward a more comprehensive understanding of the origin of CIAV contamination in vaccines.

In this study, we predicted complete amino acid sequences of the new strain and aligned with other CIAV isolates from around the world. The limited genetic variation of CIAV genome is generally <5%, most of which comes from VP1 coding region, because of the extreme conservation of VP2 and VP3 (44, 45). VP1 is the viral capsid and the virulence and pathogenicity of CIAV are associated with critical amino acid residues, such as codon sites 394, 139, and 144 (46, 47). SDSPF2020 strain presented lysine (K) at amino acid site 139 and glutamic acid (E) at site 144, which were related to the rate of replication in culture (48). At amino acid sites 75, 89, 125, SDSPF2020 strain presented valine (V), threonine (T), and leucine (L),

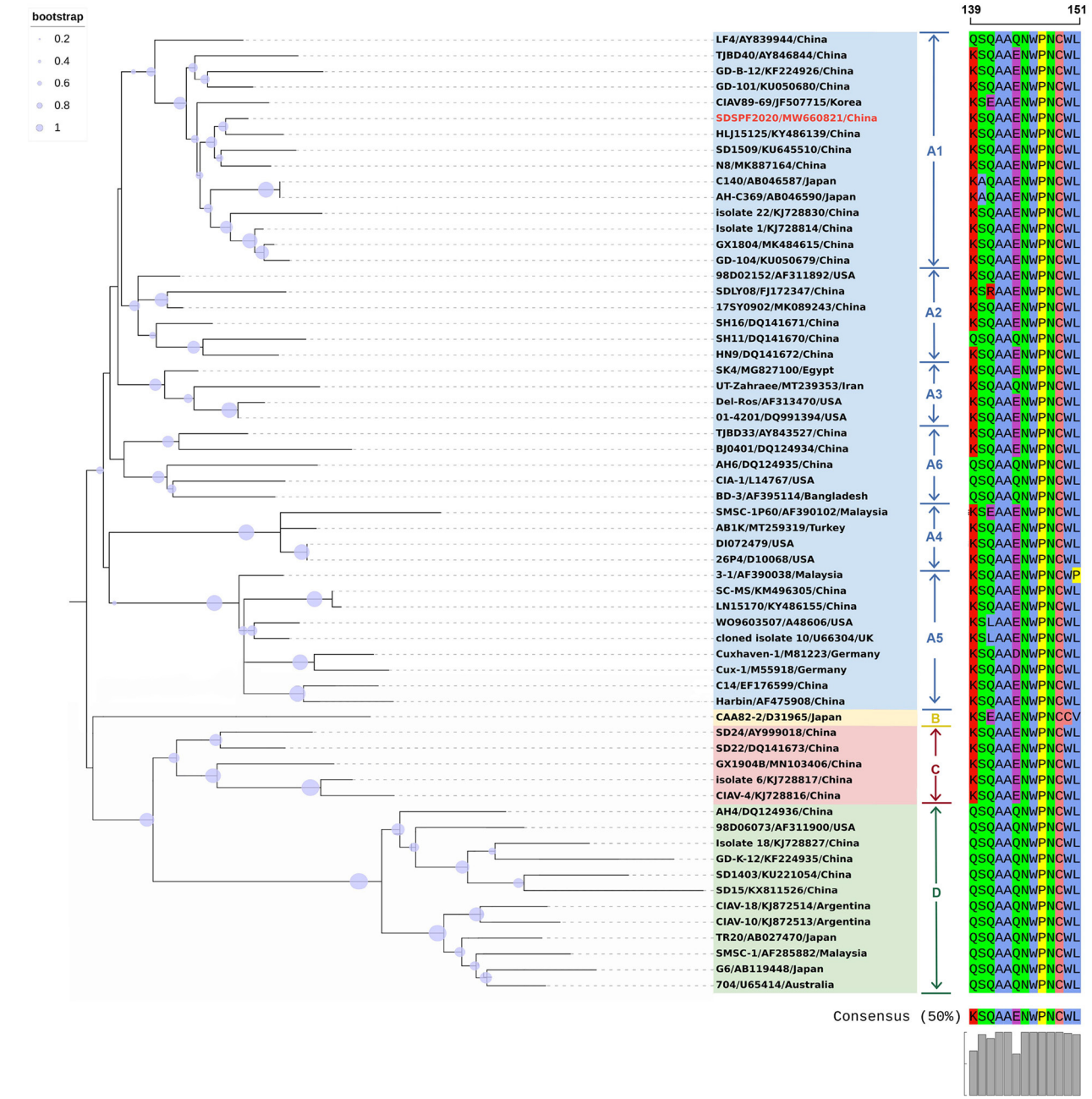

FIGURE 1 | Phylogenetic relationships of SDSPF2020 and other available reference CIAVs in GenBank based on complete genome nucleotide sequences. The phylogenetic trees were generated by neighbor-joining method (1,000 bootstraps) using MEGA X software. The red label represents the strain of the CIAV-SDSPF2020, and a multiple sequence alignment of VP1 protein hypervariable regions (amino acid 139–151) is visualized directly next to the tree. The viruses were clearly divided into 4 genogroups from A to D, and group A included six subgroups.

respectively, sharing some VP1 amino acids with strains with lower virulent characteristics as previously speculated (32, 47, 49, 50). Therefore, we speculated that SDSPF2020 might be an attenuated virulent strain. In addition, clarifying the properties of transcription regulatory elements provide a better understanding on the mechanisms of host transcriptional regulation and viral pathogenesis. SP1 recognition sites and other transcription factor binding sites are involved in regulation of the CIAV-promoter/enhancer activity (1, 27, 29). Persengiev and Green. reported that the ATF/CREB family of transcriptional regulators have diversified functions in controlling cell proliferation and apoptosis (51). We observed the motifs of these binding sites were

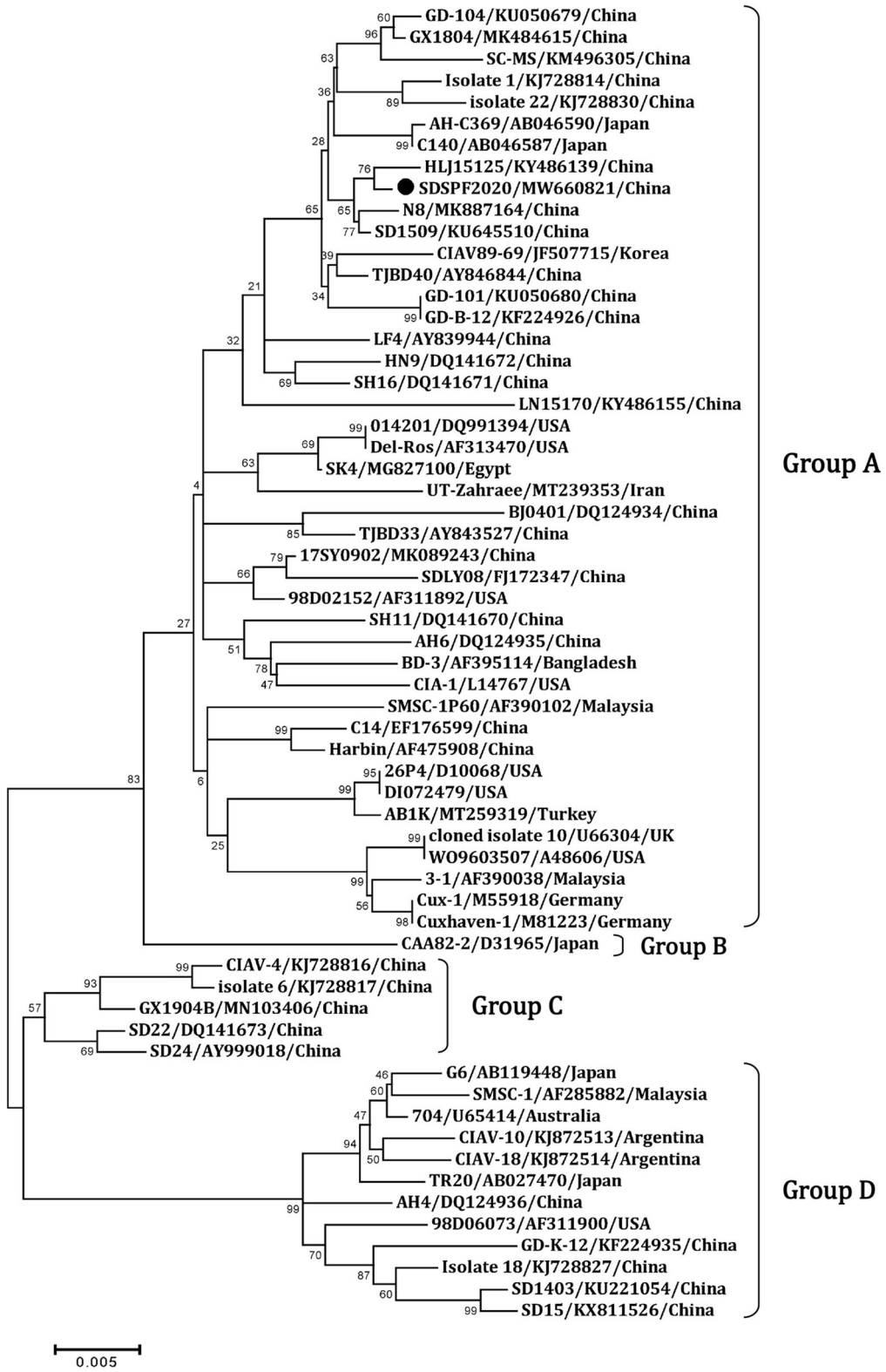

FIGURE 2 | Phylogenetic diagram of viral protein 1 genes among CIAV strains. The CIAV strain determined in this work is highlighted in a black dot, and reference sequences from GenBank were given the name followed by accession number and country. The numbers near the branches indicate bootstrap values. The four major groups were identified as A, B, C and D.

No.	Strain	75	89	97	125	139	144	151	157	251	287	370	394	413	447
1	01–4201	V	T	M	I	K	E	L	V	R	S	G	Q	S	G
2	26P4	V	T	M	I	K	E	L	M	R	T	S	Q	A	T
3	3–1	V	T	M	I	K	E	P	V	Q	D	S	Q	A	T
4	98D02152	V	T	M	I	K	E	L	V	R	S	G	Q	S	T
5	AB1K	V	T	M	I	K	E	L	M	R	T	S	Q	A	T
6	AH4	I	T	L	I	Q	Q	L	V	R	T	S	Q	A	S
7	BD-3	I	T	L	I	Q	Q	L	V	R	A	T	Q	A	T
8	BJ0401	V	T	M	L	K	E	L	V	R	A	S	Q	A	S
9	C14	V	T	M	I	K	E	L	V	R	T	S	Q	A	S
10	CAA82-2	V	T	M	L	K	E	V	V	R	S	G	Q	S	T
11	CIA-1	I	T	L	I	Q	Q	L	V	R	A	S	Q	A	S
12	CAV-10	I	T	L	I	Q	Q	L	V	R	T	S	Q	A	S
13	CIAV89-69	V	T	D	L	K	E	L	V	R	S	G	Q	S	S
14	Cux-1	V	T	M	I	K	D	L	V	Q	A	S	Q	A	T
15	Del-Ros	V	T	M	I	K	E	L	V	R	S	G	Q	S	G
16	G6	I	T	L	I	Q	Q	L	V	R	T	S	Q	A	S
17	GD-101	V	T	M	L	K	E	L	M	R	S	G	Q	S	S
18	GX1804	V	T	M	L	K	E	L	M	R	S	G	Q	S	S
19	HLJ15125	V	T	M	L	K	E	L	M	R	S	G	Q	S	T
20	HN9	V	T	M	L	K	E	L	V	R	S	G	Q	S	T
21	Isolate 18	I	T	L	I	Q	Q	L	V	R	A	S	Q	A	P
22	LF4	I	T	M	L	Q	Q	L	V	R	S	S	Q	S	S
23	N8	V	T	M	L	K	E	L	V	R	S	G	Q	S	S
24	SD15	I	T	L	I	Q	Q	L	V	R	T	T	Q	A	S
25	SD22	V	T	M	L	K	E	L	V	R	S	S	Q	A	S
26	SDLY08	V	T	M	I	K	E	L	V	R	S	G	Q	S	T
27	SC-MZ	V	T	M	L	K	E	L	V	R	S	G	Q	S	G
28	SK4	V	T	M	I	K	E	L	V	R	S	G	Q	S	S
29	TR20	I	T	L	I	Q	Q	L	V	R	T	S	Q	A	S
30	UT-Zahraee	I	T	L	I	K	Q	L	V	R	S	G	Q	A	G
	CIAV-SDSPF2020	V	T	M	L	K	E	L	M	R	S	G	Q	S	S

FIGURE 3 | Amino acids at sites of common substitutions in VP1 protein coding sequences of different CIAVs. Each site differences are indicated by different color base box. The last row in the table shows the sites of the new strain.

also retained in the SDSPF2020 genome. It suggested that those conserved transcriptional regulatory elements may be involved in pathogenicity and viral cytotropism, but the specific regulatory mechanism needs to be further investigated.

CIAV was widely spread in chicken flocks through vertical and horizontal transmission, and the potential route of contamination of vaccines should not be ignored. Numerous studies have proved that exogenous virus contamination existed in live poultry vaccines even under strict surveillance, for example, avian leukosis virus (ALV), Reticuloendotheliosis virus (REV) and fowl adenovirus (FAdV) (52–56). Live attenuated vaccines contaminated with CIAV even in relatively low dose can lead to synergetic pathogenicity and reduce the protective effects against other pathogens (57, 58). By reason of high resistance to common disinfectants and heat treatment, chicken of all ages faces the risk of CIAV infection (17, 59). Epidemiological surveys showed that the positive rate of CIAV tended to be increasing in commercial chicken flocks in recent years, even as high as 87% in some unimmunized chickens in live bird markets (60, 61), which causes substantial economic losses to poultry farming.

However, the fact that the SPF chicken flocks used to produce chicken embryos were infected appears to be treated as if it was relatively rare. Some research groups with SPF flocks throughout the world had encountered these problems in the early 2000 s (15, 62). The work by the Cornell University team demonstrated that CIAV persists in reproductive tissues of sexually mature

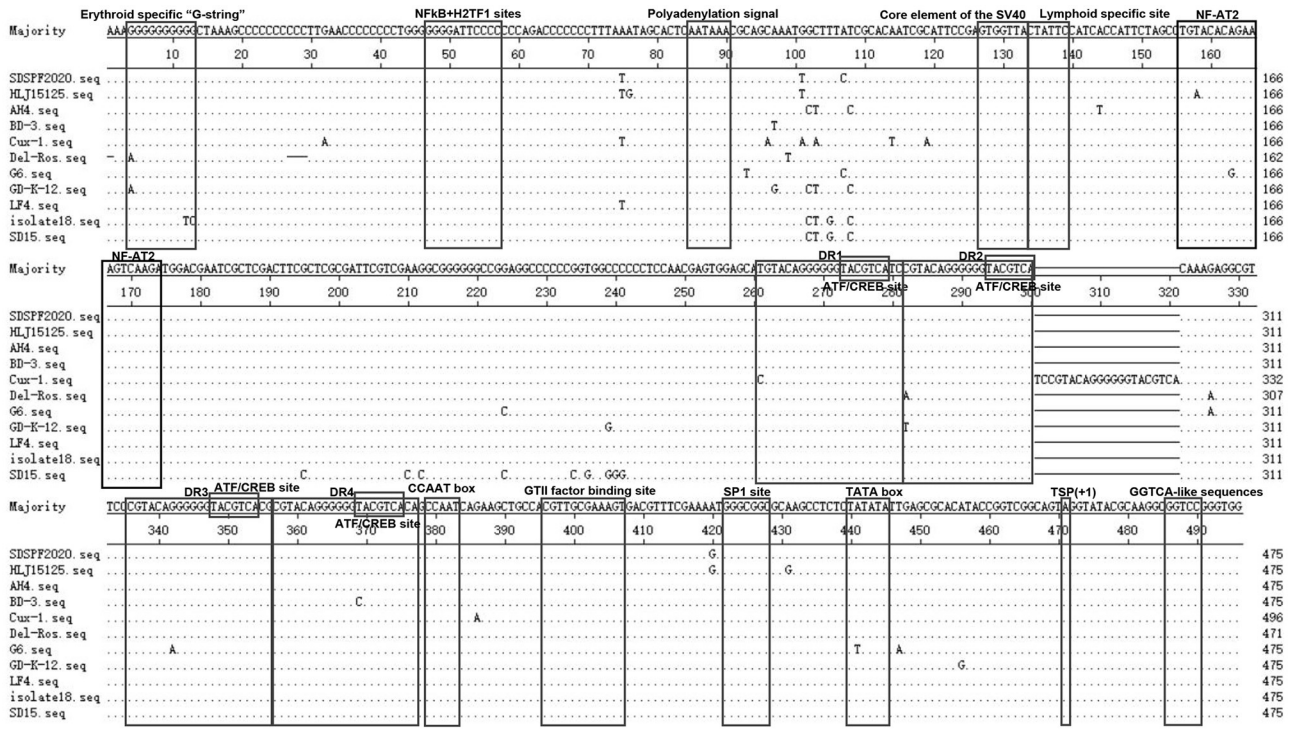

FIGURE 4 | Sequence alignment of the non-coding region sequences of SDSPF2020 and 10 reference strains. The sequences in black frames are the motifs of transcriptional regulatory elements in this study. Nucleotides matching the consensus are indicated with dots and nucleotide differences are indicated with letters.

hens and roosters, and was transmitted vertically to embryos. Brentano et al. also confirmed that CIAV genome exists in the gonads for a long time even in the presence of high neutralizing antibody titers (63). In our experiment, serum collected from a SPF layer breeder flock reacted in ELISA, and viral nucleic acid also existed in organ tissues of chicken embryos. These results demonstrated that SPF layer breeder flocks were widely infected with CIAV and transmitted the virus to chicken embryos through vertical transmission, even under rigid hygiene control and supervision, which may affect the quality of downstream biological products. Nevertheless, the elimination of the virus from infected SPF flocks is a challenging and time-consuming strategy. It is worth noting that the detection of CIAV in embryos and eggshell membranes is an excellent procedure for monitoring potential infections (64). For some vertically transmitted viruses, such as ALV and CIAV, it seems particularly important to establish intensive monitoring and careful management at the parent and grandparent levels of SPF flocks, especially on the hatchery level, which is of great significance to ensure the purity of SPF chicken embryos and vaccines. Thus, it is necessary to continue immunoprophylaxis efforts combined with optimized biosafety programs for the vaccine production.

In conclusion, this study analyzed the whole-genome sequence of CIAV (SDSPF2020) identified from contaminated NDV vaccines, which is consistent with the SPF layer breeder flock, and suggested that it is linked with epidemic wild strains. These findings showed an integrated evidence chain of a vertical transmission route from SPF chickens to vaccines, reminding us that the surveillance of vertically transmitted viruses and biosecurity control of SPF chicken farms should be strengthened continuously to reduce the potential risks of exogenous virus invasion.

DATA AVAILABILITY STATEMENT

The datasets presented in this study can be found in online repositories. The names of the repository/repositories and accession number(s) can be found here: https://www.ncbi.nlm.nih.gov/genbank/, MW660821.

ETHICS STATEMENT

The animal study was reviewed and approved by Shandong Agricultural University Animal Care and Use Committee and Shandong Agricultural University.

AUTHOR CONTRIBUTIONS

YL, JW, LC, and MZ performed the experiments. QW, HZ, and ZC analyzed the data. YL drafted the manuscript. PZ, YW, and SC revised the manuscript. All authors read and approved the final manuscript.

FUNDING

This study was funded by the National Key Research and Development Program of China (grant numbers 2018YFD0500106).

ACKNOWLEDGMENTS

The authors would like to thank YW for proofreading the draft and providing valuable feedback as well as PZ for guidance and insight into this article.

REFERENCES

1. Schat KA. Chicken anemia virus. *Curr Top Microbiol Immunol.* (2009) 331:151–83. doi: 10.1007/978-3-540-70972-5_10
2. McNulty MS. Chicken anaemia agent: a review. *Avian Pathol.* (1991) 20:187–203. doi: 10.1080/03079459108418756
3. Yuasa N, Taniguchi T, Yoshida I. Isolation and some characteristics of an agent inducing anemia in chicks. *Avian Dis.* (1979) 23:366.
4. Noteborn MH. Chicken anemia virus induced apoptosis: underlying molecular mechanisms. *Vet Microbiol.* (2004) 98:89–94. doi: 10.1016/j.vetmic.2003.10.003
5. Noteborn MH, de Boer GF, van Roozelaar DJ, Karreman C, Kranenburg O, Vos JG, et al. Characterization of cloned chicken anemia virus DNA that contains all elements for the infectious replication cycle. *J Virol.* (1991) 65:3131–9. doi: 10.1128/jvi.65.6.3131-3139.1991
6. Todd D. Circoviruses: immunosuppressive threats to avian species: a review. *Avian Pathol.* (2000) 29:373–94. doi: 10.1080/030794500750047126
7. Taniguchi T, Yuasa N, Maeda M, Horiuchi T. Chronological observations on hemato-pathological changes in chicks inoculated with chicken anemia agent. *Natl Inst Anim Health Q (Tokyo).* (1983) 23:1–12.
8. Adair BM. Immunopathogenesis of chicken anemia virus infection. *Dev Comp Immunol.* (2000) 24:247–55. doi: 10.1016/s0145-305x(99)00076-2
9. Markowski-Grimsrud CJ, Schat KA. Infection with chicken anaemia virus impairs the generation of pathogen-specific cytotoxic T lymphocytes. *Immunology.* (2003) 109:283–94. doi: 10.1046/j.1365-2567.2003.01643.x
10. Joiner KS, Ewald SJ, Hoerr FJ, van Santen VL, Toro H. Oral infection with chicken anemia virus in 4-wk broiler breeders: lack of effect of major histocompatibility B complex genotype. *Avian Dis.* (2005) 49:482–7. doi: 10.1637/7358-031805r.1
11. Hoop RK. Persistence and vertical transmission of chicken anaemia agent in experimentally infected laying hens. *Avian Pathol.* (1992) 21:493–501. doi: 10.1080/03079459208418867
12. Huynh LTM, Nguyen GV, Do LD, Dao TD, Le TV, Vu NT, et al. Chicken infectious anaemia virus infections in chickens in northern vietnam: epidemiological features and genetic characterization of the causative agent. *Avian Pathol.* (2020) 49:5–14. doi: 10.1080/03079457.2019.1637821
13. Hu LB, Lucio B, Schat KA. Abrogation of age-related resistance to chicken infectious anemia by embryonal bursectomy. *Avian Dis.* (1993) 37:157–69.
14. Smyth JA, Moffett DA, McNulty MS, Todd D, Mackie DP. A sequential histopathologic and immunocytochemical study of chicken anemia virus infection at one day of age. *Avian Dis.* (1993) 37:324–38.
15. Cardona CJ, Oswald WB, Schat KA. Distribution of chicken anaemia virus in the reproductive tissues of specific-pathogen-free chickens. *J Gen Virol.* (2000) 81:2067–75. doi: 10.1099/0022-1317-81-8-2067
16. Davidson I, Artzi N, Shkoda I, Lublin A, Loeb E, Schat KA. The contribution of feathers in the spread of chicken anemia virus. *Virus Res.* (2008) 132:152–9. doi: 10.1016/j.virusres.2007.11.012
17. Yuasa N. Effect of chemicals on the infectivity of chicken anaemia virus. *Avian Pathol.* (1992) 21:315–9. doi: 10.1080/03079459208418846
18. Urlings HA, de Boer GF, van Roozelaar DJ, Koch G. Inactivation of chicken anaemia virus in chickens by heating and fermentation. *Vet Q.* (1993) 15:85–8. doi: 10.1080/01652176.1993.9694380
19. Scott AN, Connor TJ, Creelan JL, McNulty MS, Todd D. Antigenicity and pathogenicity characteristics of molecularly cloned chicken anaemia virus isolates obtained after multiple cell culture passages. *Arch Virol.* (1999) 144:1961–75. doi: 10.1007/s007050050718
20. Meehan BM, Todd D, Creelan JL, Earle JA, Hoey EM, McNulty MS. Characterization of viral DNAs from cells infected with chicken anaemia agent: sequence analysis of the cloned replicative form and transfection capabilities of cloned genome fragments. *Arch Virol.* (1992) 124:301–19. doi: 10.1007/bf01309811
21. Pringle CR. Virus taxonomy at the XIth international congress of virology, sydney, Australia, 1999. *Arch Virol.* (1999) 144:2065–70. doi: 10.1007/s007050050728
22. Rosario K, Breitbart M, Harrach B, Segalés J, Delwart E, Biagini P, et al. Revisiting the taxonomy of the family circoviridae: establishment of the genus cyclovirus and removal of the genus gyrovirus. *Arch Virol.* (2017) 162:1447–63. doi: 10.1007/s00705-017-3247-y
23. Noteborn MH, Kranenburg O, Zantema A, Koch G, de Boer GF, van der Eb AJ. Transcription of the chicken anemia virus (CAV) genome and synthesis of its 52-kDa protein. *Gene.* (1992) 118:267–71. doi: 10.1016/0378-1119(92)90198-x
24. Peters MA, Jackson DC, Crabb BS, Browning GF. Chicken anemia virus VP2 is a novel dual specificity protein phosphatase. *J Biol Chem.* (2002) 277:39566–73. doi: 10.1074/jbc.M201752200
25. Wang D, Fan W, Han GZ, He CQ. The selection pressure analysis of chicken anemia virus structural protein gene VP1. *Virus Genes.* (2009) 38:259–62. doi: 10.1007/s11262-008-0316-z
26. Islam MR, Johne R, Raue R, Todd D, Müller H. Sequence analysis of the full-length cloned DNA of a chicken anaemia virus (CAV) strain from Bangladesh: evidence for genetic grouping of CAV strains based on the deduced VP1 amino acid sequences. *J Vet, Med B.* (2002) 49:332–7. doi: 10.1046/j.1439-0450.2002.00581.x
27. Noteborn MH, Verschueren CA, Zantema A, Koch G, van der Eb AJ. Identification of the promoter region of chicken anemia virus (CAV) containing a novel enhancer-like element. *Gene.* (1994) 150:313–8. doi: 10.1016/0378-1119(94)90444-8
28. Miller MM, Jarosinski KW, Schat KA. Negative modulation of the chicken infectious anemia virus promoter by COUP-TF1 and an E box-like element at the transcription start site binding deltaEF1. *J Gen Virol.* (2008) 89:2998–3003. doi: 10.1099/vir.0.2008/003103-0
29. Miller MM, Jarosinski KW, Schat KA. Positive and negative regulation of chicken anemia virus transcription. *J Virol.* (2005) 79:2859–68. doi: 10.1128/jvi.79.5.2859-2868.2005
30. Li Y, Yan N, Wang Y, Liu A, Liu C, Lan X, et al. Molecular evolution and pathogenicity of chicken anemia virus isolates in China. *Arch Virol.* (2021) 166:439–49. doi: 10.1007/s00705-020-04909-8
31. Zhang X, Liu Y, Wu B, Sun B, Chen F, Ji J, et al. Phylogenetic and molecular characterization of chicken anemia virus in southern China from 2011 to 2012. *Sci Rep.* (2013) 3:3519. doi: 10.1038/srep03519
32. Yao S, Tuo T, Gao X, Han C, Yan N, Liu A, et al. Molecular epidemiology of chicken anaemia virus in sick chickens in China from 2014 to 2015. *PLoS ONE.* (2019) 14:e0210696. doi: 10.1371/journal.pone.0210696
33. Tan C, Wang Z, Lei X, Lu J, Yan Z, Qin J, et al. Epidemiology, molecular characterization, and recombination analysis of chicken anemia virus in Guangdong province, China. *Arch Virol.* (2020) 165:1409–17. doi: 10.1007/s00705-020-04604-8
34. Li Y, Hu Y, Cui S, Fu J, Wang Y, Cui Z, et al. Molecular characterization of chicken infectious anemia virus from contaminated live-virus vaccines. *Poult Sci.* (2017) 96:1045–51. doi: 10.3382/ps/pew406
35. Marin SY, Barrios PR, Rios RL, Resende M, Resende JS, Santos BM, et al. Molecular characterization of contaminating infectious anemia virus of chickens in live commercial vaccines produced in the 1990s. *Avian Dis.* (2013) 57:15–21. doi: 10.1637/10056-011212-Reg.1
36. Li X, Fang L, Li Y, Cui Z, Chang S, Zhao P. Establishment of a nested-PCR method for detection of chicken infectious anemia virus in attenuated avian vaccine. *Chin Poult.* (2017) 39:18–22. doi: 10.16372/j.issn.1004-6364.2017.10.005

37. Li Y, Fang L, Wang Y, Cui Z, Chang S, Zhao P. Assessment on chicken infectious anemia virus infection in SPF chickens based on yolk antibody detection. *Chin Poult.* (2016) 38:15–18. doi: 10.16372/j.issn.1004-6364.2016.07.004
38. Meng F, Dong G, Zhang Y, Tian S, Cui Z, Chang S, et al. Co-infection of fowl adenovirus with different immunosuppressive viruses in a chicken flock. *Poult Sci.* (2018) 97:1699–705. doi: 10.3382/ps/pex414
39. Todd D, Creelan JL, McNulty MS. Dot blot hybridization assay for chicken anemia agent using a cloned DNA probe. *J Clin Microbiol.* (1991) 29:933–9. doi: 10.1128/jcm.29.5.933-939.1991
40. Fu J, Li D, Chang Z, Li Y, Fang L, Cui Z, et al. Establishment of SYBR green I fluorescent quantitative PCR method for detection of chicken infectious anemia virus and its application in vaccine contamination detection. *Chin J Anim Infect Dis.* (2017) 25:34–9. Available online at: https://zsjb.cbpt.cnki.net/
41. Li Y, Wang Y, Fang L, Fu J, Cui S, Zhao Y, et al. Genomic analysis of the chicken infectious anemia virus in a specific pathogen-free chicken population in China. *Biomed Res Int.* (2016) 2016:4275718. doi: 10.1155/2016/4275718
42. Balamurugan V, Kataria JM. Economically important non-oncogenic immunosuppressive viral diseases of chicken–current status. *Vet Res Commun.* (2006) 30:541–66. doi: 10.1007/s11259-006-3278-4
43. Hailemariam Z, Omar AR, Hair-Bejo M, Giap TC. Detection and characterization of chicken anemia virus from commercial broiler breeder chickens. *Virol J.* (2008) 5:128. doi: 10.1186/1743-422x-5-128
44. Ou SC, Lin HL, Liu PC, Huang HJ, Lee MS, Lien YY, et al. Epidemiology and molecular characterization of chicken anaemia virus from commercial and native chickens in Taiwan. *Transbound Emerg Dis.* (2018) 65:1493–501. doi: 10.1111/tbed.12886
45. Kim HR, Kwon YK, Bae YC, Oem JK, Lee OS. Molecular characterization of chicken infectious anemia viruses detected from breeder and broiler chickens in South Korea. *Poult Sci.* (2010) 89:2426–31. doi: 10.3382/ps.2010-00911
46. Todd D, Scott AN, Ball NW, Borghmans BJ, Adair BM. Molecular basis of the attenuation exhibited by molecularly cloned highly passaged chicken anemia virus isolates. *J Virol.* (2002) 76:8472–4. doi: 10.1128/jvi.76.16.8472-8474.2002
47. Yamaguchi S, Imada T, Kaji N, Mase M, Tsukamoto K, Tanimura N, et al. Identification of a genetic determinant of pathogenicity in chicken anaemia virus. *J Gen Virol.* (2001) 82:1233–8. doi: 10.1099/0022-1317-82-5-1233
48. Renshaw RW, Soine C, Weinkle T, O'Connell PH, Ohashi K, Watson S, et al. A hypervariable region in VP1 of chicken infectious anemia virus mediates rate of spread and cell tropism in tissue culture. *J Virol.* (1996) 70:8872–8.
49. Chowdhury SM, Omar AR, Aini I, Hair-Bejo M, Jamaluddin AA, Md-Zain BM, et al. Pathogenicity, sequence and phylogenetic analysis of Malaysian Chicken anaemia virus obtained after low and high passages in MSB-1 cells. *Arch Virol.* (2003) 148:2437–48. doi: 10.1007/s00705-003-0189-3
50. Abdel-Mawgod S, Adel A, Arafa AS, Hussein HA. Full genome sequences of chicken anemia virus demonstrate mutations associated with pathogenicity in two different field isolates in Egypt. *Virusdisease.* (2018) 29:333–41. doi: 10.1007/s13337-018-0467-z
51. Persengiev SP, Green MR. The role of ATF/CREB family members in cell growth, survival and apoptosis. *Apoptosis.* (2003) 8:225–8. doi: 10.1023/a:1023633704132
52. Biswas SK, Jana C, Chand K, Rehman W, Mondal B. Detection of fowl poxvirus integrated with reticuloendotheliosis virus sequences from an outbreak in backyard chickens in India. *Vet Ital.* (2011) 47:147–53. Available online at: https://www.izs.it/vet_italiana/2011/47_2/147.htm
53. Wang P, Lin L, Li H, Shi M, Gu Z, Wei P. Full-length genome sequence analysis of an avian leukosis virus subgroup J (ALV-J) as contaminant in live poultry vaccine: the commercial live vaccines might be a potential route for ALV-J transmission. *Transbound Emerg Dis.* (2018) 65:1103–6. doi: 10.1111/tbed.12841
54. Zhao P, Dong X, Cui Z. Isolation, identification, and gp85 characterization of a subgroup A avian leukosis virus from a contaminated live newcastle disease virus vaccine, first report in China. *Poult Sci.* (2014) 93:2168–74. doi: 10.3382/ps.2014-03963
55. Li J, Dong X, Yang C, Li Q, Cui Z, Chang S, et al. Isolation, identification, and whole genome sequencing of reticuloendotheliosis virus from a vaccine against Marek's disease. *Poult Sci.* (2015) 94:643–9. doi: 10.3382/ps/pev034
56. Su Q, Hou L, Gao Y, Liu X, Cui Z, Chang S, et al. Research note: molecular relationship of the fowl adenovirus serotype 4 isolated from the contaminated live vaccine and wild strains isolated in China, 2013-2018. *Poult Sci.* (2020) 99:6643–6. doi: 10.1016/j.psj.2020.08.063
57. Su Q, Wang T, Meng F, Cui Z, Chang S, Zhao P. Synergetic pathogenicity of newcastle disease vaccines LaSota strain and contaminated chicken infectious anemia virus. *Poult Sci.* (2019) 98:1985–92. doi: 10.3382/ps/pey555
58. Zhang Y, Cui N, Han N, Wu J, Cui Z, Su S. Depression of vaccinal immunity to marek's disease by infection with chicken infectious anemia virus. *Front Microbiol.* (2017) 8:1863. doi: 10.3389/fmicb.2017.01863
59. Welch J, Bienek C, Gomperts E, Simmonds P. Resistance of porcine circovirus and chicken anemia virus to virus inactivation procedures used for blood products. *Transfusion.* (2006) 46:1951–8. doi: 10.1111/j.1537-2995.2006.01003.x
60. Su Q, Zhang Y, Li Y, Cui Z, Chang S, Zhao P. Epidemiological investigation of the novel genotype avian hepatitis E virus and co-infected immunosuppressive viruses in farms with hepatic rupture haemorrhage syndrome, recently emerged in China. *Transbound Emerg Dis.* (2019) 66:776–84. doi: 10.1111/tbed.13082
61. Ducatez MF, Chen H, Guan Y, Muller CP. Molecular epidemiology of chicken anemia virus (CAV) in southeastern Chinese live birds markets. *Avian Dis.* (2008) 52:68–73. doi: 10.1637/8049-070407-Reg
62. Cardona C, Lucio B, O'Connell P, Jagne J, Schat KA. Humoral immune responses to chicken infectious anemia virus in three strains of chickens in a closed flock. *Avian Dis.* (2000) 44:661–7.
63. Brentano L, Lazzarin S, Bassi SS, Klein TA, Schat KA. Detection of chicken anemia virus in the gonads and in the progeny of broiler breeder hens with high neutralizing antibody titers. *Vet Microbiol.* (2005) 105:65–72. doi: 10.1016/j.vetmic.2004.09.019
64. Miller MM, Ealey KA, Oswald WB, Schat KA. Detection of chicken anemia virus DNA in embryonal tissues and eggshell membranes. *Avian Dis.* (2003) 47:662–71. doi: 10.1637/7007

Conflict of Interest: The authors declare that the research was conducted in the absence of any commercial or financial relationships that could be construed as a potential conflict of interest.

The handling editor AQ declared a past collaboration with the author PZ.

frontiers | Frontiers in Veterinary Science

ORIGINAL RESEARCH
published: 07 July 2022
doi: 10.3389/fvets.2022.847194

Establishment and Application of a Real-Time Recombinase Polymerase Amplification Assay for the Detection of Avian Leukosis Virus Subgroup J

Guanggang Qu[1], Yun Li[1,2], Zhongwei Zhao[3], Lizhong Miao[1], Feng Wei[1], Na Tang[1], Qingqing Xu[1], Venugopal Nair[4], Yongxiu Yao[4]* and Zhiqiang Shen[1,3]**

[1] Binzhou Animal Science and Veterinary Medicine Academy and UK-China Centre of Excellence for Research on Avian Diseases, Binzhou, China, [2] College of Veterinary Medicine, Shandong Agricultural University, Tai'an, China, [3] Shandong Lvdu Biotechnology Co., Ltd, Binzhou, China, [4] The Pirbright Institute and UK-China Centre of Excellence for Research on Avian Diseases, Guildford, United Kingdom

OPEN ACCESS

Edited by:
Rajeev Ranjan,
Indian Council of Agricultural Research (ICAR), India

Reviewed by:
Sabri Saeed Sanabani,
Clinical Hospital, Faculty of Medicine, University of São Paulo, Brazil
Sunil Bhausaheb Kokane,
Central Citrus Research Institute (ICAR), India

***Correspondence:**
Guanggang Qu
guanggangqu@163.com
Yongxiu Yao
yongxiu.yao@pirbright.ac.uk
Zhiqiang Shen
bzshenzq@163.com

Specialty section:
This article was submitted to Veterinary Infectious Diseases, a section of the journal Frontiers in Veterinary Science

Received: 01 January 2022
Accepted: 01 June 2022
Published: 07 July 2022

Citation:
Qu G, Li Y, Zhao Z, Miao L, Wei F, Tang N, Xu Q, Nair V, Yao Y and Shen Z (2022) Establishment and Application of a Real-Time Recombinase Polymerase Amplification Assay for the Detection of Avian Leukosis Virus Subgroup J. Front. Vet. Sci. 9:847194. doi: 10.3389/fvets.2022.847194

Avian leukosis caused by avian leukosis virus (ALV), belonging to the genus *Alpharetrovirus* of the family *Retroviridae*, is associated with benign and malignant tumors in hemopoietic cells in poultry. Although several methods have been developed for ALV detection, most of them are not suitable for rapid on-site testing due to instrument limitations, professional operators, or the low sensitivity of the method. Herein, we described the real-time recombinase polymerase amplification (RPA) assay for rapid detection of ALV subgroup J (ALV-J). The major viral structural glycoprotein gp85, highly specific for the subgroup, was used as the molecular target for the real-time RPA assay. The results were obtained at 38°C within 20 min, with the detection sensitivity of 10 copies/μl of standard plasmid pMD18-T-gp85 as the template per reaction. Real-time RPA was capable of ALV-J-specific detection without cross-reaction with other non-targeted avian pathogens. Of the 62 clinical samples tested, the ALV-positive rates of real-time RPA, PCR, and real-time PCR were 66.13% (41/62), 59.68% (37/62), and 67.74% (42/62), respectively. The diagnostic agreement between real-time RPA and real-time PCR was 98.39% (61/62), and the kappa value was 0.9636. The developed real-time ALV-J assay seems promising for rapid and sensitive detection of ALV-J in diagnostic laboratories. It is suitable for on-site detection, especially in a poor resource environment, thus facilitating the prevention and control of ALV-J.

Keywords: Avian Leukosis Virus Subgroup J, recombinase polymerase amplification assay, real-time RPA, rapid diagnosis, on-site

HIGHLIGHTS

- Establishment of the Real-Time Recombinase Polymerase Amplification (RPA) Method for Rapid Detection of Avian Leukosis Virus Subgroup J.
- The Specificity and Sensitivity (Detection Limit of the Assay Is 10 Copies/Reaction of Standard Plasmid) of the Optimized Real-Time RPA Assay Were Evaluated.
- Clinical Application Revealed More Sensitivity of the Real-Time RPA Assay Than the Conventional PCR and Had Good Consistency With Real-Time PCR, Suggesting the Potential for Clinical Diagnosis.

INTRODUCTION

Avian leukosis virus (ALV) is the avian leukosis/sarcoma virus that causes various tumors in chickens (1). It is divided into endogenous and exogenous viruses. The exogenous viruses infecting chickens are classified into five major subgroups, namely, A–D, and J, based on the envelope glycoprotein (gp85) identified by virus serum neutralization tests (1, 2). The ALV subgroup J (ALV-J) is a recombinant between exogenous ALVs and the family of endogenous avian retroviruses (3). The most common subgroups identified in the field are A, B, and J. ALV-J is spread by horizontal and vertical transmission and causes myeloid leukosis and other tumors in meat-type and egg-type chickens (1, 2), resulting in significant economic losses due to increased mortality, decreased productivity, and the cost for eradication. There is no commercial vaccine to prevent avian leukosis (1); thus, eradication of ALV from the breeding flocks is the primary method to control avian leucosis (4, 5). Although ALV-J has been eradicated in most Western countries, it is a major challenge for the poultry industry in Asian countries, including China (4, 6, 7).

Avian leukosis virus (ALV) eradication is based on regular monitoring and strictly eliminating the infected birds. Presently, the commonly used methods for detecting ALV include virus isolation and identification, enzyme-linked immunosorbent assay (ELISA), real-time PCR (RT-PCR), conventional PCR, immunofluorescence assay (IFA), and quantitative competitive reverse-transcription PCR (QC-RT-PCR) (8, 9). The method of virus isolation in cell culture is time-consuming as it requires a minimum of 7 days to obtain results (9–11). Antigen capture ELISA (AC-ELISA) plays a major role in eradicating ALVs (8). However, ELISA detects group-specific antigen p27 but cannot distinguish between endogenous and exogenous ALV (8, 12). Thus, RT-PCR and immunofluorescence methods for antigen detection and identification of endogenous and exogenous ALVs have been developed (8), but these tests require complicated and expensive instruments, which are not suitable for field detection of ALVs (8, 9).

In recent years, isothermal amplification methods have attracted increasing attention because of their ease of use, short duration, and independence of specialized equipment for rapid diagnosis (13). Among the isothermal amplification methods, recombinase polymerase amplification (RPA), an isothermal amplification technology, was developed as an alternative to PCR assay to amplify nucleic acids under isothermal conditions (14, 15). The RPA assay depends on several enzymes and proteins at a constant temperature, such as recombinase, single-strand binding protein, Exonuclease III, and strand displacing DNA polymerase to facilitate gene amplification (16). The recombinase binds to the primer to form a complex and searches for the homologous sequences in the double-stranded DNA. Subsequently, the chain exchange reaction is initiated to form and initiate DNA synthesis, and the target region on the template is amplified exponentially. The replaced DNA strand binds to the single-stranded binding protein, preventing further replacement (17). One significant advantage of RPA is that the amplifications could be detected by agarose gel electrophoresis (AGE) and a real-time fluorescence detection platform (18) or visualized by a lateral flow dipstick (LFD) assay (19). Moreover, RPA has the advantage of amplification at a low temperature (37–42°C), with a 20-min reaction time, which is considerably shorter than many isothermal techniques. Different types of RPA-based assays have been successfully used in the detection of pathogens in plants (20, 21), animals (19, 22, 23), and humans (24–26). Thus, the present study aimed to establish a real-time RPA assay with an exo probe for rapid, specific, and sensitive detection of ALV-J in the field.

TABLE 1 | Primers and probe of real-time RPA.

Name	Sequence (5′–3′)	Location
ALV-J-F1	CAATCATGGACGATGGTAAGTCCAATAAAC	726–755
ALV-J-F2	RTTGCGTGACTTCATAGVAAAATGGAAAAG	666–695
ALV-J-F3	CTATGTCAACCAATCATGGACGATGGTAAG	717–746
ALV-J-R1	AGCCCTGTCCCCACAAATCAAGAAAATACC	1,021–1,050
ALV-J-R2	ATTYTGTCCCRTTRCTGTAYCCCGCTGACC	863–892
ALV-J-R3	CAAGCCCTGTCCCCACAAATCAAGAAAATA	1,023–1,052
ALV-J-R4	CGAAGGTAAACCCATATGCATAATAATTCCATTC	934–963
ALV-J-R5	CCTCCCAAGGCATTACGCGGGATGCCTTGC	1,053–1,082
ALV-J-probe	TAGATATTGTGGATTCACCAGYAACGAGAC[FAM-dT][THF]G[BJQ1-dT]TAYTATMGAGGGRAC-C3 Spacer	780–828

MATERIALS AND METHODS

Virus Strains and Clinical Samples

Archived ALV viral DNA from different subgroups, namely, J (ALV-J), A (ALV-A), B (ALV-B), D (ALV-D), and K (ALV-K), preserved in the key laboratory of Shandong Binzhou Animal Science and Veterinary Medicine Academy, were used in this study. Various batches of commercial lyophilized live vaccines include Newcastle disease bivalent vaccines (Batch No. 007, 142, 152, and 063), Newcastle disease live vaccines (Batch No. 145 and 179), live pox vaccines (Batch No. 134 and 147), chicken infectious bursal disease vaccines (Batch No. 118 and 124), and live duck plague vaccines (Batch No. 153 and 177). IBDV, IBV, ILTV, NDV, and AIV H9 viruses were isolated from the clinical samples. The suspected ALV samples were collected from the chicken farms in Shandong Province.

Viral Nucleic Acid Extraction

An equivalent of 50 mg of each tissue sample was homogenized in 200 μl phosphate-buffered saline (PBS), and the supernatant was collected by centrifugation at 3,000 g, 4°C for 10 min for DNA extraction. Vaccine samples were resuspended in 1 ml of PBS for DNA/RNA extraction. DNA/RNA was extracted using Axygen® AxyPrep™ Body Fluid Viral DNA/RNA Miniprep Kit (Axygen BioScience, Inc., USA), according to the manufacturer's instructions. The RNA extracted from the RNA virus vaccines was reverse transcribed into cDNA (Life Technologies, USA). All templates were stored at −80°C until further analysis.

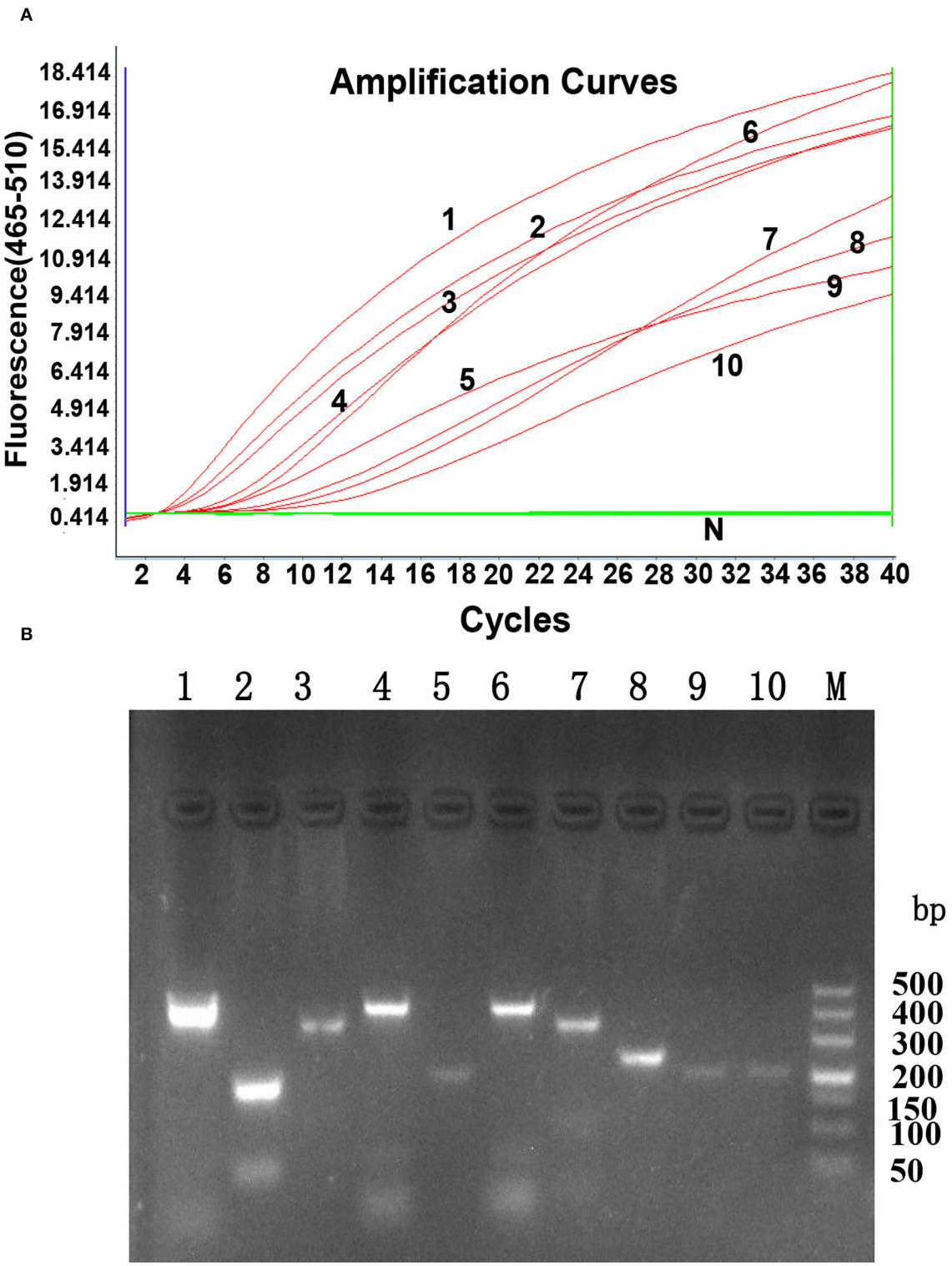

FIGURE 1 | The generated amplification plot for different combinations of primers and probes in real-time RPA. **(A)**. Amplification curve by LightCycler 480 Instrument II. N: Negative control; 1: ALV-J F1-R1; 2: ALV-J F1-R2; 3: ALV-J F1-R5; 4: ALV-J F2-R1; 5: ALV-J F2-R2: 6: ALV-J F2-R3; 7: ALV-J F3-R3; 8: ALV-J F3-R4; 9: ALV-J F3-R5; 10: ALV-J F3-R1. Reactions were scored positive when the change in fluorescence exceeded 1.0 units. **(B)**. Nucleic acid detection on agarose gel electrophoresis. 1: ALV-J F1-R1; 2: ALV-J F1-R2; 3: ALV-J F1-R5; 4: ALV-J F2-R1; 5: ALV-J F2-R2: 6: ALV-J F2-R3; 7: ALV-J F3-R3; 8: ALV-J F3-R4; 9: ALV-J F3-R5; 10: ALV-J F3-R1; M: DL500 DNA marker.

TABLE 2 | Screening of the best real-time RPA primer pairs.

No.	Primer pairs	Ct	Fluorescence signal reading (wavelength: 465–510 nm)
1	ALV-J F1-R1	5.12	18.032
2	ALV-J F1-R2	5.78	16.884
3	ALV-J F1-R5	5.85	16.509
4	ALV-J F2-R1	7.56	18.759
5	ALV-J F2-R2	8.24	11.259
6	ALV-J F2-R3	6.92	16.884
7	ALV-J F3-R3	11.05	14.259
8	ALV-J F3-R4	9.89	12.759
9	ALV-J F3-R5	12.54	10.134
10	ALV-J F3-R1	6.35	8.259

RPA Primers and Exo Probe Designing

The genome sequences of ALV-J (GenBank number: Z46390.1, KP284572.1, KC149972.1, KC149971.1, FJ216405.1, AF307949.1, and AF307950.1), ALV-A (GenBank number: M37980.1), ALV-B (GenBank number: AF052428.1), ALV-C (GenBank number: J02342.1), ALV-D (GenBank number: D10652.1), and ALV-E strains (GenBank number: DQ412728.1 and DQ412729.1) were retrieved from GenBank and aligned using DNAStar software (DNASTAR, Madison, USA). The sequence of ALV-J gp85 had a low homology to that of other exogenous subgroups (3), making it an ideal molecular target for the real-time RPA. The design of the primers and the probe of RPA is crucial for the specificity and amplification efficacy. Since there is no optimal design software available, all the primers and the probe of RPA were designed using Primer Premier 5.0, following the instructions of TwistDX. To avoid the formation of the primer's hairpin structure and dimers, the RPA primer design should avoid multiple guanines at the 5' end and ensure that the GC content is 30–70%. Furthermore, to ensure the sensitivity of the detection and the rapid progress of the reaction, the length of the RPA product was set to 100–200 bp.

The forward and reverse primers and the exo probe were designed according to the gp85 sequences following the RPA manufacturer's guidelines (TwistDx. Cambridge, UK). The primers are listed in **Table 1**. The primers and the probe were analyzed and screened using NCBI Primer-Blast to ensure specificity. All primers and the probe were synthesized by Sangon (Shanghai, China).

Construction of Standard DNA Plasmid

ALV-J-gp85 gene was amplified by PCR using forward primer 5'-GACTTCATAGVAAAATGGAAAAG-3' and reverse primer 5'-CTGTCCCCACAAATCAAGAAAATA-3'. The standard DNA plasmid pMD18-T-gp85 was obtained by cloning purified gp85 PCR product into plasmid pMD18-T according to the manufacturer's instructions for pMD18-T Vector Cloning Kit (Takara Bio Inc., Japan). The concentration of the constructed plasmids was measured on a NanoDrop 2000c spectrophotometer (Thermo Scientific, USA) at 260 nm. The copy number of the plasmid was calculated using the following formula: Number of copies = (amount of target DNA in nanograms) × Avogadro's number (6.0221×10^{23}) / length of DNA amplicon in base pair (bp) × 660 × (1×10^9) (27). The generated DNA standard was used as an initial template in the sensitivity analysis.

Real-Time RPA Assay

The exo-RPA reaction was performed in 50 μl using a TwistAmp™ exo kit (TwistDX, UK). A master mixture was prepared according to the manufacturer's instructions. The mixture contained 25 μl 2× reaction buffer, 8.2 μl dNTPs (1.8 μM), 5 μl 10× Probe E-mix, 2.1 μl forward Primer (10 μM), 2.1 μl reverse primer (10 μM), 0.6 μl TwistAmp™ exo probe (10 μM), 2.5 μl 20× Core Reaction Mix, 1 μl 50× EXO. Subsequently, 2.5 μl of 280 mM magnesium acetate and 1 μl nucleic acid were added to the mixture to initiate the amplification reaction on the LightCycler 480 Instrument II (Roche Diagnostics Corporation, IN, USA) for 40 cycles at 38°C for 20 min (30 s/cycle).

Sensitivity and Specificity Analysis

To determine the sensitivity of the RPA assay, 10-fold serial dilutions of pMD18-T-gp85 standard plasmid ranging from 10^6 to 10^0 copies/μl were tested. All the samples and positive/negative controls were evaluated in duplicate. The specificity of the assay was assessed using other viral pathogens of chicken. A panel of viruses, including ALV-J, ALV-A, ALV-B, ALV-D, ALV-K, IBDV, ILTV, IBV, NDV, and AIV H9, were significant pathogens of poultry and hence utilized in the test. Also, the positive and negative controls were tested simultaneously. The RNA extracted from RNA viruses, such as IBDV, IBV, NDV, and AIV H9, was reverse transcribed into cDNA (Life Technologies) for subsequent RPA test.

Conventional PCR

ALV-J conventional PCR was developed for the detection of ALV-J in a 25 μl reaction using primers PF: 5'-CGGAGAAGACACCCTTGCT-3'and JR: 5'-CGAACCAAAGGTAACACACG-3', as described previously [Gao et al., (8)]. Briefly, the reaction mixture consisted of 12.5 μl of 2× Premix Taq (TaKaRa, China), 2 μl forward primer PF (10 μM) and 1 μl reverse primer JR (10 μM), 2 μl of sample DNA, and the appropriate volume of DNase-free water.

The PCR reaction was as follows: initial denaturation at 94°C for 5 min, followed by 30 cycles at 94°C for 30 s for denaturation, 56°C for 30 s for annealing, and 72°C for 1 min for extension, and a final extension at 72°C for 1 min. To confirm the results, all specific fragments amplified from the clinical samples by RPA and conventional PCR were purified using a DNA gel extraction kit (Omega Bio-Tek, Inc., GA, USA) and sequenced by Sangon.

Reproducibility of the RPA Assay

The reproducibility of the assay was confirmed using three dilutions of standard plasmid pMD18-T-gp85. To determine the interassay variations, each sample was tested in triplicate using 2 μl of each plasmid per reaction. The assay was also repeated three times to evaluate the intraassay variations. The coefficients

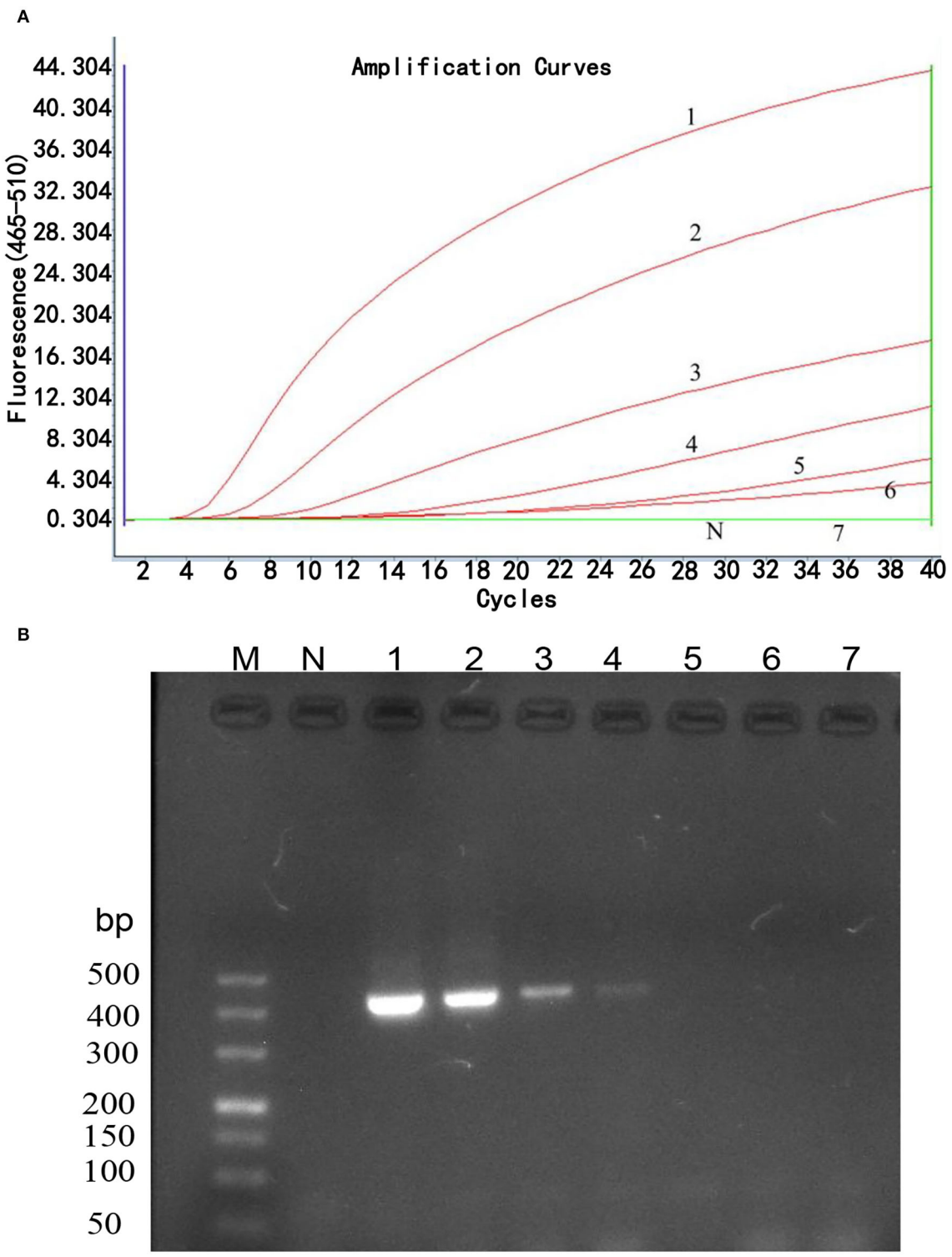

FIGURE 2 | Sensitivity analysis of real-time RPA assay. Serial dilutions of plasmid pMD18-gp85 DNA (10^6-10^0 copies corresponding to curves 1–7) were used as the templates for real-time RPA reactions. **(A)**. Sensitivity analysis by LightCycler 480 Instrument II. The detection limit was 10 copies of DNA/reaction for the real-time RPA assay (curve 6). Reactions were scored positive when the change in fluorescence exceeded 1.0 units. Curve N used nuclease-free water as a negative control. **(B)**. Sensitivity analysis by electrophoresis. M: DL500 DNA marker; 1: 1×10^6 copies/μl; 2: 1×10^5 copies/μl; 3: 1×10^4 copies/μl; 4: 1×10^3 copies/μl; 5: 1×10^2 copies/μl; 6: 1×10^1 copies/μl; 7: 1×10^0 copies/μl.

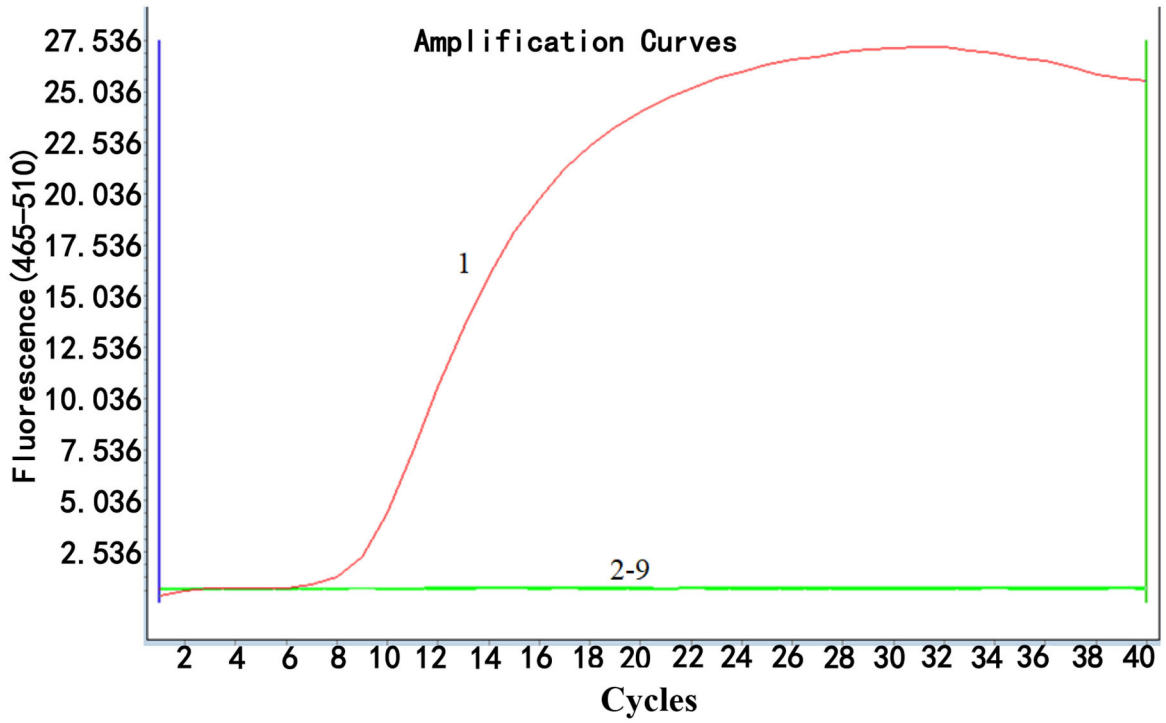

FIGURE 3 | Specificity analysis of real-time RPA assay. Only DNA from ALV-J infected samples was positively amplified (curve 1), while no amplification of other DNA or RNA viruses (cDNA) (curves 2–9 were from the following viruses: ALV-A, ALV-B, ALV-D, ALV-K, IBDV, ILTV, IBV, NDV, and H9, respectively) was observed. Nuclease-free water was used for curve N as a negative control. The results suggested that the developed real-time RPA assay was highly specific. Reactions were scored positive when the change in fluorescence exceeded 1.0 units.

of variation (CVs) for Ct values of the intra- and interassay comparisons were determined.

Real-Time RPA Assay Validation

To validate the developed assay, 50 clinical samples collected from several poultry flocks and 12 different batches of poultry lyophilized vaccines, randomly purchased from the licensed companies in China, were examined. RPA was also performed concurrently with conventional PCR and real-time PCR, as described previously (8, 9). The total agreement of RPA assay with conventional PCR and real-time PCR was verified. The calculation of the kappa value has been reported previously (28).

RESULTS

Real-Time RPA Primer Screening

According to the principles of RPA primer design, three forward primers, five reverse primers, and one RPA exo probe were designed, as shown in **Table 1**. The oligonucleotide backbone of the probe includes an inverse arrangement of fluorophore [6-carboxyfluorescein (FAM)], quencher [black hole quencher 1 (BHQ-1)], internal abasic site mimic [tetrahydrofuran spacer (THF)], and a 3'-polymerase extension blocking group C3-spacer. The primers and probe were assessed using the TwistAmp exo kit according to the manufacturer's instructions. All ten primer sets successfully generated the amplification curve within 20 min, as shown in **Figure 1**. The best primer pair ALV-J-F1/R1 with the highest amplification efficiency was identified and used for further analysis. The data are shown in **Table 2**.

Sensitivity of the Real-Time RPA Assay

The sensitivity of the real-time RPA assay was assessed by testing 10-fold serial dilutions of DNA standards ranging from 1×10^6 to 1×10^0 copies/μl. The results showed (**Figure 2A**) that the detection limit of the real-time RPA assay was 10 copies/μl of *gp85* gene per reaction by exo probe on a LightCycler 480 Instrument II. In contrast, the detection limit of the real-time RPA assay was 10^3 copies/μl of *gp85* gene per reaction, as analyzed by AGE and ethidium bromide staining (**Figure 2B**). The results demonstrated that the sensitivity of the established real-time RPA assay with an exo probe was 100 times higher than that of the real-time RPA assay.

Specificity of Real-Time RPA

The specificity of real-time RPA was determined by examining the ability of the method to detect ALV-J and differentiate it from ALV-A, ALV-B, ALV-D, ALV-K, and other common avian viruses, namely, IBDV, ILTV, IBV, NDV, and H9. As shown in **Figure 3**, the fluorescence signal was only detected from ALV-J, while no fluorescence signal was observed from other viruses, demonstrating high specificity of the

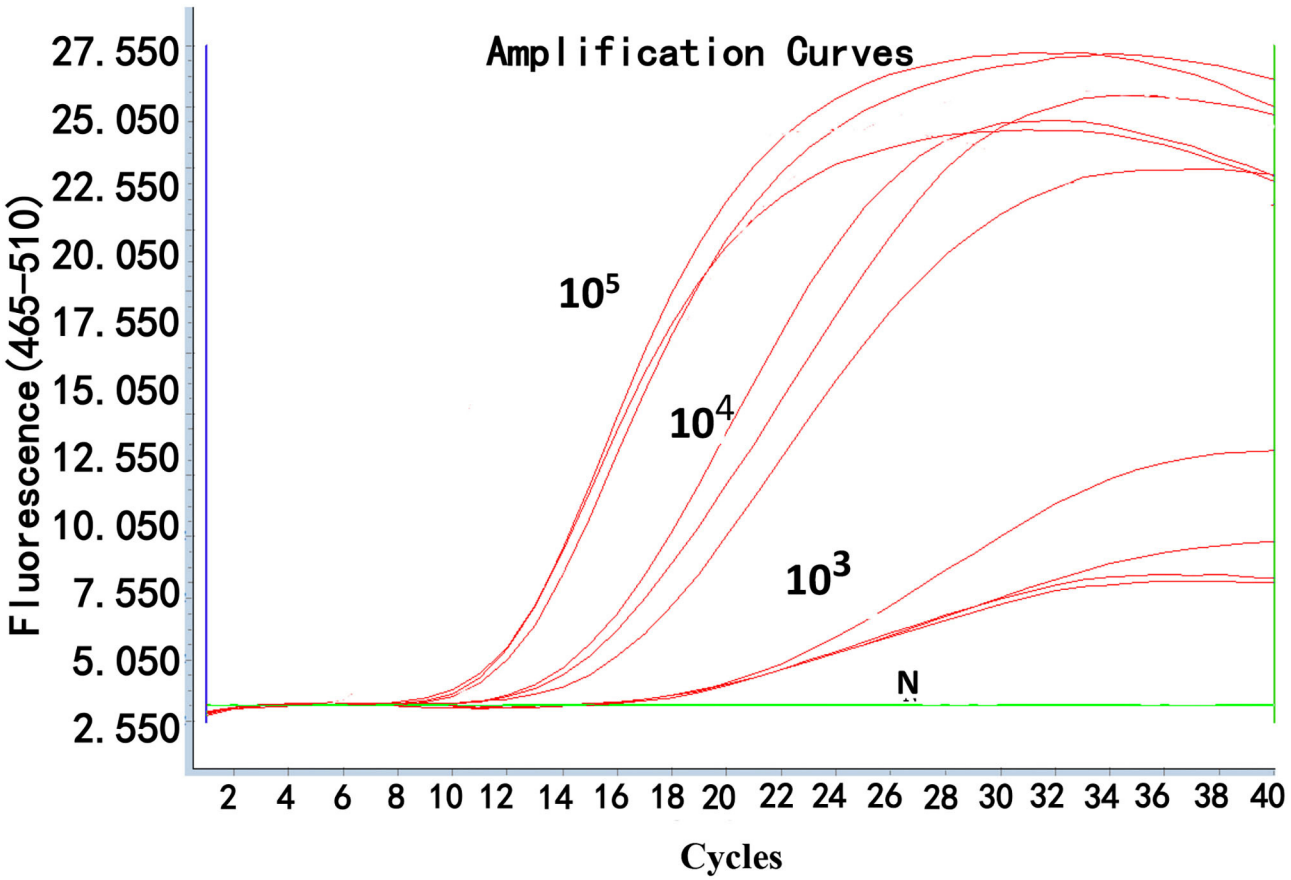

FIGURE 4 | Reproducibility of real-time RPA.

TABLE 3 | Intrareproducibility and interreproducibility assay.

Dilution of plasmid	Interassay					Intraassay				
	Ct value				CV%	Ct value				CV%
	Assay 1	Assay 2	Assay 3	Average SD		Assay 1	Assay 2	Assay 3	Average SD	
10^5	9.87	9.60	9.89	0.16	1.65%	9.64	9.15	9.51	0.25	2.69%
10^4	11.59	12.18	11.72	0.31	2.62%	11.49	11.56	11.42	0.07	0.61%
10^3	17.45	17.51	17.55	0.05	0.29%	17.61	17.78	17.67	0.09	0.49%

real-time RPA assay for ALV-J detection without cross-reactions with other subgroups of ALVs and other common avian viruses.

Reproducibility of Real-Time RPA

To determine the reproducibility of real-time RPA, the interassay and intraassay of reproducibility were assessed using testing standard plasmids (10^5, 10^4, and 10^3 copies/μl) three times independently (**Figure 4**). Also, the SDs were calculated. The inter-CV and intra-CV values ranged from 0.05 to 0.16% and 0.49 to 2.69%, respectively, indicating that the assay was highly reproducible (**Table 3**).

Comparison of Real-Time RPA Assay, Conventional PCR Assay, and Real-Time PCR Assay in Clinical Samples and Commercial Vaccine Detection

The clinical performance of the real-time RPA assay was evaluated by testing 50 suspected clinical samples and 12 batches of commercial vaccines and compared to conventional PCR and real-time PCR methods. As shown in **Table 4**, 39 of these clinical samples were ALV-positive by real-time RPA method, 35 were ALV-positive by conventional PCR method, and 40 samples were ALV-positive by real-time PCR method. The commercial vaccine test results showed that 2 samples were ALV-positive and 10

TABLE 4 | Agreement between real-time RPA detection, real-time PCR, and conventional PCR.

Sr. No	Sample	Real-time RPA	Real-time PCR	Conventional PCR
1	Heart	+	+	+
2	Heart	+	+	+
3	Heart	−	+	−
4	Heart	−	−	−
5	Heart	+	+	−
6	Heart	+	+	+
7	Heart	+	+	+
8	Heart	+	+	+
9	Heart	+	+	+
10	Heart	+	+	+
11	Heart	+	+	+
12	Heart	+	+	+
13	Heart	+	+	+
14	Spleen	−	−	−
15	Spleen	−	−	−
16	Spleen	−	−	−
17	Spleen	+	+	+
18	Spleen	+	+	−
19	Spleen	+	+	+
20	Spleen	+	+	+
21	Spleen	+	+	+
22	Liver	−	−	−
23	Liver	−	−	−
24	Liver	−	−	−
25	Liver	+	+	+
26	Liver	−	−	−
27	Liver	+	+	+
28	Liver	+	+	+
29	Liver	−	−	−
30	Liver	+	+	−
31	Liver	+	+	+
32	Liver	+	+	+
33	Liver	+	+	+
34	Liver	+	+	+
35	Bursa	+	+	+
36	Bursa	+	+	+
37	Bursa	+	+	+
38	Bursa	+	+	−
39	Bursa	+	+	+
40	Bursa	+	+	+
41	Bursa	+	+	+
42	Bursa	+	+	+
43	Kidney	+	+	+
44	Kidney	+	+	+
45	Kidney	+	+	+
46	Kidney	+	+	+
47	Kidney	+	+	+
48	Kidney	+	+	+
49	Kidney	+	+	+
50	Kidney	−	−	−
51	NDV Vaccine-007	−	−	−
52	NDV Vaccine-142	+	+	+
53	NDV Vaccine-152	−	−	−
54	NDV Vaccine-063	−	−	−
55	NDV Vaccine-145	−	−	−
56	NDV Vaccine−179	−	−	−
57	Duck plague-153	−	−	−
58	Duck plague-177	+	+	+
59	Fowlpox live vaccine-134	−	−	−
60	Fowlpox live vaccine-147	−	−	−
61	IBD vaccine-118	−	−	−
62	IBD vaccine-124	−	−	−

vaccine samples were negative, as assessed by the real-time RPA method (**Figure 5A**), which was consistent with the findings of conventional PCR (**Figure 5C**) and real-time PCR (**Figure 5B**). The ALV-positive rates of real-time RPA, PCR, and real-time PCR were 66.13% (41/62), 59.68% (37/62), and 67.74% (42/62), respectively. Among the 62 samples, only 1 tested negative for ALV by real-time RPA method but was positive by real-time PCR method. The diagnostic agreement between real-time RPA and real-time PCR was 98.39% (61/62) (**Table 4**), and the kappa value was 0.9636. Therefore, based on these test results, it could be inferred that the real-time RPA assay of ALV-J is more sensitive than the conventional PCR assay and has good consistency with real-time PCR, indicating its potential for clinical diagnosis.

DISCUSSION

Since 2008, ALV-J has caused severe economic losses owing to the induction of various malignant tumors and other reproductive problems in birds in China (8). Due to the high level of vertical and horizontal transmission of ALV-J and the lack of effective vaccines and drugs to prevent this disease (4, 29, 30), it is essential to improve the efficiency of eradication and accelerate the elimination process.

Real-time RPA assay has been widely utilized to detect human and animal pathogens (31, 32). The current study describes specific, sensitive, and rapid ALV-J methods based on exo probe real-time RPA assay, which provides accurate results in 20 min at the isothermal conditions without elaborate methods for the detection of the amplified productions (33). Although RPA has the advantage of rapid reaction, it still needs the laboratory operation step of nucleic acid extraction when used in the field. The nucleic acid quick extraction reagents currently available in the market are easy to operate, and the extraction can be completed within 5 min of heating. To better apply this method to rapid on-site detection, we will combine the RPA method with the nucleic acid direct extraction method in the next step. The entire detection process would require only 25 min, providing rapid on-site detection.

Since the ALV-J *gp85* gene shows approximately 40% identity with the corresponding regions of other exogenous ALV

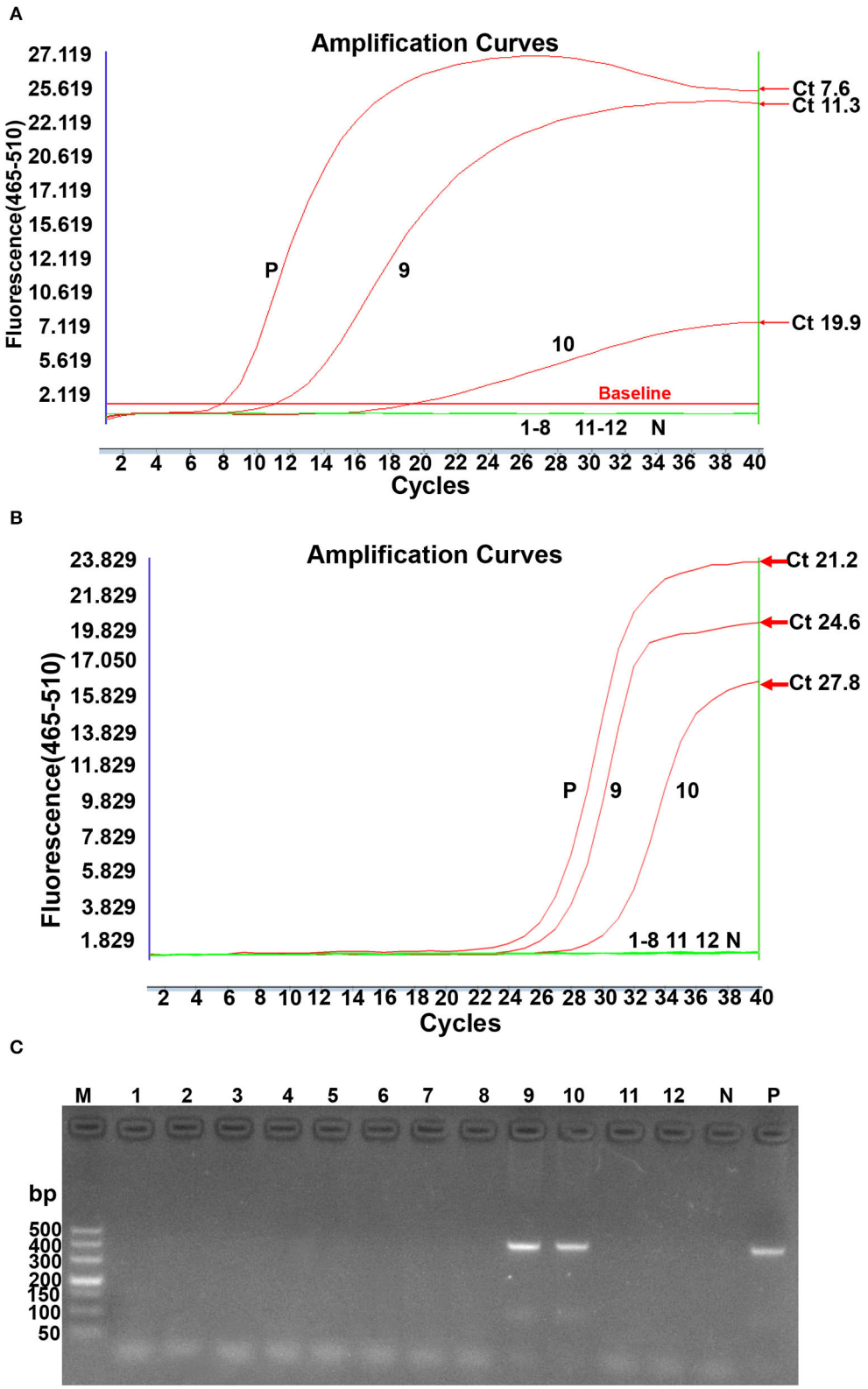

FIGURE 5 | ALV subgroup J contamination of lyophilized vaccines detected by real-time RPA, real-time PCR, and conventional PCR simultaneously. **(A)**. Real-time RPA detection. N: Negative; P: Positive; 1–8 lanes: Newcastle disease bivalent vaccines (Batch No. 007, 142, 152, and 063), Newcastle disease live vaccines (Batch

(Continued)

FIGURE 5 | No. 145 and 179), live duck plague vaccines (Batch No. 153 and 177); 9: fowl pox live vaccine 134; 10: fowl pox live vaccine 147; 11–12: infectious chicken bursa (Batch No. 118 and 124). **(B)**. Real-time PCR detection. N: Negative; P: Positive: 1∼8 lanes: Newcastle disease bivalent vaccines (Batch No: 007, 142, 152, and 063), Newcastle disease live vaccines (Batch No: 145 and 179), Live duck plague vaccines (Batch No: 153 and 177); 9: Fowlpox live vaccine 134; 10: Fowlpox live vaccine 147; 11-12: chicken infectious bursa (Batch No: 118 and 124). Reactions were scored positive when the change in fluorescence exceeded 1.0 units. **(C)**. Conventional PCR detection. M: DL500 DNA marker; 1∼8 lanes: Newcastle disease bivalent vaccines (Batch No: 007, 142, 152, and 063), Newcastle disease live vaccines (Batch No: 145 and 179), Live duck plague vaccines (Batch No: 153 and 177); 9: Fowlpox live vaccine 134; 10: Fowlpox live vaccine 147; 11–12: chicken infectious bursa (Batch No: 118 and 124); N: Negative; P: Positive.

subgroups (3). The ALV-J real-time RPA primers and probes were designed based on the sequence alignment of *gp85* genes with different strains of the ALV-J subgroup. The specificity results showed that the ALV-J real-time RPA did not amplify other exogenous subgroups (ALV-A, ALV-B, ALV-B, and ALV-K) and other common avian viruses. Therefore, this ALV-J real-time RPA using ALV-J *gp85* as the target gene showed good subgroup specificity. We also established a highly sensitive subgroup-specific real-time RPA assay for ALV-J, which can detect 10 copies/reaction. The validation of clinical samples and commercial vaccines demonstrated that the real-time RPA assay was practical in the laboratory and more sensitive than the conventional PCR assay. Additional studies are required to test more clinical samples from natural outbreaks and confirm that the RPA assay has potential for epidemiological surveillance and facilitates the eradication of ALV-J in the poultry industry and vaccine companies. Although in the current study, a Roche LightCycler 480 Instrument was used to develop RPA, the assay can also realize on-site diagnosis of clinical samples using a point-of-care (POC) instrument, Thermostatic Fluorescent Biosensor (Xianda, China) with fluorescence detection in the FAM channel (excitation 470 nm and detection 520 nm). This equipment is designed for cost-efficiency, accessibility, and the potential for scale-up. Although the sensitivity of the real-time RPA is still lower than the limit of real-time PCR, the advantages of this assay are obvious.

In summary, a rapid, reliable, simple real-time RPA assay has been developed for the detection of ALV-J. This assay is promising for specific and sensitive detection of ALV-J in diagnostic laboratories and suitable for on-site detection, deeming it a robust diagnostic tool to aid in the detection of ALV-J and subsequently decrease the rate of ALV-J transmission, thus reducing the economic impact on the poultry drastically.

DATA AVAILABILITY STATEMENT

The datasets presented in this study can be found in online repositories. The names of the repository/repositories and accession number(s) can be found in the article/supplementary material.

ETHICS STATEMENT

The animal study was reviewed and approved by the Animal Care and Use Committee of Binzhou Animal Science and Veterinary Medicine Academy.

AUTHOR CONTRIBUTIONS

GQ and YL designed the primers and probes and optimized the reaction conditions and wrote the manuscript. GQ, YY, and ZS designed the experiments and revised the manuscript. LM, FW, and NT collected the clinic samples. ZZ and QX tested the diagnostic method. VN reviewed the manuscript and polished the English. All authors contributed to the article and approved the submitted version.

FUNDING

This work was supported by the National Natural Science Foundation of China (grant No. 31761133002), the Biotechnology and Biological Sciences Research Council (BBSRC) Newton Fund grant BB/R012865/1, BBSRC Newton Fund Joint Centre Awards on UK-China Centre of Excellence for Research on Avian Diseases and 2017 China-UK Double-Hundred Talent Plan of Shandong Province.

ACKNOWLEDGMENTS

This work was supported by the National Natural Science Foundation of China (Grant No. 31761133002), the Biotechnology and Biological Sciences Research Council (BBSRC), Newton Fund grant BB/R012865/1, BBSRC Newton Fund Joint Centre Awards on UK-China Centre of Excellence for Research on Avian Diseases, and 2017 China-UK Double-Hundred Talent Plan of Shandong Province.

REFERENCES

1. Li N, Xu B, Dong W, Qiao S, Lee LF, Zhang HM, et al. Detection and localization of naturally transmitted avian leukosis subgroup J virus in egg-type chickens by *in situ* PCR hybridization. *J Vet Med A Physiol Pathol Clin Med.* (2007) 54:553–8. doi: 10.1111/j.1439-0442.2007.01008.x
2. Venugopal K, Smith LM, Howes K, Payne LN. Antigenic variants of J subgroup avian leukosis virus: sequence analysis reveals multiple changes in the env gene. *J Gen Virol.* (1998) 27:S91–2. doi: 10.1080/03079459808419307
3. Bai J, Howes K, Payne LN, Skinner MA. Sequence of host-range determinants in the env gene of a full-length, infectious proviral clone of exogenous avian leukosis virus HPRS-103 confirms that it represents a new subgroup (designated J). *J Gen Virology.* (1995) 76:181–7. doi: 10.1099/0022-1317-76-1-181
4. Venugopal K. Avian leukosis virus subgroup J: a rapidly evolving group of oncogenic retroviruses. *Res Vet Sci.* (1999) 67:113. doi: 10.1053/rvsc.1998.0283

5. Feng M, Zhang X. Immunity to avian leukosis virus: where are we now and what should we do? *Front Immunol.* (2016) 7:624. doi: 10.3389/fimmu.2016.00624
6. Li H, Tan M, Zhang F, Ji H, Zeng Y, Yang Q, et al. Diversity of avian leukosis virus subgroup J in local chickens, Jiangxi, China. *Sci Rep.* (2021) 11:4797. doi: 10.1038/s41598-021-84189-7
7. Xu M, Hang F, Qian K, Shao H, Ye J, Qin A. Chicken hepatomegaly and splenomegaly associated with novel subgroup J avian leukosis virus infection. *BMC Vet Res.* (2022) 18:32. doi: 10.1186/s12917-022-03139-1
8. Gao Q, Yun B, Wang Q, Jiang L, Zhu H, Gao Y, et al. Development and application of a multiplex PCR method for rapid differential detection of subgroup A, B, and J avian leukosis viruses. *J Clin Microbiol.* (2014) 52:37–44. doi: 10.1128/JCM.02200-13
9. Qin L, Gao Y, Ni W, Sun M, Wang Y, Yin C, et al. Development and application of real-time PCR for detection of subgroup J avian leukosis virus. *J Clin Microbiol.* (2013) 51:149–54. doi: 10.1128/JCM.02030-12
10. Smith LM, Brown SR, Howes K, Mcleod S, Payne LN. Development and application of polymerase chain reaction (PCR) tests for the detection of subgroup J avian leukosis virus. *Virus Res.* (1998) 54:87–98. doi: 10.1016/S0168-1702(98)00022-7
11. García M, El-Attrache J, Riblet SM, Lunge VR, Fonseca ASK, Villegas P, et al. Development and application of reverse transcriptase nested polymerase chain reaction test for the detection of exogenous avian leukosis virus. *Avian Dis.* (2003) 47:41–53. doi: 10.1637/0005-2086(2003)047[0041:DAAORT]2.0.CO;2
12. Yun B, Li D, Zhu H, Liu W, Qin L, Liu Z, et al. Development of an antigen-capture ELISA for the detection of avian leukosis virus p27 antigen. *J Virol Methods.* (2013) 187:278–83. doi: 10.1016/j.jviromet.2012.11.027
13. Wang JC, Liu LB, Han QA, Wang JF, Yuan WZ. An exo probe-based recombinase polymerase amplification assay for the rapid detection of porcine parvovirus. *J Virol Methods.* (2017) 248:145–7. doi: 10.1016/j.jviromet.2017.06.011
14. Abd El Wahed A, El-Deeb A, El-Tholoth M, Abd El Kader H, Ahmed A, Hassan S, et al. A portable reverse transcription recombinase polymerase amplification assay for rapid detection of foot-and-mouth disease virus. *PLoS ONE.* (2013) 8:e71642. doi: 10.1371/journal.pone.0071642
15. Xia X, Yu Y, Weidmann M, Pan Y, Yan S, Wang Y. Rapid detection of shrimp white spot syndrome virus by real time, isothermal recombinase polymerase amplification assay. *PLoS ONE.* (2014) 9:e104667. doi: 10.1371/journal.pone.0104667
16. El-Tholoth M, Branavan M, Naveenathayalan A, Balachandran W. Recombinase polymerase amplification-nucleic acid lateral flow immunoassays for newcastle disease virus and infectious bronchitis virus detection. *Mol Biol Rep.* (2019) 46:6391–7. doi: 10.1007/s11033-019-05085-y
17. Li J, Macdonald J, von Stetten F. Correction: review: a comprehensive summary of a decade development of the recombinase polymerase amplification. *Analyst.* (2020) 145:1950–60. doi: 10.1039/C9AN90127B
18. Yang Y, Qin X, Wang G, Zhang Y, Shang Y, Zhang Z. Development of a fluorescent probe-based recombinase polymerase amplification assay for rapid detection of orf virus. *Virol J.* (2015) 12:206. doi: 10.1186/s12985-015-0440-z
19. Yang Y, Qin X, Zhang X, Zhao Z, Zhang W, Zhu X, et al. Development of real-time and lateral flow dipstick recombinase polymerase amplification assays for rapid detection of goatpox virus and sheeppox virus. *Virol J.* (2017) 14:131. doi: 10.1186/s12985-017-0792-7
20. Ghosh DK, Kokane SB, Kokane AD, Warghane AJ, Motghare MR, Bhose S, et al. Development of a recombinase polymerase based isothermal amplification combined with lateral flow assay (HLB-RPA-LFA) for rapid detection of "Candidatus Liberibacter asiaticus". *PloS ONE.* (2018) 13:e0208530. doi: 10.1371/journal.pone.0208530
21. Ghosh DK, Kokane SB, Gowda S. Development of a reverse transcription recombinase polymerase based isothermal amplification coupled with lateral flow immunochromatographic assay (CTV-RT-RPA-LFICA) for rapid detection of Citrus tristeza virus. *Sci Rep.* (2020)10:20593. doi: 10.1038/s41598-020-77692-w
22. Liljander A, Yu M, O'Brien E, Heller M, Nepper JF, Weibel Db, et al. Field-Applicable recombinase polymerase amplification assay for rapid detection of mycoplasma capricolum subsp capripneumoniae. *J Clin Microbiol.* (2015) 53:2810–5. doi: 10.1128/JCM.00623-15
23. Amer HM, Abd El Wahed A, Shalaby MA, Almajhdi FN, Hufert FT, Weidmann M, et al. New approach for diagnosis of bovine coronavirus using a reverse transcription recombinase polymerase amplification assay. *J Virol Methods.* (2013) 193:337–40. doi: 10.1016/j.jviromet.2013.06.027
24. Crannell ZA, Rohrman B, Richards-Kortum R. Quantification of HIV-1 DNA using real-time recombinase polymerase amplification. *Anal Chem.* (2014) 86:5615–9. doi: 10.1021/ac5011298
25. Boyle DS, Lehman DA, Lillis L, Peterson D, Singhal M, Armes N, et al. Rapid detection of HIV-1 proviral DNA for early infant diagnosis using recombinase polymerase amplification. *MBio.* (2013) 4:e00135–13. doi: 10.1128/mBio.00135-13
26. Lillis L, Lehman D, Singhal MC, Cantera J, Singleton J, Labarre P, et al. Non-instrumented incubation of a recombinase polymerase amplification assay for the rapid and sensitive detection of proviral HIV-1 DNA. *PLoS ONE.* (2014) 9:e108189. doi: 10.1371/journal.pone.0108189
27. Ghosh DK, Kokane S, Kumar P, Ozcan A, Warghane A, Motghare M, et al. Antimicrobial nano-zinc oxide-2S albumin protein formulation significantly inhibits growth of "candidatus liberibacter asiaticus" in planta. *PLoS ONE.* (2018) 13:e0204702. doi: 10.1371/journal.pone.0204702
28. Faye M, Abd El Wahed A, Faye O, Kissenkötter J, Hoffmann B, Sall AA, et al. A recombinase polymerase amplification assay for rapid detection of rabies virus. *Sci Rep.* (2021) 11:3131. doi: 10.1038/s41598-021-82479-8
29. Wang P, Lin L, Shi M, Li H, Gu Z, Li M, et al. Vertical transmission of ALV from ALV-J positive parents caused severe immunosuppression and significantly reduced marek's disease vaccine efficacy in three-yellow chickens. *Vet Microbiol.* (2020) 244:108683. doi: 10.1016/j.vetmic.2020.108683
30. Wang P, Li M, Li H, Bi Y, Lin L, Shi M, et al. ALV-J-contaminated commercial live vaccines induced pathogenicity in three-yellow chickens: one of the transmission routes of ALV-J to commercial chickens. *Poult Sci.* (2021) 100:101027. doi: 10.1016/j.psj.2021.101027
31. Zeng F, Wu M, Ma L, Han Z, Shi Y, Zhang Y et al. Rapid and sensitive real-time recombinase polymerase amplification for detection of Marek's disease virus. *Mol Cell Probes.* (2019) 48:101468. doi: 10.1016/j.mcp.2019.101468
32. Zhang X, Guo L, Ma R, Cong L, Wu Z, Wei Y, et al. Rapid detection of salmonella with recombinase aided amplification. *J Microbiol Methods.* (2017) 139:202–4. doi: 10.1016/j.mimet.2017.06.011
33. Niemz A, Ferguson TM, Boyle DS. Point-of-care nucleic acid testing for infectious diseases. *Trends Biotechnol.* (2011) 29:240–50. doi: 10.1016/j.tibtech.2011.01.007

Conflict of Interest: ZZ and ZS were employed by Shandong Lvdu Biotechnology Co., Ltd.

The remaining authors declare that the research was conducted in the absence of any commercial or financial relationships that could be construed as a potential conflict of interest.

Publisher's Note: All claims expressed in this article are solely those of the authors and do not necessarily represent those of their affiliated organizations, or those of the publisher, the editors and the reviewers. Any product that may be evaluated in this article, or claim that may be made by its manufacturer, is not guaranteed or endorsed by the publisher.

frontiers | Frontiers in Microbiology

TYPE Original Research
PUBLISHED 22 July 2022
DOI 10.3389/fmicb.2022.912908

OPEN ACCESS

EDITED BY
Yongxiu Yao,
The Pirbright Institute, United Kingdom

REVIEWED BY
Tara Patricia Hurst,
Birmingham City University, United Kingdom
Muhammad Suleman,
University of Veterinary and Animal Sciences, Pakistan

*CORRESPONDENCE
Changbo Ou
ouchangbo@gxu.edu.cn
Xingyou Liu
lxingyou@sohu.com

†PRESENT ADDRESS
Fatma Eldemery,
US National Poultry Research Center, Agricultural Research Service, United States Department of Agriculture, Athens, GA, United States

SPECIALTY SECTION
This article was submitted to Virology, a section of the journal Frontiers in Microbiology

RECEIVED 05 April 2022
ACCEPTED 27 June 2022
PUBLISHED 22 July 2022

CITATION
Wang Q, Chu F, Zhang X, Hu H, Lu L, Wang F, Yu Y, Zhang Y, Ma J, Xu Z, Eldemery F, Ou C and Liu X (2022) Infectious bursal disease virus replication is inhibited by avain T cell chemoattractant chemokine CCL19. *Front. Microbiol.* 13:912908. doi: 10.3389/fmicb.2022.912908

Infectious bursal disease virus replication is inhibited by avain T cell chemoattractant chemokine CCL19

Qiuxia Wang[1], Fuming Chu[1], Xin Zhang[1], Huilong Hu[1], Lang Lu[1], Fang Wang[1], Yan Yu[1], Yanhong Zhang[1], Jinyou Ma[1], Zhiyong Xu[1], Fatma Eldemery[2†], Changbo Ou[1,3*] and Xingyou Liu[1,4*]

[1]College of Animal Science and Veterinary Medicine, Henan Institute of Science and Technology, Xinxiang, China, [2]Department of Hygiene and Zoonoses, Faculty of Veterinary Medicine, Mansoura University, Mansoura, Egypt, [3]College of Animal Science and Technology, Guangxi University, Nanning, China, [4]College of Life Science, Xinxiang University, Xinxiang, China

Chemokine CCL19, together with its receptor CCR7, is one of the most important factors recruiting immune cells into target organ during virus infection. Our previous study has shown that CCL19 played a vital role in the process of T cell trafficking into bursae during bursal disease virus (IBDV) infection. In this study, we hypothesized that CCL19 could exert direct influences on IBDV replication other than recruiting immune cells. A eukaryotic expression vector of pEGFP-N1/CCL19 was successfully constructed and identified by PCR, double enzymes digestion, and sequencing. Different concentrations of pEGFP-N1/CCL19 plasmids were transfected into DF1 cells and CCL19 protein was highly expressed. Then, DF1 cells were infected with IBDV B87 strain post-transfection. Based on PCR and Western blot results, CCL19 could obviously decrease the gene levels of VP1 and VP2 and the protein levels of VP2 and VP3. When CCL19 was knocked down, the gene levels of VP1 and VP2 were significantly upregulated. Moreover, indirect immunostaining revealed that the IBDV content was largely decreased after CCL19 overexpression. Additionally, CCL19 inhibitory effects might rely on activation of the JNK signal pathway. Taken together, chemokine CCL19 directly blocks IBDV replication in DF1 cells, indicating that CCL19 could play crucial functions other than recruiting T cells during the pathogenesis of IBDV.

KEYWORDS

CCL19, infectious bursal disease virus, virus replication, T cell, chemokine

Introduction

Infectious bursal disease virus (IBDV) is one of the most economically important viruses affecting poultry industry worldwide. It induces acute, highly contagious immunosuppressive diseases in young chickens aged 3 to 15 weeks (Sharma et al., 2000; Eterradossi and Saif, 2013). IBDV is a non-enveloped Avibirnavirus,

which belongs to the family Birnaviridae that group viruses enclosing bisegmented (segments A and B) double-stranded RNA genomes (Eterradossi and Saif, 2013; He et al., 2021). Genome segment B encodes viral protein VP1, an RNA-dependent RNA polymerase. Genome segment A contains two partially overlapping open reading frames that encode a non-structural polypeptide, known as VP5, and a large precursor polyprotein, which is further cleaved into VP2 (outer capsid), VP3 (inner capsid), and VP4 (a serine protease). VP2 and VP3 are the major structural proteins, comprising 51 and 40% of the virion, respectively, that have a crucial role in the morphogenesis and encapsulation of the viral genome (Berg, 2000; Luque et al., 2009).

Following IBDV infection in chicken, there was a dramatic infiltration of T cells into the bursa of Fabricius, and was first detectable as early as 1-day post-infection and persisted for several weeks (Tanimura and Sharma, 1997; Kim et al., 2000; Sharma et al., 2000). It has been indicated that the highest number of bursal cells were T cells (up to 65% of lymphocytes) (Kim et al., 2000; Sharma et al., 2000). The number of infiltrating T cells have been shown to be correlated with the IBDV virulence; however, the way in which the T cells inhibited the IBDV infection was different (Tippenhauer et al., 2013; Yu et al., 2015), and that may be due to the inconclusive differentiation of T cells into bursa of Fabricius. Ruan et al. believed that the infiltrating T lymphocytes in bursa of Fabricius were mainly $CD4^+$T cells and $CD4^+CD8^+$T cells after IBDV infection (Ruan et al., 2020). The study of Dobner et al. showed that the infiltrating T cells reached the maximum in the bursa of Fabricius on the 7th day after IBDV infection, and the number of $CD8^+$T cells was more than that of $CD4^+$T cells; $CD4^+$T cells increased by 4–11 times, $CD8^+$T cells increased by 11–38 times, and then gradually decreased, and the decline rate of $CD8^+$T cells was more moderate (Dobner et al., 2020). This may be due to differences in virulence of the virus used for infection or in the genotype of the chicken. Previous reports have demonstrated various biological functions of the infiltrating bursal T cells, such as promoting viral clearance, tissue damage and delaying follicular recovery, early immunopathology during an IBDV infection, and contribution to B cell genomic instability (Kim et al., 2000; Rautenschlein et al., 2002; Yu et al., 2015; Ciccone et al., 2017).

CC chemokine ligand 19 (CCL19), also known as macrophage inflammatory protein-3β and EBI-1 ligand chemokine, always, together with its chemokine receptor CCR7, plays a pivotal role in T cell and dendritic cell trafficking into lymphoid tissue (Forster et al., 2008). Previous studies indicated that chemokines, especially CCL19, played an important role in T cell migration into bursae during IBDV infection (Ou et al., 2017a,b; Wang et al., 2019). The mRNA expressions of CCL19 were largely increased on day 1 and day 3 post-IBDV infection, and it could interact with many differentially expressed genes after IBDV infection (Ou et al., 2017b). Moreover, our previous study showed that, during the process of T cell migration into bursae of Fabricius, the axis of CCR7/CCL19 was significantly elevated and the chemokine CCL19 acts as a chicken chemotactic factor facilitating the infiltration of T cells into the bursae in IBDV infection (Wang et al., 2019). Although the role of chemokines is recruiting immune cells to the site of virus infection, the chemokines could directly regulate the virus replication. For instance, five chemokines have been identified to contribute to the control of human immunodeficiency virus (HIV) replication. In HIV-infected individuals, the combination of the five chemokines (CCL14, CCL21, CCL27, XCL1, and SDF-1BETA) was found to upregulate the activation markers CD69 and CCR6, and downregulate the key HIV coreceptors CXCR4 and CCR7 on CD4+ T cells. Meanwhile, the anti-HIV host restriction factors IFITM1 and IFITM2 were significantly expressed, resulting in HIV replication reduction (Jacobs et al., 2017). In addition, Yu et al. provided insights for the roles of cytokines in porcine epidemic diarrhea virus (PEDV) replication and demonstrated that overexpression of CCL2, CCL5, and CCL8 significantly inhibited the virus replication, but silencing of these chemokine genes significantly promoted PEDV replication (Yu et al., 2019). Yan et al. found that CCL19 could rapidly clear HBV in the liver of mice by enhancing the responses of $CD8^+$T cells (Yan et al., 2021). Goto et al. demonstrated that human CAR-T cells producing human IL-7 and CCL19 can generate the potent therapeutic efficacy against solid tumors (Goto et al., 2021). But the effects of cytokines and chemokines on IBDV replication are still unclear.

Therefore, in this study, we aimed to investigate whether CCL19 could regulate the IBDV replication. The role of CCL19 on IBDV replication was evaluated *in vitro* through over-expression and knockdown of CCL19. CCL19 has further biological effects during the process of IBDV pathogenesis.

Materials and methods

Cells and virus

Chicken fibroblast cell line DF1 cells (ATCC CRL-12203) were cultured in Dulbecco's modified eagle's medium (DMEM) with 10% fetal bovine serum (Gibco, USA). After DF1 cells were split for transfection, the cells were maintained in 2% fetal bovine serum. Intermediate virulence vaccine strain IBDV B87 was purchased from Vland Biotech Group (Qingdao, China) and amplified in DF1 cells.

Reagents and antibodies

The JNK inhibitor, p38 inhibitor, Akt inhibitor, and Erk inhibitor were purchased (MedchemExpress, Shanghai, China).

DF1 cells were treated with either dimethyl sulfoxide (DMSO), which is the solvent for these four inhibitors, or 20 μM of each of these four inhibitors for 2 h before infection at 37°C in 5% CO_2 incubator. Then, the cells were inoculated with IBDV B87 virus at a multiplicity of infection (MOI) of 10 $TCID_{50}$ at 37°C in 5% CO_2 incubator. After 1 h of virus adsorption, the virus medium was removed and fresh medium containing fresh inhibitor was added into the culture.

Mouse antibodies against VP2 and VP3 were purchased from Wuhan Biorbyt. Rabbit antibodies against JNK and p-JNK were purchased from Cell Signaling. Mouse antibody against GAPDH and horseradish peroxidase (HRP)-labeled goat antibody against mouse and rabbit IgG were purchased from Nanjing Bioworld. Cy3-conjugated goat anti-mouse IgG antibody (1:100) was purchased from Wuhan Boster.

Construction of eukaryotic expression vector PEGFP-N1/CCL19

Previously constructed pMD T/CCL19 plasmid was used as the template for amplifying CCL19 gene (Wang et al., 2018). A pair of primers with restriction enzyme sites *Hind* III and *BamH* I was designed to amplify CCL19 by polymerase chain reaction (PCR). The purified CCL19 fragment was inserted into empty vector pEGFP-N1 by using double enzymes digestion method to generate pEGFP-N1/CCL19. Then, the plasmid was transformed into competent cells DH5α. The positive clones were selected, purified using plasmid extraction kit (Omega), and confirmed by PCR, double enzymes *Hind* III and *BamH* I digestion, and sequenced by a commercial company (Sangon Biotech, Shanghai, China).

CCL19 knockdown by siRNA

Three siRNA oligos segments (si817, si717, and si582) as well as the NT siRNA were designed and synthesized by Genepharma (Shanghai, China). The DF1 cells were seeded in six-well culture plates (Corning Inc., USA) at a density of 2×10^5 cells/well in six-well plates and incubated for 24 h before transfection at 37°C in 5% CO_2 incubator. Then, siRNA into CCL19 and NT siRNA were transfected into the cells mediated by Lipofectamine2000™, respectively. At 48 h after transfection, total RNA was extracted and reversely transcribed into cDNA to detect the inhibitory efficiency of siRNA through real-time PCR (qRT-PCR).

Transfection and virus challenge

The DF1 cells seeded in six-well culture plates (Corning Inc., USA) using DMEM medium and supplemented with 8% fetal bovine serum (Gibco, USA) were transfected with different concentrations (0.5, 1.0, 1.5, and 2.0 μg) of pEGFP-N1/CCL19 plasmids using Lipofectamine™ 2000 (Invitrogen, Grand Island, USA) following the manufacturer's protocols. Meanwhile, mock DF1 cells transfected with empty plasmid pEGFP-N1 were used as a control. At 24 h post-transfection, DF1 cells were gently washed with serum-free DMEM medium and challenged with 1 $TCID_{50}$ of IBDV B87 strain and incubated at 37 °C in a 5% CO_2 incubator. Cells were collected at 24, 36, 48, 60, and 72 h after infection.

Cell viability assay

Cell viability in DF-1 cells was measured by the Cell Counting Kit-8 (CCK-8) assay kit (Solarbio, Beijing, China). Briefly, DF-1 cells were seeded at a density of 2×10^5 cells/ml in 96-well culture plates (100 μl/well) in media, and then, the culture plates were incubated in 5% CO_2 atmosphere incubator at 37°C 24 h before transfection with pEGFP-N1-CCL19 at different concentrations. At 4 h after transfection, medium was replaced with 2% serum maintenance solution and incubated for 24 h; then, the medium was changed with serum-free media. Notably, 10 μl CCK-8 was added to each well and incubated for 1 h at 37°C.The optical density (OD) was measured at 452 nm. The percentage of viable cells was determined by the formula: ratio (%) = [OD (CCL19)–OD (Blank)]/[OD (Control)–OD (Blank)] ×100%.

Real-time polymerase chain reaction (qRT-PCR)

To quantify the copy number of IBDV and type I interferons, the IBDV VP1 and VP2, IFN-α and IFN-β, interferon regulatory factor 7 (IRF7) genes were selected for qRT-PCR with β-actin as the housekeeping gene (Staines et al., 2016). Total RNA was extracted from collected DF1 cells using Tissue RNA extraction kit (Omega™, Beijing, China) and reversely transcribed into cDNA with M-MLV reverse transcriptase (Promega, CA, USA) in accordance with the manufacturer's instructions. All primers used for the qRT-PCR are listed in Table 1. The qRT-PCR was carried out using SYBR Green PCR Master Mix (Invitrogen, Shanghai, China). The PCR conditions were as follows: 30 s at 95°C for initial denaturation, followed by 40 cycles at 95°C for 5 s, 58°C for 20 s, and 72°C for 20s. The data were analyzed using the threshold cycle (CT) values and gene expression calculated using the $2^{-\Delta\Delta Ct}$ method. All reactions were performed in three replicates to ensure the reproducibility of the amplification.

TABLE 1 Primers used for RT-PCR amplications.

Primer name	Sequence (5'-3')
CCL19-N1-F	CCG**AAGCTT** GCCACCATGCAGCGGCTGCACGTT
CCL19-N1-R	CCG**GGATCC**CTAATTGCCTTGATTTGGGAC
VP1-F	GAGGCGTTGAGGTTGGTA
VP1-R	ACTCAGTCCGGCTTCGTT
VP2-F	GGAGCCTTCTGATGCCAACAAC
VP2-R	CAGGAGCATCTGATCGAACTTGTAG
β-Actin-F	TTGTGATGGACTCTGGTGATGGTG
β-Actin-R	TTCTCTCTCGGCTGTGGTGGTG

Underlined bold letters indicated the *Hind* III and *BamH* I restriction enzyme sites.

Western blotting

The DF1 cells were harvested at 24, 48, and 72 h post-IBDV infection and washed twice with pre-cold phosphate-buffered saline (PBS). The cells were lysed with RIPA Lysis Buffer (Solarbio, China) with 1% PMSF proteinase inhibitor (Sigma, USA) and the total protein was collected following the protocol instructions. The collected protein was separated using 12% SDS-PAGE and then blotted onto nitrocellulose membranes. Subsequently, the membranes were blocked in 5% non-fat milk at 37 °C for 2 h. After washing with PBS, the membranes were incubated with primary antibody, including mouse anti-VP2 and anti-VP3 (1:1,000) and anti-GAPDH antibody (1:5,000) at 4°C for 12 h. The membranes were washed three times with PBS, and incubated for 1 h at 37°C with horseradish peroxidase (HRP)-labeled goat anti-mouse IgG (1:5,000). After being washed four times with PBS, the proteins on the membranes were visualized using the Chemiluminescent ECL western blotting substrate (Solarbio, Beijing, China). Mock-infected DF1 cells were used as the negative control.

Indirect immunostaining

DF1 cells collected at 24, 48, and 72 h post-infection were rinsed gently with PBS (pH 7.4), and fixed for 15 min at room temperature with 4% formaldehyde in PBS. Then, the cells were permeabilized with 1% Triton X-100 for 15 min at room temperature. The samples were blocked in 5% normal rabbit serum for 1 h. Furthermore, blocking solution was aspirated, and the samples incubated with mouse anti-VP2 antibody (1:1,000) for 1 h at 37°C. After removal of the primary antibody, the samples were incubated with Cy3-conjugated goat anti-mouse IgG secondary antibody (1:100) for 1 h at room temperature in a dark place. Then, the samples were analyzed using confocal microscopy immediately after being rinsed with PBS.

Statistical analysis

All data were analyzed by one-way analysis of variance and the statistical significance between the negative control group and CCL19 infection group was indicated as follows: * ($p < 0.05$) and ** ($p < 0.01$). All experiments were performed with three replicates, and the results were expressed as mean ± standard deviation (SD).

Results

IBDV B87 strain could grow in DF1 cells

In order to determine the growth and replication of B87 in DF-1 cells, DF-1 cells were infected with different doses of virus, and $TCID_{50}$ was detected and a growth curve was drawn. The results showed that IBDV B87 strain could replicate and proliferate in DF1 cells (Figure 1). With an increase in concentration and over time, B87 can cause marked pathological cell death.

Identification and expression of PEGFP-N1/CCL19

After construction of pEGFP-N1/CCL19 plasmid, it was identified by double enzyme digestion and PCR (Figure 2A). As seen in Figure 2A, plasmid digestion with *Hind* III and *Bam*H I showed two bands. Moreover, there was a 300 bp target band after amplification with the specific primers of CCL19 (Figure 2A). Also, the plasmid was confirmed by sequencing through a commercial sequencing company (data not shown). All results indicated that the CCL19 was correctly inserted into the pEGFP-N1 plasmids.

To further confirm the expression efficacy of the plasmids in DF1 cells, different concentrations of pEGFP-N1/CCL19 plasmids were transfected into DF1 cells. At 24 h post-transfection, all tested concentrations of plasmids showed efficacy expression in DF1 cells (Figure 2B).

Effect of different concentration PEGFP-N1/CCL19 on the cell viability of DF-1 cells

Before evaluating the role of CCL19 on IBDV infection, we observed the effect of different concentrations of pEGFP-N1/CCL19 on DF-1 cells viability by CCK-8 assay. Notably, concentrations of 0.8, 1.0, 1.2, 1.5, and 2.0 μg pEGFP-N1/CCL19 were transfected into DF-1 cells, respectively. The result showed that pEGFP-N1/CCL19 plasmid had certain cytotoxicity to DF-1 cells, and with the increase of

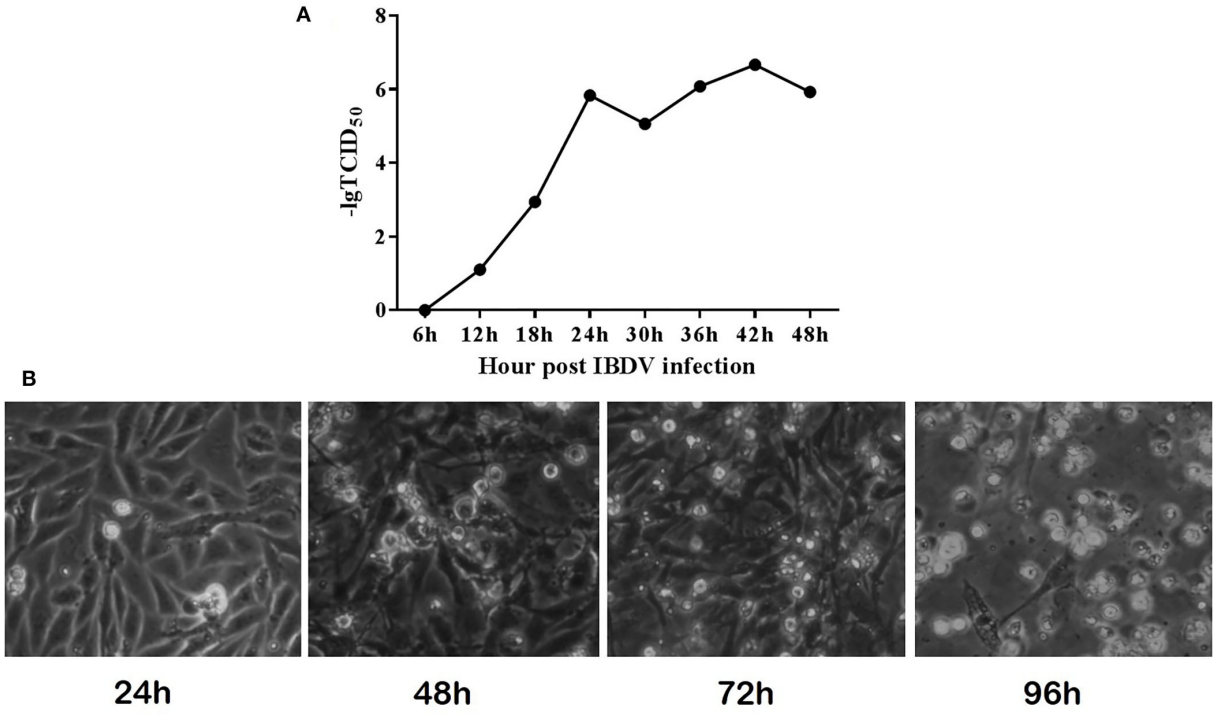

FIGURE 1
IBDV B87 strain could grow in DF-1 cells. **(A)** $TCID_{50}$ of IBDV B87 strain in DF-1 cells. **(B)** Cell morphology at different time points after IBDV infection.

transfection concentration, the cytotoxicity increased. When the transfection concentration was greater than 1.2 μg, the cell viability was lower than 60% (Figure 2C). Hence, pEGFP-N1/CCL19 was used at concentrations of 1.0 μg in all subsequent experiments.

Overexpressed CCL19 suppresses IBDV replication and release in DF-1 cells

To test whether CCL19 can protect DF1 cells from IBDV infection, pEGFP-N1/CCL19 (1.0 μg) was transfected into DF1 cells before cells were infected with IBDV. Figure 3 demonstrates the direct effects of CCL19 overexpression in DF1 cells on IBDV replication.

Figures 3A,B display the VP1 and VP2 gene expression levels in IBDV-infected DF1 cells, respectively. At 24 h post-infection with IBDV, there were no significant differences in VP1 and VP2 gene expression levels between the pEGFP-N1/CCL19 group and the empty vector control group. However, from 36 h post-IBDV-infection, the pEGFP-N1/CCL19 plasmids strongly inhibit the gene expressions of both IBDV VP1 and VP2. These inhibitory effects lasted until the end of the experiment except at 48 h post-infection, where VP1 and VP2 genes displayed similar gene expression trends.

Moreover, the protein expression levels of VP2 and VP3 were determined by western blot (Figure 3C). As shown in Figure 3C, VP2 and VP3 protein levels were largely decreased by CCL19 at 24, 48, and 72 h post-IBDV-infection, which were consistent with the results of the gene expression levels. Then, the IBDV numbers were semi-quantified by indirect immunofluorescent method (Figure 3D). Obviously, there were more IBDV-positive cells in the empty vector negative control group and those of the pEGFP-N1/CCL19 group at 24, 48, and 72 h post-infection.

The effect of chemokine CCL19 on the release of IBDV virions was further investigated. DF-1 cells were seeded at a density of 2×10^5 cells/well in six-well culture plates and incubated in 5% CO_2 atmosphere incubator at 37°C 24 h before transfection with 1 μg pEGFP-N1-CCL19. Meanwhile, 1 μg empty vector was transfected as the control group. Then, cells were challenged with 1 $TCID_{50}$ of IBDV B87 strain and incubated at 37°C in a 5% CO_2 incubator. The cell supernatants were collected at 24, 36, 48, 60, and 72 h, respectively. $TCID_{50}$ of the virus in the supernatant was detected (Figure 3E). The results showed that the virus titer in the PEGFP-N1-CCL19 transfected

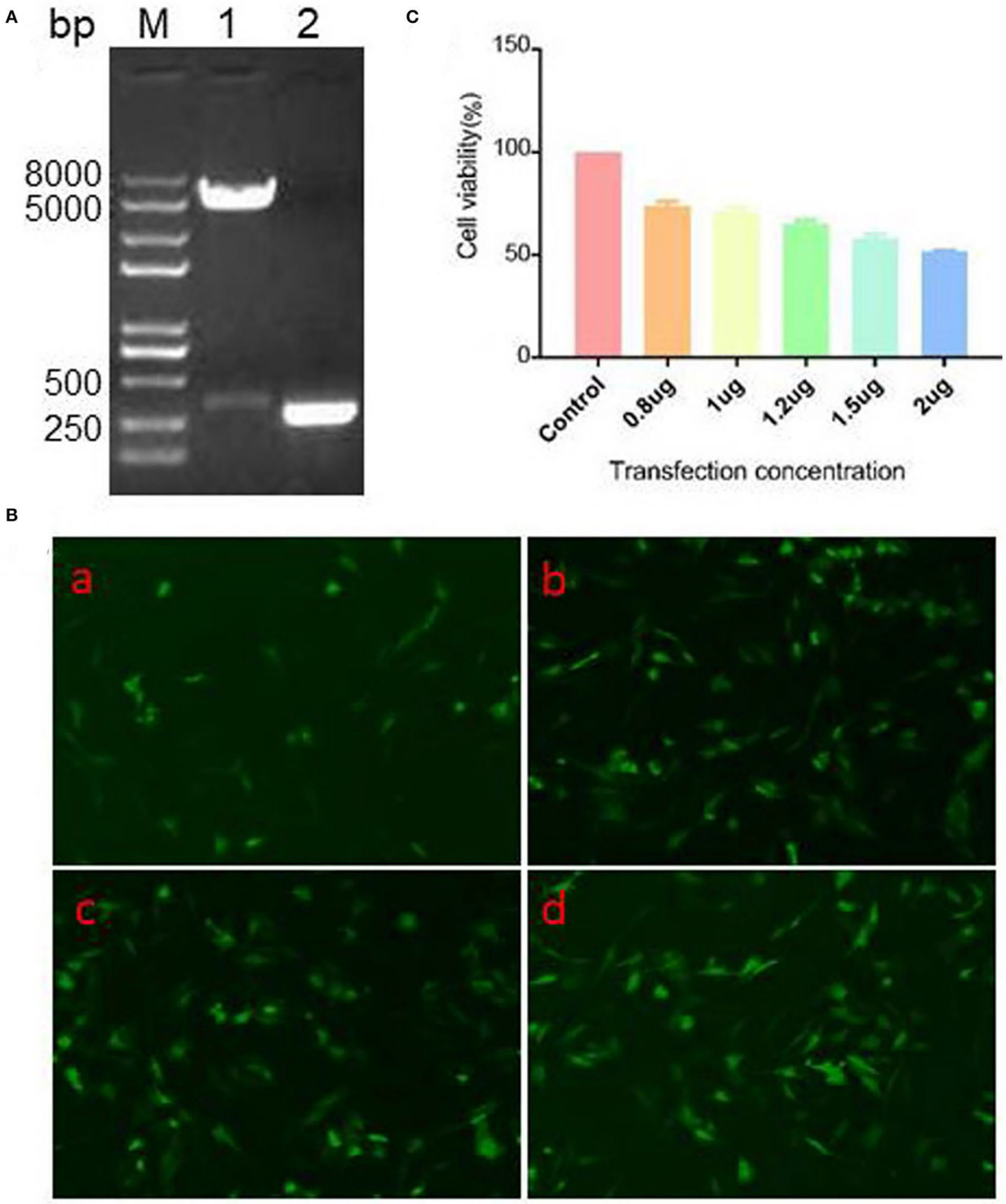

FIGURE 2
Identification, expression efficacy, and cell viability on DF1 cells of pEGFP-N1/CCL19. **(A)** PCR and double restriction enzyme digestion identification of eukaryotic expression vector pEGFP-N1/CCL19. Lane M: Trans 2K Plus II DNA marker; Lane 1: double enzymes digestion; Lane 2: PCR of CCL19. **(B)** Different concentrations (0.5, 1.0, 1.5, and 2.0 μg) of plasmid pEGFP-N1/CCL19 in DF1 cells were transfected into DF1 cells in **(B)** (a–d), respectively. **(C)** Effects of different concentrations of plasmid pEGFP-N1/CCL19 on cell viability. Concentrations of 0.8, 1.0, 1.2, 1.5, and 2.0 μg plasmids were transfected in DF1 cells.

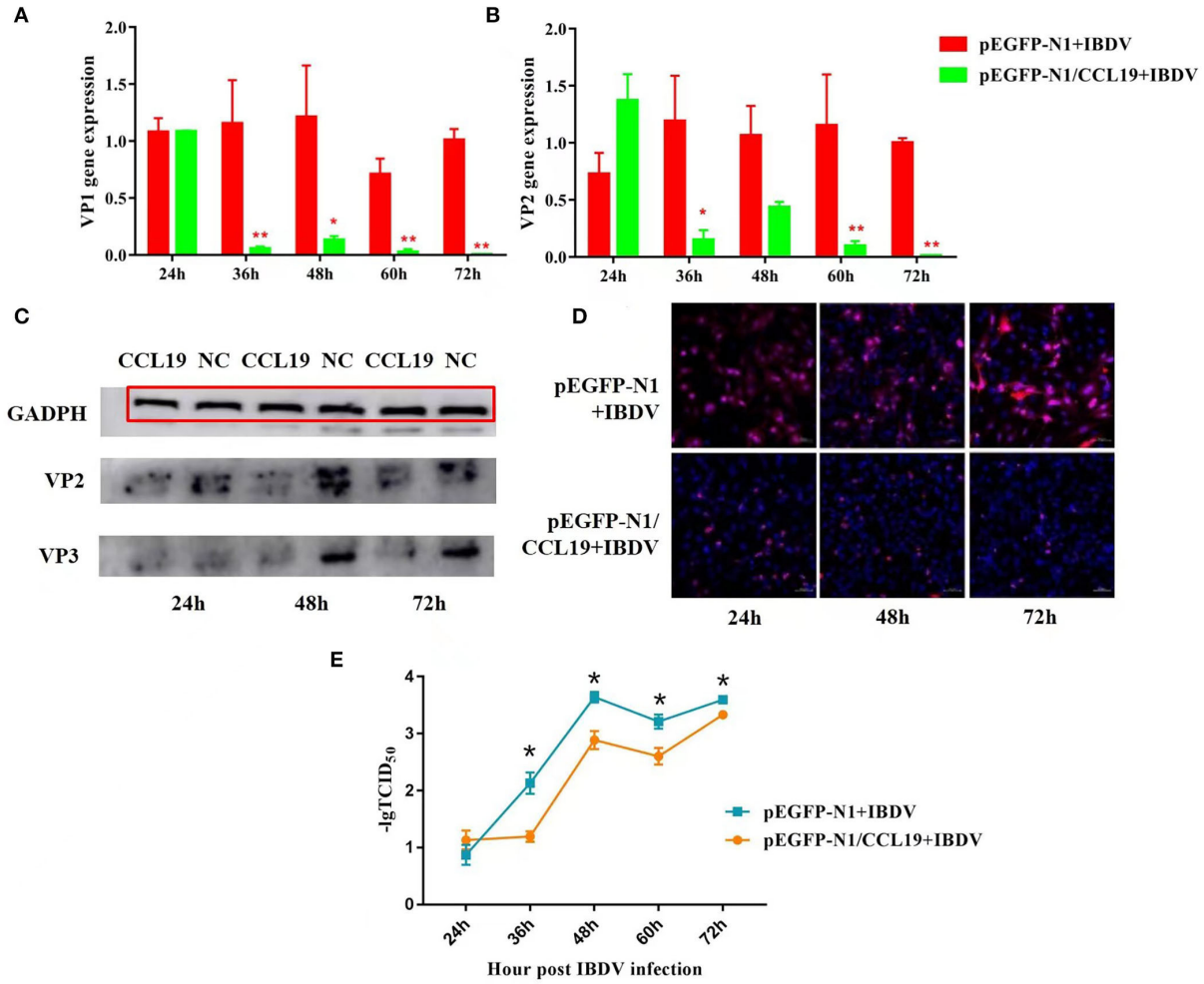

FIGURE 3
Negative regulation of overexpression CCL19 on IBDV replication at different time points in DF1 cells. Gene expression levels of VP1 **(A)** and VP2 **(B)** at 24, 36, 48, 60, and 72 h post-infection with IBDV B87 strain in pEGFP-N1/CCL19 group compared with empty vector plasmid pEGFP-N1 control group. **(C)** VP2 and VP3 protein expression levels of the empty vector plasmid pEGFP-N1 negative control group (NC) and pEGFP-N1/CCL19 group (CCL19) at 24, 48, and 72 h post-infection with IBDV. **(D)** Semi-quantification of IBDV by indirect immunofluorescent method of pEGFP-N1/CCL19 group compared with empty vector plasmid pEGFP-N1 negative control group at 24, 48, and 72 h post-infection with IBDV. Notably, 1.0 μg empty vector or pEGFP-N1/CCL19 plasmid was used in virus infection experiment. **(E)** $TCID_{50}$ at 24, 36, 48, 60, and 72 h post-infection with IBDV B87 strain in pEGFP-N1/CCL19 group compared with empty vector plasmid pEGFP-N1 control group. * or ** indicates that there were significant differences of VP1, VP2 gene expression levels or $TCID_{50}$ between pEGFP-N1 and pEGFP-N1/CCL19 groups ($p < 0.05$ or $p < 0.01$). The red box indicates the GAPDH band.

group was significantly lower than that in the control group from 36 h after IBDV infection.

CCL19 knockdown promotes IBDV replication and release in DF-1 cells

To further determine the role of CCL19 in IBDV infection, we first assessed the endogenous level of CCL19 in DF-1 cell lines (Figure 4A). We found that DF-1 cell exhibited general CCL19 expression levels. DF-1 cell lines were used for CCL19 knockdown using three different siRNAs (si817, si717, and si582). A subsequent qRT-PCR analysis showed that the CCL19 gene levels were reduced in the DF-1 cells transfected with si717 compared with the respective NT siRNA transfected control cells (Figure 4B). We selected si717 for further experiments; as the knockdown was more robust, qRT-PCR data showed that CCL19 mRNA levels were reduced by > 70% in DF-1 cell lines. Hence, DF-1 cells transfected with si717 were used in subsequent experiments.

Following siRNA transfection, we found that CCL19 knockdown slightly impacted DF-1 cell growth at 24 h (Figure 4C), although no significant change was observed in cell viability (Figure 4D). Indeed, IBDV VP1 and VP2 gene

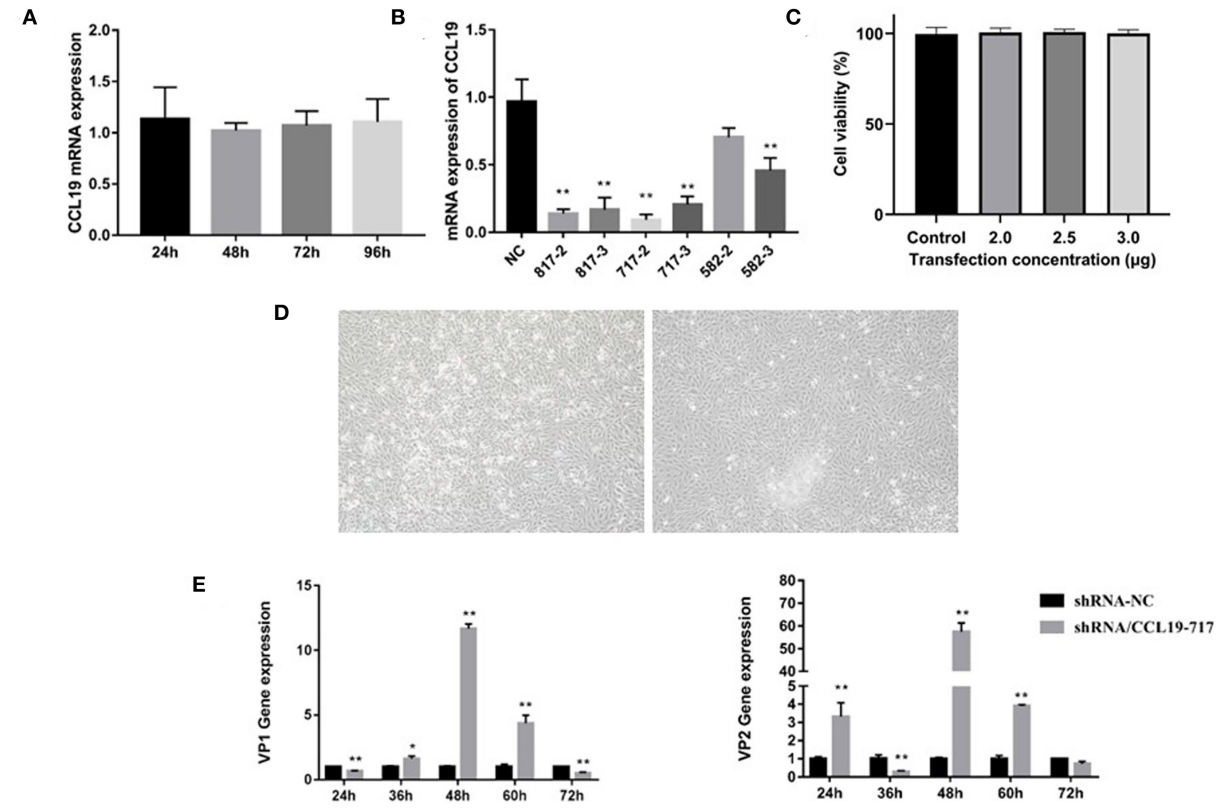

FIGURE 4
siRNA knockdown of CCL19 promotes IBDV replication. **(A)** Gene expression levels of CCL19 in DF1 cells. **(B)** The efficiency of different CCL19-siRNA. **(C)** Cell viability at 2 h after si717 transfection. **(D)** Cell morphology at 24 h after si717 transfection. **(E)** Gene expression levels of VP1 (left) and VP2 (right) at 24, 36, 48, 60, and 72 h post-infection with IBDV B87 strain in si717 group compared with NT control group. * or ** indicates that there were significant differences of VP1, VP2, and CCL19 gene expression levels between siCCL19 and NT groups ($p < 0.05$ or $p < 0.01$).

expression levels were increased obviously when there was a knockdown of CCL19 (Figure 4E). These findings indicate that the reduction of CCL19 expression may promote replication of IBDV in DF-1 cells.

Blockage of JNK and p38 signal pathway inhibited the negative regulation of CCL19 on IBDV replication

As the above data indicated that CCL19 can decrease proliferative and survival capabilities of DF-1 cells and inhibit replication of IBDV in DF-1 cells, we next set out to investigate the molecular mechanisms underlying these effects. To screen the signal pathway by which CCL19 inhibited IBDV replication, p38, JNK, Akt, and Erk signal pathway inhibitors were administrated into DF1 cells before pEGFP-N1/CCL19 plasmid transfection. Figure 5A displayed relative IBDV VP2 gene expression levels for each group (p38 + CCL19, JNK + CCL19, Akt + CCL19, and Erk + CCL19) at 60 h after IBDV infection. When DF1 cells were treated with p38 and JNK signal pathway inhibitors, the inhibition effects of CCL19 on IBDV replication were offset, or even promoted IBDV replication, indicating that CCL19 could inhibit IBDV replication. Both Akt and Erk pathway inhibitors treatment had no effects on negative regulation of CCL19 on IBDV replication.

To further study why JNK pathway inhibitor treatment could promote IBDV replication even after CCL19 expression, pEGFP-N1-CCL19 plasmids were transfected into DF1 cells and JNK phosphorylation level were determined by western blotting on 4, 6, 8, 12, and 24 h after plasmids transfection. Obviously, pEGFP-N1-CCL19 could significantly elevate JNK phosphorylation level and activate JNK signal pathway, while the pEGFP-N1 control plasmids could not change JNK phosphorylation level (Figures 5B,C).

Discussion

Similar to other chemokines, the functions of CCL19 mainly rely on immune cell trafficking. When CCL19 is mentioned,

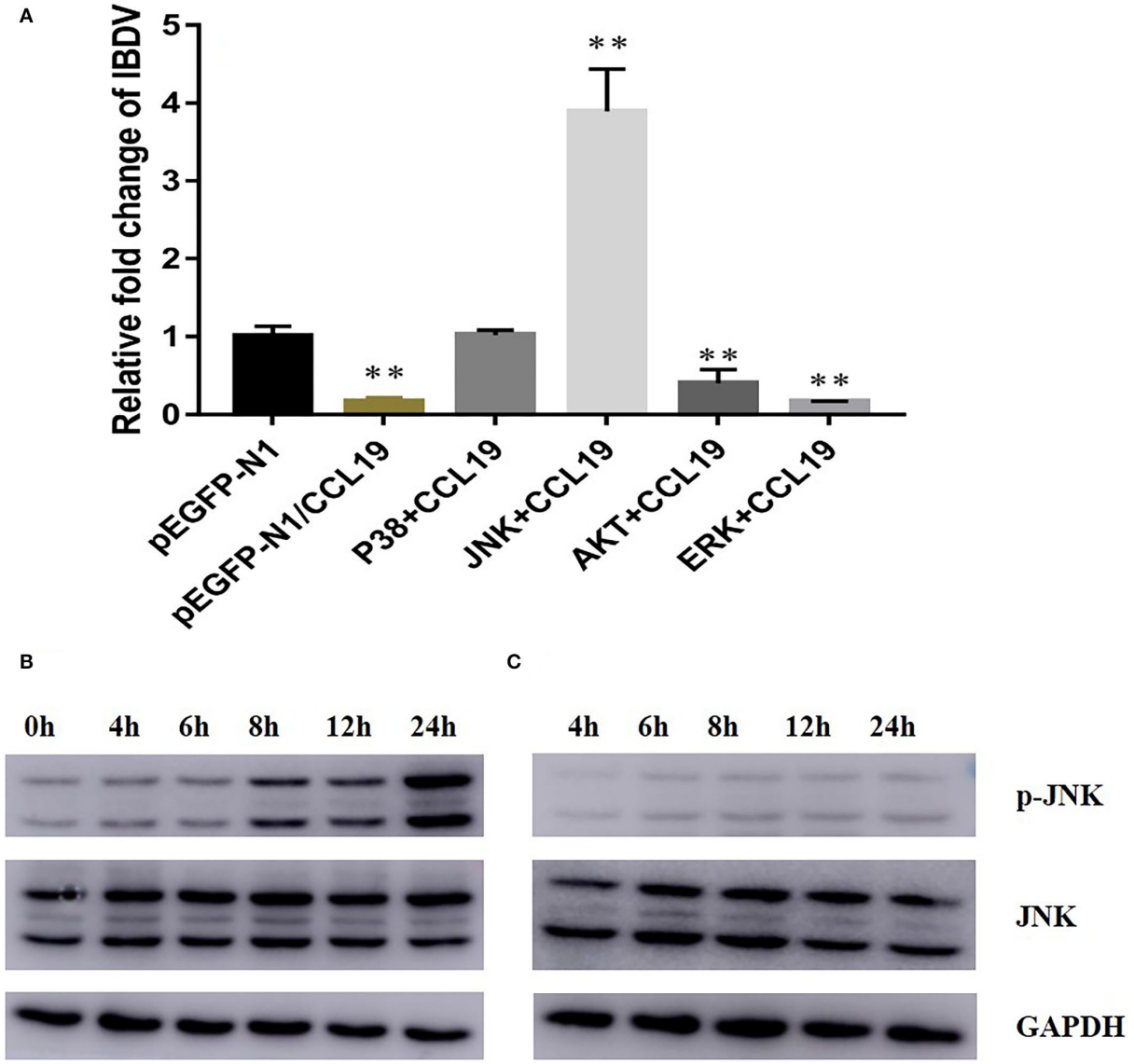

FIGURE 5
CCL19 activates JNK signal pathway to inhibit IBDV replication. **(A)** DF1 cells were pretreated with 20 μM of four signal pathway inhibitors before transfection with pEGFP-N1/CCL19 plasmid and then infected with IBDV. At 48 h post-infection with IBDV, DF1 cells were collected for determination of IBDV VP2 gene expression levels. DF1 cells were transfected with either pEGFP-N1/CCL19 and sampled at 0, 4, 6, 8, 12, and 24 h post-transfection **(B)** or pEGFP-N1 control plasmid and sampled at 4, 6, 8, 12, and 24 h post-transfection **(C)**; then, p-JNK, JNK, and GAPDH expression were determined by western blotting. ** Indicates significant differences of relative fold changes on IBDV between pEGFP-N1 and other groups ($p < 0.01$).

it is usually referred to the axis of CCR7/CCL19 and its effects on immune cell migration (Comerford et al., 2013). There are rare reports on the direct antiviral effects of CCL19. Herein, a eukaryotic expression vector pEGFP-N1/CCL19 was successfully constructed, and it could express in DF1 cells. More importantly, the plasmid pEGFP-N1/CCL19 was proved to inhibit IBDV replication *in vitro* at the gene level and protein level of IBDV. Moreover, the gene level of IBDV was recovered when CCL19 was knockdown by siRNA. The antiviral effects of CCL19 may be related to the activation of JNK signal pathway.

All the time, the main function of CCL19 is to control a serial of migratory events in immune responses, especially promoting T cells and DCs infiltration to microbial infection sites (Comerford et al., 2013). During the process of IBDV infection, one of the characteristics of IBDV pathogenesis is that with the depletion and inactivation of B cells in the bursa of Fabricius (Huang et al., 2021), numerous T cells are infiltrated

into the target organ bursae of Fabricius after IBDV infection (Sharma et al., 2000). Our previous work has proved that CCL19 indeed played an important role in T cell migration during the process of IBDV infection (Wang et al., 2019). However, after RNA-seq was applied to analyze the transcriptional profiles of the responses of bursae of Fabricius in the early stage of IBDV infection, CCL19 was found that it could interact with a number of genes, such as regulator of G protein signaling 4 (RGS4), Annexin A1 (ANXA1), Bradykinin Receptor B2 (BDKRB2), Cytidine/Uridine Monophosphate Kinase 2 (CMPK2), and Eukaryotic Translation Initiation Factor 2 Alpha Kinase 2 (EIF2AK2) (Ou et al., 2017b). These results indicated that CCL19 not only took part in T cell migration during IBDV infection, but also might interact with other genes to affect IBDV pathogenesis. In this study, we justified our hypothesis that CCL19 could interfere the process of IBDV infection by inhibiting IBDV replication.

Avian T cell mediated immune responses were suspected to play a vital role in fighting virus infection, including IBDV, infectious bronchitis virus, avian influenza virus, and avian leukosis virus subgroup J (Seo and Webster, 2001; Wang et al., 2014; Tan et al., 2016; Xu et al., 2016). Indeed, T cell cytotoxic responses were activated by IBDV infection and could inhibit IBDV replication through Fas-FasL and perforin-granzyme pathways (Rauf et al., 2012). However, T cell exerted negative effects on an individual's health due to the delay in follicular recovery (Rautenschlein et al., 2002). As far as we know, almost no research has been directed toward the effects of T cell chemoattractant chemokine on IBDV replication. This is the first study to display that T cell chemoattractant chemokine CCL19 had positive effects on inhibiting IBDV replication besides the direct inhibition functions of T cell on IBDV replication.

Another interesting thing was that CCL19 could significantly inhibit the gene levels of VP1 and VP2, but not other three virus protein genes (data not shown). To further determine the effects of CCL19 on virus protein expression levels, monoclonal antibodies against VP2 and VP3 were acquired from a commercial company. As shown in Figure 3C, the antibody against VP2 was not so good and the target bands were very faint. There were always faint background dots on the blot. These results indicated that CCL19 could inhibit expression levels of VP2 and VP3 despite the limitations of primary antibodies. Moreover, when there was a knockdown of CCL19, IBDV VP1 and VP2 gene expression levels were increased obviously. These results indicated that CCL19 might influence the aspects of transcriptions and translations of IBDV. Of course, further studies on inhibition mechanisms of CCL19 on IBDV replication would be required.

Many signal pathways were involved with IBDV pathogenesis, including p38 MAPK pathway, JNK signaling pathway, and Akt signaling pathway (Khatri and Sharma, 2006; Wei et al., 2011; Zhang et al., 2020). Four important signaling pathway inhibitors for IBDV were chosen and administrated to find which pathway would take part in the process of CCL19 on IBDV inhibition in this study. First, the ERK pathway inhibitor did not influence the effects of CCL19 on IBDV replication, which indicated that ERK pathway did not interfere with the process of IBDV replication. To the authors' knowledge, there are no reports on the relationship of ERK pathway with IBDV replication. Interestingly, Akt pathway inhibitor could not stop the inhibition effects of CCL19 on IBDV replication. Host cell phosphatidylinositol 3-kinase (PI3K)/Akt signaling seems to be a sentinel pathway after virus infection and take part in a number of physiological changes in the process of virus infection, including IBDV growth (Wei et al., 2011), virus entry into cells (Ye et al., 2017), and inhibition of host cell autophagy (Zhang et al., 2020). Thus, the result that CCL19 still inhibited the IBDV replication after administration of Akt pathway inhibitor is uncanny. Our only reasonable explanation for this result is that CCL19 relies on another pathway to inhibit IBDV replication. After blockage of p38 pathway and JNK pathway, CCL19 did not inhibit IBDV replication. However, JNK pathway inhibitor promoted the IBDV growth. Therefore, JNK pathway plays an important role in the process of inhibiting IBDV growth by CCL19. Further study displayed that CCL19 activates JNK pathway. Actually, activation of CCL19 and its receptor CCR7 usually could induce JNK phosphorylation and promote cell migration (Liu et al., 2014), which further justifies our result.

To conclude, the T cell chemoattractant CCL19 possessed the ability of inhibiting IBDV replication other than recruiting T cell into IBDV target organ bursae. The antiviral effects of CCL19 might be related to the activation of JNK signal pathway. Further research will be also applied to explore the detailed mechanism of CCL19 on IBDV replication. Moreover, this study is only an *in vitro* study and whether CCL19 could be applied to control IBDV infection in poultry is still unknown. Antiviral roles of CCL19 and its administration time, frequency, and dosage form will be determined in an IBDV-infected chicken model.

Data availability statement

The original contributions presented in the study are included in the article/supplementary material, further inquiries can be directed to the corresponding author/s.

Author contributions

QW, FC, and XZ did experiment and wrote the manuscript. CO and XL designed the study and review the manuscript. HH, LL, FW, YY, YZ, JM, ZX, and FE took part in study design, data statistical analysis and reviewing. All authors contributed to the article and approved the submitted version.

Funding

This study was supported by grant from the key Scientific and Technological Project of Henan Province (212102110009 and 202102110102), the Modern agricultural industrial technology system of Henan Province (S2012-06-G02), the Program for Innovative Research Team (in Science and Technology) in University of Henan Province (20IRTSTHN025), and the Key Scientific Research Project in University of Henan Province (21A230003).

Conflict of interest

The authors declare that the research was conducted in the absence of any commercial or financial relationships that could be construed as a potential conflict of interest.

Publisher's note

Supplementary material

The Supplementary Material for this article can be found online at: https://www.frontiersin.org/articles/10.3389/fmicb.2022.912908/full#supplementary-material

References

Berg, T. P. (2000). Acute infectious bursal disease in poultry: a review. *Avian. Pathol.* 29, 175–194. doi: 10.1080/03079450050045431

Ciccone, N. A., Smith, L. P., Mwangi, W., Boyd, A., Broadbent, A. J., Smith, A. L., et al. (2017). Early pathogenesis during infectious bursal disease in susceptible chickens is associated with changes in B cell genomic methylation and loss of genome integrity. *Dev Comp Immunol.* 73, 169–174. doi: 10.1016/j.dci.2017.03.014

Comerford, I., Harata-Lee, Y., Bunting, M. D., Gregor, C., Kara, E. E., and McColl, S. R. (2013). A myriad of functions and complex regulation of the CCR7/CCL19/CCL21 chemokine axis in the adaptive immune system. *Cytokine Growth Factor Rev.* 24, 269–283. doi: 10.1016/j.cytogfr.2013.03.001

Dobner, M., Auerbach, M., Mundt, E., Icken, W., and Rautenschlein, S. (2020). Genotype-associated differences in bursal recovery after infectious bursal disease virus (IBDV) inoculation. *Vet. Immunol. Immunopathol.* 220, 109993. doi: 10.1016/j.vetimm.2019.109993

Eterradossi, N., and Saif, Y. M. (2013). *Infectious Bursal Disease in Disease of Poultry*. Ames: Iowa State Press. p. 219–246. doi: 10.1002/9781119421481.ch7

Forster, R., Davalos-Misslitz, A. C., and Rot, A. (2008). CCR7 and its ligands: balancing immunity and tolerance. *Nat. Rev. Immunol.* 8, 362–371. doi: 10.1038/nri2297

Goto, S., Sakoda, Y., Adachi, K.eishi., Sekido, Y., Yano, S., Eto, M., et al. (2021). Enhanced anti-tumor efficacy of IL-7/CCL19-producing human CAR-T cells in orthotopic and patient-derived xenograft tumor models. *Cancer Immunol. Immunother.* 70, 2503–2515. doi: 10.1007/s00262-021-02853-3

He, Z., Ma, Y., Wu, D., Feng, W., and Xiao, J. (2021). Protective effects of the NLRP3 inflammasome against infectious bursal disease virus replication in DF-1 cells. *Arch. Virol.* 166,1943–1950. doi: 10.1007/s00705-021-05099-7

Huang, X., Liu, W., Zhang, J., Liu, Z., Wang, M., Wang, L., et al. (2021). Very virulent infectious bursal disease virus-induced immune injury is involved in inflammation, apoptosis, and inflammatory cytokines imbalance in the bursa of fabricius. *Dev. Comp. Immunol.* 114, 103839. doi: 10.1016/j.dci.2020.103839

Jacobs, E. S., Keating, S. M., Abdel-Mohsen, M., Gibb, S. L., Heitman, J. W., Inglis, H. C., et al. (2017). Cytokines elevated in HIV elite controllers reduce HIV replication *in vitro* and modulate HIV restriction factor expression. *J. Virol.* 91, e02051–e02016. doi: 10.1128/JVI.02051-16

Khatri, M., and Sharma, J. M. (2006). Infectious bursal disease virus infection induces macrophage activation via p38 MAPK and NF-kappaB pathways. *Virus Res.* 118, 70–77. doi: 10.1016/j.virusres.2005.11.015

Kim, I. J., You, S. K., Kim, H., Yeh, H. Y. and Sharma, J. M. (2000). Characteristics of bursal T lymphocytes induced by infectious bursal disease virus. *J Virol.* 74, 8884–8892. doi: 10.1128/jvi.74.19.8884-8892.2000

Liu, Q. R., Liu, J. M., Chen, Y., Xie, X. Q., Xiong, X. X., Qiu, X. Y., et al. (2014). Piperlongumine inhibits migration of glioblastoma cells via activation of ROS-dependent p38 and JNK signaling pathways. *Oxid. Med. Cell Longev.* 2014, 653732. doi: 10.1155/2014/653732

Luque, D., Saugar, I., Rejas, M. T., Carrascosa, J. L., Rodriguez, J. F., and Castón, J. R. (2009). Infectious bursal disease virus: ribonucleoprotein complexes of a double stranded RNA virus. *J. Mol. Biol.* 386, 891–901. doi: 10.1016/j.jmb.2008.11.029

Ou, C., Wang, Q., Yu, Y., Zhang, Y., Ma, J., Kong, X., et al. (2017a). Chemokine receptor CCR5 and CXCR4 might influence virus replication during IBDV infection. *Microb. Pathog.* 107, 122–128. doi: 10.1016/j.micpath.2017.03.031

Ou, C., Wang, Q., Zhang, Y., Kong, W., Zhang, S., Yu, Y., et al. (2017b). Transcription profiles of the responses of chicken bursae of Fabricius to IBDV in different timing phases. *Virol. J.* 14, 93. doi: 10.1186/s12985-017-0757-x

Rauf, A., Khatri, M., Murgia, M. V., and Saif, Y. M. (2012). Fas/FasL and perforin-granzyme pathways mediated T cell cytotoxic responses in infectious bursal disease virus infected chickens. *Results Immunol.* 2, 112–119. doi: 10.1016/j.rinim.2012.05.003

Rautenschlein, S., Yeh, H. Y., Njenga, M. K., and Sharma, J. M. (2002). Role of intrabursal T cells in infectious bursal disease virus (IBDV) infection: T cells promote viral clearance but delay follicular recovery. *Arch. Virol.* 147, 285–304. doi: 10.1007/s705-002-8320-2

Ruan, Y., Wang, Y., Guo, Y., Xiong, Y., Chen, M., Zhao, A., et al. (2020). T cell subset profile and inflammatory cytokine properties in the gut-associated lymphoid tissues of chickens during infectious bursal disease virus (IBDV) infection. *Arch. Virol.* 165, 2249–2258. doi: 10.1007/s00705-020-04735-y

Seo, S. H., and Webster, R. G. (2001). Cross-reactive, cell-mediated immunity and protection of chickens from lethal H5N1 influenza virus infection in Hong Kong poultry markets. *J. Virol.* 75, 2516–2525. doi: 10.1128/JVI.75.6.2516-2525.2001

Sharma, J. M., Kim, I. J., Rautenschlein, S., and Yeh, H. Y. (2000). Infectious bursal disease virus of chickens: pathogenesis and immunosuppression. *Dev. Comp. Immunol.* 24, 223–235. doi: 10.1016/S0145-305X(99)00074-9

Staines, K., Batra, A., Mwangi, W., Maier, H. J., Van Borm, S., Young, J. R., et al. (2016). A versatile panel of reference gene assays for the measurement of chicken mRNA by quantitative PCR. *PLoS ONE.* 11, e0160173. doi: 10.1371/journal.pone.0160173

Tan, L., Liao, Y., Fan, J., Zhang, Y., Mao, X., Sun, Y., et al. (2016). Prediction and identification of novel IBV S1 protein derived CTL epitope in chicken. *Vaccine*. 34, 380–386. doi: 10.1016/j.vaccine.2015.11.042

Tanimura, N., and Sharma, J. M. (1997). Appearance of T cells in the bursa of Fabricius and cecal tonsils during the acute phase of infectious bursal disease virus infection in chickens. *Avian Dis*. 41, 638–645. doi: 10.2307/1592155

Tippenhauer, M., Heller, D. E., Weigend, S., and Rautenschlein, S. (2013). The host genotype influences infectious bursal disease virus pathogenesis in chickens by modulation of T cells responses and cytokine gene expression. *Dev. Comp. Immunol*. 40, 1–10. doi: 10.1016/j.dci.2012.10.013

Wang, Q., Li, P., Liu, X., Yu, Y., Zhang, Y., Jiang, J., et al. (2018). Expression of avian origin chemokine CCL19 and preparation of its polyclonal antibody. *Chin. Vet. Sci*. 48,155–160. doi: 10.16656/j.issn.1673-4696.2018.0024

Wang, Q., Ou, C., Wei, X., Yu, Y., Jiang, J., Zhang, Y., et al. (2019). CC chemokine ligand 19 might act as the main bursal T cell chemoattractant factor during IBDV infection. *Poult. Sci*. 98, 688–694. doi: 10.3382/ps/pey435

Wang, Y., Wang, G., Wang, Z., Zhang, H., Zhang, L., and Cheng, Z. (2014). Chicken biliary exosomes enhance CD4(+)T proliferation and inhibit ALV-J replication in liver. *Biochem. Cell Biol*. 92,145–151. doi: 10.1139/bcb-2013-0096

Wei, L., Hou, L., Zhu, S., Wang, J., Zhou, J., and Liu, J. (2011). Infectious bursal disease virus activates the phosphatidylinositol 3-kinase (PI3K)/Akt signaling pathway by interaction of VP5 protein with the p85alpha subunit of PI3K. *Virology*. 417, 211–220. doi: 10.1016/j.virol.2011.03.003

Xu, Q., Cui, N., Ma, X., Wang, F., Li, H., Shen, Z., et al. (2016). Evaluation of a chimeric multi-epitope-based DNA vaccine against subgroup J avian leukosis virus in chickens. *Vaccine*. 34, 3751–3756. doi: 10.1016/j.vaccine.2016.06.004

Yan, Y., Zhao, W., Liu, W., Li, Y., Wang, X., Xun, J., et al. (2021). CCL19 enhances CD8+ T-cell responses and accelerates HBV clearance. *J. Gastroenterol*. 56, 769–785. doi: 10.1007/s00535-021-01799-8

Ye, C., Han, X., Yu, Z., Zhang, E., Wang, L., and Liu, H. (2017). Infectious bursal disease virus activates c-Src to promote alpha4beta1 integrin-dependent viral entry by modulating the downstream Akt-RhoA GTPase-Actin rearrangement cascade. *J Virol*. 91. doi: 10.1128/JVI.01891-16

Yu, L., Dong, J., Wang, Y., Zhang, P., Liu, Y., Zhang, L., et al. (2019). Porcine epidemic diarrhea virus nsp4 induces pro-inflammatory cytokine and chemokine expression inhibiting viral replication in vitro. *Arch. Virol*. 164, 1147–1157. doi: 10.1007/s00705-019-04176-2

Yu, X., Rui, L., Shao, Q., Liu, H., Lu, Y., Zhang, Y., et al. (2015). Changes of CD4+CD25+ cells ratio in immune organs from chickens challenged with infectious bursal disease virus strains with varying virulences. *Viruses*. 7, 1357–1372. doi: 10.3390/v7031357

Zhang, Y., Hu, B., Li, Y., Deng, T., Xu, Y., Lei, J., et al. (2020). Binding of Avibirnavirus VP3 to the PIK3C3-PDPK1 complex inhibits autophagy by activating the AKT-MTOR pathway. *Autophagy*. 16, 1697–1710. doi: 10.1080/15548627.2019.1704118

frontiers | Frontiers in Microbiology

TYPE Original Research
PUBLISHED 29 July 2022
DOI 10.3389/fmicb.2022.909252

OPEN ACCESS

EDITED BY
Nicolas Eterradossi,
Agence Nationale de Sécurité Sanitaire de l'Alimentation, de l'Environnement et du Travail (ANSES), France

REVIEWED BY
Muhammad Kashif Saleemi,
University of Agriculture Faisalabad, Pakistan
Huibin Yu,
Yale University, United States

*CORRESPONDENCE
Xiaole Qi
qixiaole@caas.cn

†These authors have contributed equally to this work

SPECIALTY SECTION
This article was submitted to Virology, a section of the journal Frontiers in Microbiology

RECEIVED 31 March 2022
ACCEPTED 04 July 2022
PUBLISHED 29 July 2022

CITATION
Fan L, Wang Y, Jiang N, Gao Y, Niu X, Zhang W, Huang M, Bao K, Liu A, Wang S, Gao L, Li K, Cui H, Pan Q, Liu C, Zhang Y, Wang X and Qi X (2022) Residues 318 and 323 in capsid protein are involved in immune circumvention of the atypical epizootic infection of infectious bursal disease virus. *Front. Microbiol.* 13:909252. doi: 10.3389/fmicb.2022.909252

Residues 318 and 323 in capsid protein are involved in immune circumvention of the atypical epizootic infection of infectious bursal disease virus

Linjin Fan[1,2†], Yulong Wang[1,2†], Nan Jiang[1,2], Yulong Gao[1,2], Xinxin Niu[1,2], Wenying Zhang[1,2], Mengmeng Huang[1,2], Keyan Bao[3], Aijing Liu[1,2], Suyan Wang[1,2], Li Gao[1,2], Kai Li[1], Hongyu Cui[1], Qing Pan[1], Changjun Liu[1], Yanping Zhang[1], Xiaomei Wang[1,2,4] and Xiaole Qi[1,2*]

[1]Avian Immunosuppressive Diseases Division, State Key Laboratory of Veterinary Biotechnology, Harbin Veterinary Research Institute, The Chinese Academy of Agricultural Sciences, Harbin, China, [2]OIE Reference Laboratory for Infectious Bursal Disease, Harbin Veterinary Research Institute, The Chinese Academy of Agricultural Sciences, Harbin, China, [3]National Laboratory of Biomacromolecules, CAS Center for Excellence in Biomacromolecules, Institute of Biophysics, Chinese Academy of Sciences, Beijing, China, [4]Jiangsu Co-innovation Centre for Prevention and Control of Important Animal Infectious Disease and Zoonoses, Yangzhou University, Yangzhou, China

Recently, atypical infectious bursal disease (IBD) caused by a novel variant infectious bursal disease virus (varIBDV) suddenly appeared in immunized chicken flocks in East Asia and led to serious economic losses. The epizootic varIBDV can partly circumvent the immune protection of the existing vaccines against the persistently circulating very virulent IBDV (vvIBDV), but its mechanism is still unknown. This study proved that the neutralizing titer of vvIBDV antiserum to the epizootic varIBDV reduced by 7.0 $\log_2$, and the neutralizing titer of the epizootic varIBDV antiserum to vvIBDV reduced by 3.2 $\log_2$. In addition, one monoclonal antibody (MAb) 2-5C-6F had good neutralizing activity against vvIBDV but could not well recognize the epizootic varIBDV. The epitope of the MAb 2-5C-6F was identified, and two mutations of G318D and D323Q of capsid protein VP2 occurred in the epizootic varIBDV compared to vvIBDV. Subsequently, the indirect immunofluorescence assay based on serial mutants of VP2 protein verified that residue mutations 318 and 323 influenced the recognition of the epizootic varIBDV and vvIBDV by the MAb 2-5C-6F, which was further confirmed by the serial rescued mutated virus. The following cross-neutralizing assay directed by MAb showed residue mutations 318 and 323 also affected the neutralization of the virus. Further data also showed that the mutations of residues 318 and 323 of VP2 significantly affected the neutralization of the IBDV by antiserum, which might be deeply involved

in the immune circumvention of the epizootic varIBDV in the vaccinated flock. This study is significant for the comprehensive prevention and control of the emerging varIBDV.

KEYWORDS

atypical infectious bursal disease, epizootic varIBDV, antigenicity difference, immune circumvention, VP2

Introduction

Infectious bursal disease (IBD), an acute, highly contagious and immunosuppressive disease in chickens, has been threatening poultry farming worldwide (Müller et al., 2003; Jackwood, 2017). IBD is caused by the infectious bursal disease virus (IBDV), an RNA virus that belongs to the genus *Avibirnavirus* of the family *Birnaviridae*. The IBDV has a non-enveloped capsid structure containing a double-stranded RNA genome with two segments, A and B (Brown and Skinner, 1996; Müller et al., 2003). Segment A encodes four viral proteins that include two structural proteins VP2 and VP3, a viral protease VP4, and a nonstructural protein VP5 (Raja et al., 2016). The capsid protein VP2 is located on the surface of the virus, and its outermost surface is composed of four loop regions, namely, P_{BC} (aa 204-236), P_{DE} (aa 240-265), P_{FG} (aa 270-293), and P_{HI} (aa 305-337) (Coulibaly et al., 2005). In addition to VP2 being the icosahedral capsid protein, it is also the major protective immunogen of the IBDV and the primary determinant of viral virulence and antigenic variation (Brandt et al., 2001; Qi et al., 2016). Segment B is approximately 2.8 kb and contains only one open reading frame (ORF), which encodes viral protein VP1. As an RNA-dependent RNA polymerase (RdRp), VP1 plays important role in viral replication and genetic evolution (Escaffre et al., 2013; Yu et al., 2013; Gao et al., 2014).

The IBDV has two serotypes. Serotype I includes virus strains that are pathogenic to chickens, whereas serotype II viruses, isolated from turkeys, are apathogenic to chickens. Since the identification of the classic strain during the first outbreak of IBD in 1957 (Cosgrove, 1962), a variant IBDV (varIBDV) in North America (Jackwood and Saif, 1987) and a very virulent IBDV (vvIBDV) in Europe (Chettle et al., 1989) have successively emerged. The varIBDV of the genotype A2aB1/A2bB1/A2cB1 (the early varIBDV) has always been the circulating strain in North America (Jackwood and Sommer-Wagner, 2005; Kurukulsuriya et al., 2016; Wang Y. et al., 2021). However, the vvIBDV, characterized by acute death, quickly swept the world and became one of the important threats to the poultry industry in the past 30 years (van den Berg, 2000; Müller et al., 2003; Jackwood, 2017; de Wit et al., 2018; Wang Y. et al., 2021). Since 2017, atypical IBD infection, widespread in immunized chicken flocks in East Asia (Fan et al., 2019; Xu G. et al., 2019; Li et al., 2020; Aliyu et al., 2021; Myint et al., 2021; Thai et al., 2021; Wang Y. et al., 2021), has been causing serious economic losses. Our laboratory identified its pathogen as a novel variant IBDV of genotype A2dB1 (hereinafter referred to as the epizootic varIBDV) for the first time, which is genetically different from the early varIBDV in North America (Fan et al., 2019; Wang Y. et al., 2021). The newly epizootic varIBDV and the persistently circulating vvIBDV are the two dominant strains, especially in China (Jiang et al., 2021).

The epizootic varIBDV can partly break through the immune protection of the existing vaccine against the vvIBDV, which is one of the important factors for the virus to become widespread in immunized chickens (Fan et al., 2020a; Li et al., 2020). It was speculated that the epizootic varIBDV might have antigenicity differences compared with vvIBDV. This study proved this speculation and revealed that residues 318 and 323 of the capsid protein VP2 were deeply involved in the antigenicity difference between the epizootic varIBDV and vvIBDV, which would provide important insights into viral evolution and comprehensive prevention of the IBDV.

Materials and methods

Cells, viruses, antibodies and plasmids

DF-1 cells were cultured in Dulbecco's modified Eagle medium (DMEM) (Invitrogen, USA) supplemented with 10% fetal bovine serum (FBS) at 37°C in a humidified incubator with 5% CO_2. DT40 cells were cultured in Roswell Park Memorial Institute (RPMI) 1,640 Medium (Invitrogen, USA) with 10% FBS, 1% glutamine, 2% chicken serum, and 0.1% β-mercaptoethanol at 37°C in a humidified incubator. The epizootic varIBDV representative strain SHG19 (Fan et al., 2020b,c) was previously isolated and identified by the Avian Immunosuppressive Disease Laboratory, Harbin Veterinary Research Institute (HVRI), Chinese Academy of Agricultural Sciences (CAAS) (hereinafter referred to as "our lab"). The Chinese vvIBDV representative strains HLJ0504 (Qi et al., 2011) and Gx (Wang et al., 2004) also were previously identified by our lab. The monoclonal antibodies (MAbs) against IBDV VP2 (2-5C-6F and 7D4) were developed by our lab. The MAb 2-5C-6F can neutralize the vvIBDV, but not 7D4. The eukaryotic

expression vector pCAGGS (Niwa et al., 1991; van den Berg et al., 1991) was kindly supplied by Dr. J. Miyazaki, University of Tokyo, Tokyo, Japan. The infectious clones pCAmGtAHRT and pCAmGtBHRT, each containing segments A and B of attenuated IBDV Gt flanked by ribozyme sequences, were previously constructed (Qi et al., 2007).

Chickens

Specific pathogen-free (SPF) chickens were purchased from the Experimental Animal Center of the HVRI of the CAAS (Harbin, China) and were housed in negative pressure-filtered air isolators. All the animal experiments were approved by the HVRI of the CAAS and were performed according to the animal ethics guidelines and approved protocols.

Indirect immunofluorescence assay

Indirect immunofluorescence assay (IFA) directed by MAbs 7D4 and 2-5C-6F against IBDV VP2 was performed to determine the antigenicity difference between the epizootic varIBDV and vvIBDV. For the IFA, DT40 cells or DF1 cells, cultured in a 24-well tissue culture plate, were separately infected with IBDVs (200 $TCID_{50}$/well) (50% tissue culture infective dose) or transfected with recombinant plasmids (1 μg/well). Cells treated with PBS were used as a negative control. At 24 h post-infection or 48 h post-transfection, the cells in different wells were fixed and then incubated with MAbs (2-5C-6F or 7D4) for 1 h, followed by staining with a fluorescein-labeled goat anti-mouse antibody (1:200 dilution) (Sigma, USA) for another 1 h. The cells were examined by fluorescence microscopy after washing five times with PBS. The quantitative analysis of fluorescence was performed as described previously (Jensen, 2013).

Serum cross-neutralization assay

The serum cross-neutralization assay was performed using the antiserum against each virus strain to further evaluate the antigenicity difference between the epizootic varIBDV and vvIBDV and explore its key residues. First, the $TCID_{50}$ of IBDV strains was determined in DT40 cells by IFA using an IBDV-specific MAb, then IBDV strain was diluted with 10-fold serial dilutions, and each dilution had 8-well repeats. The $TCID_{50}$ detection was performed three times. Then 200 $TCID_{50}$ of viruses were incubated for 1 h at 37°C with equal volumes of antiserum at 2-fold serial dilutions. The virus–serum mixture (100 μl) was cultured with DT40 cells at 37°C in a humidified incubator. After 24 h, the infection-positive wells were detected by IFA, and the homologous or heterologous neutralization titers were determined. Each neutralization assay was performed at least three times.

Identification of the antigen epitopes

A series of overlapping VP2 peptides of the vvIBDV Gx strain were cloned into pGEX-6P-1 and expressed in *E. coli* BL21 (DE3) as fusion proteins with a GST tag to investigate the epitopes of the MAbs 2-5C-6F or 7D4. For the first round, three overlapping peptides spanning the VP2 amino acid (aa) sequences, aa 1-167 (VP2A), aa 141-305 (VP2B), aa 261-441 (VP2C), were expressed in *E. coli*. The VP2X was further divided into three peptides for the second round of screening. For the last round, the peptide amino acids were truncated one by one from both ends until the minimal epitope was identified. The schematic diagrams of all peptides are listed in Figure 2A, and the primers are shown in Supplementary Table 1. The reactivity of the MAbs was detected by Western blot (WB), and the IRDye 800CW goat anti-mouse antibody (LI-COR) was used as the secondary antibody.

Epitope sequence alignment

The amino acid sequence of the VP2, containing the identified epitopes, was compared with that in other subtypes of serotype I of IBDV, including classic, very virulent, attenuated, and variant strains, using MegAlign software (DNASTAR, Madison, WI, USA). The three-dimensional (3-D) structure of the VP2 protein of the IBDV SHG19 strain was predicted by using the I-TASSER algorithm (Yang et al., 2015). The predicted structure of SHG19 VP2 was compared with that of VP2 of the vvIBDV Gx strain (Bao et al., 2021) using PyMOL software (http://pymol.org/).

Construction of the mutated VP2

The major protective antigen gene VP2 of SHG19 and Gx strains were amplified with primers VP2F/VP2R (Table 1) and then cloned into the plasmid pCAGGS, and the recombinant plasmid was named pCASHG19VP2 and pCAGxVP2. Using PCR for site-directed mutagenesis as described previously (Qi et al., 2007), direct mutations were introduced into the VP2 gene of the SHG19 and Gx strains. Based on the plasmid pCASHG19VP2, primer pairs 19-318F/318R and 19-323F/323R (Table 1) were used to introduce direct mutations A953G, A969C, and A953G/A969C (which resulted in amino acid mutations of D318G, E323D, and D318G/E323D in VP2) into the VP2 gene of the SHG19 strain, and the mutated plasmids

TABLE 1 Primers.

Primer	Sequence	Orientation	Position (nt)
A1	**AAAGAATTCGATCTC**ATCGATTGTTAAGCGTCTGAT	Sense	A: −58 to −44
A2	AGACCGATCGTATCCGACTATAGGAATTC	Antisense	A: 15 to −14
A3	GGAATTCCTATAGTCGGATACGATCGGTCT	Sense	A: −15 to 15
A4	ATGCCATGCCGACCCGGGGACCCGCGAACG	Antisense	A: +15 to 3245
A5	CGTTCGCGGGTCCCCGGGTCGGCATGGCAT	Sense	A: 3245 to +15
A6	**GCTCGAGCATGCCCG**GGTACCCGCCCTCCCTTAGC	Antisense	A: +88 to +75
B1	**TTTGGCAAAGAATTC**GAGCTCTGTTAAGCGTCTGAT	Sense	B: −58 to −44
B2	CAGACCCATCGTATCCGACTATAGGAATTCC	Antisense	B: 16 to −15
B3	GGAATTCCTATAGTCGGATACGATGGGTCTG	Sense	B: −15 to 16
B4	GATGCCATGCCGACCCTTGGGGGCCCCCGC	Antisense	B: +18 to 2,816
B5	GCGGGGGCCCCCAAGGGTCGGCATGGCATC	Sense	B: 2,816 to +18
B6	**ATCTGCTAGCTCGA**GCATGCCGCCCTCCCTTAGCCAT	Antisense	B: +88 to +72
19–318F	GTGACCTCCAAAAGTG***G***TGGCCAGGCAGGGG	Sense	A:1,067 to 1,097
19–318R	GTTCCCCTGCCTGGCCA***C***CACTTTTGGAGGTCACTA	Antisense	A: 1,100 to 1,065
19–323F	GATGGCCAGGCAGGGGA***C***CAGATGTCGTGGTC	Sense	A: 1,082 to 1,113
19–323R	GCCGACCACGACATCTG***G***TCCCCTGCCTGGCCATCAC	Antisense	A: 1,116 to 1,080
Gx−318F	TAACCTCCAAAAGTG***A***TGGTCAGGCGG	Sense	A: 1,068 to 1,094
Gx−318R	TCCCCCGCCTGACCA***T***CACTTTTGGAGGTTAC	Antisense	A: 1,098 to 1,067
Gx−323F	TCAGGCGGGGGA***A***CAGATGTCATGG	Sense	A: 1,087 to 1,111
Gx−323R	TGACCATGACATCTG***T***TCCCCCGCCTGACC	Antisense	A: 1,114 to 1,085
VP2F	**AAAGAATTCGATCTC**GGATCCATGACAAACCTGCAAGATC	Sense	A: 131 to 149
VP2R	**TAGCTCGAGCATGCCCG**AAGCTTTGCTCCTGCAATCTTC	Antisense	A: 1,453 to 1,438

Primers were designed according to the sequence of IBDV strain Gx (GenBank accession no. AY444873) and SHG19 (GenBank accession no. MN393076, MN393077). The ribozyme sequences are surrounded by boxes, the introduced restriction sites are underlined, the homology arms sequences are boldfaced, and the mutated nucleotides are shown in italic and bold. Orientation and position of the virus-specific sequences of the primers are shown. The "+" or "−" symbols in front of the positions of nucleotides indicate the upstream or downstream of the genome, respectively. "A" and "B" in the last column represent segments A and B of IBDV genome.

were named pCASHG19VP2-D318G, pCASHG19VP2-E323D, and pCASHG19VP2-D318G/E323D. Based on the plasmid pCAGxVP2, primer pairs Gx-318F/318R and Gx-323F/323R (Table 1) were used to introduce mutations using the same approach, and the mutated plasmids were named pCAGxVP2-G318D, pCASHG19VP2-D323E, and pCASHG19VP2-G318D/D323E.

Rescue of the mutated IBDV

A fusion PCR was performed as described previously (Qi et al., 2009) to construct infectious clones of the SHG19 strain. First, with pCAmGtAHRT as a template, two PCR fragments, F1 and F3, were amplified with two pairs of primers (A1/A2 and A5/A6 in Table 1), and the lengths of PCR products were 94 bp and 120 bp, respectively. Second, with the SHG19 strain as a template, the PCR fragment F2 of 3290 bp was amplified with primers A3/A4 (Table 1). Finally, a fragment SHG19AHRT was fused by three fragments F1, F2, and F3. The purified PCR product SHG19AHRT was digested with *Cla* I/*Kpn* I and ligated into pCAGGS to obtain the infectious clone pCASHG19AHRT of segment A. Based on the plasmid SHG19AHRT, primer pairs 19-318F/318R and 19-323F/323R (Table 1) were used to introduce direct mutations, and the mutated plasmids were named pCASHG19A-A953GHRT, pCASHG19A-A969CHRT, and pCASHG19A-A953G/A969CHRT. Simultaneously, with pCAmGtBHRT as a template, the fragment SHG19BHRT was amplified by three pairs of primers (B1/B2, B3/B4, and B5/B6), as given in Table 1. The purified PCR product SHG19BHRT was digested with *Sac* I/*Sph* I and ligated into pCAGGS to obtain the infectious clone pCASHG19BHRT of segment B. The schematic diagrams of infectious clones are shown in Figure 4A.

Mutated IBDVs were rescued by using an RNA polymerase II-driven reverse genetic system (Qi et al., 2007). The purified infectious clone plasmids of segment A and segment B (2 μL of each plasmid at 1 μg/μL) were co-transfected into DF-1 cells using a TransIT-X2 Dynamic Delivery System (Mirusbio, Madison, Wisconsin, USA). At 72 h post-transfection, after

freezing and thawing three times, the cell suspension was injected into bursae of 14-day-old SPF chickens. At 7 d post-injection, the bursal tissues were collected, and then the rescued viruses were detected. To characterize the rescued viruses, a fragment of 930 bp was amplified by RT-PCR using primer pairs 2U/2L (bp 628-1557 of segment A) and then sequenced (Fan et al., 2019). The full-length genomes of the rescued viruses were further amplified and sequenced to confirm the accuracy as designed. The rescued viruses were also identified by IFA directed by MAbs 7D4 in DT40 cells. The replication of the rescued viruses in DT40 cells was detected at 24, 36, 48, and 60 h post-infection by RT-qPCR, as previously described (Wang S. et al., 2021). The correctly identified rescued viruses were named SHG19, SHG19-318, SHG19-323, and SHG19-318/323, respectively.

Statistical analysis

The significance of the variability between different groups was determined by two-way analysis of variance (ANOVA), using GraphPad Prism software (version 8.0). Significant treatment means were separated using Tukey's honestly significant difference (Tukey's HSD) at $P = 0.05$.

Results

The antigenicity of the epizootic varIBDV is different from vvIBDV

To determine the antigenicity difference between the epizootic varIBDV and vvIBDV, the cross-neutralizing assay for the varIBDV representative strain SHG19 and the vvIBDV representative strain HLJ0504 was performed. The results indicated that HLJ0504 antiserum had a high homologous neutralization titer against HLJ0504 at 10.33 ± 3.06 $\log_2$, but its heterologous neutralization titer (3.33 ± 0.58 $\log_2$) for SHG19 reduced by 7.0 $\log_2$ (Figure 1A). Similarly, SHG19 antiserum had a homologous neutralization titer against SHG19 at 5.40 ± 1.14 $\log_2$, but its heterologous neutralization titer (2.20 ± 0.84 $\log_2$) for HLJ0504 reduced by 3.2 $\log_2$ (Figure 1B). In addition, with IFA in DT40 cells, the MAbs against IBDV VP2 (2-5C-6F and 7D4) were used to further detect the antigenicity difference between the epizootic varIBDV (SHG19) and vvIBDV (HLJ0504 and Gx). The results showed that all the epizootic varIBDVs (SHG19) and vvIBDVs (HLJ0504 and Gx) could be recognized by MAb 7D4, while the MAb 2-5C-6F could only recognize vvIBDV (HLJ0504 and Gx), but not the epizootic varIBDV (SHG19) (Figure 1C). These results confirmed that the antigenicity of the epizootic varIBDV was different from that of vvIBDV.

The antigen epitopes of IBDV were identified by neutralizing MAb

The neutralizing MAb 2-5C-6F of vvIBDV could not well recognize the epizootic varIBDV SHG19 by IFA. To explore the molecular basis, the antigen epitope recognized by MAb was identified step by step by using the peptide-scanning method based on a series of overlapping VP2 (Figure 2A). First, it was identified that the MAb 2-5C-6F and MAb 7D4 reacted with an epitope of aa 261-441 and an epitope of aa 141-305 (data not shown). Then the epitope of aa 261-441 was gradually truncated, and the MAb 2-5C-6F targeting antigen epitope was identified as aa 317-336 of VP2 (Figure 2B), which is located in the P_{HI} loop of VP2 (Figure 3A). Simultaneously, the epitope of aa 141-305 was gradually truncated, and the antigen epitope targeted by MAb 7D4 was determined as aa 183-191 of VP2 (Figure 2C), which is located outside of the projection (P) domain of VP2 (Figure 3A).

Sequence analysis showed that the epitope recognized by 7D4, 183PIPAIGLDPKM191, was conserved for all IBDV subtypes of serotype 1 (Figure 3D). However, for the epitope recognized by 2-5C-6F (317SGGQAGDQMSWSASGSLAVT336), both the epizootic varIBDV and the early varIBDV were different from other IBDV subtypes. The varIBDV showed 318D and 323E, but other IBDV subtypes including vvIBDV showed 318G and 323D (Figure 3E). The alignment results indicated that residues 318D and 323E are conserved in different varIBDV strains isolated from broiler, layer, and local breed chickens (Supplementary Figure 1). According to the predicted VP2 structure, the mutations G318D and D323E might alter the structure of the extreme outermost region of the VP2 P domain and the associated electrostatic potential (Figures 3B,C). Especially the G318D mutation presents a negatively charged surface at the region of SHG19 (Figure 3C).

Residue mutations of 318 and 323 of VP2 influence the recognition of IBDV by MAb

To determine the influence of residue mutations of 318 and 323 on the recognition of the MAb 2-5C-6F to viral VP2, three recombinant eukaryotic expression plasmids were transfected into DF1 cells to express the wild type of SHG19 VP2, its single-mutated type (SHG19VP2-D318G or SHG19VP2-E323D), and its double-mutated type (SHG19VP2-D318G/E323D). At 48 h post-transfection, the recognition of the MAb to viral VP2 was detected with IFA. The IFA results directed by MAb 7D4 confirmed the expression of all four VP2 mentioned before. The IFA results showed that MAbs 2-5C-6F did not recognize SHG19 VP2 but could recognize its single-mutated

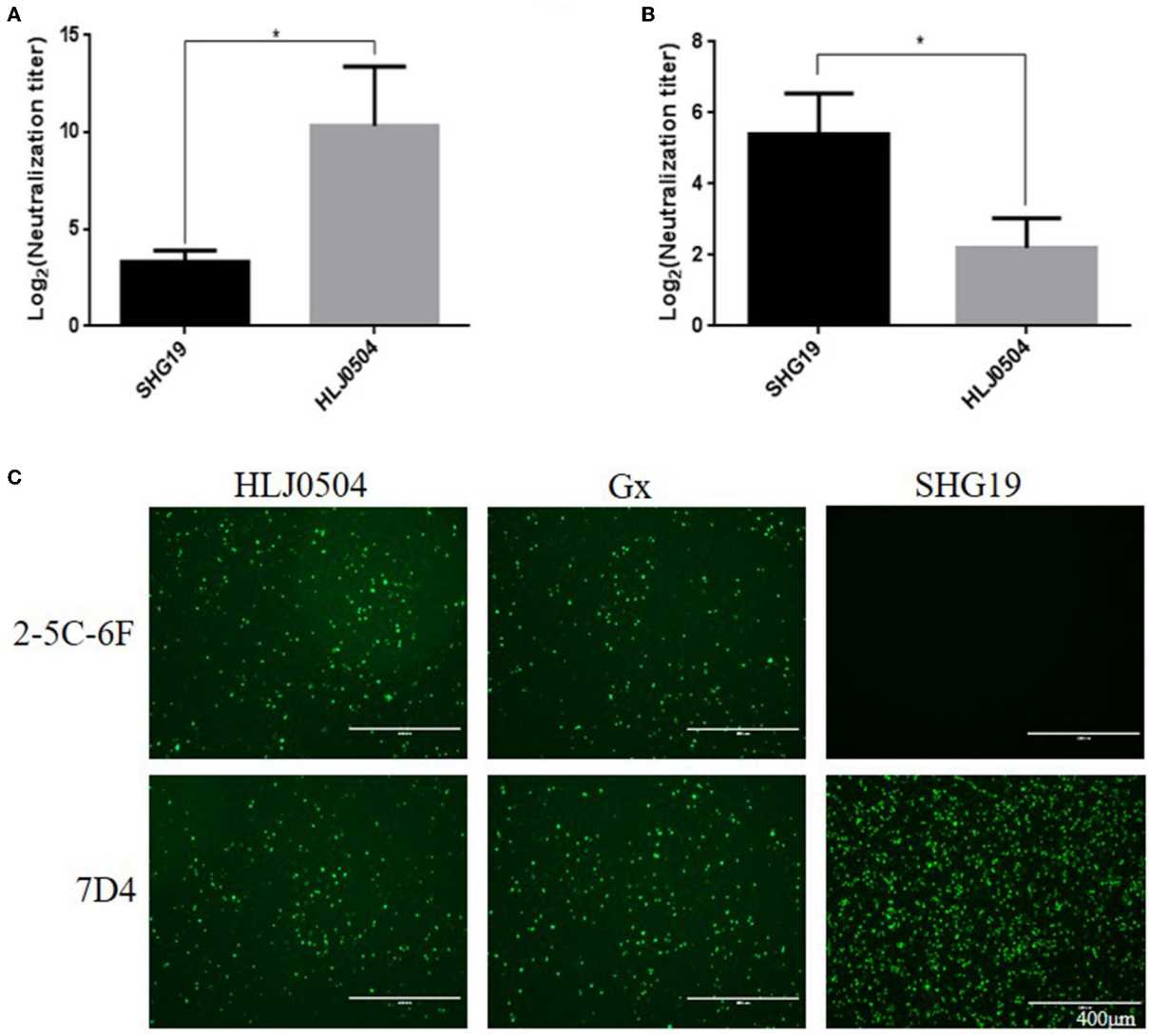

FIGURE 1
Detection of antigenicity difference between the epizootic varIBDV (SHG19 strain) and vvIBDV (HLJ0504 strain and Gx strain). **(A)** Cross-neutralizing assay of HLJ0504 antiserum for SHG19 and HLJ0504 on DT40 cells directed. **(B)** Cross-neutralizing assay of SHG19 antiserum for SHG19 and HLJ0504 on DT40 cells directed. **(C)** IFA on DT40 cells directed by MAbs 2-5C-6F and 7D4. The mean titers and standard deviations (error bars) from three **(A)** or five **(B)** independent samples are shown. * represents $p < 0.05$.

type (SHG19VP2-D318G or SHG19VP2-E323D) and its double-mutated type (SHG19VP2-D318G/E323D) (Figure 4A). The relative fluorescence intensity results confirmed this (Figure 4C). Conversely, MAbs 2-5C-6F could recognize Gx VP2 and its single-mutated type (GxVP2-G318D or GxVP2-D323E) but could not well recognize its double-mutated type (GxVP2-G318D/D323E) (Figures 4B,D). The data from both directions identified that residues mutations of 318 and 323 of VP2 was involved in the recognition of the MAb 2-5C-6F to viral VP2.

To further verify the involvement of residues 318 and 323 of VP2 in the recognition of the MAb 2-5C-6F to the virus, the mutated IBDVs SHG19, SHG19-318, SHG19-323, and SHG19-318/323 were successfully rescued (Figure 5A), which was confirmed by RT-PCR, sequencing, and IFA (data not shown). The mutated viruses SHG19-318, SHG19-323, and SHG19-318/323 showed similar replication properties as the parental IBDV SHG19 (Supplementary Figure 2). In the following experiment of MAb recognition, at 24 h post-infection in DT40 cells, the recognition of MAb to viral VP2 was detected with IFA. The IFA results directed by MAb 7D4 confirmed the infection of all four IBDV mentioned before. The IFA results directed by the MAb 2-5C-6F showed that the MAb 2-5C-6F did not well recognize SHG19 but could recognize its single-mutated strain (SHG19-318 or SHG19-323) and its double-mutated strain (SHG19-318/323) (Figures 5B,C). These data from both aspects of protein and virus discovered that residues mutations

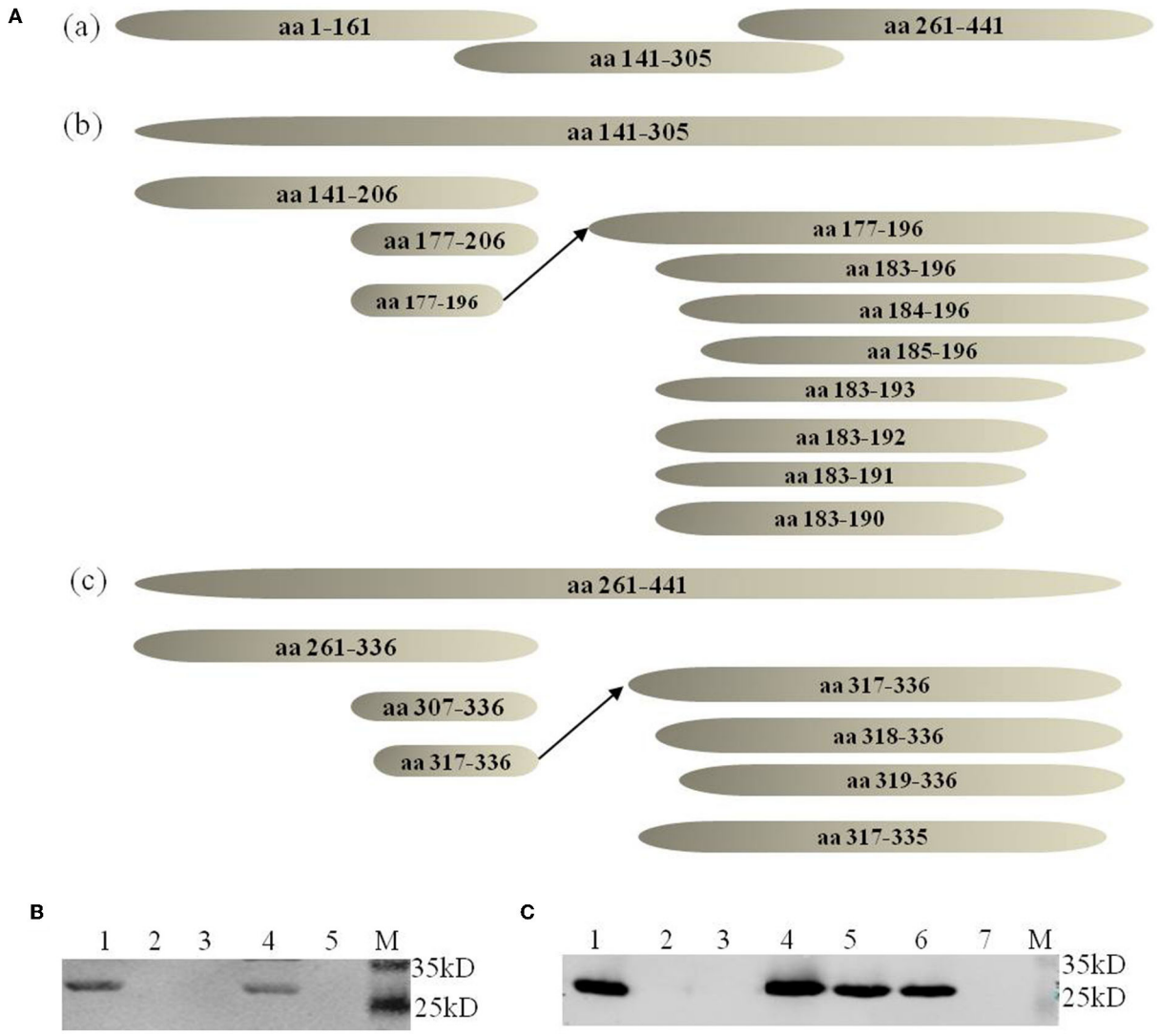

FIGURE 2
Identification of antigen epitopes with MAbs 7D4 and 2-5C-6F. **(A)** Schematic diagrams of all peptides (not drawn to scale) used in the peptide-scanning method. (a) Three overlapping peptides spanning the VP2 aa sequences. (b) Identification of the antigen epitope with MAb 7D4. (c) Identification of the antigen epitope with the MAb 2-5C-6F. **(B)** Recognition of the minimal epitope with 2-5C-6F by Western blotting. Lane 1 corresponds to the epitope of aa 317-336; 2, aa 318-336; 3, aa 319-336, 4 corresponds to aa 317-336; 5, aa 317-335; M, marker. **(C)** Recognition of the minimal epitope with MAb 7D4 by Western blotting. 1, aa 183-196; 2, aa 184-196; 3, aa 185-196; 4, aa 183-193, 5, aa 183-192, 6, aa 183-191; 7, aa 183-190; M, marker.

of 318 and 323 of VP2 influenced the recognition of IBDV by the MAb.

Residue mutations of 318 and 323 of VP2 influence the neutralization of IBDV by MAb

To further study whether residue mutations of 318 and 323 of VP2 influence the neutralization of IBDV by antiserum, cross-neutralizing assays on DT40 cells were performed. First, the neutralizing MAb 2-5C-6F against the vvIBDV was used. The neutralizing results showed that the MAb 2-5C-6F could neutralize the vvIBDV Gx strain and HLJ0504 strain, but could not neutralize the epizootic varIBDV SHG19. However, the MAb 2-5C-6F could neutralize the double-mutated SHG19 (SHG19-318/323) with a neutralization titer of 7.33 ± 0.58 $\log_2$ (Figure 6A). Furthermore, the neutralization ability of the MAb 2-5C-6F to single-mutated SHG19 (SHG19-318 or SHG19-323) was detected. the MAb 2-5C-6F could neutralize SHG19-318 and SHG19-323, with average neutralization titers of 2 ± 0 $\log_2$ and 5 ± 0 $\log_2$, which were 5.33 $\log_2$ and 2.33 $\log_2$ lower than those of SHG19-318/323, respectively (Figure 6B). These results showed that residue mutations of D318G/E323D

10.3389/fmicb.2022.909252

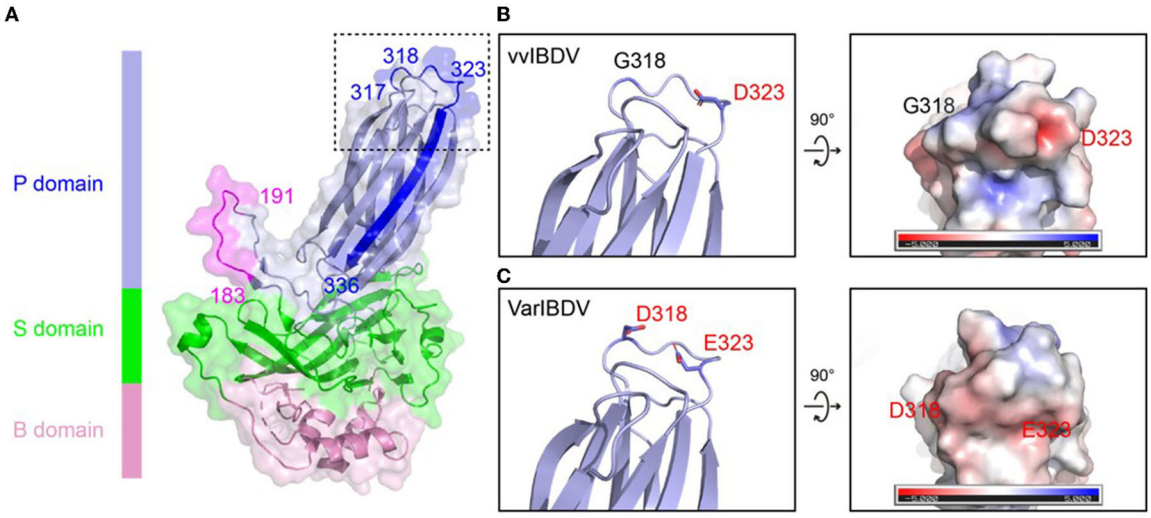

D

Subtype	Representative strain	Epitope recognized by MAb 7D4
vvIBDV	Gx	183PIPAIGLDP191
	HLJ0504	183PIPAIGLDP191
	89163	183PIPAIGLDP191
aIBDV	Gt	183PIPAIGLDP191
cIBDV	IM	183PIPAIGLDP191
Early VarIBDV	Variant E	183PIPAIGLDP191
Epidemic VarIBDV	SHG19	183PIPAVGLDP191

E

Subtype	Representative strain	Epitope recognized by MAb 2-5C-6F
vvIBDV	Gx	317SGGQAGDQMSWSASGSLAVT336
	HLJ0504	317SGGQAGDQMSWSASGSLAVT336
	89163	317SGGQAGDQMSWSASGSLAVT336
aIBDV	Gt	317SGGQAGDQMSWSARGSLAVT336
cIBDV	IM	317SGGQAGDQMSWSASGSLAVT336
Early VarIBDV	Variant E	317SDGQAGEQMSWSASGSLAVT336
Epidemic VarIBDV	SHG19	317SDGQAGEQMSWSASGSLAVT336

FIGURE 3
Location and sequence alignment of MAb antigenic epitopes. **(A)** Structure of IBDV VP2. P, S, and B domains were marked with different colors. The antigen epitopes of MAbs 7D4 (blue or magenta) and 2-5C-6F (blue or magenta) and the key residues are highlighted, respectively. The antigen epitopes of MAbs 7D4 and 2-5C-6F and key amino acid residues are highlighted. **(B)** Left: Zoom-in view of dashed box in **(A)** showing the key residues 318 and 323 of vvIBDV VP2. Right: 90° rotated view of the left panel showing the electrostatic surface representation of the vvIBDV. The side chains of residues 318 and 323 are displayed as a stick. **(C)** Left: Zoom-in view of dashed box in **(A)** showing the key residues 318 and 323 of varIBDV VP2 predicted by using the I-TASSER algorithm. Right: 90° rotated view of the left panel showing the electrostatic surface representation of varIBDV. The side chains of residues 318 and 323 are displayed as stick. **(D)** Amino acid sequence of the antigen epitope recognized by MAb 7D4 among different subtype strains of IBDV. **(E)** Amino acid sequence of the antigen epitope recognized by the MAb 2-5C-6F among different subtype strains of IBDV. The amino acid residues 318 and 323 of the antigen epitope recognized by the MAb 2-5C-6F are highlighted.

were deeply involved in the neutralization circumvention of the epizootic varIBDV SHG19 from the MAb 2-5C-6F. In terms of affecting the ability of the MAb 2-5C-6F to neutralize the epizootic varIBDV SHG19, the double-mutated strain was more efficient than the single-mutated strain, and the residue 323 of VP2 played more important roles (Figure 6B).

10.3389/fmicb.2022.909252

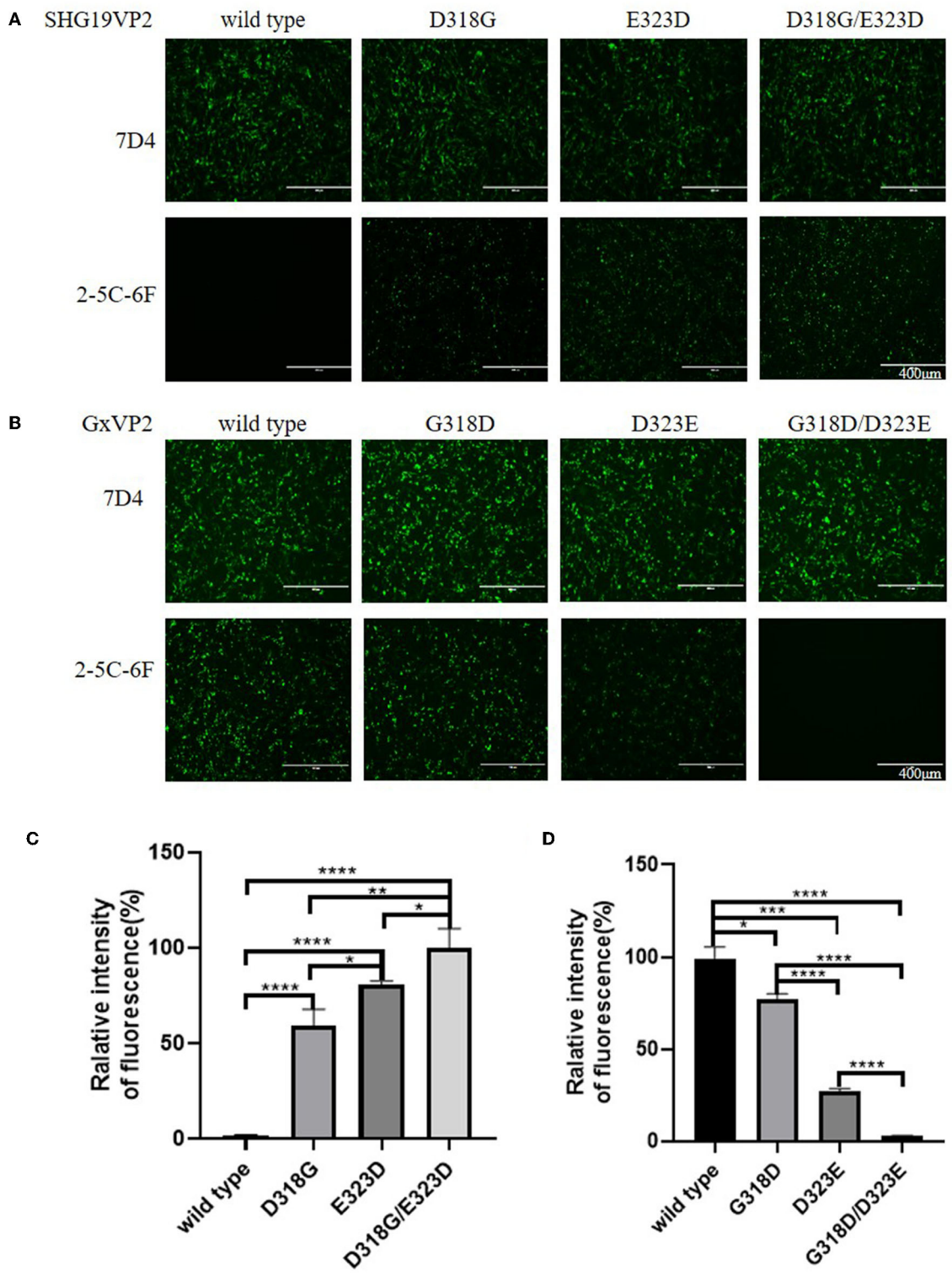

FIGURE 4
Antigen recognition detection of the wild and mutated types of VP2 in DF1 cells directed by MAbs 7D4 and 2-5C-6F. **(A)** VP2 of the SHG19 strain (SHG19VP2) and its mutated types (SHG19VP2-D318G, SHG19VP2-E323D, and SHG19VP2-D318G/E323D). **(B)** VP2 of the Gx strain (GxVP2) and its mutated types (GxVP2-G318D, GxVP2-D323E, and GxVP2- G318D/ D323E). **(C)** Quantitative analysis of fluorescence of **(A)**. **(D)** Quantitative analysis of fluorescence of **(B)**. The mean fluorescence intensity and standard deviations (error bars) from three independent samples are shown. * represents $P < 0.05$, ** represents $P < 0.01$, *** represents $P < 0.001$, **** represents $P < 0.0001$.

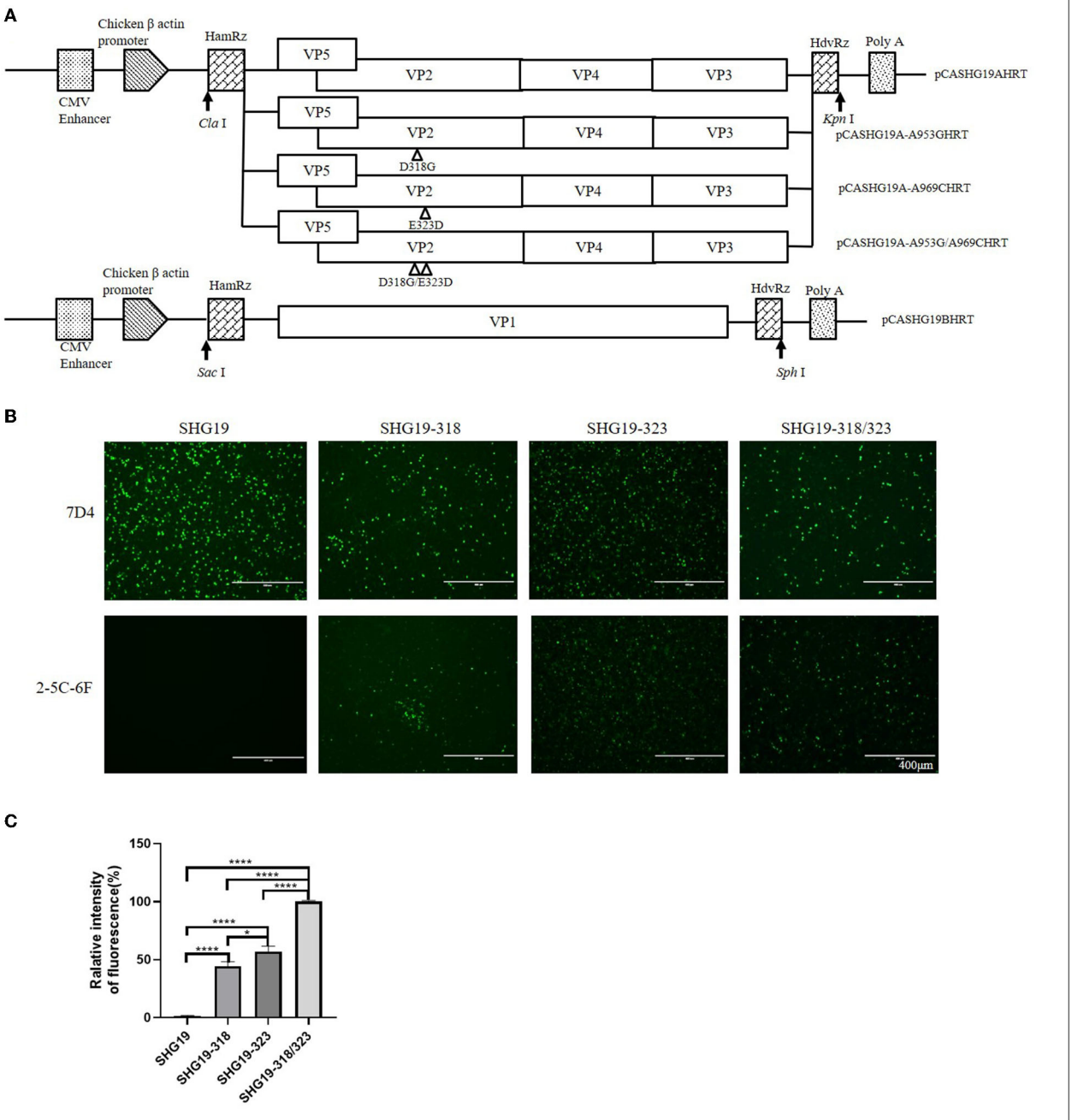

FIGURE 5
Antigen recognition detection of the epizootic varIBDV SHG19 and its mutants in DT40 cells directed by MAbs 7D4 and 2-5C-6F. **(A)** Schematic diagrams of the infectious clones containing segment A and segment B of SHG19. In plasmid pCASHG19A-A953GHRT, pCASHG19A-A969CHRT, and pCSHG19A-A953G/A969CHRT, the nucleotide substitutions A953G, A969C, and A953G/A969C resulted in the amino acid substitutions D318G, E323D, and D318G/E323D of the VP2 protein of SHG19, respectively. The genomic cDNA sequences are preceded by a cytomegalovirus enhancer and a chicken β-actin promoter and are flanked by the cDNAs of hammerhead ribozyme (HamRz) and hepatitis delta ribozyme (HdvRz). The restriction enzyme sites used to construct recombinant vectors are also shown. **(B)** IFA of SHG19 and its mutants (SHG19-318, SHG19-323, and SHG19-318/323) on DT40 cells directed by MAbs 7D4 and 2-5C-6F at 24 h post-infection. **(C)** Quantitative analysis of fluorescence. The mean fluorescence intensity and standard deviations (error bars) from three independent samples are shown. * represents $P < 0.05$, **** represents $P < 0.0001$.

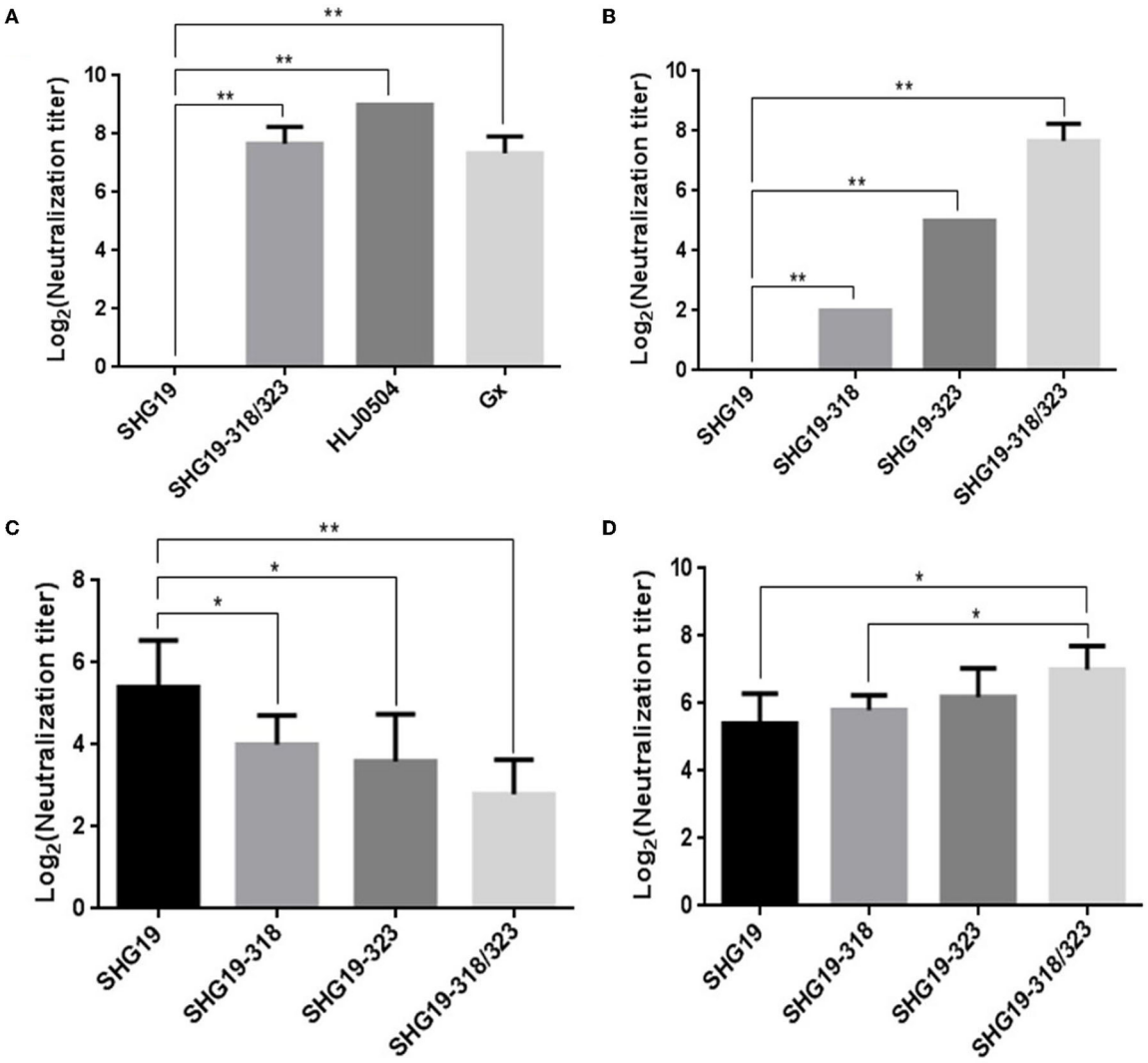

FIGURE 6
Cross-neutralizing assay. **(A)** Cross-neutralizing assay directed by the MAb 2-5C-6F for the epizootic varIBDV (SHG19 strain), vvIBDV (HLJ0504 strain and Gx strain), and double-mutated virus (SHG19-318/323). **(B)** Cross-neutralizing assay directed by the MAb 2-5C-6F for the SHG19 strain and its mutants (SHG19-318, SHG19-323, and SHG19-318/323). **(C)** Cross-neutralizing assay directed by SHG19 antiserum for the SHG19 strain and its mutants. **(D)** Cross-neutralizing assay directed by SHG19-318/323 antiserum for the SHG19 strain and its mutants. The mean titers and standard deviations (error bars) from three **(A,B)** or five **(C,D)** independent samples are shown. * and ** represent $P < 0.05$ and $P < 0.01$.

Residue mutations of 318 and 323 of VP2 influence the neutralization of IBDV by antiserum

The MAb targets only one antigen epitope, while antiserum contains antibodies against multiple antigenic epitopes. Although residues mutations of 318 and 323 of VP2 can affect the neutralization ability of its monoclonal antibody to the virus, is it enough to interfere with the neutralization ability of antiserum to virus? So the neutralization of the IBDV by antiserum was further identified. Compared with homologous neutralization to SHG19 by SHG19 antiserum (5.40 ± 1.14 $\log_2$), the neutralization titer to the single-mutated viruses SHG19-318 (4.00 ± 0.71 $\log_2$) and SHG19-323 (3.60 ± 1.14 $\log_2$) was obviously reduced by 1.40 $\log_2$ and 1.80 $\log_2$, respectively. For double-mutated virus (SHG19-318/323, 2.80 ± 0.84 $\log_2$), the neutralization titer of SHG19 antiserum was reduced more by 2.60 $\log_2$ (Figure 6C). Moreover, the SHG19-318/323 antiserum was used to detect the neutralization ability to different viruses. Compared with the homologous neutralization to SHG19-318/323 (7.00 ± 0.71 $\log_2$) by SHG19-318/323 antiserum, the neutralization titer to SHG19-323 (6.20 ± 0.84 $\log_2$), SHG19-318 (5.80 ± 0.45 $\log_2$), and the wild type of SHG19 (5.40 ± 0.89 $\log_2$) was reduced by 0.8 $\log_2$, 1.20 $\log_2$, and 1.60 $\log_2$, respectively (Figure 6D). The evidence from various angles identified that residues 318 and 323 were

important factors affecting the cross-neutralization between the epizootic varIBDV and vvIBDV.

Discussion

Since the late 1980s, the vvIBDV has spread globally and become one of the greatest threats to the healthy development of the poultry industry. With the use of vaccines and the improvement of feeding management, the vvIBDV is gradually being controlled, especially in large-scale intensive farms. However, since 2017, the atypical epizootic IBD has gradually become severe, mainly in poultry breeding areas of China (Fan et al., 2019; Xu A. et al., 2019; Jiang et al., 2021; Wang Y. et al., 2021), South Korea (Thai et al., 2021), Japan (Myint et al., 2021), and Malaysia (Aliyu et al., 2021). Although not fatal to chickens, atypical IBD causes severe atrophy of the central immune organs of the infected chickens, weakens host immunity, interferes with the immune response to other vaccines, causes complications and secondary infections by other pathogens, and reduces production performance including weight (Fan et al., 2019, 2020c; Xu A. et al., 2019; Li et al., 2020). The varIBDV appeared in the United States as early as the late 1980s and mainly circulated in North America. It is one of the important diseases severely threatening in the poultry industry in the United States (Ojkic et al., 2007; Stoute et al., 2019) and Canada (Amini et al., 2015). However, the newly epizootic varIBDV of the genotype A2bB1 in East Asia is genetically different from the early varIBDV circulating in North America (Fan et al., 2019; Wang Y. et al., 2021). In addition to the vvIBDV, the newly epizootic varIBDV has become another important threat to the healthy development of the poultry industry at least in China (Jiang et al., 2021; Wang Y. et al., 2021).

In China, to prevent and control the vvIBDV, almost all chicken flocks are immunized with vaccines including live vaccine, subunit vaccine, immune complex vaccine, and combined vaccine. Interestingly, what are the reasons for the wild spread of the epizootic VarIBDV of the genotype A2bB1 in immunized chicken flocks? Sequence analysis showed that the epizootic VarIBDV had the same characteristic amino acids as the reference strain of the early VarIBDV (variant E), including 213N, 222T, 242V, 249K, 253Q, 279N, 284A, 286I, 294L, 318D, 323E, and 330S, which is an indication of possible antigenic changes compared to the vvIBDV. The cross-neutralization test in this study proved the speculation that the neutralizing ability of the vvIBDV antiserum to the epizootic varIBDV decreased by 7 $\log_2$, and the average neutralizing titer of the epizootic varIBDV antiserum to vvIBDV decreased by 3.2 $\log_2$. In our next plan, the immune protection of the available vvIBDV vaccine against the epizootic varIBDV will be continuously monitored. However, our current research shows that enough attention should be paid to the application of the cross-neutralization test to evaluate the immune protection spectrum of vaccine in advance. In addition, the MAb 2-5C-6F, which had good neutralizing activity against the vvIBDV, could not recognize the epizootic VarIBDV well. These results discovered that the epizootic varIBDV had different antigenicity from the vvIBDV.

What is the molecular basis of the antigenic difference between the epizootic varIBDV and vvIBDV? First, the epitope of the neutralizing MAb 2-5C-6F of the vvIBDV was identified to be located at aa 317-336 of the P_{HI} of the capsid protein VP2. The P_{HI} is an important domain for immunoreactivity (Lee et al., 2006; Letzel et al., 2007). Compared with the vvIBDV, the epizootic varIBDV had two amino acid differences in this epitope, G318D, and D323E. Subsequently, the IFA based on protein mutants of VP2 showed that the double-mutations of G318D/D323E made the VP2 of the vvIBDV no longer be well recognized by the MAb 2-5C-6F, while the D318G or/and E323D mutations could make the epizootic varIBDV acquire the ability to be recognized by the MAb 2-5C-6F. Furthermore, using mutated viruses, it was further confirmed that the mutations of D318G, E323D, or D318G/E323D could enable the unrecognized epizootic varIBDV to acquire the ability to be recognized by the MAb 2-5C-6F. These data indicated that aa 318 and aa 323 of VP2 were important molecular bases for the antigenic difference between the epizootic varIBDV and vvIBDV.

Are the antigenicity changes induced by aa 318 and aa 323 mutations enough to affect the antiserum viral neutralization ability? For the first time, our study showed that the MAb 2-5C-6F could neutralize the vvIBDV but had little neutralizing activity against the epizootic varIBDV. When residues 318G and 323D of the epizootic varIBDV were mutated to 318D and 323E of the vvIBDV, 2-5C-6F could neutralize the corresponding mutant viruses, and its ability to neutralize the double-mutated virus (SHG19-318/323) was stronger than that of the single-mutated virus (SHG19-318 or SHG19-323). It is well known that antiserum targets various antigen epitopes, while the MAb only targets one, so the mutations that can escape the MAb might not be enough to escape antiserum. Furthermore, the viral neutralizing ability changes of the SHG19 antiserum were evaluated. Results showed that compared to the parental strain SHG19, the ability to neutralize single-mutated viruses (SHG19-318 or SHG19-323) was significantly downregulated, and the ability to neutralize the double-mutated virus (SHG19-318/323) was further downregulated by 2.60 $\log_2$. On the contrary, compared to SHG19-318/323, the neutralizing titer of SHG19-318/323 antiserum to SHG19 was also reduced by 1.60 $\log_2$. About the effect on MAb or antiserum viral recognition and neutralization ability, residue 323 was stronger than residue 318, and double-mutation was greater than single-mutation. According to the predicted VP2 structure, residues 318 and 323 are located on the outermost region of viral capsid protein VP2, and the mutations G318D and D323E might alter the structure and the associated electrostatic potential.

Both aspects of data identified that the mutations of residues 318 and 323 of VP2 significantly affected the recognition and neutralization of IBDV by antiserum, which might be deeply

involved in the immune circumvention of the epizootic varIBDV in the vaccinated flock. To be mentioned, the newly epizootic varIBDV exhibits the same amino acids as the early varIBDV variant E strain at positions 318 and 323 of VP2, which is a case for the selection of converging antigenically significant mutations. It was reported that aa 318-324 of VP2 were critical for vvIBDV typical and atypical antigenicity (Eterradossi et al., 1998). Letzel et al. (2007) found that residues 318 and 323 of VP2 were critical for the reactivity of MAb 10 (Letzel et al., 2007). It has been also reported that residue 323 might influence the binding of more than one MAb to the IBDV directly or indirectly (Vakharia et al., 1994; Letzel et al., 2007). In this study, it was further proved that residues 318 and 323 of VP2 could affect the neutralizing activity of antiserum, which was involved in the immune circumvention of the epizootic varIBDV in the vaccinated flock. Our research not only further proved the function of these key mutation hotspots but also clarified the important molecular mechanism of the epizootic varIBDV prevalence. In addition, these key mutation hotspots including residues 318 and 323 of VP2 could be mentioned as a good indication of possible antigenic changes.

Modern molecular biology techniques such as reverse genetics make it possible to edit vaccine strains manually (Yu et al., 2016; Fan et al., 2020b). To develop new vaccines that match the antigenicity of varIBDV, the key residues involved in immune circumvention should be taken into account. A recent research indicated that the emerging varIBDV and the persistently circulating vvIBDV are two important threats (Jiang et al., 2021). So the currently used vvIBDV vaccine needs to continue to be used scientifically. It is a more meaningful to develop broad-spectrum vaccines that can prevent both varIBDV and vvIBDV.

Conclusion

This study revealed a significant difference in antigenicity between the epizootic varIBDV and vvIBDV and further proved that residues 318 and 323 of the VP2 protein P_{HI} interfered with antiserum viral neutralization, which provided insights into one important reason for the prevalence of the epizootic varIBDV in immunized chickens. This study is significant for the comprehensive prevention and control of the emerging varIBDV.

Data availability statement

The raw data supporting the conclusions of this article will be made available by the authors, without undue reservation.

Ethics statement

The animal study was reviewed and approved by Ethics and Animal Welfare Committee of HVRI.

Author contributions

XQ, LF, and YW contributed conception and design of the study. LF and YW performed the experiments and wrote the manuscript. NJ and XN performed the relevant experiments. WZ, MH, and KB analyzed the data. AL and SW contributed to figures. YG, LG, KL, HC, QP, CL, YZ, and XW advised on experimental design and data interpretation. XQ supervised the study, interpreted the data, wrote the manuscript, and acquired the research funds. All authors contributed to the article and approved the submitted version.

Funding

This study was supported by the National Natural Science Foundation of China (Grant Nos. 32072852 and 32102649), the Heilongjiang Provincial Natural Science Foundation of China (Grant Nos. ZD2020C006 and TD2019C003), the Key Research and Development Program of Heilongjiang Province (Grant No. GA21B004), and China Agriculture Research System (CARS-41-G15).

Conflict of interest

The authors declare that the research was conducted in the absence of any commercial or financial relationships that could be construed as a potential conflict of interest.

Publisher's note

Supplementary material

The Supplementary Material for this article can be found online at: https://www.frontiersin.org/articles/10.3389/fmicb.2022.909252/full#supplementary-material

SUPPLEMENTARY FIGURE 1
Characteristic amino acid substitutions in VP2 among varIBDV strains isolated from broiler, layer, and local breed chickens. Asterisks indicate residues identical to the sequence of varIBDV strain SHG19. Residues 318 and 323 were highlighted.

SUPPLEMENTARY FIGURE 2
The replication of the mutated IBDV in DT40 cells, and the viral genome copies were detected at 24, 36, 48, and 60 hours post-infection by RT-qPCR. The mean fluorescence intensity and standard deviations (error bars) from three independent samples are shown.

References

Aliyu, H. B., Hair-Bejo, M., Omar, A. R., and Ideris, A. (2021). Genetic Diversity of Recent Infectious Bursal Disease Viruses Isolated From Vaccinated Poultry Flocks in Malaysia. *Front. Vet. Sci.* 8, 643976. doi: 10.3389/fvets.2021.643976

Amini, K., Zachar, T., Popowich, S., Knezacek, T., Goodhope, B., Willson, P., et al. (2015). Association of increased rate of condemnation of broiler carcasses due to hepatic abnormalities with immunosuppressive diseases in the broiler chicken industry in Saskatchewan. *Can. J. Vet. Res.* 79, 261–267.

Bao, K., Qi, X., Li, Y., Gong, M., Wang, X., and Zhu, P. (2021). Cryo-EM structures of infectious bursal disease viruses with different virulences provide insights into their assembly and invasion. *Sci. Bull.* 6, 646–654. doi: 10.1016/j.scib.2021.12.009

Brandt, M., Yao, K., Liu, M., Heckert, R. A., and Vakharia, V. N. (2001). Molecular determinants of virulence, cell tropism, and pathogenic phenotype of infectious bursal disease virus. *J. Virol.* 75, 11974–11982. doi: 10.1128/JVI.75.24.11974-11982.2001

Brown, M. D., and Skinner, M. A. (1996). Coding sequences of both genome segments of a European 'very virulent' infectious bursal disease virus. *Virus Res.* 40, 1–15. doi: 10.1016/0168-1702(95)01253-2

Chettle, N., Stuart, J. C., and Wyeth, P. J. (1989). Outbreak of virulent infectious bursal disease in East Anglia. *Vet. Rec.* 125, 271–272. doi: 10.1136/vr.125.10.271

Cosgrove, A. S. (1962). An apparently new disease of chickens: avian nephrosis. *Avian Dis.* 6, 385–389. doi: 10.2307/1587909

Coulibaly, F., Chevalier, C., Gutsche, I., Pous, J., Navaza, J., Bressanelli, S., et al. (2005). The birnavirus crystal structure reveals structural relationships among icosahedral viruses. *Cell* 120, 761–772. doi: 10.1016/j.cell.2005.01.009

de Wit, J. J., Cazaban, C., Dijkman, R., Ramon, G., and Gardin, Y. (2018). Detection of different genotypes of infectious bronchitis virus and of infectious bursal disease virus in European broilers during an epidemiological study in 2013 and the consequences for the diagnostic approach. *Avian Pathol.* 47, 140–151. doi: 10.1080/03079457.2017.1387231

Escaffre, O., Le Nouen, C., Amelot, M., Ambroggio, X., Ogden, K. M., Guionie, O., et al. (2013). Both genome segments contribute to the pathogenicity of very virulent infectious bursal disease virus. *J. Virol.* 87, 2767–2780. doi: 10.1128/JVI.02360-12

Eterradossi, N., Arnauld, C., Toquin, D., and Rivallan, G. (1998). Critical amino acid changes in VP2 variable domain are associated with typical and atypical antigenicity in very virulent infectious bursal disease viruses. *Arch. Virol.* 143, 1627–1636. doi: 10.1007/s007050050404

Fan, L., Wang, Y., Jiang, N., Chen, M., Gao, L., Li, K., et al. (2020a). Novel variant infectious bursal disease virus suppresses Newcastle disease vaccination in broiler and layer chickens. *Poultry Sci.* 99, 6542–6548. doi: 10.1016/j.psj.2020.09.037

Fan, L., Wang, Y., Jiang, N., Gao, L., Li, K., Gao, Y., et al. (2020b). A reassortment vaccine candidate of the novel variant infectious bursal disease virus. *Vet. Microbiol.* 251, 108905. doi: 10.1016/j.vetmic.2020.108905

Fan, L., Wu, T., Hussain, A., Gao, Y., Zeng, X., Wang, Y., et al. (2019). Novel variant strains of infectious bursal disease virus isolated in China. *Vet. Microbiol.* 230, 212–220. doi: 10.1016/j.vetmic.2019.01.023

Fan, L., Wu, T., Wang, Y., Hussain, A., Jiang, N., Gao, L., et al. (2020c). Novel variants of infectious bursal disease virus can severely damage the bursa of fabricius of immunized chickens. *Vet. Microbiol.* 240, 108507. doi: 10.1016/j.vetmic.2019.108507

Gao, L., Li, K., Qi, X., Gao, H., Gao, Y., Qin, L., et al. (2014). Triplet amino acids located at positions 145/146/147 of the RNA polymerase of very virulent infectious bursal disease virus contribute to viral virulence. *J. Gen. Virol.* 95, 888–897. doi: 10.1099/vir.0.060194-0

Jackwood, D. H., and Saif, Y. M. (1987). Antigenic diversity of infectious bursal disease viruses. *Avian Dis.* 31, 766–770. doi: 10.2307/1591028

Jackwood, D. J. (2017). Advances in vaccine research against economically important viral diseases of food animals: infectious bursal disease virus. *Vet. Microbiol.* 206, 121–125. doi: 10.1016/j.vetmic.2016.11.022

Jackwood, D. J., and Sommer-Wagner, S. E. (2005). Molecular epidemiology of infectious bursal disease viruses: distribution and genetic analysis of newly emerging viruses in the United States. *Avian Dis.* 49, 220–226. doi: 10.1637/7289-101404R

Jensen, E. C. (2013). Quantitative analysis of histological staining and fluorescence using ImageJ. *Anat. Rec. (Hoboken)* 296, 378–381. doi: 10.1002/ar.22641

Jiang, N., Wang, Y., Zhang, W., Niu, X., Huang, M., Gao, Y., et al. (2021). Genotyping and molecular characterization of infectious bursal disease virus identified in important poultry-raising areas of China during 2019 and 2020. *Front. Vet. Sci.* 8, 759861. doi: 10.3389/fvets.2021.759861

Kurukulsuriya, S., Ahmed, K. A., Ojkic, D., Gunawardana, T., Gupta, A., Goonewardene, K., et al. (2016). Circulating strains of variant infectious bursal disease virus may pose a challenge for antibiotic-free chicken farming in Canada. *Res. Vet. Sci.* 108, 54–59. doi: 10.1016/j.rvsc.2016.08.002

Lee, M., Doong, S., Lai, S., Ho, J., and Wang, M. (2006). Processing of Infectious Bursal Disease Virus (IBDV) Polyprotein and self-assembly of IBDV-like particles in Hi-5 cells. *Biotechnol. Prog.* 22, 763–769. doi: 10.1021/bp050426n

Letzel, T., Coulibaly, F., Rey, F. A., Delmas, B., Jagt, E., Van Loon, A. A., et al. (2007). Molecular and structural bases for the antigenicity of VP2 of infectious bursal disease virus. *J.Virol.* 81, 12827–12835. doi: 10.1128/JVI.01501-07

Li, G., Kuang, H., Guo, H., Cai, L., Chu, D., Wang, X., et al. (2020). Development of a recombinant VP2 vaccine for the prevention of novel variant strains of infectious bursal disease virus. *Avian Pathol.* 49, 557–571. doi: 10.1080/03079457.2020.1791314

Müller, H., Islam, M. R., and Raue, R. (2003). Research on infectious bursal disease—the past, the present and the future. *Vet. Microbiol.* 97, 153–165. doi: 10.1016/j.vetmic.2003.08.005

Myint, O., Suwanruengsri, M., Araki, K., Izzati, U. Z., Pornthummawat, A., Nueangphuet, P., et al. (2021). Bursa atrophy at 28 days old caused by variant infectious bursal disease virus has a negative economic impact on broiler farms in Japan. *Avian Pathol.* 50, 6–17. doi: 10.1080/03079457.2020.1822989

Niwa, H., Yamamura, K., and Miyazaki, J. (1991). Efficient selection for high-expression transfectants with a novel eukaryotic vector. *Gene* 108, 193–199. doi: 10.1016/0378-1119(91)90434-D

Ojkic, D., Martin, E., Swinton, J., Binnington, B., and Brash, M. (2007). Genotyping of Canadian field strains of infectious bursal disease virus. *Avian Pathol.* 36, 427–433. doi: 10.1080/03079450701598408

Qi, X., Gao, H., Gao, Y., Qin, L., Wang, Y., Gao, L., et al. (2009). Naturally occurring mutations at residues 253 and 284 in VP2 contribute to the cell tropism and virulence of very virulent infectious bursal disease virus. *Antiviral Res.* 84, 225–233. doi: 10.1016/j.antiviral.2009.09.006

Qi, X., Gao, L., Qin, L., Deng, X., Wu, G., Zhang, L., et al. (2011). Genomic sequencing and molecular characteristics of a very virulent strain of infectious bursal disease virus isolated in China. *Agr. Sci. Tech.* 12, 1946–1949.

Qi, X., Gao, X., Lu, Z., Zhang, L., Wang, Y., Gao, L., et al. (2016). A single mutation in the P_{BC} loop of VP2 is involved in the in vitro replication of infectious bursal disease virus. *Sci. China Life Sci.* 59, 717–723. doi: 10.1007/s11427-016-5054-1

Qi, X., Gao, Y., Gao, H., Deng, X., Bu, Z., Wang, X., et al. (2007). An improved method for infectious bursal disease virus rescue using RNA polymerase II system. *J. Virol. Methods* 142, 81–88. doi: 10.1016/j.jviromet.2007.01.021

Raja, P., Senthilkumar, T. M., Parthiban, M., Thangavelu, A., Gowri, A. M., Palanisammi, A., et al. (2016). Complete genome sequence analysis of a naturally reassorted infectious bursal disease virus from India. *Genome Announc.* 4, e00709–00716. doi: 10.1128/genomeA.00709-16

Stoute, S. T., Jackwood, D. J., Crossley, B. M., Michel, L. O., and Blakey, J. R. (2019). Molecular epidemiology of endemic and very virulent infectious bursal disease virus genogroups in backyard chickens in California, 2009–2017. *J. Vet. Diagn. Invest.* 31, 371–377. doi: 10.1177/1040638719842193

Thai, T. N., Jang, I., Kim, H. A., Kim, H. S., Kwon, Y. K., and Kim, H. R. (2021). Characterization of antigenic variant infectious bursal disease virus strains identified in South Korea. *Avian Pathol.* 50, 174–181. doi: 10.1080/03079457.2020.1869698

Vakharia, V. N., Snyder, D., Lütticken, D., Mengel-Whereat, S. A., and Goodwin, M. A. (1994). Active and passive protection against variant and classic infectious bursal disease virus strains induced by baculovirus-expressed structural proteins. *Vaccine* 12, 452–456. doi: 10.1016/0264-410X(94)90124-4

van den Berg, T. P., Gonze, M., and Meulemans, G. (1991). Acute infectious bursal disease in poultry: isolation and characterisation of a highly virulent strain. *Avian pathol.* 20, 133–143. doi: 10.1080/03079459108418748

van den Berg, T. P. V. D. (2000). Acute infectious bursal disease in poultry: a review. *Avian pathol.* 29, 175–194. doi: 10.1080/03079450050045431

Wang, S., Yu, M., Liu, A., Bao, Y., Qi, X., Gao, L., et al. (2021). TRIM25 inhibits infectious bursal disease virus replication by targeting VP3 for ubiquitination and degradation. *PLoS Pathog.* 17, e1009900. doi: 10.1371/journal.ppat.1009900

Wang, X., Zeng, X., Gao, H., Fu, C., and Wei, P. (2004). Changes in VP2 gene during the attenuation of very virulent infectious bursal disease virus strain Gx isolated in China. *Avian Dis.* 48, 77–83. doi: 10.1637/7061

Wang, Y., Fan, L., Jiang, N., Gao, L., Li, K., Gao, Y., et al. (2021). An improved scheme for infectious bursal disease virus genotype classification based on both genome-segments A and B. *J. Integr. Agr.* 20, 1372–1381. doi: 10.1016/S2095-3119(20)63424-4

Xu, A., Pei, Y., Zhang, K., Xue, J., Ruan, S., and Zhang, G. (2019). Phylogenetic analyses and pathogenicity of a variant infectious bursal disease virus strain isolated in China. *Virus Res.* 276, 197833. doi: 10.1016/j.virusres.2019.197833

Xu, G., Li, J., Shen, Q., Hou, L., Xia, Y., Li, Q., et al. (2019). Complete genome characterization of a novel infectious bursal disease virus strain isolated from a chicken farm in China. *Microbiol. Resour. Announc.* 8, e00632–e00619. doi: 10.1128/MRA.00632-19

Yang, J., Yan, R., Roy, A., Xu, D., Poisson, J., and Zhang, Y. (2015). The I-TASSER Suite: protein structure and function prediction. *Nat. Methods* 12, 7–8. doi: 10.1038/nmeth.3213

Yu, F., Ren, X., Wang, Y., Qi, X., Song, J., Gao, Y., et al. (2013). A single amino acid V4I substitution in VP1 attenuates virulence of very virulent infectious bursal disease virus (vvIBDV) in SPF chickens and increases replication in CEF cells. *Virology* 440, 204–209. doi: 10.1016/j.virol.2013.02.026

Yu, H., Huang, L., Zhang, Y., Hu, L., Wang, S., Li, J., et al. (2016). An attenuated EMCV-HB10 strain acts as a live viral vector delivering a foreign gene. *J. Gen. Virol.* 97, 2280–2290. doi: 10.1099/jgv.0.000541

Advantages of publishing in Frontiers

OPEN ACCESS
Articles are free to read for greatest visibility and readership

FAST PUBLICATION
Around 90 days from submission to decision

HIGH QUALITY PEER-REVIEW
Rigorous, collaborative, and constructive peer-review

TRANSPARENT PEER-REVIEW
Editors and reviewers acknowledged by name on published articles

Frontiers
Avenue du Tribunal-Fédéral 34
1005 Lausanne | Switzerland

Visit us: www.frontiersin.org
Contact us: frontiersin.org/about/contact

REPRODUCIBILITY OF RESEARCH
Support open data and methods to enhance research reproducibility

DIGITAL PUBLISHING
Articles designed for optimal readership across devices

FOLLOW US
@frontiersin

IMPACT METRICS
Advanced article metrics track visibility across digital media

EXTENSIVE PROMOTION
Marketing and promotion of impactful research

LOOP RESEARCH NETWORK
Our network increases your article's readership